TOWARDS CLINICAL TRIALS OF A NOVEL BIONIC EYE: BUILDING EVIDENCE OF SAFETY AND EFFICACY

THE UNIVERSITY OF SYDNEY

Samuel Christian Eggenberger

School of Biomedical Engineering

Faculty of Engineering

The University of Sydney

This dissertation is submitted to fulfil requirements
for the degree of Doctor of Philosophy

September 2022

The template was produced by Malcolm Morgan and Kayla Friedman for the Centre for Sustainable Development, University of Cambridge, UK

Towards clinical trials of a novel bionic eye: building evidence of safety and efficacy

Samuel C. Eggenberger – September 2022

To my Mother, Bethli

To my Father, Kurt, the real doctor

To Pauline, Ellin and Maylis, I am who I am because you are who you are.

Ethics is knowing the difference between
what you have a right to do
and what is right to do.

Potter Stewart

DECLARATION

This dissertation is the result of my own work and includes nothing, which is the outcome of work done in collaboration except where specifically indicated in the authorship attribution statement, below. It has not been previously submitted, in part or whole, to any university of institution for any degree, diploma, or other qualification.

In accordance with the University of Sydney thesis and examination of higher degrees by research policy 2015, this thesis is does not exceed 80,000 words.

Signed:_____

Date:_____

Samuel Christian Eggenberger

Sydney

AUTHORSHIP ATTRIBUTION STATEMENT

Chapter 3 of this dissertation was published in Biomaterials with the title *Implantation and long-term assessment of the stability and biocompatibility of a novel 98 channel suprachoroidal visual prosthesis in sheep* [1]. I participated in the development of the methodology with the co-authors, curated, visualised and formally analysed the data, and wrote the original draft of the manuscript. See Appendices for details on roles of co-authors. Minor adjustments of the last paragraphs of the article were made for the benefit of continuity.

Chapter 4 is the result of a collaboration with Innes K. Wise and Chris Burrows. I identified the need for a structured approach to the anaesthetic protocol selection and designed the tool based on the expert advice on laboratory animal care and anaesthesia provided by IKW and CB. I co-wrote the chapter, which will be submitted as a methods journal article, with CB. The individual contributions are listed below as per the Contributor Role Taxonomy (CRediT) guidelines [2].

SCE: Conceptualisation, methodology, formal analysis, investigation, data curation, writing, visualisation, supervision, project administration.

IKW: Methodology, formal analysis, writing – review and editing

CB: Methodology, formal analysis, investigation, writing – original draft

Additionally, the *in vivo* data used as demonstration of the concept presented in Chapter 4 was acquired with the assistance of Ariastity Mega Pratiwi (PhD candidate) during the experiments detailed in Chapter 5.

The study described in Chapter 5 was performed in collaboration with Ariastity Mega Pratiwi (PhD candidate) and with the support of Dr. Orsolya Kekesi. The individual contributions are listed below as per the CRediT guidelines [2].

SCE: Conceptualisation, methodology, software, formal analysis, investigation, data curation, writing, visualisation, project administration.

AMP: Methodology, software, investigation

OK: Methodology, investigation

Note that the CRediT statement above is true and transparent about the data and results presented in this dissertation, and doesn't exclude that further data curation, analysis or visualisation may be performed on the same dataset subsequently.

Chapter 6 contains the outcome of a joint project with Ariastity M. Pratiwi, which I presented as a poster titled “Towards Calibrated Computer Models for the Optimization of Parallel Stimulation” at The Eye and the Chip: 12th World Research Congress on the Relationship between Neurobiology and Nano-Electronics Focusing on Artificial Vision (TEatC 2021), Detroit MI, USA (see poster and link to the associated web page in the Appendices). I identified the need for a model, developed the concept based on the potential field of application for the model, including the definition of worst-case parameters for chronic safety testing, and I analysed and interpreted the results. AMP built the computational model. CRediT author statement [2]:

SCE: Conceptualisation, methodology, formal analysis, writing, visualisation

AMP: Methodology, software, formal analysis, data curation, investigation

Chapter 7 of this thesis was based on existing data acquired as described in the present dissertation by Dr. Niras Cheeckottu Vayalil, Graduate School of Biomedical Engineering, University of New South Wales, Sydney. I developed the methodology (except for the ageing parameters: temperature; current; frequency; and duration of the experiment), curated, visualised, and analysed the data and wrote all related sections of this dissertation.

In addition to the statements above, in cases where I am not the corresponding author of a published item, permission to include the published material has been granted by the corresponding author.

Signed:_____

Date:_____

Samuel Christian Eggenberger

Sydney

As supervisor for the candidature upon which this thesis is based, I can confirm that the authorship attribution statements above are correct.

Signed:_____

Date:_____

Prof. Dr. Gregg Jørgen Suaning

Towards clinical trials of a novel bionic eye: building evidence of safety and efficacy

Samuel C. Eggenberger – September 2022

ABSTRACT

In the quest for therapeutic solutions for the visually impaired, electrical stimulation of the retina is, and has been, the focus of intense research. Some of these efforts have led to the development of the Phoenix^{99} Bionic Eye, a device which combines promising technological features with novel stimulation strategies.

For medical devices, considerable challenges must be overcome before they're allowed to be trialled in their target population. The requirements for a study to be performed include the demonstration of a positive risk-benefit ratio of the research. The present dissertation is an attempt to address how pre-clinical trials in animals can be used to understand and minimise risks.

A positive risk-benefit ratio means that the potential benefits of the research outweigh the risks of the intervention. In the case of retinal prostheses, the risks include the surgical intervention, the immune response to the device, the safety of the electrical stimuli, and the effects of device ageing.

In this work, successful demonstration of the surgical safety and biocompatibility of passive Phoenix^{99} devices during long-term implantation in sheep called for the evaluation of the chronic effects of the novel stimulation paradigms it can deliver. As preparation for this study, the techniques used to evaluate the safety and efficacy of the stimuli in animals were refined. A systematic approach to minimise the impact of anaesthesia on the experimental results is presented, as well as a novel *in vivo* retinal recording technique. To maximise the clinical relevance of all animal trials, a computer model for the prediction of thresholds was developed.

Finally, *in vitro* device ageing was performed to deepen our understanding of the design's potential for long-term implantation. Protocols for a long-term device safety study in sheep and for an acute human trial are also presented, thus taking concrete and sensible steps towards the first clinical use of the Phoenix^{99} Bionic Eye.

ACKNOWLEDGEMENTS

I would like to thank Prof. Gregg Suaning for his trust, for opening the doors of his laboratory to me, and for giving me access to the results of the many years of work, which have led to the development of the Phoenix^{99}. I wish that my contribution to this gigantic project may have brought this endeavour one step closer to giving someone a spark of light, where it's most needed. Thank you also for the review and constructive critique of this dissertation.

My gratitude goes to Innes Wise and Chris Burrows for sharing their passion and expertise about veterinary anaesthesia. Thank you for the fascinating discussions which have guided me through a rather unexpected, yet fascinating "detour" in my career as an engineer and a scientist. I thank Andrew Nessiem for his role with animal care and review of the relevant literature about anaesthetic protocols. Thank you to Emma Johnson providing her expertise in veterinary anaesthesia during the prolonged procedures.

Thank you to Ariastity Mega for her patient and constructive translation of my vision into a promising computer model. Thank you also for the help with the preparation and execution of the sheep trials. The long nights and – even longer – debates about stimulation strategies were all worth it.

Thank you to Dr. Orsolya Kekesi for the support provided during the preparation and execution of the animal experiments, for the advice on quantitative analysis of immunohistochemistry, and for the critical review of this thesis.

I thank Matthew Kolibac and Sebastian Parsons for their assistance with manufacturing the electrode arrays for the *in vivo* experiments.

Thank you to Dr. Niras Vayalil for his assistance with all matters related to electronics and for his help with the investigation of the Phoenix^{99} ageing properties. I would also like to thank Prof. Torsten Lehmann for taking the time to answer my many questions about stimulation artefacts and artefact-reduction strategies, and Dr. Alejandro Barriga-Rivera for sharing his experience with the acquisition of cortical signals.

I'm grateful to Elaine Chew, Andrew Fortis, Karen Barnes and the Veterinary Pathology Diagnostic Services, Sydney School of Veterinary Science for the help with immunohistochemical staining and in slide scanning, and to Dr. Kathrin Schemann of the Sydney Informatics Hub, a Core Research Facility of the University of Sydney, for the technical assistance with regards to statistical analysis. Thank you to Kayla Friedman and

Malcolm Morgan of the Centre for Sustainable Development, University of Cambridge, UK for producing the Microsoft Word thesis template used to produce this document.

Thank you to Dr. Maria Büchner and Dr. Matias Kagias for their critical comments on this thesis.

My gratitude goes to Dr. Görkem Serbes for sharing his knowledge and wisdom, and for making me benefit from his endless patience. Thank you for your friendship and for helping me through the rough patches as a growing scientist.

I'd also like to thank my parents for teaching me resilience and for their never-failing trust in me.

A special thank you goes to Red and Blue, who graze peacefully on a cloud.

Finally, I find no words to express my gratitude to the person who has kept our growing family alive and happy while I dedicated my time to the work presented here. Pauline Eggenberger, this entire adventure only made sense because you were here by my side. Thank you.

CONTENTS

LIST OF TABLES

LIST OF FIGURES

LIST OF ABBREVIATIONS AND ACRONYMS

Abbreviation	Definition
ACT	AUSTRALIAN CAPITAL TERRITORY
AE	ADVERSE EVENT
AMP	AGE RELATED MACULAR DEGENERATION
ANOVA	ANALYSIS OF VARIANCE
CAP	COMPOUND ACTION POTENTIAL
CRediT	CONTRIBUTOR ROLE TAXONOMY
CRI	CONSTANT RATE INFUSION
CT	COMPUTED TOMOGRAPHY
ECAP	ELECTRICALLY EVOKED COMPOUND ACTION POTENTIAL
ECG	ELECTROCARDIOGRAPHY
EEG	ELECTROENCEPHALOGRAPHY
EEP	ELECTRICALL EVOKED POTENTIAL
ERG	ELECTRORETINOGRAPHY
FDA	FOOD AND DRUG ADMINISTRATION (UNITED-STATES OF AMERICA)
GFAP	GLIAL FIBRILLARY ACIDIC PROTEIN
IM	INTRAMUSCULAR
IOP	INTRAOCULAR PRESSURE
IV	INTRAVENOUS
LCA	LEBER'S CONGENITAL AMAUROSIS
LED	LIGHT EMITTING DIODE
LGN	LATERAL GENICULATE NUCLEUS
MAC	MINIMUM ALVEOLAR CONCENTRATION
MAR	MINIMUM ANGLE OF RESOLUTION
MEA	MULTIELECTRODE ARRAY
NSAID	NON-STEROIDAL ANTI-INFLAMMATORY DRUG
NSW,	NEW SOUTH WALES
NY	NEW YORK
OCT	OPTICAL COHERENCE TOMOGRAPHY
PBS	PHOSPHATE-BUFFERED SALINE
PDMS	POLYDIMETHYLSILOXANE
PIVA	PARTIAL INTRAVENOUS ANESTHESIA
QMP	QUASIMONOPOLAR
RCD1	RADICAL-INDUCED CELL DEATH 1
RCS	ROYAL COLLEGE OF SURGEONS
RF	RADIOFREQUENCY
RGC	RETINAL GANGLION CELL
ROI	REGION OF INTEREST
RP	RETINITIS PIGMENTOSA
RPE	RETINAL PIGMENTED EPITHELIUM
SA	SOUTH AUSTRALIA
SAE	SEVER ADVERSE EVENT

SEM	SCANNING ELECTROM MICROSCOPE
SOP	STANDARD OPERATING PROCEDURE
TIVA	TOTAL INTRAVENOUS ANAESTHESIA
TM	TRADEMARK
TMS	TRANSCRANIAL MAGNETIC STIMULATION
UNSW	UNIVERSITY OF NEW SOUTH WALES
USD	UNITED-STATES DOLLARS
VCD	VERTICAL CORNEAL DIAMETER
VEGF	VASCULAR ENDOTHELIAL GROWTH FACTOR
VEP	VISUALLY EVOKED POTENTIAL
VIC	VICTORIA
VS	VISUAL STIMULATOR
WHO	WORLD HEALTH ORGANISATION

List of Appendices

1 INTRODUCTION

ELECTRIFYING BLINDNESS

Retinal implants are little pieces of electronics designed to electrically stimulate the retina of blind people and trick their brains into perceiving images where the eyes are no longer functional. To use such devices to restore a form of vision, the electrical – neural – path to the brain must be preserved. Multiple pathologies fulfill this criterion, including rare genetic disorders like Stargardt disease or Leber's congenital amaurosis. Because of their higher prevalence, two blindness-causing diseases have been identified as principal target for retinal stimulation: retinitis pigmentosa (RP) and age-related macular degeneration (MD). Both pathologies affect the light-sensitive cells of the retina while leaving a functional neuronal connection to the brain [3, 4].

RP is a genetic disease, which leads to gradual vision loss from the periphery of the visual field towards the centre, eventually leading to severe visual impairment. With a prevalence of approximately 1 in 4000 [5], it is the leading cause of blindness in young people in developed countries [6, 7]. The disease generally causes first symptoms, such as diminished dark adaptation, in pre-adulthood and vision further degrades over several years [8]. The timeline of disease development is very variable. Many patients lose central vision by the age of 60 [5], although a large population will retain useful vision their entire life [8].

On the other hand, AMD causes gradual vision loss starting in the central area – the macula – and extending towards the periphery, eventually causing severe visual impairment and blindness, although peripheral vision may remain largely intact. The

disease affects mostly the older population and the prevalence of AMD-related visual impairment and blindless is very low under the age of 60 [9]. It is the leading cause of blindness in developed countries and accounted for 5.6% of the blind population in the world in 2020 [9].

The Phoenix^{99} Bionic Eye is a fully implantable system, designed to deliver electrical stimuli to the retina of late-stage AMD or RP patients to restore visual sensations. It implements novel current focusing strategies designed to enable simultaneous stimulation from multiple sites while minimising electrical interference – crosstalk between electrodes [10]. Compared to other retinal prostheses in development, which are mostly restricted to sequential stimulation due to crosstalk, the Phoenix^{99} may be used to explore ways to elicit more spatiotemporally natural and higher acuity vision [10, 11]. Additionally, it also implements a technology enabling direct recording of the retinal response which may be used to further understand, refine, and tune the stimulation [12]. A detailed review of the literature of relevant retinal implants will be presented in Chapter 2 to establish the potential benefits of the device compared to the current clinical landscape of visual prostheses.

The Phoenix^{99} is the result of more than two decades of intense research in the field of implantable electronics and neural stimulation and has reached a point in its development where a clinical trial appears as the natural next step. Beyond the good intentions and the technological features, there is a multitude of challenges that such a device will face until visually impaired people can use it. Many of those challenges are influenced by the regulatory landscape, and competing devices and technologies, rather than solely the devices potential. A closer look at the context in which a device will have to fit is therefore warranted.

1.1 Reality check

Retinal implants have been in development for at least three decades and multiple devices have since been implanted in more than 500 patients [13] as part of clinical trials or as commercial devices. Although different implantation sites have been tested, including epiretinal, subretinal, or suprachoroidal prostheses, the principles behind the restoration of a sense of vision is shared between the devices: electrical stimulation of the retina using small electrodes designed to interface with the surviving neural network.

To date, the best restored visual acuity measured was 6/150 using a prosthesis called Alpha AMS (Retina Implant AG, Reutlingen, Germany) [14]. Although it represents

amazing progress and would have been a very useful improvement for the recipient, this value is still below the threshold of legal blindness defined by the World Health Organisation as a visual acuity worse than 3/60 [15].

From the three retinal implants which received clearance by some regulatory body (American Food and Drug Administration approval or European Conformity marking) none remain on the market today. The manufacturers having voluntarily ceased production of their retinal devices to focus on other visual prostheses such as cortical stimulators or having been forced to cease operations due to financial hardship. This reflects multiple factors that affect the viability of retinal prostheses, namely the reportedly limited quality of the restored vision and the financial viability of the products.

Research and development in the field of complex implantable devices such as vision prostheses is an inherently difficult process. Beyond the challenges of designing and building reliable, miniature, high tech devices, we will see that such implants appear to fall into a "gap", where safety and efficacy are hard to demonstrate and improve without the use of human subjects. Yet simultaneously, tests on humans are difficult to justify without extensive safety and efficacy data. This contradiction blurs the line between basic research, applied research, and the development of commercial devices. Indeed, as *in vitro* experiments and animal research have shown to be limited with regards to their applicability to humans [16], performing even exploratory research on neural interfaces requires devices and stimulation paradigms that are sufficiently safe and reliable to be used in the clinic. Once such devices are available, given the challenges that will have been overcome to this point, it would be beneficial if the same technology could be applied more widely.

To become truly useful to a larger population, and therefore achieve its goal as a vision prosthesis, a device should be perceived as economically viable, at least in the long term. Should it be only for the purpose of supporting the colossal development and clinical trial costs, a concept must be able to attract investors; naturally, investments are more likely if a model is expected to generate profit. As long as prospective financial sustainability isn't in sight, prostheses are likely to remain within the boundaries of research-oriented organisations that can attract public and philanthropic support, and therefore to be produced and used at a relatively small scale. Inside academic structures, which have different key performance indicators than the industry, there are few incentives to dedicate huge resources to basic verification and validation campaigns. Although a crucial step towards regulatory clearance for medical devices and wider availability for

potential recipiends, such campaigns often fail to meet some of the criteria for publication in scientific journals – one of the key performance indicators in research – such as innovative and original work. Instead, resources are often dedicated to further developing novel technologies or techniques, sometimes resulting in a lag of the required industry-level demonstration of repeatability, performance, safety or durability of the device.

Although quantification is beyond the scope of this thesis, several metrics can be identified, which will influence the financial sustainability of a project and hence the long-term survival of a device. By influencing how many devices can and will be made and sold each year, versus the costs of maintaining the infrastructure required to build them, the following parameters all play an important role in the calculation aiming to determine the chances of success of a venture; it's potential profitability and attractivity to investors.

- Quality of the restored vision
- Number of potential patients
- Device lifetime
- Development costs
- Manufacturing costs
- Complexity and costs of the surgery and medical follow-up
- Risks associated with the surgery
- Risks associated with the implanted device (biocompatibility, stimulation safety)

The population of potential patients – the *market size*, to use economics terminology – is an example where numbers may seem to play in favour of retinal implants. In practice, things are quite different.

Given the prevalence of late stage AMD alone, which was estimated to more than 10 million people in 2020 [17], there is a big market for therapies. Nonetheless, the proportion of potential recipients for retinal implants is much lower. Firstly, even with at advanced stages of AMD, most people retain some form of vision [18]. If the vision may be poor, it often remains above the best acuity ever restored by a retinal implant. In these cases, the benefits of an intervention may not outweigh the risks of the related surgery.

Secondly, therapies aiming to slow-down – or even reverse – degenerative diseases are the subject of active research. For example, neovascular (wet) AMD is one of the two

main forms of the disease. It evolves faster and, in the past, has been responsible for 80% of the AMD-related cases of severe visual impairment and blindness [18]. Fortunately, effective treatments have been developed for wet AMD, which delay the degeneration so that patients may maintain visual acuity above that of legal blindness for the rest of their life [17]. To date, there are no known treatments for the dry form of AMD but considering that, at this stage of development at least, retinal prostheses are most likely to be used in legally blind people, the market size may effectively be reduced to approximately 2 million people worldwide. Furthermore, given the high cost of retinal implants, such devices are likely to be available primarily in developed countries, hence further reducing the market size.

Finally, the market is shared between several vision restoration strategies; some of them already in clinical trials, such as electrical stimulation of the visual cortex [19], or optogenetics [20], where cells that are not naturally sensitive to light are "taught" to become photosensitive to replace lost photoreceptors.

To summarise, the history of retinal prostheses has seen enormous achievements represented by the development and clinical use of devices which often provided patients with the first glimpses of their surroundings in many years. Nonetheless, the restored vision provided by retinal implants remains relatively underwhelming and is characterised as "ultra-low vision" [21]. Additionally, the devices are costly to develop, manufacture, trial, and commercialise[1], while the population of potential recipients is small.

1.2 Way forward for retinal implants

Given the seemingly discouraging observations above, one might rightfully wonder why retinal prostheses are still being developed and doctoral dissertations dedicated to them. The answer lies somewhere between the tales of the immense success of cochlear implants, which use the same principle of electrical stimulation and are providing a sense

[1] For example, the Argus II (Second Sight Medical Products, Inc., 12744 San Fernando Road Suite, 400 Sylmar, CA 91342 USA) costs $115,000 to $150,000 (U.S. dollars) excluding the costs of surgery, postoperative follow-up and treatments, and training to use the prosthesis. (Rohan Bajaj, G.D., James T. Handa, Adrienne W. Scott. *Retinal Implants for RP: An Update on Argus II and Others*. 2019 [cited 2022 09.01]; Available from: https://www.aao.org/eyenet/article/retinal-implants-for-rp.)

of hearing to more than 700'000 people around the world [22] and the trust that we are yet to achieve the full potential of retinal implants for the people who could benefit from them. It is worth noting that despite the relatively low restored visual acuity and high costs of the device and associated interventions, a study found the Argus II (Second Sight Medical Products, Inc., 12744 San Fernando Road Suite, 400 Sylmar, CA 91342 USA) to be cost-effective compared to standard care for RP patients [23]. Any further improvements of the restored vision will be a step in the right direction and therefore academic research activities on the topic are needed and justified.

To maximise the chances of having a positive impact on the life of even a single visually-impaired person; on the path to further develop a retinal prosthesis and bringing it to the clinic, it is crucial to carefully consider the many points listed above and to focus our work not only on the concept of the device and the questions associated with the pursuit of vision restoration, but also on the context in which it will have to fit. That is one in which the regulatory landscape is merciless – even if righteous – and where medical, scientific, ethical, and financial aspects merge into one intricate labyrinth. In particular, the short, and medium-term use of the devices as research platforms, most likely driven by organisations with a scientific rather than industrial and financial focus, should be considered when planning their future.

In this context, the intention of this dissertation is to focus on the primary concern of any modern medical device: *safety and efficacy*; and propose approaches to gather satisfactory evidence for the purpose of the Phoenix^{99} being granted approval for clinical trials in a research environment, hopefully opening doors towards a wider use of the device outside the research world.

1.3 Risks and benefits in clinical research

Research should be ethical, or as per definition 3 of the Merriam-Webster dictionary, research should "follow accepted rules of behaviour"; "research should be morally right and good" [24].

In 2000, Emanuel, Wendler and Grady proposed seven requirements which must be fulfilled so that clinical research can be considered ethical:

- Value – enhancements of health or knowledge must be derived from the research
- Scientific validity – the research must be methodologically rigorous

- Fair subject selection – scientific objectives, not vulnerability or privilege, and the potential for and distribution of risks and benefits, should determine communities selected as study sites and the inclusion criteria for individual subjects
- *Favorable risk-benefit ratio – within the context of standard clinical practice and the research protocol, risks must be minimized, potential benefits enhanced, and the potential benefits to individuals and knowledge gained for society must outweigh the risks*
- Independent review – unaffiliated individuals must review the research and approve, amend, or terminate it
- Informed consent – individuals should be informed about the research and provide their voluntary consent
- Respect for enrolled subjects – subjects should have their privacy protected, the opportunity to withdraw, and their well-being monitored. [25]

While each of the requirements should be subject of careful consideration and planning as projects move forward towards clinical trials, it is the concept of *device and stimulation safety evaluation* for the purpose of demonstrating a *favourable risk-benefit ratio* that will be the centre of attention in the present dissertation.

According to Emanuel et al. "the potential benefits to individuals and knowledge gained for society must outweigh the risks" [25]. While in some cases, one may be able to quantify the risks and benefits, this definition remains profoundly subjective. Nevertheless, the terminology emphasizes the need to develop a deep understanding of the potential benefits *and limitations* of the research, as well as an intimate knowledge of all risks.

At this stage, it is interesting to consider the somewhat subtle differences between two apparently related requirements in the list above. In the case of visual prostheses for the blind, such as retinal implants, the "value" of the research is straightforward. The trial of a device designed and built for the purpose of restoring vision will either enhance the health and quality of life of the recipients, or it will demonstrate the limitations of the implant, thus improving the knowledge and allowing progress towards improved, functional devices. On the other hand, the potential "benefits" of the intervention relate rather to the quality and functionality of the restored vision for the recipients.

As such, the value of retinal implant research appears rather immovable; the first people to consider this approach may have used very similar wording if tasked to define its value. The understanding of the intervention's potential benefits, though, has evolved with each experiment that was performed and each piece of evidence acquired. After more than 15 years of clinical trials with retinal prostheses, it has become clear that the current strategies used in electrical stimulators are unlikely to restore high acuity vision with natural temporal characteristics. Instead, they provide a sense of vision that "is certainly distinct from natural perception and requires rehabilitative training and extensive practice to optimise outcomes", as described by Ayton et al. [13].

Reflecting on the concept of "favourable risk-benefit ratio", it follows that each prosthesis approaching clinical trials should undergo an objective assessment of its potential benefits, acknowledging the limitations and carefully considering the specific design features and technological advances of the proposed device. In other words, new devices and concepts should specifically tackle the limitations highlighted in previous research so that their potential added benefits justify *any* risk for the recipients. Meanwhile, "risks must be minimized" [25], particularly so as to ensure that the benefits – which may be limited – outweigh them.

The Phoenix^{99} implements novel and promising stimulation strategies, which may present increased benefits to recipients. It is also built using only materials with a proven track-record in biocompatibility that are sterilizable, the risk of adverse events such as infection or severe immune responses are minimised. As such the device is in a favourable position to demonstrate a positive risk-benefit ratio. While risks can be managed and minimised through careful design and choice of materials, testing remains the best evidence that the implemented measures are efficacious.

1.4 Preclinical testing

Beyond bench testing on which we will elaborate in Chapter 7, *in vivo* trials in animal models are often the last and most important steps ahead of a clinical application of an implantable device.

To demonstrate the readiness of the Phoenix^{99} with regards to safety, two major trials are required. The first one, which will be the focus of Chapter 3, is the demonstration of the biocompatibility and stability of the device, as well as the safety and efficacy of the surgical procedure used to position the implant.

The second will be the long-term safety study of the novel stimulation paradigms developed to enhance the benefits of the retinal prosthesis. To ensure that the results of this complex, yet crucial experiment will be truly representative of a future clinical application, it is worth dwelling on some its parameters and challenges.

1.5 Neither too much, nor too little

The effects of retinal stimulation, such as the evocation of visual percepts or potential tissue damage, are strongly dependant on the electrical stimulation parameters, including the current amplitude (I) [26], the duration of the pulses (PW) [27], the waveform [28] and frequency [29] of the stimuli. The safety and efficacy of the stimulation also depend on the material and surface area (A) of the electrodes. The surface charge density (σ) at the electrode is a commonly accepted – even if somewhat rough – indicator of stimulation safety [30]. This metric, which is also related to the efficacy of the stimulation [31], combines some of the main stimulation parameters as shown in Equation (1).

$$\sigma = \frac{I \cdot PW}{A} \quad \textbf{(1)}$$

Stimulation at high charge density can cause damage within minutes [32-34] or over time [30] while stimulation with lower charges is considered safe [30, 35] but may not reliably elicit percepts [36-38].

Several preclinical studies for electrical stimulation of the retina have been reported [33, 35, 39-44] but there is no consensus with regards to the chosen stimulation parameters such as the charge density. As an example of the complexity of performing representative safety testing of implants, one preclinical study used a maximum charge density of 77 $\mu C/cm^2$ to demonstrate the safety of the stimulation [35]. The successful study was then used as evidence of safety to progress towards clinical trials. However, during the clinical testing, the 'safe charge injection limit' had to be redefined using a theoretical model of safety as justification [45] because the 77 $\mu C/cm^2$ tested in animals weren't sufficient to elicit percepts. In some patients, the thresholds were even very close to the safe injection limit as given by the model (237 $\mu C/cm^2$) [45]. Despite the discrepancy between the parameters used in the preclinical experiments and the clinical trials, it is noteworthy that the electrode array and stimulation were well tolerated in humans [45].

Effectively, because of the complexity of the task to perform representative preclinical testing, the first studies in humans with a specific device generally have safety evaluation as primary outcome [46-48]. Nonetheless, the researchers shall always do their best to obtain the most representative evidence of safety during the preclinical phase; should it be only to be better prepared for a possible "industrial" evolution of the device which may follow successful clinical trials.

For the purpose of obtaining market approval in the United-States of America, the Food and Drug Administration specifies that non-clinical testing must be performed in such manner as to represent clinically relevant 'worst case' scenarios[2] [49]. In the case of retinal stimulation, a clinically relevant worst case would be the most damaging stimulus that may ever be used clinically. Establishing with certainty what this stimulus probably is as complex as it is important.

Indeed, if a safety study was performed with stimulation parameters that are too favourable, potential risks may be overlooked. On the other hand, if a study is performed with parameters that are too disadvantageous, a device or stimulation strategy may be falsely deemed unsafe. To study the safety of stimulation paradigms, researchers should therefore aim to test their chronic effects with stimulation parameters that are relevant with regards to eliciting percepts[3]. As challenging as this may be, some opportunities

[2] In the USA alone, multiple paths to market exist and there may be exceptions where worst-case testing is not a *sine qua non*.

[3] Systematically testing a wide range of stimulation amplitudes, or injected charge densities, should provide information with regards to a 'safety threshold' above which chronic stimulation will most likely cause irreversible damage. This threshold could be used to define what parameters are acceptable for clinical use. Nonetheless, because of the gradual appearance of stimulation-related damage with increasing charge densities, it is unlikely to yield decisive threshold value, leaving researchers to make arbitrary decisions with regards to what can be defined as 'safe'. Such systematic testing is also likely to require very large cohorts. Finally, it would not ensure that the safety threshold lies in a domain where the stimulus is likely to elicit percepts. This approach may therefore be complementary to the one presented in this dissertation by jointly developing an understanding of the relationship between stimulation parameters and damage, as well as the perceptual thresholds. Nayagam et al. have reported interesting development work to assess the "the safety limits of chronic electrical stimulation of the retina". (Nayagam, D.A.X., et al., *A Pre-clinical Model for Safe Retinal Stimulation*. Investigative Ophthalmology & Visual Science, 2017. 58(8): p. 4204-4204.)

exist, including examples to take from the retinal prostheses' close "relative": the cochlear implant.

1.6 Getting feedback

Hearing tests are performed daily and are a very powerful tool to evaluate the sensitivity of a subjects hearing. During the test, the individual sits in a sound-treated room and is asked to signal whenever a sound is heard, while tones of varying frequencies and volume are delivered to one ear at a time. From this example, it is obvious that certain conditions must be met to perform this test. Amongst others, the subject must be awake, understand the task they need to perform, and be able to provide feedback.

Because of these requirements, the test typically can't be used to detect hearing loss in newborns and young children. For this population, other solutions must be found, such as recording the electrical response from the brainstem. Although these tests are very effective to detect severe hearing loss in newborns [50], the level of details that can be obtained, for example with regards to sensitivity at various frequencies is not comparable to an audiometry test performed in a cooperating subject.

In people with severe hearing impairment, cochlear implants that deliver electrical stimulation to the auditory nerve fibres can be used to provide a useful sense of hearing [51] and even support language development for children with congenital hearing loss [52]. Like newborns during hearing tests, people under general anaesthesia during the implantation surgery of a cochlear device are unable to provide feedback. Intraoperative information on device functionality, including whether the recipient is likely to perceive sounds is nonetheless very valuable as it can allow immediate action in case of issues and avoid multiple surgeries.

To overcome this issue, prosthetic hearing researchers and manufacturers have developed techniques to record the response from the auditory nerve fibres, so-called electrically evoked compound action potentials (ECAP), from electrodes adjacent to the stimulation site [53]. The ECAP recording can be used to check the implant's ability to elicit a neural response, ensure adequate electrode position and may even help with initial implant tuning [54, 55], where the adequate stimulation parameters are determined for each patient.

In the field of vision prosthesis, this type of technology is yet to be implemented. To the best of the author's knowledge, there have been no reports of such measurements even

being attempted *in vivo*. As a result, researchers aiming to study electrical stimulation of the retina to restore vision face challenges when gathering information about the response to the delivered stimuli.

When visual prostheses are implanted in adult human subjects, and when they are switched on when the patient is awake, the situation can be compared to the ideal example of a hearing test in a cooperating adult. The researchers can use the device to deliver a variety of stimuli and receive detailed feedback about the sensations caused [36-38]. They can then use this information to refine the stimulation and tune it to for the recipient. Note that given the complexity of the elicited percepts, such as spatial and temporal distortion [56], this is not always a straightforward process and can be time-consuming for arrays with a multitude of electrodes. Nonetheless, the verbal feedback is immensely useful.

On the path which would have led to a retinal implant, or a novel stimulation paradigm, being tested in a human patient, animal models will most certainly have been used to study them. With regards to their ability to understand the test and provide feedback, animals would have to be compared to newborn babies in the hearing test example. Even in non-human primates, reliably defining something as critical as the lowest stimulation amplitude which causes a percept – the perceptual threshold – is arduous. It requires creativity from the researchers and intense training with the animals. For example, Prévot et al. trained macaques to perform saccades in the direction of a peripheral visual stimulus. After implantation, the saccade detection task was repeated during electrical stimulation at different powers and the perceptual threshold was inferred from the rate of successful saccades [57].

Even in this model, where the animals can be trained to perform complex tasks, and with this elaborate methodology, the accuracy with which of the perceptual threshold can be *estimated* is unknown. In another study in cats, stimuli causing a “distinct attending motion of the head” were considered to have cause a “perceptual response” [35]. The absence of verbal reports is indeed one of the most important limitations of animal models in the field of visual prostheses, where they are often used for safety testing only [16].

Another approach is commonly used to gather further insights into the effects of stimulation without verbal feedback, which is comparable to the technique used for hearing loss screening in preverbal children: Recording the cortical response to electrical stimulation of the retina.

Multichannel electrophysiology systems and penetrating multielectrode arrays with high electrode count and density, such as the 96-probe, 4x4 mm^2 Utah array (BlackRock Neurotech, Salt Lake City, UT, USA) have enabled researchers to capture, qualify and quantify the electrically evoked cortical response to retinal stimulation in the primary visual cortex of animals [58-60] with a high level of refinement and sensitivity. This technique was used successfully to compare stimulation paradigms with different return configurations [31, 60, 61], evaluate the effects of spatiotemporal interference from multiple electrodes [62] or investigate "virtual electrodes" where the combination of stimulation from multiple sites produce patterns with unique spatial characteristics [63].

Although beneficial in the development of innovative stimulation techniques, the approach presents several limitations. Firstly, a craniotomy must be performed to access the cortex. This intervention is therefore often performed during terminal, acute experiments, as opposed to experiments where animals are recovered and followed over a longer term. Secondly, they rely on the recording electrode array being located very precisely in the cortical area primarily activated by the retinal electrodes under investigation. A recording array located in an area distant from this target may produce weak signals, if any activity can be recorded at all. Finally, the recordings may provide information on the stimulus amplitude which will cause measurable cortical activation, but any correlation between the cortical thresholds and the true perceptual thresholds must be inferred.

The cortex shows a gradual increase in response amplitude, often quantified by the number of neuronal spikes, with increasing retinal stimulation current amplitude [31], which then saturates at high stimulation amplitude. The lower threshold, at which any response is detected, and which would most likely be closest to the perceptual threshold, is therefore difficult to identify. To overcome this issue, researchers often use an arbitrary threshold definition known as the 'P50', or the stimulation threshold at which the cortical response reaches 50% of its saturation value [61].

Although the P50 is a useful tool to compare stimulation paradigms and learn about the stimulation amplitude required to elicit a similar response, it doesn't provide detailed information about what happens at the interface between the device and the neural system: the retina.

1.7 Listen to the retina

Between a stimulus delivered close to the retina and its interpretation by the brain, a complex network of neurons is involved along the visual pathway, which processes the information [56]. Relying solely on the measurable cortical activity triggered by retinal stimulation to study the effects of the stimulation could be compared to a chef attempting to determine the ingredients of recipes only by looking at the expression of someone trying them. While the chef may be able to guess which dish is very sour and which one might be sweet, under no circumstances will an exhaustive list of ingredients result from the exercise.

The ideal scenario would obviously be where the chef is invited into the kitchen as the dishes are prepared but a lot of useful information may already be gathered by listening to a foodie describe the tasting experience. Recording the response from the retinal neurons during stimulation may be compared to this last scenario, with regards to the ability to provide more detailed insights into the perception. As an attempt to evaluate the true perceptual thresholds[4], which could be used to refine the parameters of chronic stimulation studies, retinal recordings will be explored experimentally in Chapter 5.

As previously mentioned, modern cochlear implants already implement a comparable technology, which allows for information to be gathered directly from the stimulated nerve bundles. Thanks to the very large number of recipients, the researchers and manufacturers have access to an immense source of data, including patient feedback, that can be used to develop new techniques [53] or deepen our understanding of the stimulation.

In the field of visual prostheses, although electrophysiology experiments on explanted retinas are quite common [64, 65], there have been no reports of this technology being

[4] Stronks, Barry and Dagnelie measured electrically evoked potentials with electrodes placed on the scalp of humans implanted with the Argus II system. They concluded that it "yielded fairly accurate predictions" of the perceptual thresholds. Nevertheless, the recordings exhibited a low signal to noise ratio and were strongly influenced by the location of the retinal stimulation. Additionally, the subjects were awake and could describe the elicited sensations. Because of the effects of anaesthesia and lack of verbal feedback, the correlation between the cortical response and the percepts must still be inferred in anaesthetised animals. (Stronks, H.C., M.P. Barry, and G. Dagnelie, *Electrically elicited visual evoked potentials in Argus II retinal implant wearers.* Invest Ophthalmol Vis Sci, 2013. **54**(6): p. 3891-901)

tested *in vivo*, let alone in humans. At this stage, as retinal recordings have not yet been implemented in subjects with the ability to provide constructive feedback, it is necessary to determine the type of relationship that exists between the retinal response and the more commonly recorded cortical response.

Due to the invasive nature of the experiments, cortical recordings are most often performed in anaesthetised animals. Unfortunately, anaesthetic drugs are known to modify, depress or even suppress cortical activity [66-68]. To minimise the anaesthesia-related disruption of the cortical response during electrophysiology experiments of the visual system, careful consideration of the chosen anaesthetic regime is necessary. In collaboration with veterinary anaesthetists and veterinarians, a framework decision making tool was developed to guide the selection of the anaesthetic protocols for this type of experiments which will be detailed in Chapter 4. A refined technique aimed at providing physiologically stable animals with minimal cortical depression and selected using the tool was used successfully during retinal-cortical recording sessions in sheep.

Even in optimal conditions such as with minimal effects of anaesthesia on the results, cortical electrophysiology experiments are long, complex, and costly. Most importantly, they use an immensely precious resource: the life of an animal for the progress of science. As such, we have a moral obligation to ensure that the outcomes of animal trials are maximized.

1.8 The role of simulations

Computer simulations are an extremely powerful tool to test new ideas, or new designs. They can also be used to push the limits of what can be done or has been done experimentally. Using empirical data, computer models can be calibrated to represent as closely as possible real-life conditions. From there, new conditions can be tested with an increased confidence in the applicability of the results, ultimately minimising risks, increasing the potential benefits, and therefore improving the risk-benefit ratio.

As we refine the methods to determine adequate stimulation parameters for safety studies – clinically relevant worst-cases – we seek to design tools to demonstrate their validity and serve in the identification of worst-case parameters for other stimulation paradigms without the need for additional animal testing. An approach to computer model calibration based on existing empirical data will be presented in Chapter 6, where we successfully calibrated a computational model designed to predict the effects of parallel stimulation.

With a refined understanding of the conditions required for clinically relevant stimulation safety studies of promising stimulation paradigms, the researchers will then be ready to embark for the last leg of the preclinical journey: performing the long-term stimulation safety in sheep, for which a concept will be presented in Chapter 8.

1.9 Step by step

Acquiring definitive evidence of a novel retinal implant's safety and efficacy is as challenging as it is necessary for it to progress towards the clinic where it will be facing its ultimate test. Gathering this evidence requires numerous parameters to be carefully considered, their effects analysed and interpreted. From the biocompatibility of the device (Chapter 3, published in *Biomaterials* [1]) to novel ways to record the body's response to electrical stimulation (Chapter 5), via the optimisation of the anaesthetic protocols to ensure that electrophysiology experiments provide unbiased results (Chapter 4), the present dissertation describes some of the concrete steps that are being taken to bring the Phoenix^{99} Bionic Eye at the door of clinical trials.

With a focus on the clinical relevance of the stimulation parameters used for testing, we endeavour to get as close to the perceptual thresholds as possible, using this important transition from "nothing to something" as a target to guide the research efforts. On the way, we will also discuss how empirical cortical responses can be used to build reliable computer simulations (Chapter 6), review some of the device lifetime requirements for a prosthesis (Chapter 7), and make conceptual proposals of chronic trials in animals and a first acute test in humans (Chapter 8). But first, to better understand the potential benefits of the Phoenix^{99} to which all identified risks will be compared on the road to clinical trials, we will look at the current landscape of vision restoration technologies and the preclinical trials that led to some of the devices being applied clinically.

2 VISUAL PROSTHESES

REVIEW OF THE LITERATURE

2.1 Introduction

In performing everyday tasks, humans and a large majority of other animals rely on a flow of information from the outside world transmitted through the eyes and to the brain in the form of visual percepts. Vision allows us to interpret our environment, navigate it and react to it appropriately.

2.1.1 Vision loss and blindness

In humans, visual impairment can be a debilitating condition which increases the risks of depression and anxiety, as well as it reduces the general well-being and social functioning [69, 70]. Vision loss is also associated with high financial load. In Australia alone, direct and indirect costs of vision loss have been evaluated at about AUD 5 billion (USD 3.56 billion) [71].

This number includes not only the costs of medical care, but also considers the value which is not produced because of the lower employment rate and increased mortality of the visually impaired, as well as the "lost earnings of carers during their caring activities" [71]. Vision loss can be caused by a wide range of conditions such as uncorrected refractive errors, genetic disorders, tumours, or accidents. Changes in vision can be sudden or spread over a long period and the age at which a condition appears is also strongly variable. The elderly population is nevertheless particularly affected by visual impairment with as much as 17% of the population between the age of 65 and 74 and 26% of the population above the age of 75 self-reporting as visually impaired [72].

Worldwide, the most common causes of visual impairment are cataract and uncorrected refractive errors with cataract being the main cause of blindness (visual acuity < 3/60) while uncorrected refractive errors cause the majority of moderate or severe vision impairment (visual acuity < 6/18 but ≥ 3/60) [73]. Glaucoma, age-related macular degeneration (AMD) and diabetic retinopathy (DR) are also amongst the main causes of vision loss [73].

In some cases, prevention and treatments such as cataract surgery are efficacious to avoid blindness. Other disorders are more complex to prevent or cure. Retinitis pigmentosa (RP), a degeneration of the photoreceptors which causes gradual loss of vision starting in the peripheral visual field, is an inherited disease. Genetic mutations in at least 45 genes have been identified to cause the disease [5]. The variety of causes for such a disease complexify the quest for a cure. Age-related macular degeneration (AMD) is a degenerative disease that primarily touches the central, high-acuity visual field. Further causes of blindness are accidents or tumours that affect part of the visual path. The list of causes for visual impairment is long, and each pathology not only acts on a specific region of the visual path, but it may also manifest distinct symptoms and leave behind a specific type of residual vision. Accordingly, the development of any therapy must consider this large number of factors to maximize the benefits for patients.

2.1.2 Vision and visual processing

To make useful information out of the data carried by the light reflected or emitted by everything that surrounds us, it must go through a formidable amount of processing. It begins when photons, appropriately focused on the retina by the lens, hit the light sensitive cells: the photoreceptors.

The photoreceptors are located at the back of the retina. They synapse with the second layer of neural tissue which in turn transmit information to the retinal ganglion cells (RGC) [74]. More accurately, before it exits the eye via the axons of the RGCs, the image was already processed by a complex system of excitatory and inhibitory feedback and feedforward network involving the horizontal cells at the interface between the photoreceptors and the bipolar cells, as well as the amacrine cells at the junction between the bipolar cells and RGCs [56, 74] (Figure 2-1).

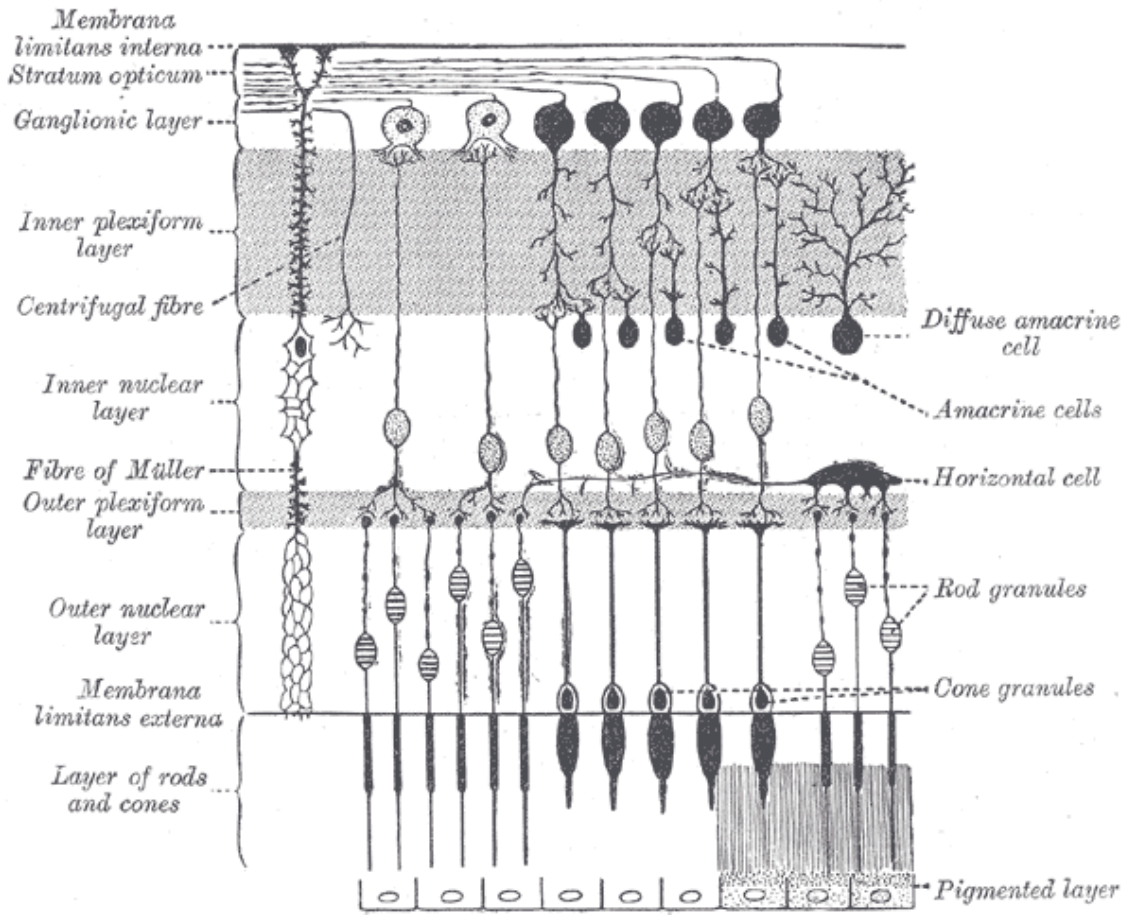

Figure 2-1 Anatomy of the retina. The neurons involved in the detection of light (rods and cones), as well as the processing and transmission of the visual information towards the brain (bipolar cells – oval shaped cells in the inner nuclear layer, horizontal cells, amacrine cells and RGCs) are shown in this engraving. From the 1918 edition of Gray's Anatomy of the human body (Figure 882, public domain) [75].

The axons of the RGCs exit the eyeball through the optic disc and form a bundle – the optic nerve - which transmits the visual information to the lateral geniculate nucleus

(LGN)[5], where the RGCs synapse with further neurons to bring impulses to the visual cortex. In the striate cortex, the information is further transmitted to deeper cortical layers until it can finally be combined, through the complex wiring of the brain, into outputs such as movement [76].

In the visually impaired, the unused neural network (beyond the layer causing the disability) can be recruited by other functions. The visual cortex, for example, has been shown to play a role in tactile and auditory functions as well as language or mathematics in people who become blind early in life [76]. Merabet et al. demonstrated the plasticity of the occipital cortex in normally sighted individuals that are temporarily subject to visual deprivation (blindfolded for five days). Using repetitive transcranial magnetic stimulation (rTMS) they could "transiently disrupt the function of the occipital cortex". It resulted in an increased error rate in the blindfold group when reading Braille while no difference was observed in the control group under the same condition. This experiment demonstrated that the occipital cortex had been recruited for Braille reading in the subjects with no visual inputs but not in the subjects who were allowed to use their eyes [77].

Photoreceptor degeneration also has consequences on the neural network in the retina. The death of the photoreceptors is followed by the death, migration, or rewiring of the other retinal neural cells such as the bipolar, horizontal, amacrine cells and RGCs [4]. This effect could have major effects on any strategy which uses the surviving neural network to restore sight as it may not only be degenerate and compute incomprehensible information, it may also lose the ability to transmit signals to the brain altogether [4]. Luckily, a significant portion of the RGC population has been shown to survive the sensory deprivation secondary to photoreceptor death and retinal remodelling [3]. The

[5] For completeness, besides the LGN, RGCs also project to three further brain nuclei which aren't considered part of the visual pathway: the superior colliculus, the hypothalamus, and the pretectum of the midbrain, where the visual inputs influence the control of the eye movements, pupillary reflexes, diurnal rhythms and hormonal changes. (Dragoi, V., *Visual Processing: Cortical Pathways*, in Neuroscience Online: An Electronic Textbook for the Neurosciences, J.H. Byrne, Editor. 2020, Department of Neurobiology and Anatomy McGovern Medical School at The University of Texas Health Science Center: Houston)

availability of RGCs to transmit signals to deeper layers of the brain is crucial to some vision restoration strategies.

The reorganization and degeneration that take place in the visual pathway due to blindness must therefore be considered during the development and testing of visual prosthesis. For example, the use of sighted animals during in-vivo safety and efficacy testing of a prosthesis may introduce biases. On one hand, the healthy cells may participate in the responses in a sighted subject, while they may not in a model of retinal degeneration [58]. On the other hand, while the presence of an electrode array may cause disturbances to functional, “healthy” retinas, the relevance of the device-related changes must be determined in a context where the corresponding cells would be already degenerate in a blind subject [1]. This adds another layer of complexity in an equation with an already high number of variables.

2.1.3 Vision preserving therapies

Many different strategies are being used or investigated to protect vision in patients with degenerative diseases and restore vision in patients that have lost it. While this review will focus mainly on the restorative part of the therapeutic spectrum, it is to be noted that the development of preventive therapies may one day render visual prosthetics obsolete if degenerations can be stopped at a sufficiently early stage. It is interesting to note that retinal prostheses may also provide a form of neuroprotection which slows down the retinal degeneration. In some cases, implantation of subretinal devices have been shown to be linked to improved vision due to neurotrophic effects only, even when the device wasn’t able to deliver sufficiently high currents to elicit a neural response [78, 79].

Several encouraging examples exist, where vision is effectively protected in subgroups of patients with specific affections. Considering the example of age-related macular degeneration, the neovascular or ’wet’ subtype of AMD was known to cause 80% of the cases of severe visual impairment [18]. Ranibizumab (Lucentis R , Genentech/Novartis), bevacizumab (Avastin R , Genentech/Roche) or aflibercept (Eylea R , Bayer/Regeneron) are effective in controlling the abnormal formation of blood vessels in the choroid, which characterizes wet-AMD. These treatments prevent further degeneration and can even improve the visual acuity of patients suffering from wet- AMD [80-82].

Gene therapy as well can be used to stop retinal degeneration. The principle is to replace missing/mutated genes directly in the cells of the patient using for example adenoviral factors. A gene therapy protocol has already been clinically shown to preserve vision in

patients suffering from Leber's Congenital Amaurosis (LCA, a subtype of RP) and is approved by the American Food and Drug Administration (FDA) [83].

While this disease is rare and the treatment is extremely specific, this is an encouraging result and it demonstrates that the approach, which may be applicable to other genetic diseases, is viable. That is, provided that the required genes are sufficiently small to "fit" in an available gene delivery system.[6]

2.1.4 Vision restoring therapies

With the aim of providing a useful sense of vision to those who have lost it, researchers around the world have taken a wide variety of approaches. Some concepts are still in their early days while others have already been tested clinically over several years [84], or even granted market approval in some jurisdictions.

Ideally, vision restoration therapies which propose to replace the function of neural cells should account for the way the healthy cells were connected and what kind of processing took place at the site of the originally affected cells. Between all the different layers, the visual information is processed, data is analysed, filtered, and combined [74]. The brain is used to getting the right type of information from the right cells [56]. For the brain to understand information that is received, the natural neural paths should ideally be respected. Otherwise, information can be hard or even impossible to interpret. For example, some groups of cells react differently to the presence of light. Some are activated in its presence (ON-cells), while some are inhibited (OFF-cells). If neighbouring ON and OFF cells are activated simultaneously by a prosthesis, it could be that the conflicting information will "cancel out" before it reaches the brain, making it "disappear" [56]. Furthermore, the timing and speed of the stimulation also play an important role in the intelligibility of the restored sight [56].

---

[6] Interestingly, the Covid-19 pandemic may play a positive role in the development of gene therapies as lipid nanoparticles, which could theoretically contain genes of unlimited lengths (Ehsan and Mann, 2000), were successfully used globally for the first time (https://www.cas.org/resource/blog/understanding-nanotechnology-covid-19-vaccines).

- Ehsan, A. and M.J. Mann, *Antisense and gene therapy to prevent restenosis*. Vasc Med, 2000. 5(2): p. 103-14.

Amongst other, notable examples of vision restoration therapies that are being studied are to use stem cells to replace lost photoreceptors [85], or the use of gene therapy techniques to make parts of the surviving neural network photosensitive. Optogenetics aims at getting neurons, which are not naturally sensitive to light, to express photosensitive proteins on their surface which then either increase neuron firing rates or inhibit cell action potentials when illuminated. The idea with this technique is to replace the lost function at a different neuronal level such as in the RGC layer, albeit without the benefits of the retinal neural network [86].

Particularly relevant to this dissertation is the fact that neurons can be activated by electrical fields. Along the visual path, several areas have the potential to create percepts in the blind patient when subjected to electrical stimulation, depending on the pathology that caused the impairment. Stimulation of the visual cortex [87-90], LGN [91, 92], the optic nerve [93-97] or the retina [13, 45, 98, 99] have been explored.

In the retina itself, four sites for stimulation have been identified: epiretinal, subretinal, suprachoroidal and episcleral [13]. All those sites, including the optic nerve, the LGN or visual cortex differ in the type of cells (neurons) that are activated, the distance between the stimulation electrodes and the cells, the ease of surgical access and the type of tissue between the electrodes and the cells.

To provide visual sensations that are useful to the patient and aid in navigation, orientation or recognition, visual prosthesis should provide large numbers of individual visual percepts (phosphenes). In turn, the phosphenes should be such that they can be effectively combined in a way that the brain interprets as images, or scenes. To achieve this feat, many factors must be accounted for, including the natural image processing provided by the neural network between the eyes and the brain, and the spatiotemporal mapping of 2-dimensional images that represent our moving environment [56]. Retinal stimulation is particularly interesting because the position of a stimulus in the retina can closely correlate to the position of the perception (retinotopic mapping) [100-102]. This mapping is, for example, difficult to maintain in the optic nerve where all axons exiting the eye are bundled together, thus making the required encoding and decoding of stimulated percepts more complex.

Combining this property with the relative ease of surgical access of the eye, compared to the visual cortex for example, several groups have undertaken to develop retinal

stimulators including some that have obtained regulatory clearance in several countries [84, 103, 104] and have been used in hundreds of patients around the world [13].

2.1.5 The Phoenix^{99} Bionic Eye

The clinical experience accumulated in the field of electrical visual prostheses over the last three decades has demonstrated several shortcomings of the existing devices. Implant survival in the harsh conditions of the body and over extended durations [105], ease of surgical approach [106], number of individually elicited percepts or the capacity to combine individual phosphenes into meaningful visual information are but a fraction of the properties that an ideal visual prosthesis for the blind should possess . The Phoenix^{99} bionic eye effectively combines years of research in the fields of electrical stimulation of the retina and implantable electronics into a fully implantable and highly customizable device. This review aims at presenting the different visual prostheses that have reached the clinic in terms of stimulation strategies and resulting visual gain for the patients. The key technological features of the Phoenix^{99}, including the suprachoroidal implantation site, the retinal recording capabilities, and built-in current steering, are then reviewed to highlight the potential benefits of the prosthesis, and to serve in the risk-benefit ratio analysis which will be required to justify a clinical trial of the device. Finally, the preclinical studies which were used to demonstrate the safety of the clinically tested prostheses are reviewed.

2.2 Clinical landscape of retinal implants

Many research groups around the world have developed different approaches to deliver electrical stimulation to the retina, with the goal of providing useful vision to the profoundly visually impaired. The sites of stimulation around the retina vary, as well as the stimulation strategies and the electrodes that deliver the stimuli. Electrode material, number and density, as well as current return path and array dimensions strongly influence the theoretical best restored visual performance.

2.2.1 Argus II

The Argus II (Second Sight Medical Products) is a visual prosthesis based on an epiretinal electrode array connected to an electronics case located on the globe. The implant receives data and power through a receiving antenna wrapped around the eye from an external unit. The external unit includes a goggles-mounted camera, a video processing unit and power-pack, and a transmitting antenna [107].

During implantation, a vitrectomy (removal of the vitreous body from the posterior chamber of the eye) is performed to allow positioning of the electrode array directly against the retina where it is fixed using a retinal tack [107].

2.2.1.1 Clinical availability

The Argus II implant was the first bionic eye to receive the CE (European conformity) mark (2011) and to be approved for implantation in humans by the FDA (2013) [108]. It has since been implanted in more than 350 people world-wide [109] but is no longer available since 2019.

2.2.1.2 Type of stimulation and electrode array

The epiretinal array of the Argus II implant features 60 electrodes [107] which deliver biphasic pulses to the surviving neurons of the retina, mostly to the retinal ganglion cells (RGCs). The sclera-attached electronics case plays the role of return electrode in a so-called monopolar stimulus configuration. During monopolar stimulation, the current of each stimulation site is returned to a distant electrode. This configuration is straightforward and yields visual percepts at comparatively low currents [60], but leads to electrical interference when stimulation is delivered from multiple sites simultaneously [10, 31].

2.2.1.3 Restored acuity, functional vision, and safety

The device was used in several small- and large-scale clinical trials. Da Cruz et al. reported the 5-year follow-up of 30 patients implanted with the Argus II bionic eye as part of a long-term 10-year study [84]. To evaluate the performance of the implant, the subjects were asked to perform a set of tasks with the implant ON and OFF. Five years post-implantation, the patients performed better with the system ON than OFF when asked to localize a white square on a black background, determine the direction of motion of a high contrast white bar on a black background.

To determine visual acuity, a square grating visual test was performed and 38.1% of the patients scored 2.9 logarithm of the minimum angle of resolution (logMAR) or better, while none of them scored at least 2.9 logMAR when the system was off. Note that having a visual acuity better than 2.9 logMAR before implantation was an exclusion criterion for the study [98]. Patients also demonstrated better performance at locating and touching a simulated high contrast door on a wall and following a white line on the floor with the system ON than OFF during functional vision tests [84].

In 2012, Humayun et al. reported the interim results of the same study. At that point the best visual acuity measured between all patients was 1.8 logMAR (equivalent to 20/1262) with the implant ON [110], this acuity has been explained by the users effectively using scanning techniques (head movements) to improve acuity provided by the device [111]. Remember here that a person is considered 'legally blind' if the visual acuity is below 3/60 [15]. Also note that some patients had as few as 46 electrodes used for stimulation (range: 46 to 60, median: 55). A strict safety policy was applied with regards to charge injection and electrode impedance, which led to multiple electrodes being disabled [110].

Using observer-rated evaluation of functional low-vision, the device was found to provide significant advantages to complete vision-related tasks after a mean follow-up of 36 months [112].

In the five years follow-up, 3 devices were partially, or fully explanted following serious adverse events (SAE) and two devices had failed. There was a total of 24 SAEs reported in patients, including conjunctival erosion, ocular hypotony, conjunctival dehiscence and presumed endophthalmitis ("endophthalmitis means bacterial or fungal infection inside the eye involving the vitreous and/or aqueous humors", Durand, 2013 [113]) as most recurrent SAEs. Most patients (60% or 18/30) have not reported any serious adverse events during the first 5 years of the study [84].

Recently, a French team highlighted the "the safety and effectiveness of the Argus II System in a real-world cohort of patients and … its real functional benefit in implanted patients' daily activities" after a two-year postmarket study [114]. Out of eighteen subjects, only two adverse events were reported, which resolved without intervention, namely one case of endophthalmitis and one vitreous haemorrhage.

2.2.2 Alpha-IMS and Alpha-AMS

Retina Implant AG (Reutlingen, Germany) received CE marking for two subretinal implants. The two devices worked according to the same principles, namely a subretinal chip including a large number of microphotodiodes detected ambient light and trigger stimulation on adjacent electrodes. The signal received by ambient light was amplified using power transmitted through the skin by induction. The microphotodiode array, combined with the focussing capabilities of the eye effectively replaced the external camera required, for example, by the Argus II system [104].

Gain and sensitivity of the amplifiers in the silicon chip could be tuned by the user using an external handheld control box to adapt, for example, to light conditions. The properties of single stimulation sites couldn't be fine-tuned to adapt to different threshold values at each electrode [115].

The Alpha AMS was the second device generation and included features to extend the functional lifetime of the implant compared to the first generation (Alpha IMS) [104]. The Alpha AMS device also delivered biphasic stimuli versus the monophasic pulses produced by the Alpha IMS. It included a slightly larger chip with higher electrode count (1600 versus 1500 in the IMS chip) [115]. Further minor changes were also implemented to improve the properties of the implant [116].

The improvements were revealed necessary during a 29-participant clinical trial during which many implants failed as early as 3 to 12 months post implantation [105].

2.2.2.1 Clinical availability

The Alpha IMS and Alpha AMS devices both had received the CE marking. Thanks to the increased reliability and functional lifespan of the AMS, it had supplanted its predecessor on the market and in the clinical trials dedicated to evaluating performance and safety of subretinal prostheses (ClinicalTrials.gov NCT02720640 and NCT01024803) [116]. The company ceased all operations in 2019.

2.2.2.2 Type of stimulation and electrode array

The Alpha AMS device delivered biphasic pulses in the subretinal space with regards to a distant return electrode located in the temple region. The stimuli were delivered in a purely monopolar configuration by 1600 "pixels" measuring 70 × 70 μm² on a 3.2 mm x 4 mm chip [104]. Thanks to the location of the implant in the subretinal space, it was suspected to preferentially elicit responses in the bipolar cells. The bipolar cells are more distal in the visual pathway than the RGCs and electrical stimulation of those cells is suspected to contribute to more natural vision by better utilizing the neuronal image processing capabilities [14].

2.2.2.3 Restored acuity, functional vision, and safety

The best restored acuity ever measured with a retinal prosthesis was provided by the Alpha AMS (6/150) after intensive visual training [14]. Previously, the highest restored acuity had been 20/546 (1.43 logMAR) measured in one patient with the Alpha IMS and one with the Alpha AMS [116, 117]. Nonetheless, visual acuity could nevertheless only

be measured in a minority of participants in clinical trials. The most revealing results from the clinical studies using the Retina AG implants come from tests that represent activities of daily living. Overall, the participants were able to detect and localize objects better with the implant ON than OFF and so was hand-eye coordination, but recognition scores were not significantly different with the implant switched ON or OFF. Motion detection was also a difficult task, probably linked to the low frequency at which the implant works [116].

Out of the 15 patients implanted with the Alpha AMS device as part of two clinical studies, two devices 13/15 did not function properly due to damage to the implant. A total of 8 SAEs were reported in 4 patients, including conjunctival dehiscence in two patients (1 and 3 occurrences) [116].

2.2.3 IRIS II

The Intelligent Retinal Implant System II (IRIS II), manufactured by Pixium Vision S.A. (74 rue du Faubourg Saint-Antoine, 75012 Paris, France), is an epiretinal stimulation device. The implanted device receives data and power from special glasses via infrared and radiofrequency telemetry, respectively. A "neuromorphic image sensor" [103] acquires visual information in a continuous manner, providing information about the intensity as well as the intensity change rate of pixels. A belt-worn image processor then generates commands that are translated into stimulation patterns through 150 electrodes [103].

The most singular feature of the IRIS II is the ability to calibrate each stimulation sites not only based on the individual electrode impedance, but also depending on the type of local natural neuronal processing unit that is being excited. The idea is that using iterative methods, ON/OFF neuronal pathways can be identified and the stimulation patterns adapted to deliver information that can be better interpreted by the brain [118].

2.2.3.1 Clinical availability

The IRIS II system received the CE mark and was available as part of clinical trials. In the most recent report of chronic implantation trials, Muqit et al. have reported the 6 months preliminary results of safety and efficacy analysis of the system as part of a 36-months chronic implantation study (NCT02670980 www.clinicaltrials.gov) [119]. Despite the trials, Pixium Vision discontinued their activities on the IRIS prosthesis to focus on a photovoltaic retinal prosthesis called PRIMA [120] (see 2.2.5).

2.2.3.2 Type of stimulation and electrode array

The IRIS II implant provides epiretinal stimulation using a 150-electrode array to deliver current to the surviving neurons. The currents are delivered in a monopolar configuration between individual electrodes and a distant return electrode [103].

2.2.3.3 Restored acuity, functional vision, and safety

The 6-months preliminary results demonstrated improvements in a high-contrast square localization task and as well as in a direction-of-motion test. The device also restored a measurable visual field in 80% of the participants compared with the baseline of no visual field in all participants. Some improvements were also observed when subjects were asked to recognize objects based on pictures [119].

A total of 17 adverse events were reported including 6 SAEs in 4 patients [119]. In a separate study with an earlier version of the IRIS, the device featuring 49 electrodes was shown to be well tolerated and permitted basic shape recognition in 4 patients [121].

2.2.4 Australian suprachoroidal implants

Australian groups, originally collaborating as part of the Bionic Vision Australia research consortium, have been active in the development of devices designed to elicit visual percepts from the suprachoroidal space. Out of three implant designs, two have been tested in small clinical trials. The third device, the Phoenix^{99} is at the preclinical stage and the focus of this dissertation. As such, its design will be discussed in detail later.

Besides the common implantation site in the suprachoroidal space, all three devices feature platinum electrode arrays, sandwiched between two layers of silicone [122].

In the first device tested in humans, the implant was connected to a belt-worn image processor and stimulation electronics via a percutaneous port located behind the ear and connected to the electrode array via a helical lead wire [45]. The second generation of this implant is fully implantable and combines two distinct current sources to drive 44 electrodes [46]. All devices rely on an external camera and image processor to encode the stimulation patterns [1, 45, 46].

Compared with subretinal and epiretinal implants described above, a vitrectomy isn't required to position a device in the suprachoroidal space. The surgical procedure is therefore simplified [123]. The electrode array is located inside a pocket formed between the choroid and the sclera, providing a stable positioning without the need of retinal tacks or any other intraorbital procedure [123].

2.2.4.1 Clinical availability

A phase I, three-participant clinical study (Clinicaltrials.gov NCT01603576) was described by Ayton et al. in 2014, describing the 12-months post-operative safety and efficacy data [45]. The second-generation device, made by the company Bionic Vision Technologies (Melbourne, Victoria, Australia) has been implanted in four late-stage RP patients as part of a phase II clinical trial (Clinicaltrials.gov NCT03406416) [21, 46]. None of these devices have yet received CE marking or FDA clearance.

2.2.4.2 Type of stimulation and electrode array

During the phase I trial, arrays with 33 platinum electrodes were implanted, including 20 electrodes which could be individually stimulate. The second-generation device features 44 active electrodes. Electrode dimensions varied between studies with the first device including pads with 400 and 600 μm in diameter, versus 1000 μm diameter in the second one [45, 46].

A monopolar configuration was used to deliver charge-balanced biphasic current impulses to the surviving retinal neurons. Two distant electrodes also located in the suprachoroidal space were used as returns. In some cases, ganged electrode pairs were used to stimulate, in order to increase the amount of charge that can safely be delivered and increase the dynamic range available during testing.

2.2.4.3 Restored acuity, functional vision, and safety

During phase I testing, restored visual function was tested using a light localisation task in which the participants are required to identify the orientation of a high contrast wedge of white light on a black screen (task described as part of the Basic Assessment of Light and Motion - BaLM [124]). All patients performed significantly better with the implant ON than OFF. Visual acuity was only measurable in one participant who had a best measured value of 20/4477 (2.35 logMAR) with the implant ON while device OFF acuity was worse than 20/34756 (3.24 logMAR) [45].

The devices were successfully positioned in the suprachoroidal space with no intraoperative adverse events. Device integrity was confirmed, and all electrodes were intact after implantation.

The main reported serious adverse event was an infection around the percutaneous port. In all patients, subretinal and suprachoroidal haemorrhages developed three to four days postoperatively. All resolved without further complications but an unexplained gradual increase in the electrode-retina distance was observed in two (2/3) subjects [45].

Interim results area available for the phase II trial with a 44-channel suprachoroidal implant. Visual acuity was not measured after device fitting. Instead, the clinical outcomes were evaluated using functional testing in a variety of situations, including screen-based assessments, tabletop search tasks and obstacle courses [46]. Additionally, self- and observer-rated assessments were performed to evaluate whether the devices provided useful information in performing daily tasks. Finally, quality of life was assessed using self-reporting questionnaires.

The interim results provide evidence that visual function increases and that everyday activities are made easier with the device on versus device off [21, 46]. Interestingly, the benefits of the device appear to increase during the first six months of use. On the other hand, the self-reported quality of life questionnaires revealed no significant difference between preoperative scores and with the prosthesis.

To date, there have been no reports of severe adverse events during the trial. Like in the phase I trial, two small subretinal haemorrhages were observed postoperatively but resolved within two weeks without intervention. Similar to the phase I trials, an increase in the distance between the electrodes and the retina was observed, yet the rate of increase was slower in the second trial and was not correlated with an increase in perceptual thresholds [45, 46]. It was highlighted that the changes in electrode-retina distance and the change in thresholds in early experiments may have been related to the higher charge densities and stimulation frequencies used [46].

2.2.5 Other noteworthy clinical trials

Other interesting devices are or have been in clinical trials. Recently, Pixium Vision (74 rue du Faubourg Saint-Antoine, 75012 Paris, France) has published a press release with promising 6-months preliminary results from a 5-participant clinical trial of their PRIMA Bionic Vision System, specifically designed for patients with AMD. The 378-electrode subretinal array is well tolerated during chronic implantation. It receives power and data using infrared and has been able to safely restore some level of central light perception while preserving residual peripheral vision. The maximum restored acuity was 20/460 (1.37 logMAR) [125], which is notably amongst the best scores to date.

Endo et al. reported positive outcomes in a one-patient study with a suprachoroidal-transretinal stimulation implant during "targeted movement" tasks using a combination of residual natural vision enhanced by prosthetics [126].

2.3 The Phoenix^{99}

The Phoenix^{99} was developed as part of Bionic Vision Australia in parallel to the implants tested in humans by Ayton et al. [45]. In this device, the electrode array is manufactured using the same materials as for its sibling but includes 98 electrical stimulation sites organized in a hexagonal lattice [127]. The suprachoroidal array is connected to a visual stimulator (VS) secured on the globe via scleral sutures. The VS is connected to a telemetry implant, located behind the ear, via a helical cable. The telemetry implant receives power and data for the stimulation of the retina using wireless radiofrequency (RF) inductive communication, making the device fully implantable [128].

Image acquisition, processing and encoding into electrical stimulation are performed by an external camera and processor. The implanted electronics are highly versatile in the type of stimulation patterns they can deliver. Information delivery to the neural pathways is therefore easy to study and upgrade. Scientific research aimed at understanding the influence of varying electrical signals on the perceived visual information is therefore simplified, as well as patient-specific tuning.

Through implementation of neural response telemetry (NRT) technology, allowing to record the electrically evoked activity of the retinal neurons close to the site of stimulation, the device may also enable more detailed studies of the perceptual thresholds for a variety of stimuli, both in animals and humans.

The implant was designed for very long-term implantation, aiming at producing devices which will ideally outlive the recipients (decades of functionality without requiring replacement surgery), using biocompatible materials, and protecting all sensitive components inside hermetic capsules while ensuring electrical conductivity via hermetic platinum feedthroughs embedded in ceramics [129]. While the novel fabrication techniques call for demonstration of the *in vivo* biocompatibility (Chapter 3) and long-term functionality of the device (Chapter 7), the stimulation strategies implemented in the Phoenix^{99} deserve a high level of attention.

2.3.1 Current steering from the suprachoroidal space

Epiretinal and subretinal implants, such as the Argus II or the Alpha AMS respectively, require extensive manipulation of the globe and the retina. A vitrectomy must be performed to allow implantation in the correct space. The surgeries are complex and involve intra- and postoperative risks [123].

Comparatively, access to the suprachoroidal space in which the Phoenix[99] is located is easier and this site has the specific advantage of physical separation between the electrodes and neural tissue, potentially protecting the neurons from potential stimulation bi-products [35, 123]. On the other hand, higher stimulation thresholds are expected due to current spread over the increased distance between the electrodes and the neural tissue [31].

Current steering methods such as hexapolar stimulation – where the current is returned to a ring of electrodes surrounding the stimulation site (Figure 2-2) – were developed in part to focus the stimuli delivered from the suprachoroidal space and increase the resolution [130]. Additionally, the techniques minimize the electrical crosstalk compared to a monopolar configuration, enabling effective simultaneous stimulation [31]. Hexapolar stimulation, in return, has been shown to have a higher threshold compared to monopolar paradigms [61].

This issue is also addressed in the design of the Phoenix[99] through the implementation of a so-called "quasimonopolar stimulation paradigm" [61]. The quasimonopolar approach allows to lower the current thresholds during hexapolar stimulation by increasing the excitability of the target neurons using subthreshold monopolar stimulation via a distant return electrode [10, 61].

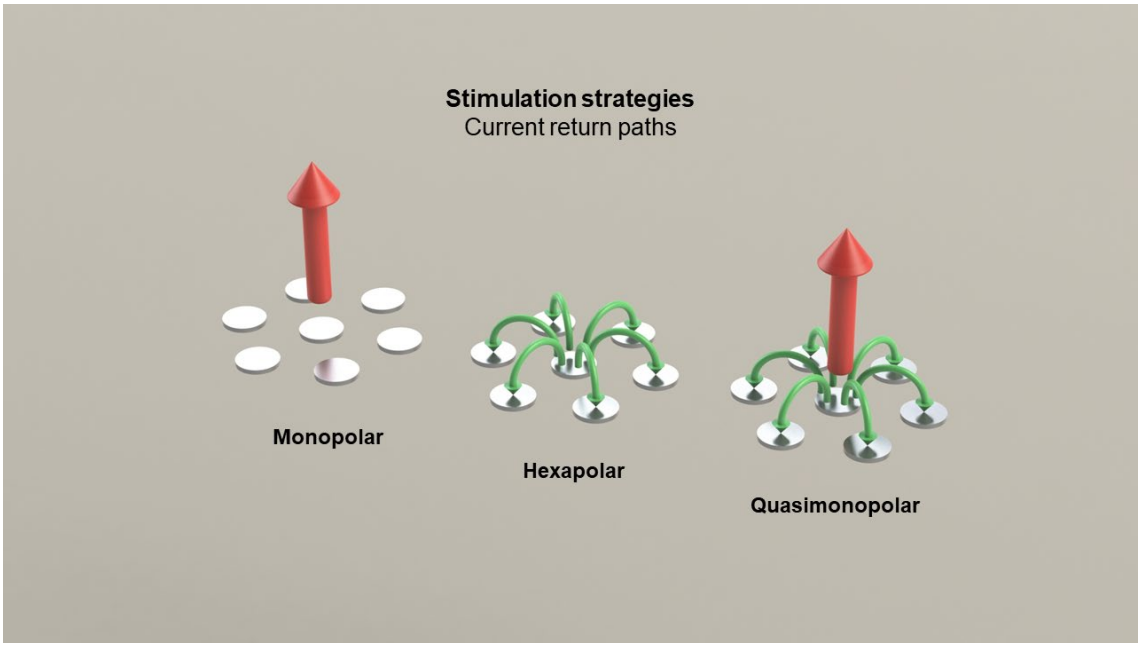

Figure 2-2 Current return configurations. During monopolar stimulation, the current is returned to a distant electrode. The hexapolar configuration sees the current returned to a ring of 'guards' surrounding the stimulation site. Quasimonopolar stimulation is a combination of both. Red arrows represent the monopolar component of stimulation, the green arrows represent the hexapolar components.

The Phoenix^{99} bionic eye uses the proven concept of suprachoroidal stimulation, which can safely and reliably elicit percepts over several years, while causing low numbers of adverse events [45, 46]. The implant also implements specific technical solutions to the potential drawbacks of the suprachoroidal approach, presenting a very promising list of potential benefits. The prosthesis is therefore a serious candidate for clinical trials, provided that the intervention- and device-related risks can be shown to be adequately low.

2.4 Preclinical studies of retinal implants

Since the first attempts to restore vision in a blind patient using electrical stimulation of the cortex by Brindley and Lewin in 1968 [87], there has been an obvious evolution in the safety requirements for medical devices. Both to clear a product for commercial use and in the field of clinical research, the level of evidence which must be produced before the authorities has been gradually increasing. This phenomenon obviously influences the number and complexity of the preclinical trials being reported, including the duration of implantation and the use of passive or active devices.

Predecessors of the prostheses that have reached the stage of clinical trials have been consistently tested in animal models during the development phase. From fundamental testing of potential materials and designs [131] to high fidelity copies of electrode arrays built for clinical trials [132], the implantation of electrically inactive devices provide insights into the host response to the surgery – including the effects of multiple consecutive surgeries [133, 134] – and materials [131, 132, 135, 136] (see Chapter 3). It also establishes a baseline, or *control* [39], to which stimulation safety experiments can be compared.

Studies with active devices generally have one of two aims: determine the ability of a device, electrode, or specific stimulation parameters to evoke brain activity, or test the safety of a device when used to deliver specific stimulation patterns. The former is usually

done in acute experiments while the latter generally aims to establish the chronic effects of stimulation to be used as evidence of safety before moving ahead to human trials.

Smaller animal models, such as rats, are usable for acute experiments [137]. Because they must be able to live as comfortably as possible with an implant and associated equipment, larger models are often required for chronic safety studies. Both for active and passive device testing, multiple animal models have been used over the years. For example, dogs were used to test early passive [135, 136] and active [39] versions of the Argus I and II (Second Sight Medical Products, Inc.). Rabbits, minipigs [138, 139], pigs [43] and cats [140] were used to examine the host response to subretinal implants as preparation for the human trials of the Alpha IMS and AMS. Because the visual system of the cat has been extensively studied, this model has often been preferred where detailed studies of the correlation between stimulus and cortical response were envisioned. As such, many reports on the Australian suprachoroidal implants, including predecessors of the Phoenix[99] focussed on this model [31, 60, 61, 141]. Notably, chronic preclinical safety studies with passive [106, 132, 142] and active [30, 35] suprachoroidal retinal stimulators that led to the clinical trials reported by Ayton et al. and Petoe et al., used the cat. Independent of the animal model used, the tools used to evaluate the effects of the implants are generally consistent.

2.4.1 Retinal health assessment tools

Histology – observation of cells and tissue under a microscope – is the most used technique besides fundus photography as it provides information about the immune and fibrotic response to the devices and stimulations. It is also used to evaluate the health of the retina by observing gross changes of the retinal anatomy or variations in neuron density in the different retinal layers [35, 132, 140]. Optical coherence tomography, as a non-invasive technique which also provides images of retinal cross-sections also allows for the evaluation of retinal changes and can be performed *in vivo* [35, 140]. Tools which allow the evaluation of the retinal function are also commonly used.

Electroretinography (ERG) is the measurement of the retinal electrical response to visual stimuli. Typically, an electrode placed in contact with the cornea measures the response to flashes with regards to a reference. Light sources are often called ‘full-field’ and are designed to illuminate as much of the retina as possible in order to elicit a strong response from both the central and peripheral visual field. The ERG recordings provide information to clinicians and researchers about physiological and pathophysiological retinal functions

[143]. ERG has been used to evaluate the impact of retinal implants on the retinal response to visual stimuli [144], for example in cases of epiretinal prostheses where the device stands between the light source and the photosensitive cells [39]. Beyond the ERG, it is also possible to record the cortical response to the visual stimuli, the so called visually evoked potentials (VEP) or electrically evoked potentials (EEP).

As previously mentioned, cortical recordings are typically quite invasive and therefore often used in acute, terminal experiments at the end of chronic studies. They nonetheless remain an effective tool to gather quantitative data about the impact of devices on the body. Used both in studies with active [145] and passive implants [133], the cortical evoked potentials can provide important insights into shifts in thresholds which may be correlated with retinal damage observed using other techniques. Other assessment methods, such as the measurement of the intraocular pressure, angiography, or X-ray computed tomography are also in the quiver of the researchers attempting to capture the multidimensional impact that retinal implants [35, 39]. Although the assessment tools appear to be widely accepted, there is no consensus on the adequate stimulation parameters to assess device safety in preclinical trials.

2.4.2 Stimulation parameters in chronic safety studies

Because the implants from the different groups around the world all have different designs, are positioned at variable distances from the retina (epiretinal, subretinal, suprachoroidal, intrascleral) and deliver different types of stimuli, it is difficult to compare them. As such, there is little value in direct comparisons of the actual stimulation values. Nevertheless, there also seems to be no consensus with regards to the approach to take to determine the adequate stimulation parameters for a given implant, or even the duration stimulation which may be considered as ‘worst-case’ for a daily implant user. For example, Nayagam et al. stimulated the retinas of cats 24 hours per day for three months at levels limited either by the device’s compliance or signs of pain [35]; Gekeler et al. stimulated the retinas of pigs for four weeks, one hour daily using variable stimulation amplitudes, while documenting “behavioural changes” [43]; finally, Terasawa, Tashiro, Nakano, Osawa (K.) and Osawa (M.) tested their device in rabbits for one month with an intra-scleral electrode, eight hours per day, at a fixed value for all animals [42].

As can be seen in Table 2-1 all reports tested the safety of sequential, monopolar stimuli. The potential additional benefits of the Phoenix^{99} compared to existing prostheses come

from the implementation of novel stimulation paradigms aimed at providing high frequency, high resolution stimulation over large electrode array such as parallel, hexapolar stimulation. To date, there have been no preclinical studies dedicated to the safety of simultaneous stimulation from multiple electrodes. As a result, further safety trials are warranted but refinement of the test parameters is required.

Table 2-1 Preclinical studies with active implants, summary of experiment parameters. The stimulation frequency applied to each electrode is shown in brackets.

Author	Animal model	Experiment duration	Daily stimulation	Return type	Stimulation upper limit	Stimulus Frequency
Güven 2005 [39]	Dogs	Mean 104.6 days, range 60 to 120	8-10 hours	Monopolar	Fixed	60 Hz, 16 electrodes (3.75 Hz)
Gekeler 2007 [43]	Pigs	1 month	1 hour	Monopolar	Fixed	20 Hz 16 electrodes (1.24 Hz)
Terasawa 2013 [42]	Rabbits	1 month	8 hours	Monopolar	Fixed	50 Hz One electrode (50 Hz)
Nayagam 2014 [35]	Cats	3 months	24 hours	Monopolar	Stimulator compliance or pain	200 Hz, 12 electrodes (16.7 Hz)

2.4.3 Safety of the Phoenix^{99}

From the implantation site in the suprachoroidal space to the size of the stimulation electrodes used, via the materials used to construct the devices, there are key similarities between all the Australia suprachoroidal devices. For some time, they were effectively developed in parallel by teams sharing the same source of funding, hence the resemblance. To demonstrate potential safety and efficacy of the Phoenix^{99} to the regulatory bodies, these similarities may play an important role. Indeed, there may be materials to claim substantial equivalence in some domains and benefit from the extensive *clinical* safety data acquired during the studies in a total of seven blind patients. These studies showed quite convincingly that the devices can be used safely to deliver sequential, monopolar stimulation to the retina for the purpose of restoring a sense of

vision. Yet the features that distinguish the Phoenix[99] from its compatriots, the novel stimulation paradigms that represent the added potential benefits of the device, and hence justify the risks of clinical research, however small they might be, need to be tested for safety.

Evidence of the paradigms' potential has been presented in multiple reports [10, 31, 60, 61, 146]. These have also shown that the ability of hexapolar stimulation to electrically isolate multiple stimulation sites from each other comes at the price of increased cortical thresholds [31, 60]. Higher cortical thresholds may correspond to higher perceptual thresholds, which in turn would mean higher injected charge densities and risk for the tissue [30]. Quasimonopolar stimulation – where the stimulation current is returned partially to a ring of guards and partially to a distant return (Figure 2-2) – may provide means to reduce the thresholds back to values close to the pure monopolar thresholds [60], but the efficacy of this technique during simultaneous stimulation is yet to be demonstrated [10].

Safety tests dedicated to these parameters are therefore required, particularly to compare them to the established sequential monopolar stimulation. An experimental design for such a study is proposed in Chapter 8 but to ensure that the proposed study compares stimuli that are clinically relevant with regards to the elicitation of percepts and delivery of functional vision, our understanding must be deepened. While the refinement exercise will be the focus of chapters 4 to 6, let's begin where all other retinal prostheses have started their clinical adventure: ensuring that passive devices can be safely implanted for extended periods of time in an animal model.

3 SURGICAL SAFETY AND BIOCOMPATIBILITY

LONG-TERM IMPLANTATION OF PASSIVE DEVICES IN SHEEP

Article published in Biomaterials [1]

Data and supplementary data published in Data in Brief [147] (see Appendices)

3.1 Introduction

As we move towards a seamless interaction between humans and therapeutic implants, the visually impaired and blind community glimpses what the future may bring for the restoration of sight. Through electrical stimulation of surviving neurons of the visual system, the emerging field of retinal neuroprosthesis aims to allow people with profound vision loss from degenerative retinal disorders to regain a useful sense of vision.

Retinitis pigmentosa (RP) is an inherited retinal disease (IRD) which can cause severe visual impairment and blindness as it results in the death of the retinal photoreceptors. Compared to pathologies that affect other retinal neurons (e.g. glaucoma, which involves damage to retinal ganglion cells (RGCs) and their axons in the optic nerve [148]), retinal degenerative diseases often leave behind a viable [149], [150], however remodelled [151], [4], network of retinal neurons that can be used to elicit visual percepts when activated through artificial stimulation [98].

Patients suffering from IRD predominantly involving the photoreceptors, such as RP, may benefit from a retinal visual prosthesis or so-called ‘bionic eye’. Improved mobility, navigation, orientation, recognition and overall quality of life are expected if the restored visual sensations can adequately transpose the visual scenery.

Akin to cochlear implants, which have restored the sense of hearing to the deaf and severely hearing impaired [152], visual prostheses electrically stimulate the visual system to effect perceptions. Individual visual perceptions elicited by electrical stimulation are known as phosphenes. Multiple phosphenes can be combined into images and referred to as prosthetic – phosphenised – vision. Electrical stimulation anywhere along the visual

pathway can elicit visual sensations. Three primary sites of intervention have been the focus of intense research: the visual cortex [87]; the optic nerve [93]; and the retina [153]. The latter being the focus of the present article. Stimulation of the retina presents advantages compared to other sites, such as improved surgical safety [154] and a more direct correspondence between the location of the stimulating electrode on the retina and its perceived location in the visual field [155]. Compared to other retinal stimulator designs, such as epiretinal or subretinal devices, suprachoroidal implants offer simplified surgical procedures and good device stability, at the expense of increased thresholds [156].

To-date, there exist a handful of prosthetic devices targeting surviving retinal neurons by way of electrical neuromodulation. These are in various stages of development - including three that have been approved for sale in some jurisdictions: The Argus II retinal prosthesis system (Second Sight Medical Products, Inc., Sylmar, CA, USA – device no longer for sale), the Alpha IMS multiphotodiode array (Retina Implant AG, Reutlingen, Germany – company ceased operation) and the IRIS II bionic vision system (Pixium Vision, Paris, France). Generically speaking, these devices modulate the activity of the surviving retinal neurons through the controlled delivery of electrical impulses from multiple interfacing sites (electrodes) [157].

Clinical trials of retinal prosthesis have highlighted the interindividual variability of the restored visual acuity [158] and phosphene shapes [100]. Challenges in developing a functional visual prosthesis include: the number [158] and morphology [100] of individual phosphenes that can be used to form patterns; the ability to consistently modulate phosphene characteristics [159]; the coexistence of a device within the body; and the capacity of the device to safely modulate the neuronal tissue over a long time [99, 105], preferably the life span of the patient.

Research within our laboratories has led to several avenues through which the foregoing may be achieved. Of particular importance is the capacity to modulate phosphene morphology through novel multiplexing and current steering approaches, and the means of implementing these into a fully implantable device [31, 61, 127]. The flexible, on-board stimulation electronics therefore provide means to optimise stimulation strategies based on individual recipient responses, including different current return configurations [10] without having to surgically replace the device.

Our device, 'the Phoenix^{99}', has 98 stimulation sites complemented by one common return electrode. It is a fully implantable device aimed at restoring useful visual percepts to the blind. The device includes a suprachoroidal electrode array, a visual stimulator (VS) and a telemetry implant (TI). This study aimed to demonstrate that it can be safely implanted in an ovine model using an established surgical procedure that results in a stable implant and electrode array position, with a fast and uneventful postoperative recovery. We present the surgical approach as well as the intra- and postoperative observations, including indirect fundus imaging, infrared imaging and optical coherence tomography (OCT). Radiographs of the heads and post-mortem orbit and eye dissections complemented the study. The effects of the surgery and the biocompatibility of the implant during extended periods were analysed at a gross microscopic and cellular level, using histopathological analysis. Using electrically inactive devices, this study establishes a reference to which future studies of active implants can be compared.

Combined with encouraging first-in-human observations of suprachoroidal stimulation applied via an externalized electrode array of similar dimensions [45], this study represents an important step for establishing a fully-implantable system for the provision of phosphenised vision.

3.2 Materials and Methods

3.2.1 Ethics statement

The procedures for this study were approved by the Animal Care and Ethics Committee (ACEC) of UNSW Sydney (protocol number 14/155B) and were conducted in accordance with the Australian Code for the Care and Use of Animals for Experimental Purposes 8th edition (2013) and the ARVO standards for use of animals in ophthalmic research.

3.2.2 Implant system

The Phoenix^{99} fully implantable system comprises a VS connected to a behind-the-ear TI via a flexible cable. The VS consists of an extraocular hermetic capsule built from alumina ceramic and titanium, connected to a suprachoroidal electrode array. The array was manufactured using medical grade silicone elastomer and pure platinum (Pt) for biocompatibility and biostability. It is formed via a novel laser micromachining process pioneered by the authors and collaborators [122].

The array is 18.7 x 10.8 mm with a nominal thickness of 500 µm, as shown in Figure 3-1. The conformable array has a tapered tip and the edges are rounded for minimal insertion and implantation trauma. In all devices but the two used in preliminary experiments, a subset of the 98 Pt electrodes were exposed using laser micro-machining of the protective electrically insulating silicone elastomer layer. An L-shaped scleral incision of 11 x 3.3 mm is required to allow for electrode array insertion, yet the larger segment is entirely sutured closed following insertion. The resulting scleral opening is 3.3 mm (Figure 3-2), which is comparable to scleral flaps routinely used in glaucoma treatments [160].

Figure 3-1 (A and C) illustrate the system architecture. Briefly, the TI (5) is placed behind the ear and is interfaced with an external transmitter via mutual inductance for transcutaneous power and data transmission, obviating the need for an implantable battery and affording the capacity to fully configure the electrical stimuli from externally derived instructions. Power and configuration data are transmitted from the TI to the VS (2) via net charge neutral signals delivered via a two-wire flexible cable (4). The cable passes around the lateral orbital rim and is secured in an incision made to the bone with a silicone grommet (3). The electrode array (1) delivers the stimuli to the retina from the suprachoroidal space.

All devices used in this study were designed to be implanted in the left eye. They were initially cleaned in 80% ethanol, rinsed in deionised water, and gas sterilised in ethylene oxide prior to surgery.

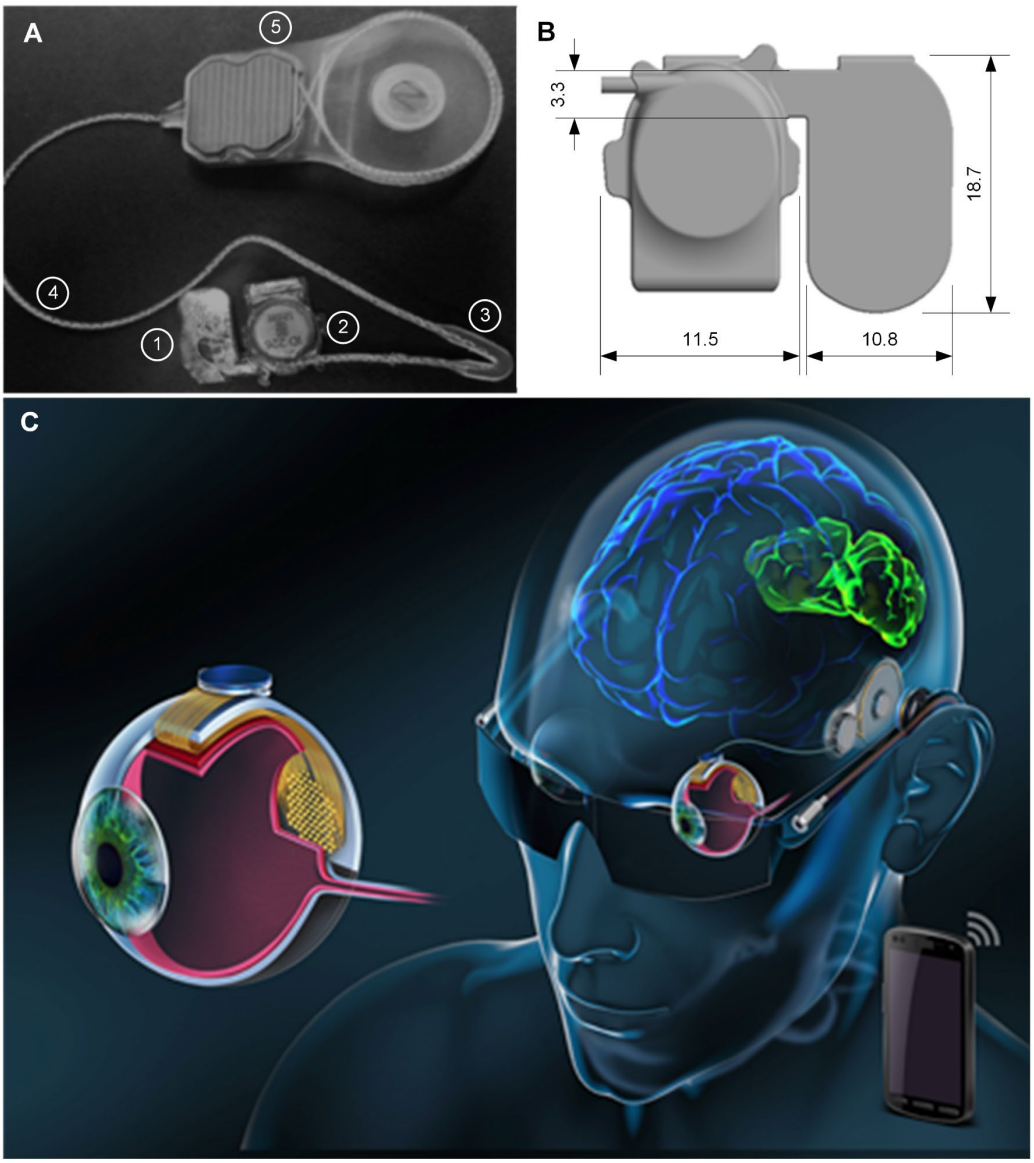

Figure 3-1 The Phoenix[99] system. A) Photograph of the whole implant including (1) the electrode array, (2) the VS capsule, (3) silicone grommet, (4) the flexible cable and (5) the TI. B) 3D rendering of the VS in its final form factor. Critical dimensions of the VS in different sections. C) Artist view of the entire system and its position in the globe (Illustration by Leanne & Jamie Tufrey). Note that the appearance of the external components, such as the camera have not yet been determined. A possible position of the camera on glasses is presented here, but other solutions could be envisioned, such as recruiting the camera of a modern smartphone.

3.2.3 Animal model

Visual neuroscience researchers tend to prefer the feline or primate model owing to the richness of information within the academic literature, relating to the visual systems in these animals. Accordingly, our choice of the ovine model warrants some justification.

The surgical technique was initially developed, tested and refined in animal and human cadaveric eyes, as well as *in vivo* feline, rabbit and sheep models. Our previous research on stimulation strategies [31, 61] utilized a feline model using electrode arrays with externalized electronics, obviating the need for the eye and the electronics to co-exist within the orbit. The feline globe dimensions closely match the orbit size, leaving little extraocular space.

The device investigated in this study will be fully implantable in humans and is designed to fit the anatomy of the host species. Among other functional units (see description of the device above), the Phoenix[99] includes a capsule that is sutured directly onto the globe and occupies part of the orbital space. The human orbit has capacity to support the implant. The device size is similar to glaucoma drainage devices which have a long history of stability attached to sclera in human patients [161]. Similarly, the ovine orbit contains a significant volume of fatty media surrounding the globe, and the bony component provides protective space for the VS (See (2) in Figure 3-1), while maintaining unimpeded ocular movement, unlike the feline orbit. In this regard, the ovine orbit is substantially more similar to the primate than the feline.

The Dorper breed ovine model was selected as a good match for the size and shape of the sheep orbit with human anatomy [162] and the suitability of the neck tissue for tunnelling and communications with the telemetry unit in future studies. Dorper sheep do not have the folds of fleece around the neck associated with sheep bred for wool production.

3.2.4 Housing and cohort

Nine adult, female sheep (*Ovis aries*) were used (two Suffolk breed sheep were used for early studies, prior to availability of Dorper breed sheep; and implanted for two days and one month). The seven other sheep were of the Dorper breed. Animals were farm-sourced, delivered, weighed (mean weight 50.5 kg, range 45 kg to 61.5 kg) and screened for any pre-existing pathology upon arrival in the study facility. The animals were housed in a physical containment 1 (PC1) facility within the Graduate School of Biomedical Engineering (GSBmE, UNSW Sydney, Australia) for the duration of the study.

A modular pen system was used so the animals were held in groups or alone while maintaining visual and vocal connections with the other animals. Directly after surgery, the sheep were kept individually in a raised pen (1800x1200x1100 mm) to assist with monitoring before return to the group pen, as soon as wound healing and recovery allowed. Flooring surfaces were non-slip and covered in straw bedding, except during the

surgery preparation phase, when straw was replaced by rubber foam flooring. Temperature was maintained at 21 ± 2°C and the humidity between 40% and 70% RH. Chaff and lucerne were provided in adequate quantities and water was available *ad libitum*.

The animals were allocated to one of four groups based on date of arrival in the study facility: 2 days (N=1), 1 month (N=2), 2 months (N=2) and 3 months (N=4). The experimental unit was defined as a single animal. Animals were given a unique number corresponding to the experimental group and group position; for example, "1M#2" was the second animal in the group implanted for one month.

3.2.5 Anaesthesia, monitoring and preparation for surgery

The animals were fasted overnight prior to surgery, with access to water maintained. Anaesthesia was induced by intramuscular injection of Zoletil 100, 12 mg/kg, (Virbac Australia Pty Ltd, Milperra, NSW, Australia) and maintained by inhalation of isoflurane in oxygen (1.5-3% in 2 L/min, I.S.O, Veterinary Companies of Australia Pty Ltd, Blacktown, NSW, Australia). Initial administration of inhalational anaesthetic was performed by mask followed by intubation with an endotracheal tube. Intravenous access was established in either the cephalic or saphenous veins to allow for the administration of fluid therapy (1 drop/second, Hartmann's solution, Compound Sodium Lactate (1L), Baxter Healthcare Pty Ltd, Old Toongabbie, NSW, Australia). Maintenance of the appropriate level of anaesthesia was determined by monitoring heart rate, respiration, blood pressure, SpO_2, mucous membrane colour, capillary refill time, temperature, and by regular checks of withdrawal reflexes. Surgical procedures were typically completed within 120 minutes.

The anaesthetised animals were administered a systemic dose of broad-spectrum antibiotics (cephalexin, 0.05ml/kg IV - 1g in 5ml sterile water, Keflin, Aspen Pharma Pty Ltd, St Leonards, NSW, Australia). The area around the surgical site was shaved, cleaned and disinfected with povidone-iodine. Povidone-iodine was used to disinfect the eye and surroundings and rinsed with sterile saline after 3 minutes. Atropine 1% (Aspen Pharma Pty Ltd, St Leonards, NSW, Australia) was topically applied to the ocular surface to dilate the pupil, and artificial tears (GenTeal, Novartis Pharmaceuticals, East Hanover, NJ, USA) were applied to maintain ocular surface hydration. Both products were used as required for the duration of the procedure.

3.2.6 Implantation surgery

Aseptic procedures were followed. The surgical approach consisted of an incision at the scapula followed by the tunnelling of the VS and flexible cable under the skin to the orbital margin with the aid of a trocar. Implantation of the electrode array into the suprachoroidal space was performed via an incision in the sclera. The VS unit was sutured directly onto the eyeball and the TI was positioned subcutaneously behind the ear before all surgical wounds were sutured close.

A full thickness incision of the skin behind the ear allowed the formation of a subcutaneous tunnel by blunt dissection. The tunnel was enlarged by consecutive passes of malleable brain retractors of increasing size (12, 17 and 25 mm), and an incision was made at the orbital margin using the brain retractor as reference. The VS was passed through this tunnel with the aid of a customised trocar.

The orbital grommet (Figure 3-1) was lodged in a key-hole shaped orbitotomy created using sequential passes with a bone drill with increasing burr size (diameter 1.8 and 2.5 mm). Connective tissue was incised and elevated at the zygomaticofrontal suture and an orbitotomy was created at this landmark. As a corrective measure following cases of grommet instability, the surgical procedure was updated after the first five surgeries. The orbitotomy was moved 2 mm superior to the zygomatic suture and the connective tissue was subsequently sutured over the orbital grommet to stabilise its position. An additional suture was also added at the orbital margin to secure the grommet.

Access to the ovine globe was simplified by means of a lateral canthotomy. A corneal stay suture of 6-0 Prolene (Johnson and Johnson, Sydney, Australia) afforded the surgeon manipulation capabilities to aid in the surgical process. The conjunctiva and Tenon's capsule were dissected to create a pocket large enough to contain the VS capsule. To allow for adequate exposure and manipulation of the globe, the superior rectus muscle was severed.

The electrode array was implanted into the suprachoroidal space through an L-shaped incision to the sclera (11 x 3.3 mm), located in the superotemporal quadrant of the globe, 10 mm posterior to the corneoscleral limbus (Figure 3-2). A silicone introducer, that mimics the size and flexibility of the electrode array, was used to establish a pocket in the suprachoroidal space. The electrode array was then advanced alongside the introducer for approximately 3 mm before the introducer was removed. The array was then completely inserted until it reached the appropriate site behind the retina. Six 7-0 Prolene sutures

were placed along the longer section of the L-shaped incision to close the scleral wound over the electrode array (Figure 3-2). A 3.3 mm passage in the sclera remained to bridge the intraocular electrode array with the VS.

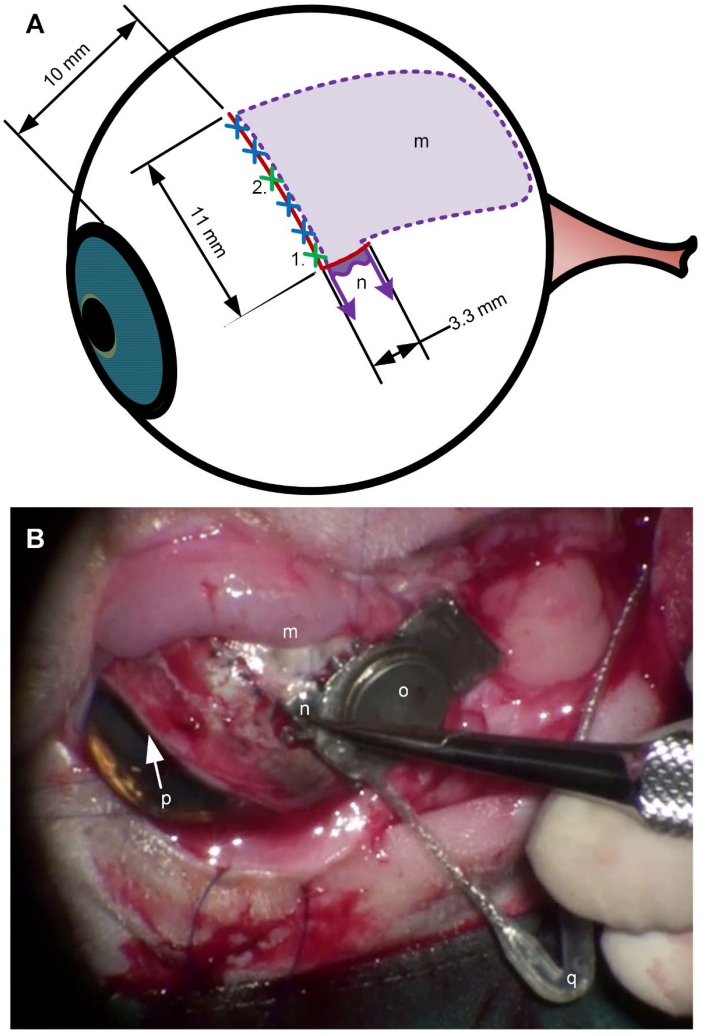

Figure 3-2 Scleral incision and sutures. (A) Schematic view of the globe and L-shaped incision. (B) Intraoperative photograph of the Phoenix[99] Bionic Eye *in situ* during suturing of the scleral incision. m) Location of the electrode array under the sclera, sutured scleral "L-shaped" incision (red line in A) and the remaining bridge (n) through which the conductors exit the globe, o) visual stimulator capsule, p) corneal limbus and q) silicone orbital grommet. The short part of the L allows minimal residual scleral opening where the electrode array exits the eye and is connected to the VS via a bridge (n). After electrode array insertion in the suprachoroidal space, the long section of the L-shaped incision is sutured with 7-0 Prolene at the six locations indicated by crosses. The green sutures are placed first, following the numbering in the figure, before placing the remaining ones.

If required for control of the eye pressure, a 30-gauge needle and 1 ml syringe was used to remove 0.5ml aqueous humour from the anterior chamber.

Eyelets, integral to the body of the VS hermetic capsule, provided anchorage points through which to secure the device directly to the eyeball, positioning it in a protected space within the orbital fat of the superotemporal orbit. The VS was fixated using two loops of 7-0 Prolene suture per eyelet. The TI was positioned subcutaneously behind the ear before all surgical wounds were closed. Incision was infiltrated with local anaesthetic at closure (Bupivacaine 0.25% diluted from 0.5% solution, 10 ml – Marcaine 0.5%, AstraZeneca, Macquarie Park, NSW, Australia).

3.2.7 Postoperative care and clinical assessments

Immediately after the surgery, the animals were returned to individual holding pens for observation. During recovery from anaesthesia, animals were monitored for any signs of pain or distress. Carprofen was administered for analgaesia (4 mg/kg, Carprieve, Norbrook Laboratories Pty Ltd, Tullamarine, VIC, Australia). Topical antibiotic (Chlorsig, Aspen Pharma Pty Ltd, St Leonards, NSW, Australia) and anti-inflammatory eye drops (Prednefrin forte, Allergan Australia, Pty Ltd, Gordon, NSW, Australia) and artificial tears (GenTeal, Novartis Pharmaceuticals, East Hanover, NJ, USA) were administered three times daily for one month, or as required by the surgeon. Systemic antibiotics were administered every four days for two weeks (Benacillin, 150 mg/ml, 4 ml, Troy Animal Healthcare, NSW Australia). If required by a veterinary care specialist, analgesia was continued during the recovery period (Carprofen, 2 mg/kg).

Animals were assessed twice a day (morning and afternoon) during the first 7 days after the operation (ophthalmoscopy, temperature, wound appearance and eye health, behaviour and general wellbeing). Further eye health checks were conducted using indirect ophthalmoscopy every 2-3 days for a minimum of 2 weeks post-surgery. Thereafter, ophthalmoscopy was conducted weekly, with general health assessment daily. Fluorescein staining (OptiStrip-FL, OptiMed Pty Ltd, Castle Hill, NSW, Australia), visualized with a Burton lamp, was used as required to identify corneal damage. Regular ophthalmoscopic assessments were performed using a hand-held setup without recording capabilities in awake animals, as opposed to the imaging sessions described below.

Any adverse events (AEs) were recorded and treatments were administered as required on a case by case basis, including but not limited to analgaesia, local antibiotics and secondary surgical interventions. Suspected AEs without the possibility to formally prove

alternate cause were all included in the results. AEs were categorised as severe if they required secondary surgical intervention, euthanasia or caused the death of the animal.

3.2.8 Intraocular pressure measurements

Intraocular pressure (IOP) measurements were made in both eyes, in the pen, without anaesthesia, on days 1 and 7 post-surgery, and after one, two and three months, where applicable, using a TonoVet rebound tonometer (Icare Oy, Helsinki, Finland).

3.2.9 Imaging

Fundus images and OCT images were obtained prior to device implantation, directly post-implantation and monthly until termination. Fundus recordings were made using a Super Quad 160 lens (Volk, Mentor OH, USA) and video camera (Galaxy S3, Samsung, Seoul, South-Korea or XR500, Sony, Tokyo, Japan), passed through the optics of an OPMI operating microscope (Zeiss, Oberkochen, Germany). OCT imaging was performed with an Envisu 2300 system (BiOptigen, Morrisvile NC, USA). Infrared images were obtained immediately after device implantation and repeated monthly using a novel technique described elsewhere [163]. X-rays of the head and neck were obtained at one month and on the day of termination in a representative sample of the animals scheduled for two- and three-months study duration to assess device stability. All imaging was performed under anaesthesia as used for primary surgery (see above). Atropine drops 1% (Aspen Pharma Pty Ltd, St Leonards, NSW, Australia) were used to dilate the pupils for imaging.

Fundus and infrared images were acquired as video files and representative frames were extracted using the automatic deinterlacing function in VLC Media Player software (Free Software Foundation, Inc., Boston, USA). Wherever possible, frames containing the area of interest around the implant tip were selected based on the image quality, for all imaging methods. For each animal, the series of images were then rotated and scaled using blood vessels as a landmark input for the Fiji [164, 165] software plugin "Align image by line ROI" [166]. The image families created were stacked and cropped to significant content using a separate Fiji plugin (Crop (3D), Mark Longair).

Implant position was observed and compared between time points in the stacked infrared images by manually drawing its contour in Fiji. Blood vessels were used as landmarks to identify the location of the electrode array and for comparison across imaging modalities.

3.2.10 Termination and eye tissue dissection and fixation

The animals were prepared using anaesthetic induction as described for implantation. Following the imaging, the animals were euthanised via an intravenous overdose of barbiturate anaesthetic, sodium pentobarbital (>365 mg/kg, approximately 20 mL, Lethabarb, Virbac Pty Ltd, Milperra, NSW, Australia). Cardiac function was monitored until no signs of life were observed.

The head was removed immediately and perfused with warm (37 °C) heparinised saline (2 L), followed by cold (4 °C) neutral buffered formalin (NBF, 10%, 1 litre) at the rate of 1.0 L/hr. Eyes were enucleated, leaving the entire implanted Phoenix^{99} implant and external leads in position in the eye and fixed in NBF for minimum 48 hours. Samples were refrigerated at 4 °C until dissection. To reduce the viscosity of the vitreous humour, 4 mL of Davidson fixative was injected to each eye, through an incision in the inferomedial quadrant of the globe, 6-8 mm posterior to the limbus. After the injection, the whole eye was immersion fixed in NBF until processing and embedding.

3.2.11 Histological processing

Following isolation of the sheep ocular tissue, the location of the array was marked with tissue marking dyes on the sclera. The implanted device was released from the eye tissue by cutting the sutures for removal from the globe. The implanted device was cleaned with 70% ethanol and stored.

The tissue at the array site was cut into approximately 14 × 4 mm sections. The tissue was further dissected, and pieces placed in embedding cassettes with biopsy pads (Muraban Laboratories, Australia) to keep the retinal-choroidal-scleral layers intact during tissue processing and embedding.

For paraffin embedding, samples were initially dehydrated in a graded series of ethanols (30%, 1 hr; 50%, 1 hr; 70%, 1 hr; 2 × 95%, 30 min and 1 hr; 2 × 100%, 30 min and 1 hr), then histolene (2 × histolene, 30 min and 1 hr), infiltrated with paraffin (2 × paraffin, 2 x 1 hr at 58 °C) and then embedded. Sections were cut at 10 μm on a rotary microtome with disposable blades (ThermoFisher Scientific, North Ryde), collected on Superfrost Plus glass slides (ThermoFisher Scientific), dried overnight at 37°C, and stored. Collected sections included regions over the implant body, at the edges of the implant, and at least 0.5 mm from the electrode array.

To determine the effect of the implant on the retinal-choroidal-scleral structure, sections were stained with hematoxylin and eosin (H&E). Sections were dewaxed in xylenes (10 and 5 min), followed by rehydration through a graded series of ethanols (2 × 100%, 2 min; 90%, 2 min; 70%, 2 min) and water (2 min). Sections were then stained with Harris Hematoxylin (7 min; prior to bluing in running tap water for 4 min) and eosin (4 min). Sections were then dehydrated by serial washes in 100% ethanol and 2 changes of xylene (5 and 10 min), prior to mounting with DePeX solution (Muraban Laboratories, Mount Kuring-Gai, Australia).

3.2.12 Histopathological assessment and scoring

Slides of representative eyes, including controls, were de-identified, randomised and examined by two veterinary pathologists. Histological assessment was made using a two-part grading system to assess a) retinal health and b) host response in the suprachoroidal space. The host response was evaluated by grading the inflammatory response and fibrosis on a scale from ‘0’ to ‘3’, adjusted on the results observed in the study (‘0’: no response, ‘3’: most severe response in the cohort). The retinal health scale provided criteria to evaluate the effects of the intervention on the retina based on the functional requirements of a visual prosthesis. Thinning and remodelling were assessed on a mild/moderate/severe scale where severe would be likely to interfere with the functionality of a visual prosthesis. Scoring for each section was done in parallel by the two pathologists and discussed until consensus. All scores were based on the strongest response observed in each eye, according to the criteria described in Table 3-1.

Sections were also analysed to detect the presence of retinal detachment or haemorrhage (retinal, subretinal or suprachoroidal). All slides were digitised using an Aperio Versa 1.0.4 (Leica Biosystems, Nussloch, Germany) slide scanner and viewed in ImageScope™ version 12.4.0.5043 (Leica Biosystems, Nussloch, Germany). When present, the length of retinal detachment was measured by drawing a line along the hypertrophied retinal pigmented epithelium (RPE).

Table 3-1 Histopathology grading system. The host response was evaluated by grading the inflammatory response and fibrosis on a scale from '0' to '3', adjusted on the results observed in the study ('0': no response, '3': most severe response in the cohort). The retinal health scale provided criteria to evaluate the effects of the intervention on the retina based on the functional requirements of a visual prosthesis. The retinal health scale provided criteria to evaluate the effects of the intervention on the retina based on the functional requirements of a visual prosthesis. Thinning and remodelling were assessed on a mild/moderate/severe scale where severe would be likely to interfere with the functionality of a visual prosthesis.

		Histology evaluation criteria			
	Grade	**None**	**Mild**	**Moderate**	**Severe**
General	**Retinal health**	No observable thinning or remodelling	Mild thinning/remodelling of the outer retinal layers (RPE, outer nuclear layer and outer plexiform layer)	Moderate remodelling of the retina extending into the inner retinal layers (inner nuclear layer, inner plexiform layer and ganglionic layer)	Severe retinal degeneration with significant retinal ganglion cell loss
	Grade	**0**	**1**	**2**	**3**
Scale calibrated on the cohort	**Fibrosis**	None	Adjacent to the end of the implant, there is a minimal increase in sparsely cellular collagen (approx. 1-2 fibrocytes thick)	Adjacent to the end of the implant, there is a mild detectable increase in fibrous connective tissue (approx. 3-4 fibrocytes thick)	Adjacent to the end of the implant, there is a mild detectable increase in fibrous connective tissue (approx. 5-6 fibrocytes thick)
	Inflammatory response	None	Rare scattered phagocytic cells (presumed histiocytes) sometimes containing small amounts of cytoplasmic pigmented material lining the implant margins and occasionally within the space vacated by the implant. Within the implant space, aggregates of mononuclear phagocytic cells and multinucleated macrophages are not a feature. When present, lining at the implant margins are one cell thick.	Small numbers of scattered phagocytic cells often containing small amounts of cytoplasmic pigmented material located within the space vacated by the implant and lining the implant margins. Within the implant space, phagocytic cells sometimes form small aggregates. Multinucleated macrophages are not a feature. Lining at the implant margins are usually one cell thick.	Moderate numbers of scattered phagocytic cells often containing small amounts of cytoplasmic pigmented material located within the space vacated by the implant and lining the implant margins. Within the implant space, mononuclear phagocytic cells sometimes form small aggregates and occasional multinucleated macrophages are present. Lining at the implant margins are usually 1-2 cells thick

3.2.13 Retinal thickness measurements

Deidentified slides were viewed in ImageScope™ and retinal thickness measured using the ruler tool to place markers perpendicular to the retinal layers. The thickness of the retina, from the photoreceptors (outer limit) to the nerve fibre layer, was measured every 200 µm over the entire length of visible retina. The measurements were recorded for four categories, separating the values obtained directly above the edge of the pocket created by the implant and over segments of detached retina. If neither of those features were visible or present, the values were temporarily qualified as "body of the implant or control retina" and assigned to either of those categories after re-identification. Where possible, measurements were taken up to 600 µm on either side of the location of the implant edge. Whenever multiple slides were available for a single eye, the values from all slides were combined into a single data set, according to the four categories described above. Areas with processing artefacts affecting the measurements, such as artefactual retinal detachment, were excluded.

3.2.14 Immunohistochemistry

Eyes were processed for fluorescence immunohistochemistry as previously described [167]. Briefly, sections were dewaxed and rehydrated through alcohols to water. For antigen retrieval, sections were incubated in 0.01 M sodium citrate buffer (pH 6) at 95 °C for 10 min, cooled to 40 °C, and washed with PBS. Sections were permeabilised with 0.1% Triton X-100/PBS for 30 min, room temperature, followed by blocking in 5% BSA/0.1% Triton X-100/PBS for 30 min, room temperature, and incubated with primary antibodies, made up in 1% BSA/0.1% Triton X-100/PBS, for 16 h, 4 °C.

The antibodies used were as follows: specific for astrocytes and activated Müller glia: GFAP-Cy3 conjugate (mouse IgG; 1:800); cone photoreceptors: opsin-red/green (opsin R/G) (rabbit IgG; 1:500, 1:1000) (Merck Millipore) and macrophage/microglia: Iba1 (goat IgG; 1:200) (Abcam, USA). Immune complexes were detected with the appropriate secondary antibodies (raised in donkey, diluted 1:1000) (2 h, room temperature) to goat IgG, mouse IgG, or rabbit IgG, conjugated with Alexa-Fluor 488, 555, or 647 (Invitrogen, USA). Nuclei were counterstained with Hoechst 33258 (1:10,000) prior to mounting in glycerol:PBS (80:20) and slides were sealed with nail varnish. All fluorescence images were captured using an LSM 700 Meta Confocal microscope system and ZEN Blue

software (Carl Zeiss, Germany). Images were assembled in Photoshop CS software (Adobe Corporation, USA).

Quantitative analysis on immunoperoxidase labelled sections was performed using the ImageScope™ Positive Pixel Count algorithm [168, 169]. Briefly, paraffin sections cut at 4um were collected on charged slides (HistoBond®, Marienfeld), dried and subsequently deparaffinized to water. Sections were then heat antigen retrieved in high pH buffer (Target Retrieval Solution, S2367, DAKO®). Slides were loaded onto a DAKO® Link Autostainer with the following steps: blocking (Bloxall, SP6000, VectorLabs®), primary antibody (macrophage/microglia, clone Iba1, BioCare Medical®, rabbit polyclonal, 1:200), secondary (Envision K5007, DAKO®), chromogen ImmPACT Nova Red (SK4805, Vector Labs®), counterstained in haematoxylin (Whitlocks, VPDS Histo Lab Manual©, 2021), cleared and mounted in DePeX and coverslipped. Negative control sections were processed identically as described above, but with the primary antibody omitted. Sections were scanned with Aperio Versa (Leica Biosystems®, UK) at 40x for analysis. The whole retina was outlined in all sections excluding the retinal pigmented epithelium (RPE), to avoid confusion with the red chromophore. The ratio of positive pixels to the total number of pixels per region of interest was calculated for each section and used as a measure of the Iba1+ macrophages/microglia (‘Positivity’ expressed in percent). To minimise false positives, the algorithm was also applied to negative controls for immunohistochemistry for all samples. Details of the parameters used in the analysis are provided in the Supplementary information.

3.2.15 Statistics

3.2.15.1 Retinal thickness

Two-tailed, Student’s t-tests were performed in GraphPad Prism version 8.4.3 for Windows (GraphPad Software, San Diego, California USA) to determine whether the average thickness was different between detached segments and the retina over the implant body, and between the implant’s edge and the implant body, in individual eyes. The tests assumed approximately normal distributions of the continuous dependent variables, as well as the absence of outliers and independence between the observations.

3.2.15.2 Histology scores

The Kendall’s Tau-b rank correlation coefficient [170] was calculated using IBM SPSS Statistics for Windows, version 26 (IBM Corp., Armonk, N.Y., USA) to measure for association between the duration of the experiment and the retinal health score.

A three-class ordinal scale was used to rank the eyes based on implant duration, according to the experimental group to which the animal had been allocated. The controls were excluded because they were not representative of any implant duration.

The Tau-b test is a non-parametric method that tests the null-hypothesis of non-monotonic association between two variables. Kendall's Tau-b test was chosen as it was specifically designed to account for the presence of ties (data points of equal value for one or more of the categories). A two-tailed significance test was run on the calculated correlation coefficient using SPSS Statistics.

3.3 Results

Nine Phoenix^{99} Bionic Eyes were successfully implanted and were well tolerated by the hosts. All electrode arrays were stable in the suprachoroidal space for the duration of the study and resulted in an immune response within the suprachoroidal space classified as being mild. Retinal thinning and remodelling were limited to the outer retinal layers for all but one animal in which mild disturbance of inner retinal layers was observed.

3.3.1 Adverse events (AEs)

One (1/9) animal died directly postoperatively due to respiratory complications unrelated to the device (2M#2). This animal, scheduled to receive an implant for two months, was therefore excluded from the following section. This severe adverse event (SAE) was reported as an intervention unrelated event.

There was a total of 41 clinically relevant AEs including all levels of severity for eight animals (median: 5, range: 2 to 7 AEs/animal). There were three, device or intervention related SAEs in three sheep, two of which were suture-related and required additional stitches. The last SAE was observed as a loose grommet which eroded through the conjunctiva (see below). AEs are summarized in Table 3-1.

Table 3-2 Clinical adverse events summary table

Adverse event types	Number of cases Total: 46
Clinical adverse events	**41**
Corneal abrasion/opacity	7
Corneal ulcer	1
Swelling	6
Limited blinking	5
Red eye	5
Weeping wound, discharge, light bleeding	4
Suture related	3
Dislodged orbital grommet (without erosion or VS movements)	2
Dislodged orbital grommet with erosion through conjunctiva and VS dislodgement	1
Retinal haemorrhage	1
Suspected retinal haemorrhage	2
Limited eye movements	2
Elevated IOP ≥35 mm Hg	1
Herniated choroid	1
Histologically observed adverse events	**3**
Retinal detachment	3
Events unrelated to the device	**2**
Hoof drop (neurological disorder)	1
Post-operative respiratory problems and death	1

All electrode arrays were successfully inserted into the suprachoroidal space and the VSs sutured to the globe at the appropriate position. The TIs were implanted without difficulty. In 2M#1, the silicone introducer was accidentally pushed entirely into the suprachoroidal pocket during electrode array insertion and the array had to be retracted to allow removal of the introducer. This double attempt to position the electrode array had no further consequences during the procedure but may have led to the suspected haemorrhage described below. Intraoperatively, a suprachoroidal haemorrhage caused by herniation of the choroid was observed using indirect ophthalmoscopy in one of the early development animals (2D#1). The sclera of this animal was unusually thin compared with the rest of the cohort and caused complications during electrode array insertion. IOP was lowered by removing 0.5 ml aqueous humour from the anterior chamber and array insertion was completed.

After surgery, swelling around the eye and surgical site was reported in most animals (6/8) at day 1, which often impeded blinking (5/8). In all but one case, this was reduced by day seven. Minor swelling was still observed after 30 days in once case. Eye

movements were noticeably reduced in two sheep (2/8) but their condition improved rapidly during the recovery period. Eye redness was observed in five animals (5/8). Occasional discharge and/or mucus as well as light bleeding were observed at the canthotomy site early after surgery in three animals (3/8) but were without consequences and without evidence of infection. Three animals (3/8) experienced suture-related complications including localised irritation of the conjunctiva at one suture site, delayed conjunctival healing requiring additional sutures to be placed (3M#3) and canthotomy wound dehiscence was also treated by additional sutures on postoperative day eight (1M#1).

Fluorescein staining revealed localised corneal abrasions extending beyond the corneal epithelium, sometimes associated with corneal opacity, in seven animals (7/8). The severity of the abrasion extended from minor, superficial, punctate lesions to deeper lesions covering a large portion of the cornea. Up to four weeks were needed for full recovery. Corneal abrasion reappeared in one animal that underwent secondary surgery and required seven days to heal. One sheep (1/8) experienced postoperative corneal ulceration which was treated with topical antibiotics after which no further complications were found. Corneal abrasion and opacity were problematic for all imaging techniques, sometimes restricting the view of the retina, resulting in some missing assessment data.

Two orbital grommets (2/8) were observed to have dislodged from the orbitotomy. The first was identified during post-mortem dissection one month after implantation and had no further consequences. The second was observed during recovery surgery for a partial conjunctival extrusion recorded on postoperative day 56 (3M#3). During the same surgery, the VS required reattachment to the sclera. The sutures attaching the VS to the sclera were not broken, but the device was no longer attached to the sclera, suggesting that they had eroded through the scleral tissue. Revision surgery re-attached the device and grommet in position. During revision surgery, tissue was observed between the VS capsule and the sclera. The tissue was removed to allow the capsule to be sutured flush on the sclera. A sample of the tissue growth was fixed, stained with H&E and analysed by two veterinary pathologists to identify the type of tissue formed in response to the presence of the capsule. The tissue removed from between the implant and the sclera presented multifocal thickened stratified squamous epithelium with prominent underlying immature scar tissue comprised of a stellate to elongate monomorphic fibroblast population with a moderately myxomatous extracellular matrix including low numbers of scattered neutrophils. Focally there was a small aggregate of multinucleate giant cell

macrophages, presumably associated with the suture material at a previous suture site. The animal proceeded to the study endpoint without further complications. As a result of the observed dislodged grommets, remedial changes to the surgical procedure were applied in all surgeries that followed, providing supplemental grommet stability. The change and its effects are discussed below.

One animal (1/8) presented an elevated IOP of 35 mmHg in the non-operated eye on day 7. This value had been defined as the threshold from which medication would be considered and this event was therefore counted as an AE. With a single borderline value, the decision was made to delay treatment and the readings recovered below the threshold without intervention.

Post-mortem histological analysis revealed localised retinal detachments in three eyes (3/8) (see histopathology section for details) but there were no clinical signs of detachments or subretinal fluid during the *in vivo* observations (fundus or OCT). In two of the three animals, a red discoloration of the retina was also observed, one close to the optic disk and the other in the superior part of the retina (2M#1 and 1M#2, respectively). A small, localised suprachoroidal haemorrhage was suspected in both cases. Redness decreased over a week in one animal and remained unchanged in the other. Correlation between the location of the red discoloured areas and the detachments observed via histological analysis could not be confirmed.

All animals, with the aforementioned exception of 2M#2, progressed to the end of the study without further issues. Fundus imaging and OCT showed no signs of endophthalmitis, vitreous haemorrhage or expulsive haemorrhage. No signs of neovascularization or physical trauma of the retina were observed. There were no ocular infections.

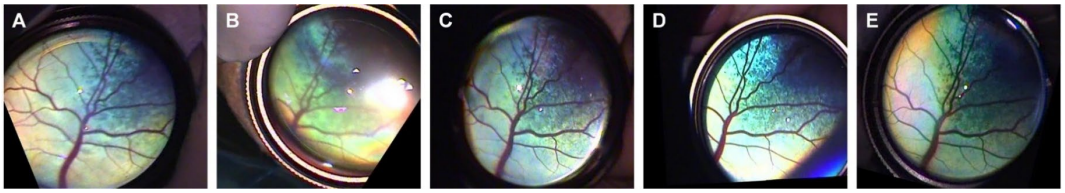

Figure 3-3 In-vivo retinal health evaluation. Fundus images of the operated eye of 3M#4 for the entire duration of the experiment. From left to right, (A) preoperative picture, (B) image acquired directly postoperatively, (C) one-month, (D) two-months and (E) three-months postoperative follow-up images. The contour of the electrode array is visible on the postoperative image but can no longer be detected after thirty days.

Figure 3-3shows a representative set of fundus images acquired preoperatively, directly postoperatively and at the one-, two- and three-months mark after implantation in 3M#4. The contour of the electrode array is visible on the postoperative image but can no longer be detected after one month. No signs of neovascularisation or haemorrhage can be seen. Localised retinal detachment is not visible on the images but was revealed during histology.

No AEs were recorded related to the TI.

One animal was diagnosed with hoof drop, a neurological condition which causes difficulties in weight bearing. The animal was treated with 2 mL Carprofen twice daily until the condition improved. The animal was able to fully bear weight within seven days. The condition is likely to have occurred due to static operative position in which the nerves of the leg may have become inflamed and was otherwise not related to the surgical approach or the implant.

3.3.2 Intraocular pressure

Pressure baseline for the study was established from both the eyes of four animals (16.8 ± 2.4 mmHg, mean ± standard deviation), which corresponds to reported values (16.36 ± 2.19 mmHg) [171]. Pressure variation from baseline was calculated for each eye by subtracting the baseline from the postoperative values. Wherever no individual baseline was available, the study baseline was used.

Overall, the pressure variations beyond the first week post-implantation were small and did not require any intervention or medication. The average day 1 absolute variation from baseline was 6.4 ± 2.9 mmHg (mean ± SD) for the operated eye and 7.6 ± 5.5 mmHg for the contralateral eye. Three operated eyes increased, two decreased and one remained stable (pressure difference ≤ 2 mmHg). IOP increased in all but one non-operated eyes.

Animals 2M#1 and 1M#2 (2/7), in which subretinal haemorrhages were suspected, had a decreased day 1 IOP in the operated eye, which is also consistent with the retinal

detachments observed histologically [172]. Note that the values recorded (9.7 and 11 mmHg) were above the value defined for ocular hypotony (5 mmHg or less [173]) in both cases. The contralateral eyes showed an increase in IOP of similar amplitude (5.3 and 6.6 mmHg) in both cases. Values recovered to baseline values within seven days.

High IOP (defined as adverse event if ≥35 mmHg) was measured in one animal (1/7) with a reading at 35 mmHg (baseline + 18.2 mmHg) in the non-operated eye of 3M#2 on day seven, following an elevated reading of 31 mmHg on day 1 (baseline + 14.2 mmHg). By day 30, the pressure had adequately recovered towards the baseline without external intervention.

3.3.3 Implant stability

3.3.3.1 Telemetry implant

The TIs were adequately positioned in a soft tissue pocket behind the ear for all animals (8/8). No displacements or any other AEs were recorded for this part of the implant system as confirmed by radiography or dissection. Tissue dissected at the end of the study revealed no abnormal tissue reaction to the presence of the implant in any animal.

3.3.3.2 Orbital grommet and visual stimulator

The stability and spatial position of the VS capsule were evaluated qualitatively using radiography and post-mortem dissection. The stability of the different components of the implant was also assessed during the secondary surgical procedure required in 3M#3.

During post-mortem dissection, a dislodged orbital grommet was observed in 1M#1, but it did not cause any harm. Movement of an additional grommet in the orbitotomy was seen when applying tension to the helical cable. Despite the absence of an adverse event, this fixation was considered as borderline acceptable. In sheep 3M#3, a dislodged orbital grommet and loose VS capsule were observed, the consequences of which are described above. The changes in the surgical protocol made to increase grommet fixation in later cases are discussed below.

In all other animals (7/8), the parts of the visual prosthesis located inside the orbital cavity appeared stable (Figure 3-4).

A detailed pathology assessment was made during post-mortem dissection in the three-months trial group. It revealed no signs of infection, neither in or around the orbit, around the helical cable or the TI. Fibrous encapsulation was deemed appropriate and as expected for all animals, with a comparatively increased fibrous layer around the surgical wounds

in the sheep which underwent revision surgery on day 56. The observed fibrous capsules were smooth and contributed largely to the stability of the VS capsules, sometimes rendering sutures redundant. No extensive fibrosis was observed between the VS capsules and the sclera. All scleral wounds showed appropriate healing.

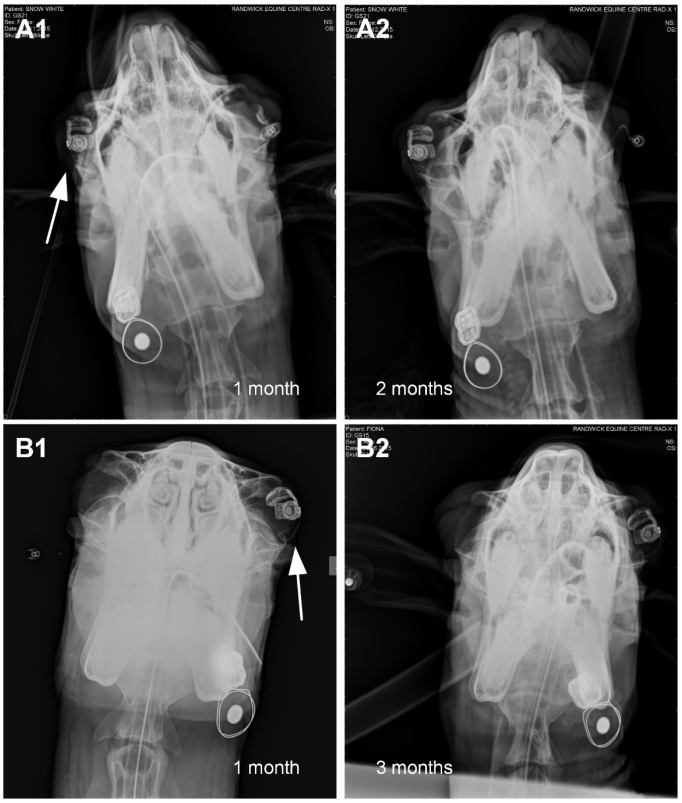

Figure 3-4 Implant stability. Radiographs showing the position of the Phoenix[99] bionic eye with the behind the ear TI and the VS connected via the helical wire. A1 and A2 compare the device position at one and two months, respectively, in 2M#1 in left posterior oblique view. B1 and B2 show the device after one and three months in 3M#2 (ventrodorsal view). Slight variations of the angular and spatial position of the implant relative with bony landmarks are attributed to the freedom of eye movement provided by the implant system, as well as different head positions during imaging. Arrows point towards the VS and electrode arrays in the left eye of the animals.

3.3.4 Suprachoroidal electrode array

To evaluate the position and stability of the electrode array, indirect ophthalmoscopy and infrared images were used. As described above, several factors including corneal opacity, directional orientation, and the experimental nature of the infrared imaging approach resulted in variable image quality for both techniques. For some animals, useful images

could not be successfully acquired at some planned time points. The full set of infrared images is shown in Figure 3-5 and reveals the variability of the image quality as well as the missing datapoints. Fundus images only were used wherever infrared imaging was not viable.

In most animals, the implant contour could be identified on the fundus images directly postoperatively due to a temporary disruption of the retinal anatomy, as discussed in the OCT section. In all but one animal (3M#1), the implant contour could no longer be identified at one month. With ophthalmoscopy, a dark irregular shaped area was often observed in the same quadrant as the implant. This was due to the known asymmetry of the tapetum fibrosum in the sheep [174] and should not be confused with the shadow of the implant.

Aligned and scaled infrared images of each animal revealed no discernible change in array positioning throughout the study (Figure 3-5). This was evaluated by drawing the contour of the implant tip onto stacked images to facilitate visual comparison. The resolution of the images, although variable, generally allowed for the identification of blood vessels which could be used as landmarks to compare the position of the implant between imaging modalities.

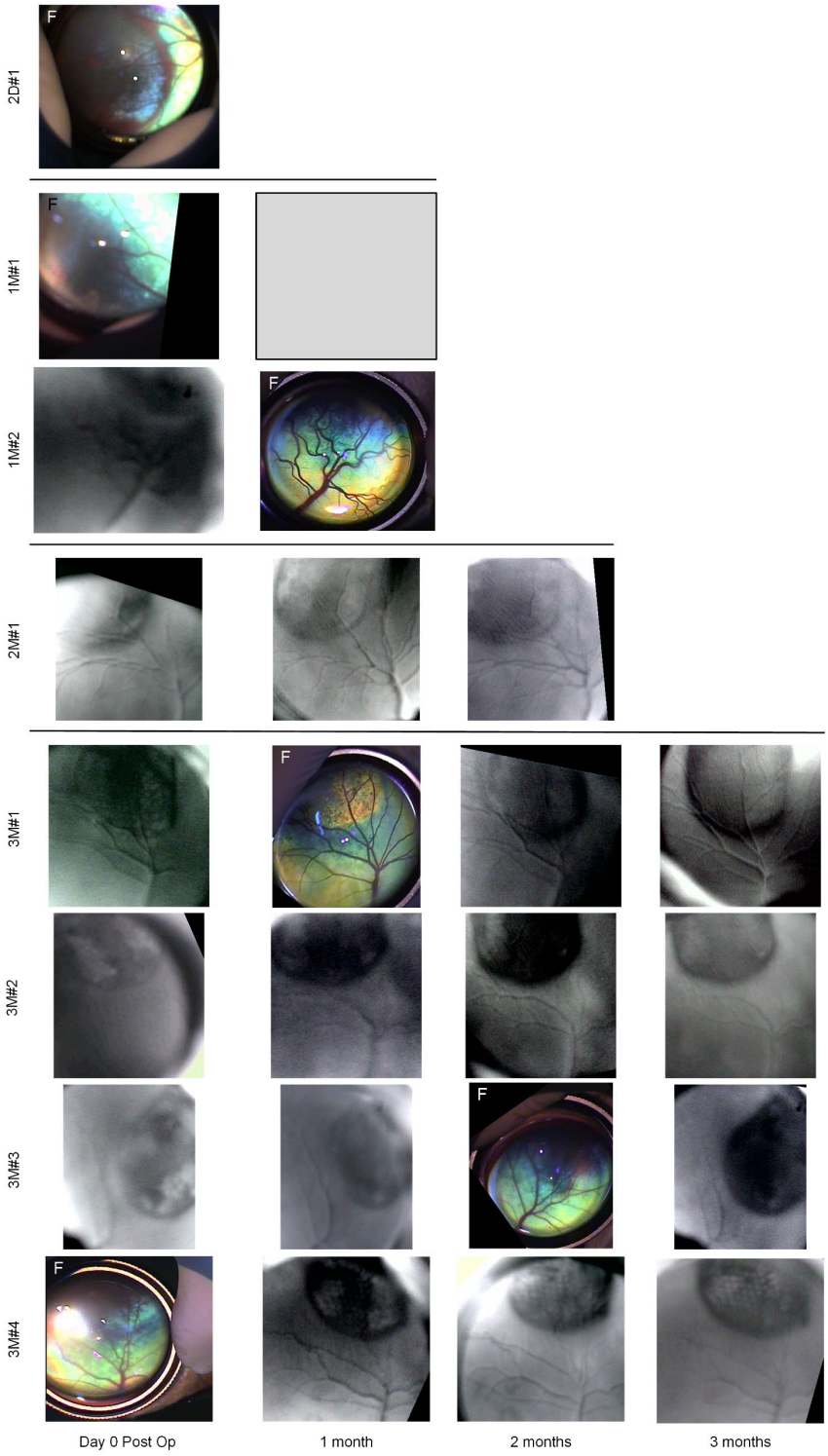

Figure 3-5 Infrared imaging. Full set of infrared images acquired for all animals, complemented by fundus images where useful infrared images could not be obtained. From left to right, images acquired postoperatively on the day of surgery, one, two and three months post implantation. The animals were grouped by experiment duration with increasing experimental duration from top to bottom.

Figure 3-6 shows two representative examples of the complementary fundus and infrared imaging techniques. By correlating blood vessel landmarks, the position of the implant can be verified on the infrared image while retinal health over the implant can be assessed even when the implant outline was not visible.

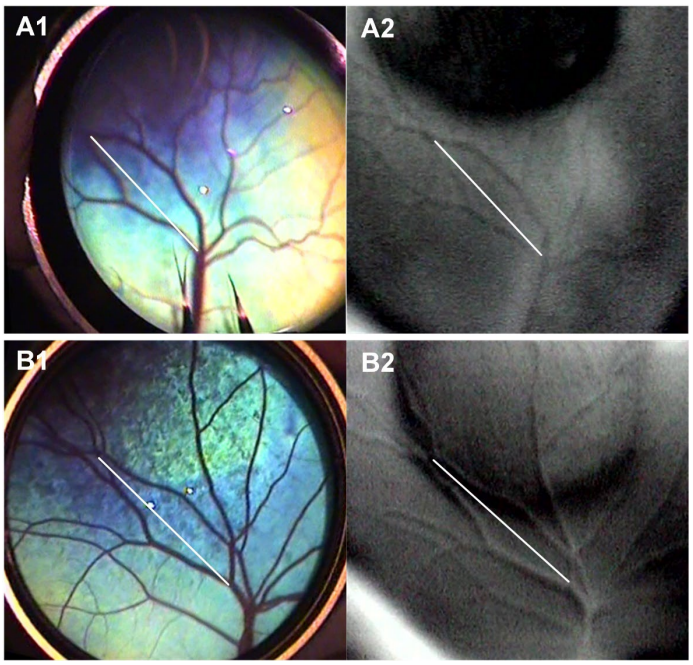

Figure 3-6 Ophthalmoscopy and infrared imaging. Complementary fundus and infrared images for 3M#2 after two months (A) and 3M#1, three months after surgery (B) aligned using blood vessels as landmarks (white lines used as input for automated scaling and alignment in Fiji). The representative examples of the cohort show how fundus images allow observation of the health of the retina and indicate the absence of neovascularisation or haemorrhage while the infrared pictures allow for the localisation of the electrode array with reference to blood vessels.

3.3.5 Optical coherence tomography (OCT)

OCT images of the implant site were acquired for each of the animals in the three-months group (3M#1, 3M#2, 3M#3 and 3M#4). On some images a small step over the edge of the implant was visible, as seen for example in Figure 3-7. Note the different scales on the X and Y axes, which magnify the stepped appearance of the transition.

No signs of retinal detachment, haemorrhage, retinal degeneration or neovascularization were seen on the OCT images. The blood vessels and all retinal layers were well preserved in all OCT rasters. The electrode array was visible under the retina in some images and coincided with the observed retinal step. In Figure 3-7, a combination of OCT,

fundus and infrared images is shown for 3M#2 (top). The location of the viewed OCT slice and intersection with the blood vessels are shown with a white line in the corresponding fundus and infrared pictures. High resolution OCT rasters could be acquired but did not permit reconstruction of the exact location of the slice. An example is shown in Figure 3-7.

Like fundus and infrared imaging, OCT acquisition was sometimes difficult due to corneal opacity. Difficulties experienced during imaging did not allow for clear and focused OCT rasters on days 60 and 90 for 3M#3 and on day 90 for 3M#4.

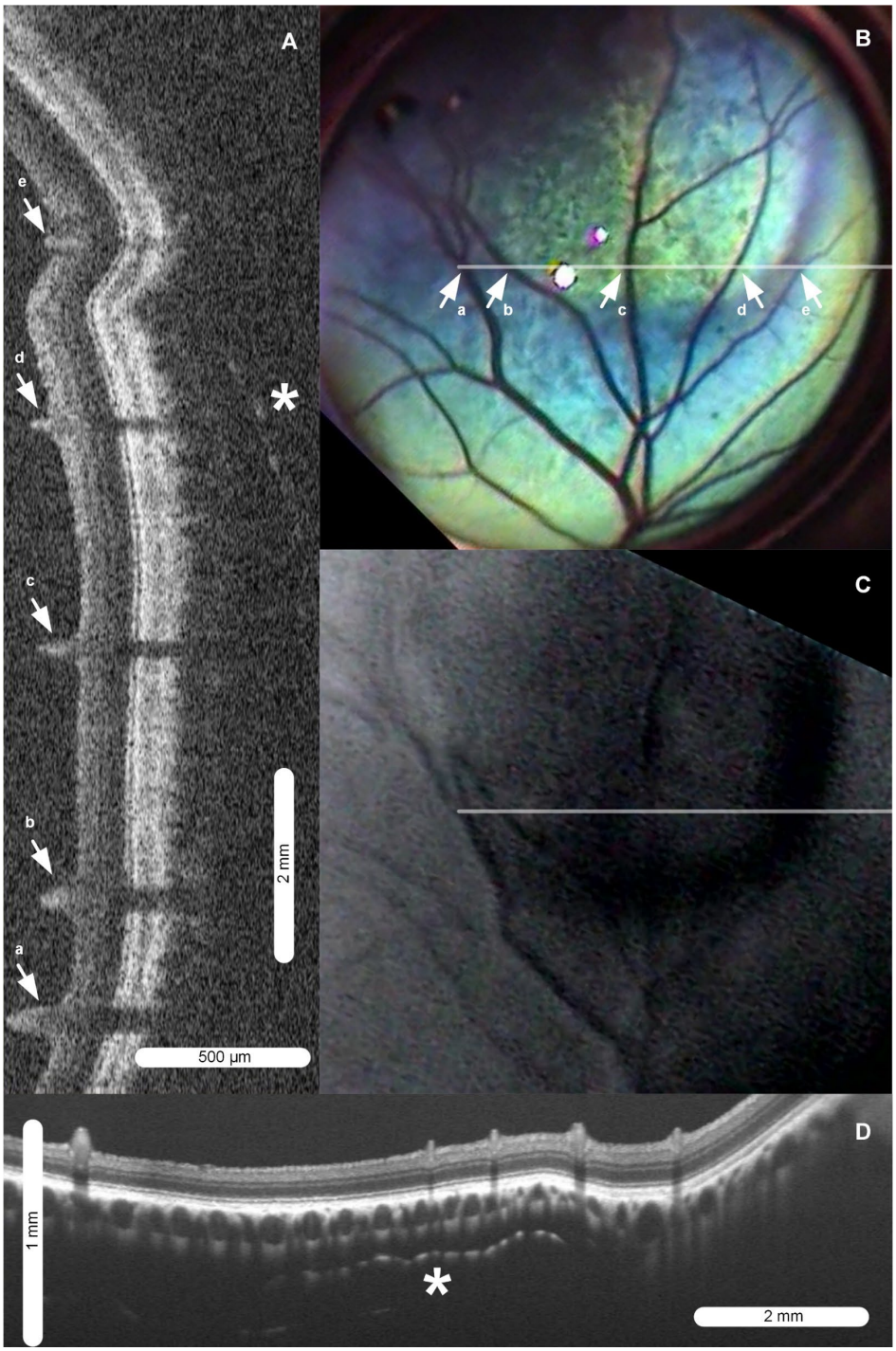

Figure 3-7 Optical coherence tomography. A) Low resolution OCT frame of 3M#1 after two months showing the electrode array under the choroid (*), B) and C) fundus and infrared images of the same animal on the same day. The location of the OCT raster is shown with a semi-transparent white line. In B), the location of the blood vessels shown in A are highlighted (a-e). D: 3M#2 Two-months high resolution OCT-raster without accurate location correspondence, stars show location of the electrode array.

3.3.6 Histopathological assessment and scoring

H&E stained tissue sections were analysed and graded according to the scale in Table 3-1. Post-mortem, processing-related retinal detachments in the eyes of three animals (2D#1, 1M#1 and 3M#1) resulted in no tissue suitable for histological assessment. However, representative samples of the three chronic study groups were available for analysis. The contralateral eyes of sheep 1M#2, 2M#1 and 3M#2 were used as controls. To minimise the total number of animals being used, the remainder of animals were shared in a separate study that required surgery on the right eye. These shared eyes were thus excluded from the control group of the study reported herein. A total of eight eyes were processed and analysed, including three controls and five implanted eyes with experimental durations of one (N=1), two (N=1) and three (N=3) months. A summary of the histology grades is presented in Table 3-3. Tissue encapsulation of the electrode array was not observed for any of the extracted arrays, suggesting that any fibrotic or inflammatory response in the tissue was seen with the histology.

In all analysed eyes (5/5), a pocket was clearly observed at the location of the implant (device removed prior to histology), in the suprachoroidal space (Figure 3-8). The highest level of fibrosis of the study, however mild (fibrotic layer approximately 5-6 cells thick), was seen in the eye of sheep 1M#2 and was graded a '3'. Apart from the two-months animal, which was fibrosis-free, all other samples were grade '2' in at least some sections, with fibrous connective tissue approximately three to four fibrocytes thick. Overall, fibrosis was predominantly detected adjacent to the ends of the implant pocket in the suprachoroidal region (Figure 3-8).

1M#2 and 3M#2 presented the strongest inflammatory response of the entire cohort and were graded '3', with moderate numbers of scattered phagocytic cells within the space vacated by the implant and lining the implant margins and occasional multinucleated macrophages. In the other animals, phagocytic cells were rare or in small numbers and multinucleated macrophages were not present (grade '1' or '2'). See Table 3-1 for details. Examples of grade '2' fibrosis and grade '3' inflammation are shown in Figure 3-8.

Retinal thinning/remodelling was rated as 'none' or 'mild' in all but one implanted eye (4/5), which had 'Moderate' retinal damage, including a reduction of the outer nuclear layer and retinal ganglion cell (RGC) layers. Localised retinal detachments were observed in three eyes (3/5) with measured detachment lengths ranging from 370 to 1250 μm. In all cases, the retinal detachment was made apparent by retinal pigment epithelium (RPE) hypertrophy, as opposed to artefactual detachments which do not show changes in RPE.

The thickness of the detached retinal segments could be measured in two samples (2/3). In 2M#1, the detached retina suffered artefactual damage during processing and its thickness couldn't be adequately determined.

In 2M#1 the retina measured at the edge of the device was significantly thinner than elsewhere along the body of the array ($P<0.0001$). This observation was most likely due to the region of interest being close to the transition from visual to non-visual retina, which shows a gradual thinning towards the periphery of the eye (ora serrata). Due to the normal anatomy of the retinal layers, a retinal health score of '0' was given to this eye. 1M#2, 3M#2 and 3M#3 had 'Mild' thinning/remodelling with a mild loss of layers and slight decrease in cellularity, particularly the photoreceptor segment. In 1M#2, this was observed in the segment of detached retina and the remaining sample did not show signs of retinal degeneration (Figure 3-8). The mean thickness of this segment was also thinner than the rest of the sample (difference between means ± SEM: 36.3 ± 9.3µm, $P=0.0002$) but this wasn't apparent when comparing the tissue directly adjacent to the detachment. Relatively thin retina was also observed close to the implant edges ($P<0.0001$) but similarly to the 2M#1, the proximity to non-visual retina is likely to explain this observation.

There was no evidence of retinal detachment in 3M#2 and 3M#3 and the edges of the array did not cause thinning. The edge of the array of 3M#2 was neighbouring a segment retina thicker than the average ($P=0.005$). The thickness appeared mostly influenced by a relatively thick nerve fibre layer (NFL), which was consistent with the neighbouring NFL and within the range measured in the other samples. There was no significant difference between the areas of interest in 3M#3 ($P=0.3243$). One animal, in the three-month experimental group (3M#4), presented a 1250 µm retinal detachment which coincided with 'Moderate' thinning and remodelling of the neural tissue. The segment was significantly thinner than the rest of the sample ($P=0.0118$). The edges did not significantly affect the retinal thickness ($P=0.0873$).

H&E stained sections indicated no identifiable differences in cellularity of control or experimental retinas, but did not provide clear evidence of gliosis or other changes to the retinal glial cells. Retinal thickness was used as a proxy marker for retinal changes, and most importantly, no major degenerative changes were seen for retinas for the entire cohort. In order to further assess the effects on astrocytes and Müller glia activation, microglia/macrophages and inflammatory responses, immunohistochemistry was also performed.

A combination of GFAP and LM-opsin immunostaining showed there was no obvious degeneration in the photoreceptor layer, nor evidence of gliosis for all sections examined. This included sections of retinal tissue overlying the edges of the suprachoroidal array pocket as well as across the body of the implant. GFAP immunostaining was localised to the astrocytes within nerve fibre layer, with processes within the ganglion cell layer, consistent with minimal gliosis and lack of Muller glia activation across the implant pocket for all retinas examined (Supplementary figure). Activated Müller glia GFAP expression typically extends across the retinal layers, to the outer retina, with hypertrophic processes extending between photoreceptors and RPE; this was not observed in any experimental eyes. Additionally, there was no noticeable difference in the presence of Iba1+ cells within the retina across the body of the electrode array as shown using immunofluorescence, with most Iba1+ cells localised to the inner plexiform/inner nuclear layer (Supplementary figure). Quantitative analysis of immunoperoxidase stained retinas [175] showed no significant difference in average Positivity (percentage of positive pixels to the total number of positive and negative pixels) between the controls and the three-month group, but the latter showed a much wider range of pixel positivity values (control: 0.3221 % ± 0.01681, three months: 0.5174 % ± 0.4249, mean ± standard deviation, supplementary figure). 3M#2 presented an increased score in the implanted eye versus its contralateral control. Even in this animal, which presented the highest Iba1+ Positivity ratio of the cohort, Iba1+ cells did not infiltrate the outer nuclear layer and minimal thinning and remodelling of the retinal layers were observed, as described above (supplementary figure, *A high-resolution version of this slide for use with the Virtual Microscope is available as eSlide: VM06308*). In the choroid, where the implant was inserted, Iba1+ microglia/macrophages were observed around the implant region consistent with a low-level inflammatory response observed within the histological sections (described above), but no overall effect on retinal structures.

Kendall's correlation coefficient between the three study groups with durations of one, two and three months showed a moderate monotonic relationship may exist between the duration of implantation and the retinal response (τ=0.429), although this was not statistically significant (P=0.35).

All controls were free of fibrosis and inflammation, and all were negative for retinal damage and detachment. Haemorrhage was absent in all samples and no other types of pathologies were observed.

Table 3-3 Histology grades. The contralateral eyes of sheep 1M#2, 2M#1 and 3M#2 were used as controls and were all free of fibrotic and inflammation, and presented no retinal thinning, remodelling or detachment. No signs of suprachoroidal haemorrhage were visible in the samples. The eyes of 2D#1, 1M#1 and 3M#1 were missing for histopathological analysis for technical reasons.

Eye	Experimental duration [Days]	Host response		Retinal health		Detachment length [µm]
		Fibrosis	Inflammation	Thinning/remodelling	Detachment	
Controls	**0**	0	0	None	Absent	-
1M#2 Left	**32**	3	3	Mild	Present	670
2M#1 Left	**60**	0	1	None	Present	370
3M#2 Left	**91**	2	3	Mild	Absent	-
3M#3 Left	**93**	2	2	Mild	Absent	-
3M#4 Left	**100**	2	1	Moderate	Present	1250

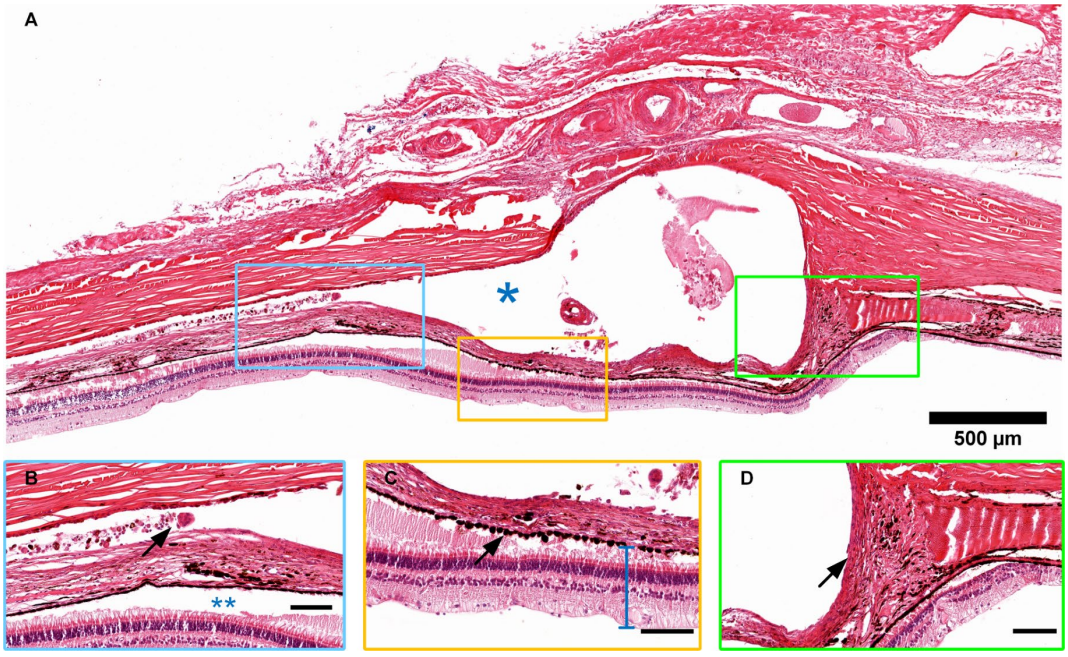

Figure 3-8 Histopathological assessment and scoring A) Low magnification of the implant site in 1M#2 (space vacated by the implant is indicated by an asterisk). B) shows an example of grade 3 inflammatory response (arrow) and artefactual retinal detachment due to processing (double asterisk). C) Hypertrophied retinal pigmented epithelium (RPE) indicating non-artefactual retinal detachment (arrow) and example of retinal thickness measurement location D) shows a higher magnification of the end of the implantation site with an example of grade 2 fibrosis (arrow). Scale bars: 100 µm unless specified otherwise. ***A high-resolution version of this slide for use with the Virtual Microscope is available as eSlide: VM06308***

3.4 Discussion

A safe surgical procedure resulting in the stable positioning of a biocompatible implant is one of the keys to success for the bionic eye. The protocol used during this study was developed over more than a decade using animal and human cadavers and is now well-established. Similar approaches have been used and their safety and efficacy demonstrated during chronic implantation in humans, for implants featuring a suprachoroidal array connected to a behind the ear transcutaneous plug [45, 176]. The experiment described here was the first *in vivo* application of this procedure with a fully implantable device.

All surgical procedures were successful, resulting in adequate spatial positioning of the device without major intraoperative AEs. Remedial procedure changes were successfully implemented to increase the long-term stability of the orbital grommet and VS. There were only three intervention-related SAEs over the course of the entire study, which required secondary surgical intervention, mainly to place additional sutures.

The use of biostable and biocompatible materials caused only a mild cellular response in the suprachoroidal space and the retinal tissue was adequately preserved during the long-term implantation of the Phoenix^{99}, demonstrating the biocompatibility of the device.

3.4.1 Surgical protocol and implant stability

Intraoperatively, two suspected and one verified suprachoroidal haemorrhages were reported. A comparatively thin sclera in an animal used for early development, as well as a manipulation error (accidental over-insertion of the introducer tool in the suprachoroidal pocket) were identified as causes. In another sheep, a discoloured retina showed no changes over time and did not suffer from any further AEs, suggesting that the discoloration may have been present prior to surgery. The retinal haemorrhages reported here can be considered as minor with limited long-term effects, as confirmed histologically. Furthermore, during a clinical study employing a similar surgical approach and suprachoroidal electrode array, Ayton et al. [45] reported subretinal and suprachoroidal haemorrhages in all (3/3) human subjects. All resolved without further sequelae and did not influence the ability of the device to deliver electrical stimulation to the retina. There are no reasons to expect that a haemorrhage of this type would have more severe effects with a fully implantable device than with the partially implantable device used in the Ayton study. These events nonetheless demonstrate the importance of a well characterised, reproducible surgical procedure and the correct microsurgical

instrumentation to facilitate electrode array insertion and to minimize the manipulation of sensitive ocular tissue such as the retina.

Recovery was overall uneventful for most of the animals. Minor, treatable post-surgical AEs were recorded such as weeping wounds, mild bleeding or red eyes and one case of wound dehiscence. In humans, these events are expected to be easier to follow and treat, as feedback about any complication can be readily shared and understood.

The most significant events were related to the stability of the orbital grommet. In two early animals, the orbital grommet dislodged from the orbitotomy. During the study, measures were taken to improve grommet stability. In the first five sheep, the orbitotomy was made at the level of the zygomaticofrontal suture and secured by a press-fit of the silicone grommet in the orbitotomy only. The protocol was revised to the current technique for the last four surgeries and included an orbitotomy located 2 mm above the zygomaticofrontal suture, as well as additional stabilisation through the suturing of a connective tissue flap on the grommet. No dislodged orbital grommets were seen in animals which underwent the revised procedure. We recommend the use of the flap technique for any future chronic implantation (human or animal) of devices. Additionally, excess tension in the helical cable may have aggravated the grommet stability issues. It occurred when the TI was implanted before the VS and placement of the orbital grommet. The protocol was revised after the fifth sheep to allow for better management of the cable slack. This consideration may not apply to humans, due to differences in their anatomy.

Further changes were made to the surgical protocol to prevent the VS capsule separating from the sclera. Two sutures per eyelet were used when securing the VS to the globe to increase its stability until the fibrous encapsulation rendered the sutures redundant. The post-mortem dissection after three months revealed that the sutures were already redundant or partially redundant in all sheep (4/4). It can reasonably be expected that a similar process of encapsulation will take place in humans as well, further ensuring capsule stability.

A dislodged orbital grommet and subsequent loose VS, which resulted in conjunctival erosion, was the most severe device-related AE in the study. The updates to the surgical protocol make the reoccurrence of these issues unlikely, as demonstrated by the positive results after implementation.

Addressing the need for assessing the stability of the electrode array throughout the course of the study, the development of a device for the acquisition of the infrared images

occurred in parallel to this study. Accordingly, some of the limitations in quality, resolution and number of images that could be acquired is linked to this process. The images that could be acquired proved very useful to verify the position and stability of the implant when the outline of the implant was no longer visible in the fundus images. Using the available tools, spatial stability of the electrode array was demonstrated in all animals, even in the animal where the VS was detached from the sclera (Figure 3-5). The observed stability of the electrode array close to the tissue targeted by electrical stimulation, is very encouraging with regards to a clinical application of the device.

Corneal abrasion and corneal opacity concerns were common events during this study. Despite the care taken to keep the cornea well hydrated during surgery, it may have been insufficient. The sheep were observed to have difficulty blinking postoperatively due to swollen eye lids and this is likely to have increased their susceptibility to corneal abrasion. Lubrication should be used intensively intraoperatively and postoperatively to avoid dehydration and abrasion of the cornea. Tarsorrhaphy should also be considered as an aid to alleviation of this concern.

In the sheep model, the superior rectus muscle was sectioned because its broad insertion interfered with access to the sclera. This step may not be required in humans due to the planned superotemporal position of the device, between the superior and lateral rectus muscles, as well as further anatomical differences. The superior rectus was re-sutured on a case-by-case basis during the first part of the present study. In two animals in which it had been re-sutured over the scleral wound, diminished or absent eye movements were observed, compared to animals in which the rectus muscle was not re-sutured. Although improvements were observed with 14 days, the surgical protocol was adapted accordingly, and the muscle was not re-sutured in the following animals. The change in surgical protocol led to apparent better eye mobility. This is counterintuitive and further investigation would be required to identify the causes. Nevertheless, it is unlikely that observations made in sheep about eye mobility in the presence of the implant would be replicated in humans. If severing the muscle is required, and unless proof of deleterious effects of muscle reattachment can be obtained, the rectus muscle should be re-sutured to the sclera, to preserve normal ocular motility in humans.

3.4.2 Ocular and cellular health

There were no cases of intervention-related ocular hypertension, which could place the implant recipients at risk to develop other pressure-related pathologies such as glaucoma.

The only IOP-related AE was a transient high pressure in the non-operated eye, for which we lack an explanation. The absence of hypertension is a very encouraging result in the context of devices designed for long-term implantation.

Clinical evaluation of the implanted and control eyes using ophthalmoscopy, infrared imaging and OCT revealed no significant impact of the surgery or presence of the implant on the retina. Despite the absence of *in vivo* evidence, small (<1.5 mm) segments of retinal detachment were seen during histopathological assessment in three sheep. An expected higher degree of retinal thinning and remodelling was observed in detached areas [177], yet the disturbance of the inner retinal layers observed was moderate even after three months, with no evidence of retinal gliosis, suggesting that the detached segments did not cause an ongoing inflammatory response and may have occurred intraoperatively or early during the postoperative recovery period. Additionally, this may suggest that eyes that were free of detachments may not have developed detachments later on. Astrocyte/Müller glia patterns of GFAP immunolabelling across the implant pocket and surrounds were similar to those seen in normal retina. This was consistent with observations in a porcine retinal implant model [144]. Outside the detached segments, thinning and reorganisation was limited to the outer retinal layers, which are likely to be highly remodelled in human patients blinded by RP [151].

The recent report on porcine subretinal implants showed increased retinal Iba1+ cells in regions of the implants. Nonetheless, it was concluded that this observation was linked to the initial response to surgical procedures and followed by an adequate retinal recovery [144]. The device presented here is positioned in a tissue pocket between the choroid and sclera, and physically separated from the retina by the choroid. Minimal retinal disruption may be expected, consistent with the observed low numbers of Iba1 positive cells within the outer nuclear layer and the retinas.

A limitation of the study is the lack of information about the localization of the exposed Pt electrodes versus silicone rubber body of the array. Identification of the areas of exposed electrodes wasn’t possible during the histological processing of the tissue. Adequate methods for the tracking of individual electrodes would be beneficial to evaluate more specifically the effects of the active versus passive Pt electrodes in future studies

Non-parametric statistical analysis showed that there may be a monotonic relationship between the severity of the retinal remodelling and the duration of the experiment,

although the statistical significance of this result was limited due to the small sample size. Overall, the data presented here suggests that most changes in the retina, including detachments, and all tissues surrounding the implant happen within the first month post-surgery. After that, the implant site stabilizes between the end of the first month and at least until the end of the third month. Demonstrating the biocompatibility of the device, the stabilization of the host response and retinal reorganisation beyond the first postoperative month is very encouraging for a clinical application.

3.5 Conclusion

This study included the implantation of nine passive Phoenix^{99} Bionic Eyes in an ovine eye model for up to 100 days and demonstrated the safety and effectiveness of the proposed surgical procedure. Few SAEs were observed and remedial changes to the initial surgical protocol were successfully implemented to further improve device stability and long-term outcomes. The biocompatibility of the device was demonstrated, as shown by the absence of infection, neovascularization, or histological evidence of tissue degeneration. Overall, the host response to the surgery and device was mild, owing to the use of biostable and biocompatible materials. Inner retinal layers, particularly the RGC layer, on which electrical stimulation relies for the transmission of the stimuli to the brain were preserved adequately.

The system, although designed for humans, was well tolerated in the ovine model. The encouraging results in the sheep are likely to translate to a positive outcome in humans. This safety study represents a critical step towards the clinical demonstration of the potential for the Phoenix^{99} to restore a sense of vision for people with retinal degenerative diseases and will represent a critical baseline to which chronic studies of stimulation safety can be compared.

On the way towards these crucial experiments, which will strongly influence the clinical fate of the implant, refining the methods for electrophysiology experiments to minimise the confounding factors is a welcome initiative.

4 ANAESTHETIC REGIME OPTIMISATION

ANAESTHESIA PROTOCOL SELECTION AND REFINEMENT TOOL FOR CORTICAL ELECTROPHYSIOLOGY EXPERIMENTS IN ANIMAL MODELS

4.1 Introduction

Electrophysiology experiments studying cortical network activity are complex. Measuring biopotentials can seem an art as much as a science. Capturing the small electrical signals from intricate neural networks to understand their mechanisms and interconnections, or explore therapeutic techniques is a challenging task in itself. To establish unequivocally whether two variables are correlated, researchers must isolate them from all other variables and aim to avoid confounding factors. In systems as complex as living animals, excluding uncontrolled variables entirely is impossible. Yet much can be done to minimise their number and their effects.

Nociception describes the process by which noxious stimulation is communicated through the central nervous system. In conscious animals, this leads to the experience of pain [178]. Therefore, for ethical reasons, the use of appropriate anaesthesia *and analgesia* are essential whenever potentially painful interventions are undertaken in live animals. Notably, not all anaesthetic agents provide analgesia, for example isoflurane, and nociception can still occur. It is well established that nociceptive inputs can create profound physiological changes and hence confounding factors. Therefore, analgesia is also essential for animals undergoing invasive procedures under anaesthesia. Similarly, the physiological effects of general anaesthesia is a common cause of confounding factors that can interfere with results of scientific studies [179].

Fortunately, the influence of both anaesthesia and nociceptive inputs can be modulated. Carefully designed anaesthetic and analgesic protocols can offer a high level of control over undesired physiological disturbances. All anaesthetic agents cause dose-dependent alterations and suppression of cortical activity. However, some agents cause significantly

less cortical depression at relevant doses for appropriate depths of anaesthesia [180]. Careful selection of the drugs used for such experiments may therefore strongly influence the research outcome. Additionally, balanced anaesthesia, during which multiple anaesthetic and analgesic agents are used in combination, is an effective approach to minimise the adverse effects of drugs [181].

Anaesthesia is typically achieved with either inhalational techniques where anaesthetic is continuously breathed in, injectable techniques where drugs are continuously or intermittently administered, or a combination of the two. In a balanced protocol, the use of injectable analgesics and/or sedatives can significantly reduce the required dose of the anaesthetic agent (gaseous or injectable). Hence, balanced protocols can be used to minimise the undesired effects of individual anaesthetic agents [182] and to provide favourable conditions for studying cortical activity [180]. Despite its widespread use in human and clinical veterinary settings [181] [183], this method is rarely reported for experiments involving cortical electrophysiological recordings in animals.

Considerable efforts are being made towards understanding the effects of anaesthetic agents on cortical activity. Sorrenti *et al*. recently published a comprehensive review of these effects on electrophysiology experiments [66]. Despite the growing body of knowledge in the field, there appears to be no consensus with regards to the choice of an ideal anaesthetic regime for cortical electrophysiology experiments.

Additionally, as described by McMillan: "[…] anaesthesia can often be viewed as a means to an end; a necessary step performed merely to facilitate the performance of another procedure" [184]. As a result, the importance of reporting and discussing the choice of anaesthetic protocols and monitoring techniques, and their potential effects on the results of *in vivo* experiments is often overlooked [185]. However, accurate reporting of the anaesthetic and analgesic protocols is a requirement to meet the ARRIVE guidelines for reporting of animal research [186]. This requirement presents an opportunity to improve the accuracy of experimental outcomes, animal welfare, reporting quality and reproducibility of electrophysiology experiments in animal models. Indeed, protocols deemed unsuitable for anaesthesia in humans and animals (ref – link 1 and link 2) due to the reported increased risk of awareness under anaesthesia [187, 188] continue

to be used in animal research protocols[7]. It is our hope that by highlighting alternative protocols that include true hypnotic agents, we may raise awareness of protocols that can be reliably used for electrophysiological experiments while significantly reducing the chance of animals being aware during experimental conditions.

To facilitate and standardise the selection of balanced anaesthetic protocols, our team has developed a methodology suitable for the preparation of projects using a wide range of animal models and involving teams with specific skill sets. The result is an 'anaesthesia and monitoring selection and refinement tool' which provides information on anaesthetic techniques, drugs, and monitoring, as well as equipment- and skill-based decision trees applicable for research involving animal models. Finally, practical inventories of required articles are provided to assist with the preparation of experiments.

The tool was developed around anaesthesia maintenance techniques and drugs, with the assumption that electrophysiology recordings are performed sufficiently long after induction. The effects of anaesthesia are then expected to be driven by the maintenance drug protocols. Different techniques were rated according to their ability to provide physiologically stable animals in which anaesthetic depth can be quickly and reliably adapted. For this reason, total intravenous anaesthesia (TIVA) was prioritised for large animals. When referring to large animals in this chapter, the specific focus was on commonly used species such as sheep, pigs and cats. Other large animal models may require management protocols to be adjusted based on the species and the drugs available. Despite this, following the principles outlined in this chapter should allow the user to prepare a robust protocol that will likely maximise results while ensuring animals remain as physiologically stable as possible. In small animal models such as mice and rats, TIVA is seldomly reported [189]. Because the present work intends to provide solutions which rely on a solid base of literature, and even though TIVA is expected to provide similar benefits in small and large animals, balanced inhalant anaesthesia is recommended for rodent models. Other commonly used anaesthetic techniques were also included to provide more flexibility where TIVA may not be practical, including partial intravenous anaesthesia (PIVA), balanced inhalant anaesthesia (BInhA), where the dose of gaseous

[7] Examples of such protocols include sufentanil or nitrous oxide combined with a neuromuscular blocking agent. Indeed, there is an increased risk of awareness under anaesthesia when these agents are not combined with inhalational or injectable anaesthetic agents (e.g. isoflurane or propofol).

agent is minimised by injecting analgesics and/or sedatives. Finally, balanced injectable anaesthesia (BInjA) should be considered, where the dose of injectable anaesthetic is minimised by combining them with analgesics and/or sedatives.

Inventories of essential equipment, skills, and consumables to allow delivery of modern, effective, and safe anaesthesia were created for small and large animal models. Completing the essential requirements inventory was considered a go/no-go gate in the anaesthesia refinement process. The availability of specific items and skills required to perform the proposed anaesthetic techniques, were then used as decision points to guide the user, based on their own facilities and team skill set. Furthermore, summary tables about the different techniques, as well as the known effects of different drugs were assembled from the literature to help the user refine their decisions.

Due to the importance of monitoring to adjust anaesthetic depth and guide the maintenance of physiological stability, and thereby control potential confounding factors, we also devised detailed checklists and guidelines with regards to the use and role of monitoring equipment. Finally, the tool was complemented with a section, including resources, to encourage users to develop, adapt or use checklists when performing anaesthesia. Indeed, checklists have a widely proven positive effect on anaesthetic safety [184].

Because of its vital role in ensuring animal welfare, anaesthesia planning and execution is a crucial task in any animal experiment. In electrophysiology experiments, proper preparation and training of the staff responsible for the anaesthesia may be even more important due to how sensitive cortical readings are to both anaesthetic agents and physiological derangements. Ideally, at least one person should be fully dedicated to anaesthesia and monitoring for the duration of the experiments.[13]

To ensure that the role and effects of the chosen anaesthetic protocol (technique, drugs, and dosages) are understood by all stakeholders, the tool should be used well in advance of commencing experiments. The whole team should be involved and transparent communication about skills and knowledge encouraged. Training should be organised where adequate proficiency cannot be guaranteed. Similarly, monitoring equipment should be operated by skilled personnel who are able to interpret readings and react appropriately. It is strongly recommended to involve veterinary and/or health professionals for any required training to increase the level of multidisciplinary expertise in planning and performing anaesthesia.

The present methodology does not aim to provide an exhaustive list of possible protocols. Instead, it focuses on the demonstrated benefits of balanced anaesthesia and drugs with a strong reputation in clinical veterinary practice. The anaesthesia refinement and selection tool assumes that the user has access to controlled (classified as Schedule 8 drugs in Australia) drugs, being mostly opioids for their role in minimising the required dose of anaesthetic agent and for provision of analgesia. Other protocols may need to be applied if opioids are unavailable and specific veterinary advice should be sought.

Using the 'anaesthesia and monitoring selection and refinement tool', we propose a propofol-morphine-isoflurane PIVA for extended electrophysiology experiments in sheep. We report two physiologically stable animals over 12:45 and 13:45 hours and strong cortical responses during bright flash visual stimulation.

4.2 Anaesthesia selection tool

Anaesthesia is a multi-facetted discipline: technique and drug selection; dosage calculations; safe induction and maintenance; monitoring and, if applicable, recovery of the animal. The tool described in the present article was designed to assist researchers in navigating some of the key anaesthesia-related factors that may influence the success of cortical electrophysiology experiments. The information provided, flowcharts and tables were built to be comprehendible by people with varying levels of expertise on the topic of anaesthesia, to foster discussions within the – often multidisciplinary – teams, during the planning phase of cortical experiments to enable information sharing and alignment of goals to maximise the scientific outcome.

4.2.1 Overview

The anaesthesia selection tool was designed to be a sequential process. Figure 4-1 shows a high-level overview of the proposed process, which is supported by concrete inventory checklists. The inventory checklists should be filled out as the user progresses through the steps of the chart. Figure 4-1should be used as the overall guide to the process as it contains the pointers to the individual charts and tables that should be used at each step.

The purpose of the tool is to serve the experiments and maximise their outcome, rather than influence the experimental design. Accordingly, the process described here assumes that decisions have already been made with regards to the animal model, the intervention (including surgical procedure), and that the experiment has been designed up to the details of the anaesthetic protocol. Using the pre-established parameters, such as the animal

model, type of experiment, data acquisition technique and location, invasiveness of the surgery, the user can use Table 4-1 to develop an understanding of the key characteristics of the different anaesthetic techniques available for selection in the tool (step A in Figure 4-1).

The anaesthetic technique selection (Figure 4-2) and premedication and induction selection (Figure 4-3) flowcharts, respectively steps B and C in Figure 4-1, should then be followed including filling out the corresponding sections of the inventory checklists provided in the appendices. Using the charts and inventory checklists, informed decisions about the equipment and skills requirements for each technique can be made, including essential monitoring capabilities. Table 4-2 provides suggestions with regards to the premedication and induction agents, guiding the selection of combinations of anaesthetic, sedative, and analgesic agents.

Having selected the most promising techniques for premedication, induction, and maintenance of anaesthesia for the planned experiment, the user can use Table 4-3 and Table 4-4 to select a balanced drug combination that is appropriate for the chosen cortical measurements planned (step D). The user should then refer to the literature available about the chosen drugs to define the details of the planned protocol (step E). If specific drugs listed in the tables are not available in the researchers' country, then consultation with a veterinarian may be required to establish a suitable alternative protocol. A concrete example of the process is presented at the end of the present paper which may assist with the exercise.

Having established the feasibility of the chosen anaesthetic technique, including sourcing of equipment and drugs, and staff training required, established using the inventory checklists, the user is encouraged to consider additional monitoring techniques, which may lead to improved physiological stability, reduced pain/nociceptive input, and overall improved experimental outcomes (step F in Figure 4-1).

Finally, due to their well-established benefits in improving efficiency and safety [184, 190], detailed checklists should be utilised. It is recommended to create or adapt existing step by step procedure checklists which describe the planned protocol that are used prior to and during the procedures to maximise reproducibility and safety. Such checklists may also assist during the reporting phase, for example by allowing for identification and reporting of inconsistencies (step G).

To ensure that all equipment, including drugs and consumables are available when required, we have developed various inventory checklists that the user is invited to complete according to their own resources, as they go through the anaesthesia selection process. Because of the multidisciplinary nature of electrophysiology experiments, we have also highlighted the anaesthesia- and animal handling-specific skills that are needed for safe and effective anaesthesia. Personnel with adequate training and experience to use the electrophysiological recording equipment and interpret readings should be available during planning and during interventions.

These checklists have been designed to be considered during the planning stage when developing protocols to ensure that all required equipment and steps in the development of the anaesthetic protocol have been considered in a logical and orderly manner. Included in these lists are “essential” sections which cover equipment and techniques that are considered indispensable when performing high quality research.

The appropriate sections of the inventory checklists are highlighted in the flowcharts and should be filled out as the tool is being used because their outcome is used as go/no-go gates.

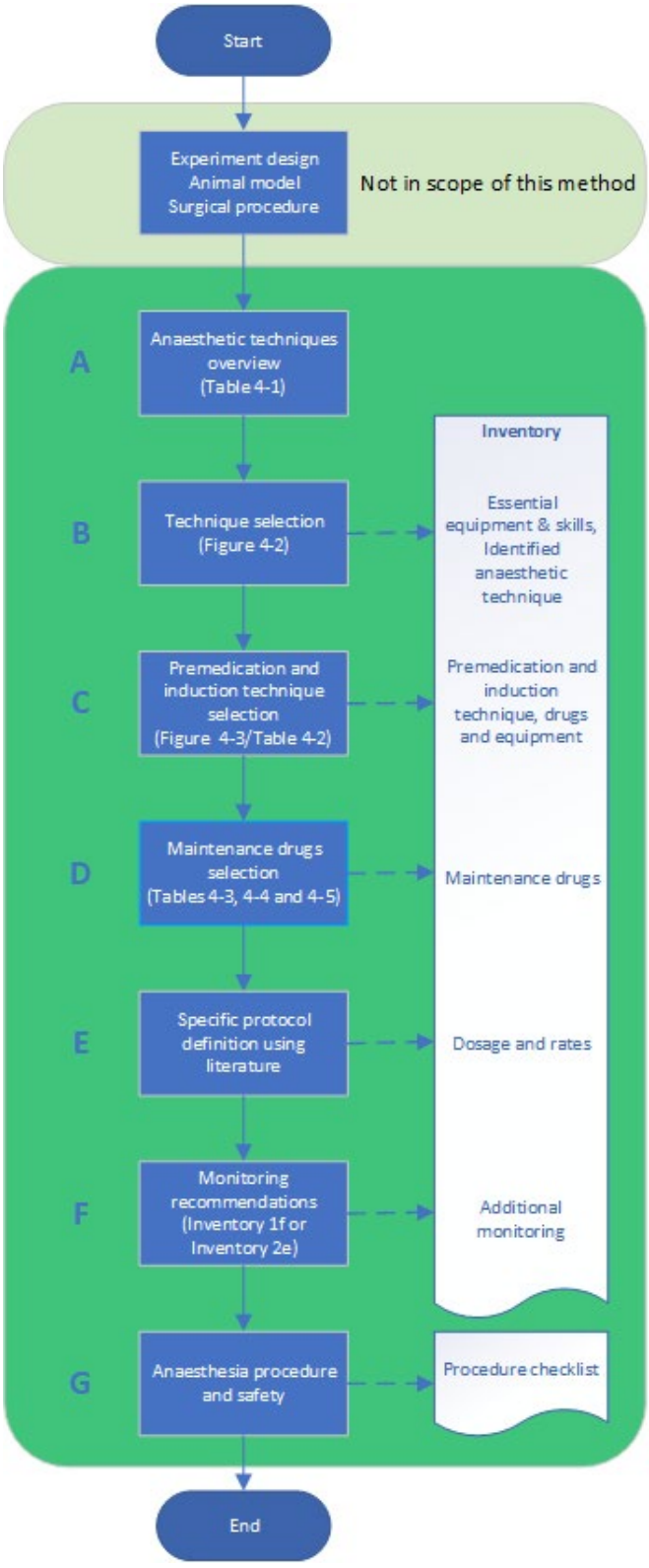

Figure 4-1 Anaesthesia selection and refinement tool overview

4.2.2 Anaesthetic techniques

Considering the available evidence, alongside expert opinion, the most appropriate anaesthetic techniques for electrophysiological experiments were selected and organised

in order of preference. Ideally, TIVA should be provided (Gold standard), followed by PIVA (Silver), BInhA (Bronze) and BInjA in that order. TIVA is the first preference for large animals as when correctly used it avoids the highly depressant effects on both cortical activity and cardiorespiratory stability that inhalant agents produce, that may subsequently impair electrophysiological readings [180]. However, TIVA is not always suitable due to both the cost associated with some large animal injectable anaesthetic protocols and the technical difficulty in small animals (e.g., rats and mice). Typically, inhalational anaesthetic agents are relatively less expensive than injectable drugs. Therefore, PIVA is considered a suitable alternative and second preference as it allows a significant reduction in inhalant used while reducing costs associated with TIVA. PIVA can also be used while assessing the impacts of new surgical procedures with the view to slowly transition to TIVA as the team becomes more confident in using infusion anaesthetic techniques which are typically technically more challenging compared to a pure inhalational technique. Provided that the equipment and skills are available (inventory 1c in the appendices), the decision to favour PIVA or TIVA is left at the user's discretion and should be made in consultation with anaesthesia professionals if possible.

Although TIVA and PIVA would most likely produce similar benefits in rodents as in large animals, it was decided for small animals to assign BInhA and BInjA as gold and silver standards, respectively. The techniques involving intravenous access (TIVA and PIVA) may be difficult in small animals for technical reasons earlier described and do not benefit from the same extensive body evidence of superiority over inhalant techniques for large animals in the literature, although reports exist for their use in rodents [137, 191]. Therefore, the use of BInhA followed by BInjA have been included as principal options for rodents. BInhA involves using a bolus injectable opioid and/or sedative administration to reduce the requirements and thus negative effects of inhalant agents. Opioids also provide analgesia which is essential when invasive protocols are undertaken [182]. However, BInhA is not as reliable or titratable as the PIVA techniques and can result in poorer recording quality and physiological stability. For example, if the duration of effect of the bolus injectable agent is shorter than the total duration of anaesthesia, blood levels, and thus the effect, will wane. Repeated bolus doses may thus be required, leading to a see-sawing blood level and effect which impacts stability of anaesthesia. Indeed, the injectable agents are continuously metabolised and plasma levels, required to reduce inhalant requirements, decrease over time. BInhA was also proposed as a further

option for large animals, in cases where constant rate infusion equipment and skills may be unavailable.

For rodents, BInjA, the combination of injectable agents to produce balanced anaesthesia is also technically easy to perform and can be used to provide varying durations of anaesthesia. Despite this, BInjA is considered inferior due to the inability to easily alter anaesthetic depth and because top-up doses are required, which risks disturbing the position of the animal [189]. Additionally, drugs are slowly eliminated [189] from the body. As a result, intermittent drug administration produces varying depths of anaesthesia over time depending on the amount of drug affecting the animal. This may lead to swings in anaesthetic depth and confound attempts at obtaining useful recordings. Constant-rate infusion (CRI) of injectable drugs will reduce such variation. Therefore PIVA (BInhA with CRI) or TIVA (BInjA as a CRI) could be considered where practical and where sufficient prior evidence is available. Note that if the rate of elimination by the body and the rate of administration are not adequately matched, the animal may become progressively more deeply anaesthetised over time. An associated decrease in physiological stability may occur, which may also affect recordings.

Table 4-1 presents a high-level comparison of some of the known anaesthetic protocols used in the clinical and research practice, including pros and cons, and suitability for small and/or large animal models.

The decision tool was built around the assumption that cortical recordings would be performed long enough after premedication (if used) and induction, so that the effects of the induction methods have a negligible impact on the cortical signals. Figure 4-2 presents the main decision chart, with regards to the choice of maintenance technique. Following the flowchart, the user is instructed to refer to and complete specific parts of the inventory checklists provided in the appendices. For example, having ticked all items and skills listed in the ‘essentials’ checklist is a go/no-go gate, and the user should ensure that all items or training will be available before proceeding with the selection and refinement of the anaesthetic protocol.

Given the order of priority assigned to the different anaesthetic techniques, the flowchart asks the user to answer questions about the availability of key pieces of equipment, such as an anaesthetic machine with a vaporiser, to determine which technique would be most suitable. Upon reaching the end of a “branch” of the chart, the user is again instructed to refer to the inventory checklist and ensure that it can be adequately completed before

committing to using a specific technique. Note that whether an experiment includes recovering animals after the intervention, or not, isn't considered as a key decision parameter for the choice of anaesthetic technique. In all cases, the anaesthesia technique should be chosen to maximise animal welfare and experimental outcome and the fate of the animal at the end of the intervention is secondary.

Table 4-1 Anaesthetic protocol comparison table. Protocols utilising the benefits of anaesthetic-sparing agents to 'balance' the anaesthesia are shown in the green columns. Gold, silver, and bronze colours match the priority given to the different protocols for small and large animal models. Note that TIVA and PIVA for small animals would most likely produce similar benefits as in large animals, yet due to the low number of reports using these techniques, it was decided to assign BInhA as gold standard. Note that induction of anaesthesia is always required prior to placing an intravenous access in small animals.

Type of protocol	TIVA Total intravenous anaesthesia	PIVA Partial intravenous anaeshesia	BInhA Balanced inhalant anaesthesia	BInjA Balanced injectable anaesthesia	Inhalant anaesthesia (not balanced)	Injectable anaesthesia (not balanced)
General	**Pros**: Less cortical depression than inhalant techniques **Cons**: Requires intravenous access and specific equipment. Costs may be significant	**Pros**: Costs (reduces required dose of hypnotics) **Cons**: Same as TIVA, Potential for waste anaesthetic gas exposure	**Pros**: Reduction of inhalant agent which may assist with animal stability as well as cortical activity **Cons**: Inferior to PIVA with regards to level of inhalant required, higher cortical depression expected	**Pros**: Low tech **Cons**: May cause swings in anaesthetic depth and effects on cortical activity, as drugs concentrations and anaesthetic depth will be in a constant state of flux	**Pros**: Basic technique, equipment generally available for small and large animals **Cons**: Significant depression of cardiovascular function and cortical activity expected. Potential for waste anaesthetic gas exposure.	**Pros**: Basic technique, low cost. **Cons**: Requires training to perform injections.
Small animals	Few reports in the literature. Little known about dosage and long-term effects. (Simpson 1997)	Few reports in the literature. Little known about dosage and long-term effects. (Barriga-Rivera 2018)	Fewer reports in small animals but is becoming the standard of practice on many centres	Reports in the literature describe this technique. Reports of increased mortality vs inhalant or BInhA techniques exist for certain protocols	Frequently reported technique for general surgery. Likely to negatively impact cortical recordings	Single agent injectable anaesthesia is not reported frequently due to increased mortality
Large animals	State of the art for cortical or EMG recordings in human and veterinary clinical practice	Provides additional control over anaesthetic depth and dose of injectable used	Technique commonly used in human and vbeterinary clinical practice with significant literature to support its use. However doesnt reduce inhlants as significantly as PIVA	Not recommended in large animals due to the availability of more suitable options that provide more stable anaesthetic planes which will allow for optimal recording sessions	Increased doses of inhalant required to maintain anaesthesia compared to BInHa which will likely negatively affect animal stability and quality of recordings.	Not suitable for large animals due to the volume of drug required to be injected and the negative affects on animal stability
Intravenous Access	Required Also used for fluid therapy and other drugs	Required Also used for fluid therapy and other drugs	Recommended for small animals if possible. Required for large animals. Also used for fluid therapy and drugs	Recommended if practical. Induction of anaesthesia required prior placing IV in small animal models	Recommended if practical for small animals. Required in large animals for fluid therapy and drugs	Recommended if practical for small animals.

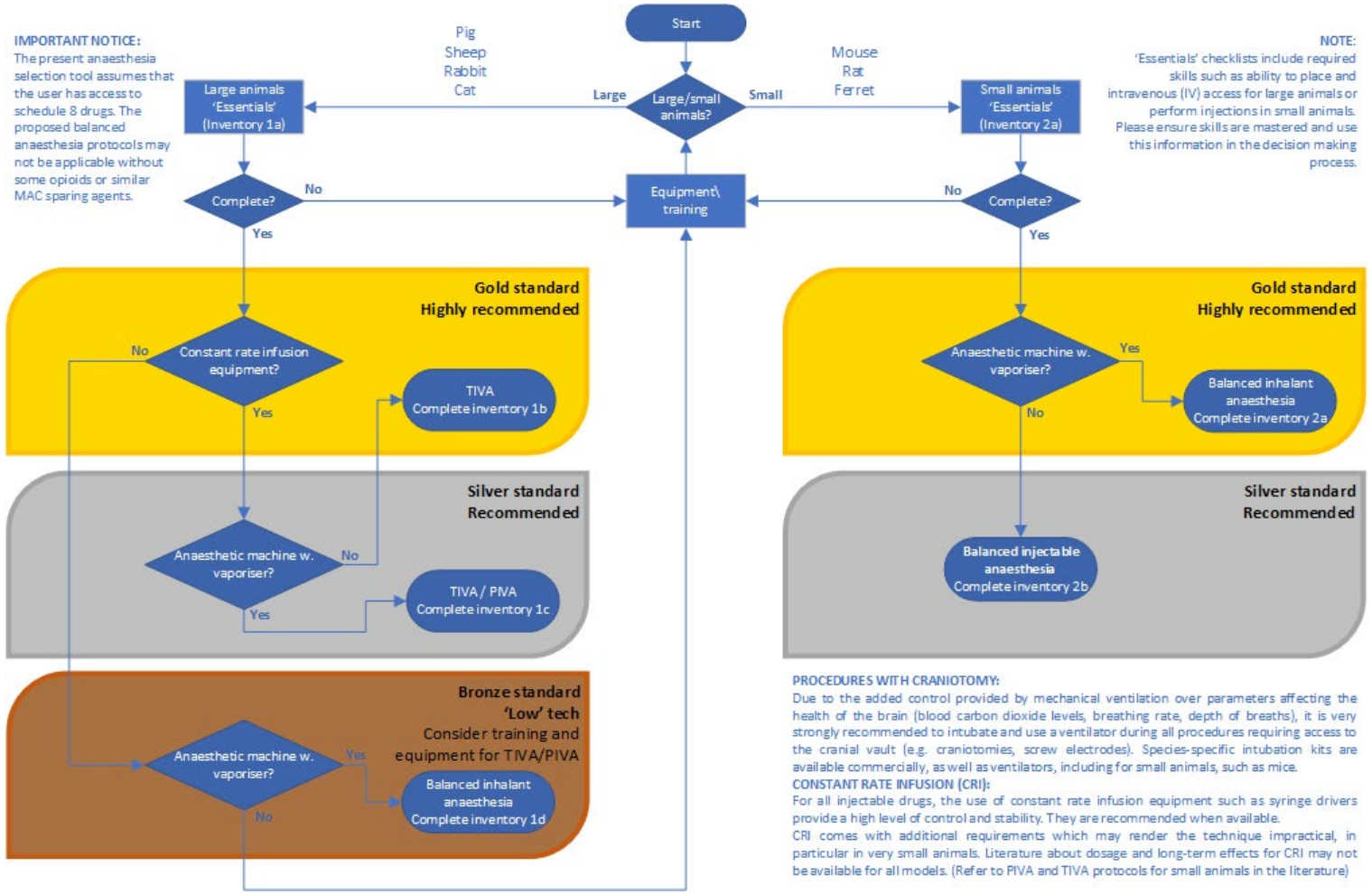

Figure 4-2 Anaesthesia protocol selection flowchart for both large and small laboratory animals undergoing electrophysiological studies of the cortex.

4.2.3 Premedication and induction

The goals and requirements of premedication and induction protocols vary significantly from species to species, particularly between large and small animal models as many common techniques used in large animals are either prohibitively difficult or not well researched in small animal species [183, 189]. The ideal premedication will provide both appropriate sedation and analgesia as appropriate for the animal model and procedure. This will ease maintenance of a stable anaesthetic plane and mitigate the physiological impacts of nociceptive input [183]. Due to the wide variety of premedication protocols available, as well as species-specific response to certain drugs, it is beyond the scope of this paper to recommend premedication protocols for every possible animal model. We do however encourage the use of premedication or sedation where appropriate prior to induction of anaesthesia. Typically, small animal protocols reported in the literature do not include premedication [189]. Despite this, the use of premedication agents prior to induction of anaesthesia in rodents provides a more balanced anaesthetic approach as described earlier. This is likely to minimise the induction requirements of anaesthetic agents and assist with maintaining optimal anaesthetic and physiological stability of animals throughout the anaesthetic event during initial surgical interventions prior to recording sessions. According to the principles of balanced anaesthesia previously presented in the context of maintenance, adequate use of sedatives will also minimise the induction requirements of anaesthetic agents. A more stable anaesthetic event is therefore expected, and premedication is recommended.

Like premedication, anaesthetic induction options will vary between species due to the intricacy of some techniques, *i.e.,* placing intravenous catheters, as well as the temperament and disposition of different animal species. The gold standard for induction of anaesthesia in veterinary and human clinical practice is via the use of injectable intravenous (IV) anaesthetic agents titrated to achieve an appropriate depth of anaesthesia. This technique also provides the advantage of a rapid, relatively stress-free induction of anaesthesia [192].

This technique may not be feasible in smaller animal models such as mice where it is difficult – if not impossible – to place intravenous catheters in conscious animals. Therefore, the use of an induction chamber to induce anaesthesia with inhalational agents is popular [189]. While this technique is technically easy and relatively rapid, it may produce significant levels of waste anaesthetic gas exposure to operators if not used

correctly. Additionally, this technique requires a deeper plane of anaesthesia to be achieved before transferring the animal to the chosen maintenance anaesthetic technique [189]. This may overly depress the central nervous and cardiorespiratory systems and thus potentially cause morbidity or affect experimental outcomes. It is noteworthy that the use of induction chambers for large animals is not safe due to the size of the animal and concerns regarding safety of personnel.

In large animal models, intramuscular (IM) injections may be used to provide sedation or general anaesthesia where IV access is not practical in a fully conscious animal (for example, establishing IV access in conscious pigs is not considered to be safe due to the temperament of the animals). After adequate premedication, IV access can be gained and the injectable IV anaesthetic agent injected for induction of general anaesthesia. In rodents, intraperitoneal (IP) – or, less frequently, IM – injections can be used in place of an induction chamber. These are less ideal anaesthetic induction techniques because the speed of induction and the depth of the achieved anaesthesia cannot be adjusted once the drugs have been administered [183, 189]. Users cannot intervene readily if animals are inadvertently overdosed. Adequate response procedures for such scenarios should be planned and documented.

The premedication and induction technique selection chart is shown in Figure 4-3. The chart considers some of the difficulties related to animal size and typical temperament to guide the decisions. The user should refer to the corresponding inventory checklists in the Appendices, as well as Table 4-2 and Table 4-5 to select appropriate drug combinations for the chosen induction technique. Note that the lists of drugs included in these tables are not exhaustive.

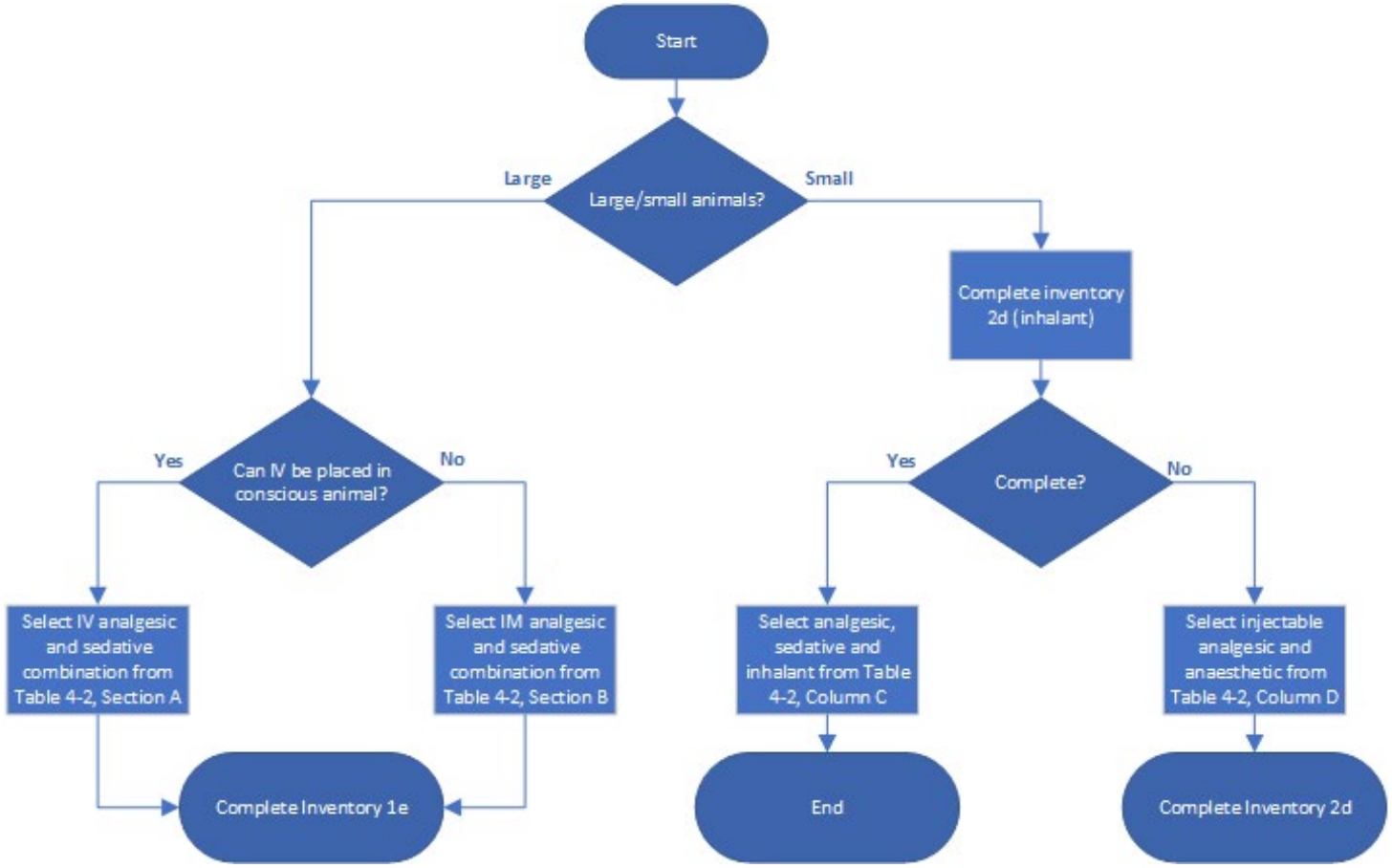

Figure 4-3 Premedication and induction selection chart.

Table 4-2 Premedication and induction drug selection table. For more details about the cardiovascular effects of each agent, refer to Table 4-5.

Chosen induction technique	Choose one from each available category			
	Large animals		Small animals	
	Intravenous	Intramuscular	Inhalant	Injectable
Refer to Figure 4-3 →	**A**	**B**	**C**	**D**
Analgesics	Methadone	Methadone	Methadone	Methadone
	Morphine	Morphine	Morphine	Morphine
	Fentanyl*			Fentanyl*
			buprenorphine	Buprenorphine
Sedatives	Midazolam	Midazolam	Midazolam	Midazolam
	Diazepam*	Diazepam*	Diazepam*	Diazepam*
	Xylazine	Xylazine	Xylazine	Xylazine
	Medetomidine	Medetomidine	Medetomidine	Medetomidine
	Acepromazine	Acepromazine		
Inhalant anaesthetics			Isoflurane	
			Sevoflurane	
			Halothane	
Injectable anaesthetics	Propofol*	Alfaxalone		Propofol*
	Alfaxalone			Alfaxalone
	Ketamine	Ketamine		Ketamine
	Etomidate*			Etomidate*
	Thiopental*			Thiopentone*

* IV only

4.2.4 Maintenance drug selection

When selecting drugs for maintenance of anaesthesia in large animal protocols, we aimed to select agents that were commonly available, had reasonably minimal side effects, were ideally able to be used with minimal training, and exhibit properties that allow rapid titration of depth of anaesthesia depending on the animals' requirements.

Alfaxalone and propofol are considered ideal amongst currently available anaesthetic hypnotic agents both for intravenous induction of anaesthesia and for TIVA and PIVA protocols. Both agents produce a relatively similar degree of cardiorespiratory depression (Table 4-5) and are suitable for long term infusion in most animal species [193]. Cost is a relevant factor when deciding between the two agents as propofol is currently significantly less expensive than alfaxalone. The use of alfaxalone for larger animals or for prolonged studies may become cost prohibitive. The combination of ketamine and midazolam was not included in the hypnotics selection due to concerns about poor recovery qualities when used as an infusion. For example, time for anaesthetic recovery

may be greatly extended due to the longer duration of action of ketamine [192]. The combination is also considered to be inferior to propofol and alfaxalone as ketamine may affect cortical recordings [192]. However, it may provide an appropriate alternative for intravenous induction and maintenance of anaesthesia in situations where propofol or alfaxalone are not available. This neuroleptic combination is inexpensive and readily available in most developed countries. It is notable that ketamine is a controlled substance in most jurisdictions, requiring more administrative effort.

Inhalant agents are known to cause dose-dependent depression of the cardiorespiratory and central nervous systems [189]. These agents are well established to produce profound depression of cortical signals depending on the agent and amount administered [180]. It has been reported that administering isoflurane at levels lower than 50% of the minimum alveolar concentration (MAC) particular for that species results in acceptable cortical recording quality [180]. This is therefore the basis of the balanced PIVA and BInhA techniques recommended by our team which both allow minimal amounts of inhalational agent administration to maintain an adequate depth of anaesthesia. Rapid elimination of inhalational agents both allows for rapid adjustment of depth of anaesthesia and, in recovery models, to produce an appropriate quality of anaesthetic recovery. Inhalational agents are also cost-effective, and the equipment and technical expertise required for administration widely available. Therefore, inhalational anaesthetic agents are potentially useful if the doses required are minimised.

Isoflurane is a cost-effective solution that is readily available in most laboratories. Halothane has been extensively studied in protocols investigating pain via electromyography signals and is considered the gold standard in veterinary clinical practice for electromyography recordings [194]. It may therefore be a more suitable agent than isoflurane, yet availability and cost may become a problem as halothane is not currently used extensively in all parts of the world. Halothane also presents safety concerns for personnel if waste anaesthetic gas scavenging is incomplete. Sevoflurane is used extensively in human clinical practice and is becoming popular in veterinary and research settings. Some reports suggest superior effects when performing recordings than other inhalant agents [180]. Nevertheless, the need for specialised equipment and the relatively high cost of sevoflurane can be problematic.

Opioid infusions are widely considered to be ideal anaesthetic-sparing agents due to their relatively minor cardiorespiratory side effects, provision of analgesia and typically being widely available due to their use in human medicine [195]. Amongst them, methadone,

morphine, and fentanyl were considered as the opioids of choice. Their gold-standard analgesic properties and significant anaesthetic-sparing effects provide cardiovascularly stable animals under anaesthesia in which the required doses of hypnotics and/or inhalant agents is minimised. As a result, cortical recordings may also be facilitated. Morphine and methadone are particularly well suited for use as an IV infusion due to low cost and wide availability in highly concentrated formulas. Fentanyl may be equally suitable for infusion yet is generally associated with higher costs and is only suitable for intravenous administration.

If infusions of opioids are not practical for any reason, then intermittent administration of methadone or morphine administered either IV or IM can be considered (BInhA). This technique is however suboptimal as the concentrations of the opioids will see-saw over time as described earlier, and thus producing relative changes in anaesthetic depth and potentially confounding cortical recordings. Table 4-3 and Table 4-5 can be used to select adequate drug combinations based on the chosen anaesthetic technique.

Table 4-3 Summary of anaesthetic drug selections suitable for large animals (e.g, cats, sheep or pigs) undergoing electrophysiological studies of the cortex. Select one agent in each category that is included in the frame of the chosen anaesthetic technique (output from Figure 4-2).

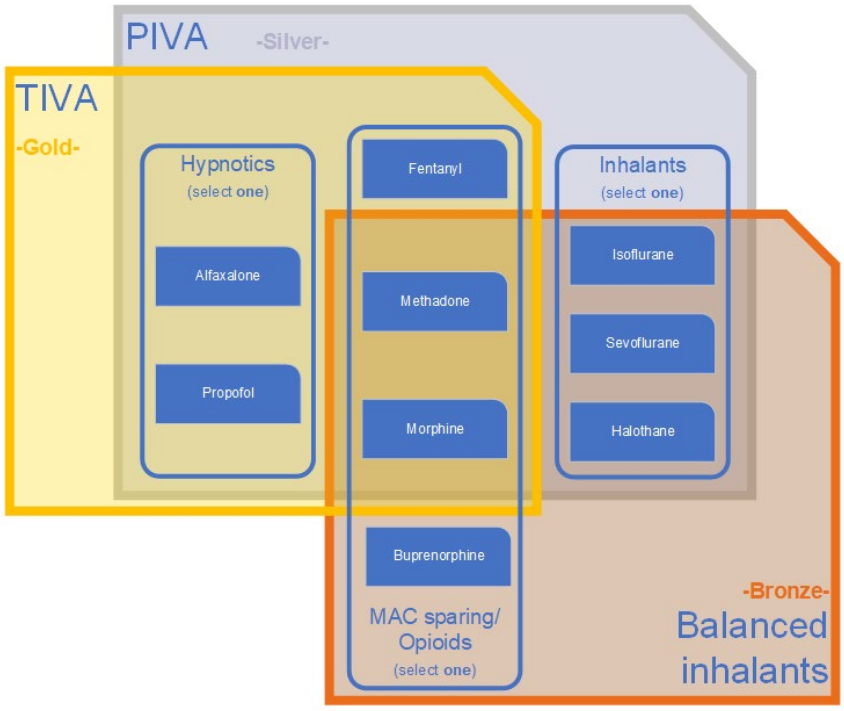

Selection of agents for small animal protocols (mice and rats) is significantly more restrictive. Due to the difficulty and potential invasiveness of placing intravenous canulae

for continuous infusion of drugs (CRI, e.g. for TIVA), many protocols will be based on inhalant anaesthetic agents [189]. While this is suboptimal, we suggest that BInhA may provide superior conditions for cortical recordings, compared to maintenance using relatively high doses of inhalational agents alone. Indeed, using anaesthetic sparing and analgesic agents, administered as boluses of drugs, or in some cases using CRI, the inhalant requirements are minimised.

Like the large animal section, isoflurane, sevoflurane, or halothane, in order of preference, may be selected with the same potential benefits and pitfalls. Injectable combinations including alfaxalone / xylazine and ketamine / xylazine have also been included in this list of options to provide additional techniques if inhalant anaesthesia is not deemed possible or appropriate [189].

Two opioid options have been included as options for small animals for their analgesic and anaesthetic sparing effects. Similar to large animals, morphine is suitable for bolus injections which may need to be repeated every few hours depending on the duration of anaesthesia, the dose administered and the route of administration [189]. Morphine infusion may be suitable for use in advanced balanced anaesthetic techniques in combination with an inhalant agent however relatively little evidence exists for the effects of these infusions in small animals so care must be exercised. Buprenorphine is commonly used in small animal models to provide analgesia and MAC sparing effects [189]. Buprenorphine is administered as a bolus dose; however, duration of action is longer at approximately 6-8 hours. A smoother anaesthetic plane may therefore be achieved while fewer injections are required over the study period, minimising the problems posed by potentially moving the position of the animal to allow injection.

Table 4-4 Summary of anaesthetic drug selections suitable for small animals (rodents) undergoing electrophysiological studies of the cortex. Select one agent in each category that is included in the frame of the chosen anaesthetic technique (output from Figure 4-2).

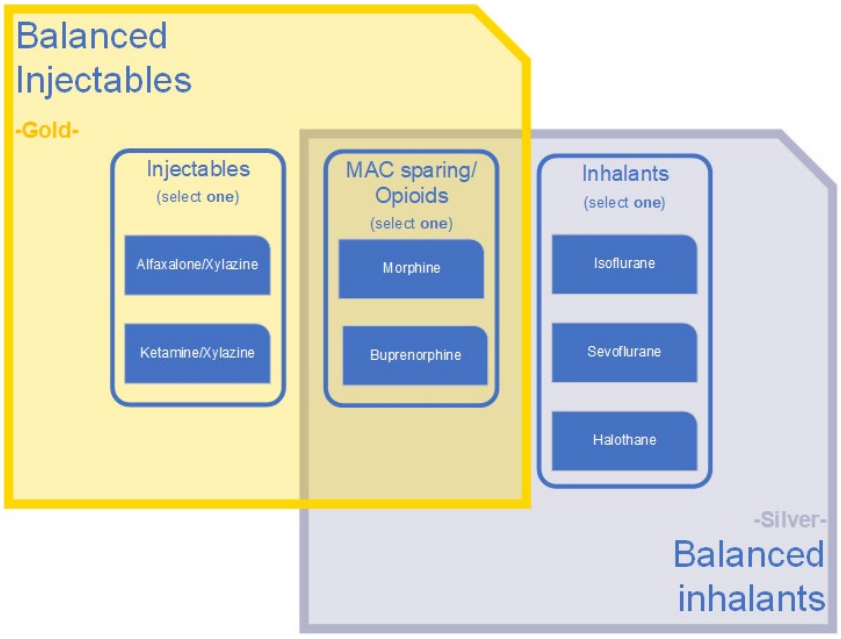

Table 4-5 Adapted from Steinbacher and Dörfelt (2013) [196] and Ohad (2014) [197]

	Drug	Heart rate	Force of cardiac contraction	Cardiac output	Vascular resistance	Blood pressure	Drug Class	Notes
Sedatives	**Midazolam**	↔	↔	↔	↔	↔	Benzodiazepine	Suitable for intramuscular injection
	Diazepam	↔	↔	↔	↔	↔	Benzodiazepine	Not suitable for intramuscular injection
	Xylazine	↓↓	↔	↓	↑	↑↓	Alpha 2 agonist	Blood pressure raises then falls slightly
	Medetomidine	↓↓	↔	↓	↑↑	↑↑	Alpha 2 agonist	Blood pressure raises then returns to near base line
	Acepromazine	↔	↓	↔	↓↓	↓↓	Phenothiazine	
Analgesics	**Methadone**	↓	↔	↔	↔	↔	Mu opioid agonist	
	Morphine	↓	↔	↔	↔	↔	Mu opioid agonist	
	Fentanyl	↓	↔	↔	↔	↔	Mu opioid agonist	
Inhalant anaesthetics	**Isoflurane**	↓	↔	↔	↓	↓	Halogenated Ether	
	Sevoflurane	↔	↔	↔	↓	↓	Halogenated Ether	
	Halothane	↓	↔	↔	↓	↓	Halogenated Ether	
Injectable anaesthetics	**Propofol**	↔	↓	↓	↓	↓		
	Alfaxalone	↑	↓	↓	↓	↓	Neurosteroid anaesthetic	
	Ketamine	↑	↑	↑	↑	↑	Dissociative anaesthetic	Not suitable for infusion
	Etomidate	↔	↔↓	↔	↔↑	↔	Non	Not suitable for infusion
	Thiopental	↑	↓	↑	↓	↓	Barbiturate	Not suitable for infusion

Legend:

↔	Stable	↓	Decrease
↑	Increase	↓↓	Strong decrease
↑↑	Strong increase	↔↓	Stable, or decrease
↑↓	Increase then decrease	↔↑	Stable, or increase

4.2.5 Dosage and refinement

Like premedication protocols, details of dose rates have not been included in the present tool as dose rate and routes of administration vary considerably between various animal models. It would be beyond the scope of this paper to recommend doses for each individual species and strain of animal that may be used. Instead, we encourage users to seek commonly available laboratory animal anaesthesia textbooks, such as the fourth edition of "laboratory animal anaesthesia" [198], which are able to provide detailed information about appropriate selection of specific drugs for the chosen species as well as appropriate dose rates. Once again, involving professional anaesthetists and/or veterinarians, at least during the planning phase, will prove very beneficial when dealing with such technicalities as dosage calculations.

4.2.6 Mechanical ventilation and brain health

Due to the added control provided by mechanical ventilation over parameters affecting the health of the brain (blood carbon dioxide levels, breathing rate, depth of breaths), it is very strongly recommended to intubate and use a ventilator during all procedures requiring access to the cranial vault (e.g., craniotomies, screw electrodes). Species-specific intubation kits are available commercially, as well as ventilators, including for small animals, such as mice. The aim of mechanically ventilating an animal that is going to have intracranial access established is to control arterial carbon dioxide levels at the low end of normal (approximately 30 mm Hg in mammals) while minimising the negative cardiovascular impact that mechanical ventilation can produce. Minimising cardiovascular depression from mechanical ventilation is achieved by using a high frequency, low pressure pattern of ventilation.

4.2.7 Anaesthetic monitoring

Large animal monitoring equipment is readily available and relatively affordable owing to its use in veterinary and human practice. Thus, we recommend at minimum the use of pulse oximetry, continuous core body temperature recording, continuous blood pressure measurement and capnography. Reasoning for these monitoring choices is described in detail in the case report section of this paper. Detailed lists of equipment and consumables for monitoring are listed in the 'Essentials' (1a) and 'Monitoring' (1f) inventory checklists for large animals in the Appendices.

Typically but unfortunately, in small animal protocols anaesthetic monitoring is minimal with the anaesthetist relying on visual observations to assess respiratory characteristics and identify signs of cyanosis [189]. The addition of some relatively low-cost monitoring equipment will increase safety for the animal significantly throughout the anaesthetic period. At a minimum, we recommend the use of pulse oximetry to allow real time assessment of changes in heart rate and oxygen saturation as cardiorespiratory depression is common when anaesthetic depth is too deep. Continuous temperature monitoring should also be carried out as standard. Hypothermia has wide-ranging deleterious physiological effects and decreases anaesthetic requirements which, if unrecognised and corrected, increases the welfare and anaesthetic risk for the animal. Hypothermia may also thus impact the quality of cortical recordings [199]. In more advanced small animal protocols of longer duration, the addition of blood pressure monitoring and the use of capnography if animals are to be intubated and ventilated is recommended. Ideally, blood gas and electrolyte monitoring are also used. Refer to the 'Essentials' (2a) and 'Monitoring' (2e) inventory checklists for small animals in the Appendices.

We strongly recommend that researchers unfamiliar with the monitoring techniques described receive formal training by veterinary staff. Researchers are also advised to seek opportunities to observe them being performed on other animals where possible. It is important that users can interpret, and trouble shoot values obtained from selected monitoring equipment to ensure optimal outcomes. The presence of monitoring equipment by itself is useless without trained staff to interpret and take corrective actions when required.

4.2.8 Procedure checklists

Checklists are used routinely in human and veterinary medical practice to improve patient safety and to ensure optimal outcomes [184, 190]. Following initial design of the research protocol and prior to commencement of the protocol these lists should be consulted again to ensure that all requirements have been met prior to anaesthetising animals. By following these checklists, users should ensure that no unexpected problems surrounding the anaesthetic event arise during surgical sessions while maximising the available time to acquire high quality recordings.

4.3 Protocol selection and execution in sheep

The anaesthesia selection tool described in the present chapter was used to identify an appropriate balanced anaesthesia protocol for an experiment that involved recording the cortical response to visual and electrical stimulation of the retina in a sheep animal model.

This section presents a typical application of the selection tool to serve as a guide to users. Based on the requirements for the experiment and the chosen animal model, as well as the skill set and equipment available in a research facility, an example is given which shows how the different parameters influence the tool outputs. Beyond the choice of an anaesthetic technique, induction and maintenance drugs, the tool also served as a resource to establish with certainty that all consumables and equipment were available to perform the experiment in good conditions. Finally, the tool suggested to monitor additional vitals to verify the physiological stability of the animals during the experiment. The vitals are presented to support the choice of anaesthetic technique and drugs, and emphasize the advantages of additional monitoring data during reporting.

The electrophysiology results presented here represent a small subset of the data acquired, which is presented in Chapter 5, namely visually evoked potentials during bright flash stimulation in light-adapted eyes of sheep.

4.3.1 Experiment overview

In the field of vision prostheses, electrical stimulation of the retina represents a promising approach to restore vision in human patients. Retinal prostheses have provided variable levels of vision restoration in over 500 people [13] worldwide. Researchers rely on preclinical animal studies to ensure safety and efficacy of devices prior to use in human patients. Anatomical similarities between the sheep and human allow sheep to be used as a suitable animal model for preclinical experiments with devices in their final (human) form [1, 162]. In the field of vision prostheses, electrical stimulation of the retina represents a promising approach to restore vision in human patients. Retinal prostheses have provided variable levels of vision restoration in over 500 people [13] worldwide. Researchers rely on preclinical animal studies to ensure safety and efficacy of devices prior to use in human patients. Anatomical similarities between the sheep and human allow sheep to be used as a suitable animal model for preclinical experiments with devices in their final (human) form [1, 162].

Visual and electrical stimulation of the retina and recording of the cortical response is commonly used to study and improve retinal stimulators for the purpose of vision restoration [31, 200, 201]. Experiments typically involve the implantation of stimulating electrodes close to the retina and positioning recording electrodes above or in the visual cortex.

4.3.2 Selection tool outputs

The anaesthesia selection tool developed was applied according to the method described above and including the following key parameters:

- • Sheep (Dorper Breed) – Large animal
- • Terminal procedure (animals not recovered)
- • Invasive surgeries to position a suprachoroidal stimulating electrode array
- • Craniotomy to position intracortical recording electrodes
- • 10-15 hours procedure duration

4.3.2.1 Anaesthetic technique and inventory

The anaesthetic technique flow chart was used to determine an appropriate protocol. The 'essential' inventory items (inventory checklist 1a) were able to be completed as our facility has these items and a team of trained specialist anaesthesia veterinary staff for use in all protocols which allowed us to meet each of the skills checkboxes. Next the gold, silver and bronze standard tiers were considered. From the gold standard selection area, it was determined that adequate constant rate infusion equipment was available. This step led to the silver standard step requiring an anaesthetic machine with a vaporiser attached suitable for inhalant anaesthesia. With this item also available, the tool guided us to the choice of a full TIVA or PIVA technique at our discretion (all items of inventory checklist 1c available). Due to our inexperience with a complete TIVA protocol in sheep for this research protocol, it was decided that a safe compromise would be to select a PIVA technique while keeping the inhalant dose minimised. This would allow us extra flexibility of increasing inhalant anaesthetic levels in response to surgical stimulation, if required, while being able to quickly and easily decrease inhalant levels and depth of anaesthesia when no longer required, for example during cortical reading sessions.

4.3.2.2 Premedication and induction

Due to the relatively docile nature and ease of handling of sheep, intravenous catheter placement is generally possible without sedation. Therefore, an intravenous premedication combination was selected from Table 4-2 and inventory 1e was completed. Methadone was selected to provide moderate sedation to allow movement of the animal to the anaesthetic induction area. Dexmedetomidine could have been used to provide higher levels of sedation, however, this was not considered to be necessary. Propofol administration was selected as the most appropriate induction agent to obtain general anaesthesia.

4.3.2.3 Maintenance drug selection

The maintenance drug selection tool was used to determine an appropriate drug combination for our proposed protocol (PIVA) using sheep weighing approximately 50 kg. When assessing the hypnotics section, we investigated the properties and costs of the available drug options. Due to the expected duration of the experiment and the high cost, alfaxalone was considered to be inappropriate. Propofol was considered the most appropriate choice due to its favourable cost and ability to maintain anaesthesia via IV infusion [193]. A combination of ketamine and midazolam may have been appropriate as an induction and maintenance agent, however there was concern due to a lack of data with prolonged ketamine and midazolam infusions in sheep.

Next, the anaesthetic sparing/opioids section was assessed for options with investigators assessing the properties of each drug option. Buprenorphine was considered inappropriate as we had the equipment to provide continuous infusions whereas buprenorphine is typically used as a longer acting agent administered in bolus doses every 6 to 8 hours. Administering an opioid as an infusion would help to maintain animal stability and optimise recording quality during the protocol by reliably and consistently reducing anaesthetic requirements. Fentanyl was considered a possible choice based on its availability, appropriateness to use as an infusion as well as being short acting therefore providing the ability to rapidly increase or decrease analgesia and degree of MAC sparing. However, morphine was selected as the agent of choice due to decreased cost compared to methadone and fentanyl. Morphine was also sourced in more concentrated forms than methadone or fentanyl making handling and preparing infusions easier.

The inhalant options were assessed. Halothane was deemed to be promising due to its extensive use in research protocols investigating electromyography recordings, indicating

that cortical depression by the agent would be minimal [194]. Unfortunately, a vaporiser or liquid inhalant could not be readily sourced which eliminated this agent from consideration. The lack of readily available equipment for use of sevoflurane, coupled with significantly increased costs when compared to other available inhalational agents led to sevoflurane being deemed unsuitable in the specific situation. Equipment for administration of isoflurane was however readily available and the cost to incorporate isoflurane into the protocol was deemed appropriate given the amount of research funding available for this experiment. Additionally, the literature has claimed that the ability to secure accurate cortical recordings would be good if isoflurane levels were kept below 0.5% - less than 50% of the MAC for isoflurane in sheep [180]. Considering the MAC sparing effects of the morphine and propofol infusions, adequate anaesthetic effects of isoflurane below this threshold were considered achievable. As a result, the risk of alteration of the cortical signals by the low levels of isoflurane was considered to be negligible compared to the required investment (costs, equipment, training) to incorporate either of the two other inhalants of choice. This is an example where the reality of the research facility and training may force teams to weigh the pros and cons of different techniques and drugs, before reaching a conclusion.

4.3.2.4 Dosage and further refinement

Dose rates were obtained from standard veterinary anaesthesia textbooks for the drugs selected. Where information was unavailable in textbooks, literature data base searches were conducted for papers that described the drug being used in the same or similar species and dose rates and general drug effects were inferred. For example, propofol TIVA dose rates for our protocol were extrapolated from papers investigating this technique in sheep and goats [202-204].

4.3.2.5 Monitoring

As previously mentioned, extensive monitoring equipment with appropriately trained staff were available for this protocol (completed inventory 1f) which allowed a high degree of monitoring, maximising chances of the animal remaining physiologically stable over the prolonged study period and maximising the chance of obtaining accurate cortical recordings. Pulse oximetry was used to continuously assess heart rate and oxygen saturation. This was considered essential as all anaesthetic agents cause dose dependent cardiorespiratory depression [189]. ECG monitoring was used to identify any arrythmias to allow treatment as required. Non-invasive blood pressure, and later invasive blood

pressure was used to ensure adequate perfusion to vital organs. Invasive blood pressure was used once the required instrumentation could be completed due to its superior accuracy and continuous measurements. Capnography was used to assess adequacy of ventilation and in combination arterial blood gas analysis, was used to ensure that the required levels of arterial carbon dioxide could be achieved. Blood gas analysis is the gold standard for assessment of adequacy of ventilation and this arterial carbon dioxide and oxygen levels. This monitoring is highly preferred in the craniotomy large animal research model as changes in arterial carbon dioxide result in changes in the volume of tissue in the intracranial vault which may affect the stability of recordings [205]. Continuous oesophageal temperature was continuously recorded to guide maintenance of normothermia with the aid of active heating devices[199].

While depth of anaesthesia monitoring using electroencephalogram has been and is being investigated in humans, as well as in research animals, this technique requires species- and protocol-specific validation [206]. To the best of the authors knowledge, such validated parameters were not available, to date, for sheep undergoing propofol-morphine-isoflurane. Electroencephalogram was therefore not recorded, and the depth of anaesthesia was monitored using the physiological parameters listed above.

4.3.2.6 Procedure checklist

Prior to induction of anaesthesia, step one of a modified surgical safety checklist [207] was employed to confirm details regarding the identity of the animal undergoing the procedure, as well as equipment and drugs had been prepared and tested prior to induction of anaesthesia. Roles and responsibilities of those team members involved in the procedure were also confirmed.

Prior to the first surgical incision, step two of the surgical safety checklist was completed to ensure that all team members were aware of the procedure being performed and that all required surgical equipment was present and in sterile condition (where required) prior to starting the procedure.

Surgical safety checklists also include a third step that is completed prior to recovering animals from anaesthesia. As this was a terminal procedure this was not completed.

4.3.3 Ethics statement and animal preparation

We conducted a prospective, interventional study in adult Dorper sheep in the Hybrid Operating Theatre of the Sydney Imaging Core Research Facility at the University of

Sydney, Australia. The study was approved by the University of Sydney (Australia) Animal Research Ethics Committee (2021/1864) and was conducted at the Charles Perkins Centre, The University of Sydney (Sydney, Australia). The study complied with institutional general guidelines and regulations and ARRIVE guidelines for in-vivo animal experiments. The experiment was defined as a hypothesis-creating pilot study. As such, the statistical analysis plan was not finalised before data collection. The investigation was performed in accordance with the Helsinki Convention guidelines for humane care of animals and the Australian code for the care and use of animals for scientific purposes [208].

4.3.4 Cohort, anaesthesia, and monitoring

Animals were acclimatised for at least two weeks prior to the procedure and received routine preventative treatments prior to arrival. Two adult, female Dorper sheep (1 year old, weighing 50 and 51 kg) retinal and cranial surgery to position stimulating and recording equipment as detailed below. Sheep were premedicated intravenously with methadone 0.4 mg/kg. Anaesthesia was induced by administering propofol intravenously to effect (4 to 6 mg/kg), to facilitate orotracheal intubation. Anaesthesia was maintained with inspired 0.5-1.5% isoflurane delivered in an air/oxygen mixture. Propofol was infused at 18 to 25 mg/kg/hr and morphine infused at 10 to 30 mg/hour throughout the anaesthesia period. All sheep were mechanically ventilated using controlled intermittent positive pressure ventilation mode used to deliver high-frequency, low volume pattern of ventilation. Animals received fluid therapy to maintain intravascular volume, cardiac output, and thus normal blood pressure.

Animals were placed in sternal recumbency with arterial blood pressure transducers zeroed immediately before the procedure at the level of the right atrium. Mechanical ventilation was conducted in synchronized intermittent positive pressure ventilation mode with a positive end expiratory pressure of 5 cm H2O maintained. Haemodynamic parameters were continuously recorded. Arterial pressure, central venous pressure and cardiac output were continuously recorded (Philips Patient Monitor, IntelliVue MX800, Philips Medizin Systeme Boeblingen GmbH, Hewlett-Packard-Str.2 71034 Boeblingen, Germany) up until euthanasia as per the original research protocol.

The selected propofol-morphine-isoflurane anaesthesia provided physiologically stable animals for the duration of the experiments. The anaesthetic depth could be adequately managed to suppress all signs of nociception during ocular and cranial surgeries in both

sheep. The physiological changes shown for both animals in Figure 4-4 have been included to demonstrate that all physiological parameters were maintained within levels that were deemed to be appropriate throughout the experiment by the attending anaesthetist. Anaesthetic depth was always deemed to be adequate throughout by the anaesthetist based on absence of reflexes and lack of movement or ventilator asynchrony.

In sheep number one, a decision was made to increase the isoflurane concentration during the initial surgical procedures to ensure adequate depth of anaesthesia and thus maintain animal welfare. Despite significantly increasing isoflurane levels from 0.5 to 1.5% during the surgical procedures, no negative physiological effects were observed with all vital signs, including mean arterial pressure (Figure 4-4 (d)) remaining in normal ranges. Importantly, immediately following reduction of isoflurane levels to the predetermined goal of 0.5%, it was possible to record visually evoked potentials, demonstrating the flexibility of the protocol while still allowing recordings to be performed as needed. Despite the lack of negative effects from increasing the isoflurane during the initial surgical procedure in sheep number one, sheep number two did not require this increase in inhalational agent delivery to maintain an appropriate anaesthetic depth for the surgical procedure. This highlights the flexibility of the anaesthetic protocol depending on individual animal requirements. As previously noted, all drugs may alter the cortical signals, yet the combination of multiple drugs into a balanced protocol allowed for the minimisation of the dose of all drugs. With dose minimisation, particularly that of isoflurane, depression and/or alteration of the recordings were also considered as minimised.

In addition to the demonstrated cardiovascular stability, no additional doses of analgesics were required during the experimental procedure in response to surgical manipulations, confirming the adequacy of the analgesic component of the protocol provided by the morphine infusion.

In sheep number one, arterial blood gas analysis at approximately the three-hour mark revealed a significant disparity between end tidal carbon dioxide values (Figure 4-4 (c)) and arterial carbon dioxide values (data not shown). Ventilation parameters were corrected, and efficacy of the measures taken were confirmed with end-tidal and arterial gas level measurements. While the values did change significantly, they are still well within normal values described for this species.

Changes in heart rate and other recorded parameters may be influenced by a variety of factors throughout the anaesthetic period and may not necessarily indicate that anaesthetic depth is inadequate. For example reasons for varying heart rate could be due to inadequacy of anaesthesia, noxious stimulation, arterial carbon dioxide levels as well as natural variability in the animals responses the anaesthetic drugs administered to name a few. The increase in heart rate, particularly in sheep one, was likely due to the nociceptive input from commencement of surgery. Thus, the isoflurane level was adjusted to ensure an adequate depth of anaesthesia was maintained during the surgical procedure. However, the heart rate range remained within normal physiological limits throughout the anaesthetic periods for both sheep.

All other monitored vitals remained within the normal range and no additional interventions were required. Missing arterial blood pressure datapoints in sheep number one were due to a fault in the pressure sensor after approximately two hours of anaesthesia. This sensor was subsequently replaced, and measurements resumed. In the last hour of the intervention on the same sheep the oxygen saturation sensor failed. However, arterial oxygenation levels were used as a substitute and confirmed that the sheep remained appropriately oxygenated throughout the final hour of procedures

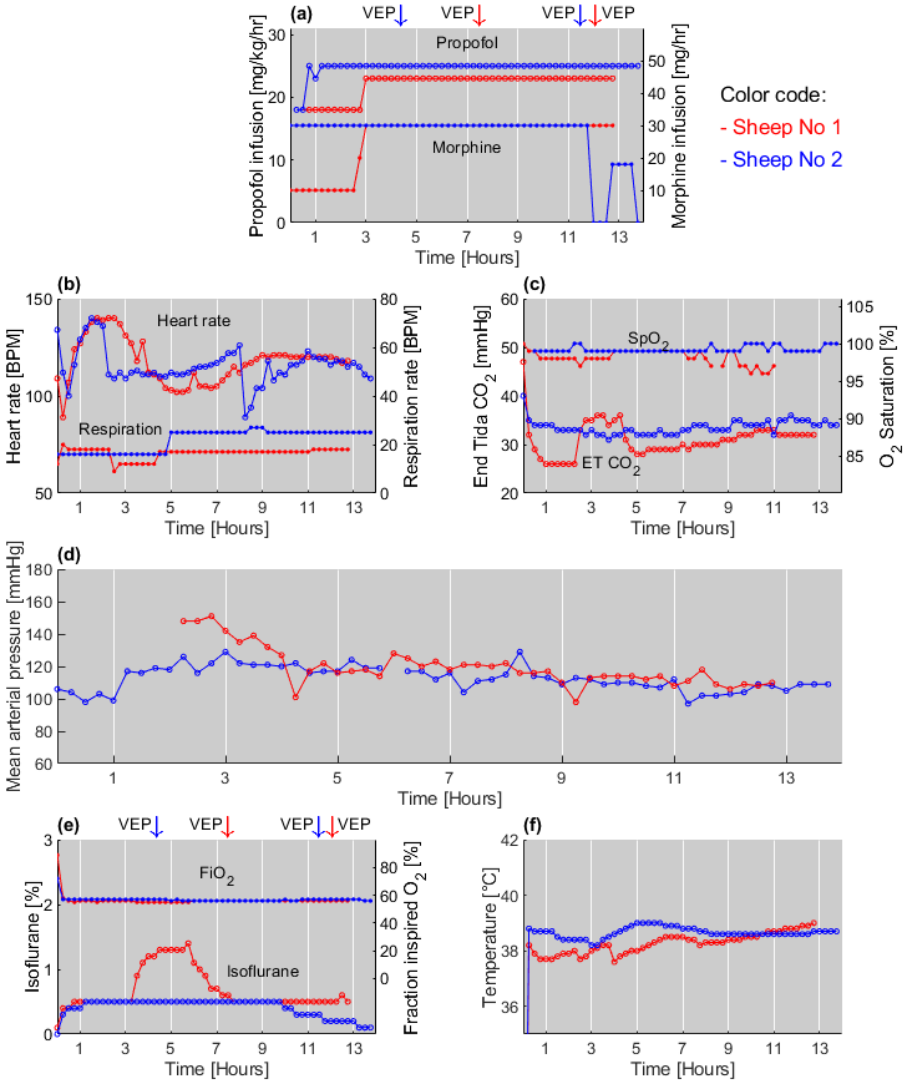

Figure 4-4 Anaesthetic records and vitals monitoring for two sheep anaesthetised using a morphine, propofol and isoflurane combination for up to 13 hours 45 minutes. (a) and (f), arrows mark the time of the visually evoked potential (VEP) recordings shown in Figure 4-5.

4.3.5 Surgeries and recordings

After dilating the pupils with Atropine 1% (Aspen Australia, St Leonards NSW, Australia), a platinum-nylon-silicone suprachoroidal electrode array was implanted in the right eye of both animals according to a technique adapted from [1]. Briefly, a lateral canthotomy was performed after crushing the tissue from the lateral canthus with haemostats to reduce localised haemorrhage. A corneal stay suture was used to manipulate the globe. The conjunctiva and tenon's capsule were dissected and a seven-

millimetre incision of the sclera was made ten millimetres posterior to the limbus. Array insertion was simplified by the creation of a suprachoroidal pocket by blunt dissection using a polyester insertion guide with the same dimensions as the array. The array was sutured to the sclera at the insertion site using three 6-0 Vicryl (Ethilon, Ethicon, Raritan, New Jersey, USA) sutures located on either sides and in the centre of the scleral incision.

The posterior segment of the skull was exposed using full-thickness, midline incision of the skin. A 30 by 30 mm craniotomy, centred 20 mm rostral and 10 mm lateral to the lambdoid suture [200], allowed access to the cortex. Visually evoked potentials were recorded with a platinum ball-electrode epidurally in one animal and subdurally in the other. In both sheep, a penetrating electrode array (Utah array, BlackRock Neurotech, Salt Lake City, Utah, USA) was pneumatically inserted in the exposed cortex and used to record VEPs in the second part of the experiments.

Visual stimulation and cortical recording from the primary visual cortex

Binocular visual stimulation was delivered using two custom-built full-field flash generators. The light sources used a two-LED (white, approximately 6740 Kelvin) system to provide light adaptation (72 lm/m2, 12.7 cd/m2) and 50-millisecond bright flashes of white light (1778 lm/m2, 422 cd/m2). The animals were light adapted for at least ten minutes before each trial [209]. The eyes were held open and eye ointment (Lacri Lube, Allergan Australia Pty. Ltd, North Sydney, NSW, Australia) was applied regularly and generously throughout the experiments.

Cortical activity was recorded using a multichannel recording/stimulation system (RHS Stimulation/Recording Controller and 32-Channel headstages). Reference and ground electrodes were shorted together via a zero-ohm resistor on the headstages. A reference/ground electrode was positioned approximately 30 mm from the recording site in (needle) or under (wire) the skin in the case of platinum-ball or Utah array recordings, respectively. All recordings were stored for off-line postprocessing.

After 12.45 and 13.45 hours, respectively, the animals were humanely sacrificed with an intravenous injection of a combination of potassium chloride and concentrated pentobarbitone (Lethabarb, Virbac Australia, Milperra NSW, Australia) following confirmation that animals were adequately anaesthetised prior to euthanasia in accordance with animal ethics requirements.

Series of 120 (Pt-Ball electrode) and 80 (Utah array) stimuli were averaged together without filtering to reduce noise and plotted over the full inter-stimulation interval of one

second (Matlab R2021b, version 9.11.0.1809720, MathWorks, Natick, MA, USA). In both animals, epidural, subdural or intracortical visually evoked potentials could be recorded throughout the experiments. Representative recordings are shown in Figure 4-5. Differences between recordings of animals' cortical signals were due to varying locations of the electrodes over the visual cortex. Extra- and intracortical recordings differed mainly due to the proximity to the neurons, the size of the array, as well as the location on the visual cortex between the platinum ball and the Utah array.

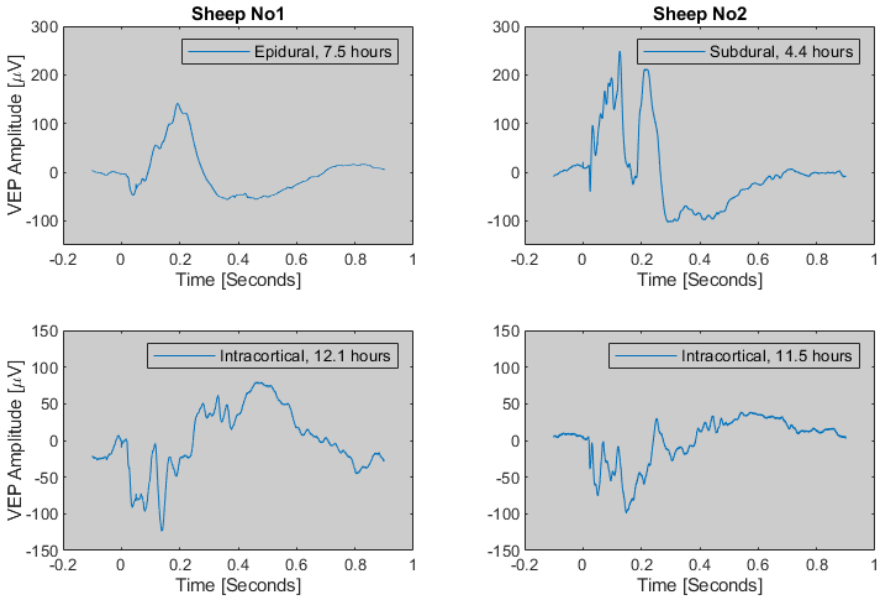

Figure 4-5 Ensemble average of visually evoked potentials acquired at different time points after anaesthesia induction in two sheep. Top: Epi- and subdural recordings with a platinum ball-electrode, left and right respectively. Bottom: Intracortical VEP recordings obtained as the average of 96 (left) and 32 (right) channels of a penetrating multielectrode array (Utah). Differences between animals are due to varying locations over the visual cortex. Extra- and intracortical recordings differ mainly due to the proximity to the neurons, the size of the array, as well as the location on the visual cortex between the platinum ball and the Utah array.

4.4 Discussion

The proposed anaesthesia selection tool was followed to identify an optimised anaesthetic protocol. Application of the protocol to an experiment involving epidural, subdural and intracortical recordings of the brain response to visual stimuli allowed for physiologically stable animals in which visually evoked potentials could be recorded for a least twelve hours of anaesthesia.

Animal welfare and physiological stability

From a practical standpoint, the chosen technique was easily administered and did not require significant both troubleshooting or deviation from the planned protocol determined using the selection tool.

While both animals remained within normal physiological values throughout the anaesthetic period, the importance of the inclusion of intermittent blood gas analysis as an additional monitoring method was highlighted in sheep number one. As discussed, previously increased arterial carbon dioxide concentrations may cause significant problems when trying to record visually evoked potentials as they may lead to increased intracranial pressure and general metabolic dysfunction. Over prolonged experimental sessions, the pressure may significantly impact animal anaesthetic and physiological stability and cortical recording quality. The inclusion of blood gas analysis in our monitoring techniques allowed for identification of a problem that would not have been able to be identified with standard monitoring equipment. The ventilation parameters were adjusted as demonstrated by the rise and eventual decline in both end tidal and arterial carbon dioxide values as the adequacy of ventilation was rectified.

When designing the anaesthesia selection tool, a review of the types of anaesthetic protocols that are reported for experiments involving visually evoked potentials was performed followed by a review of the current standards of practice in humans and veterinary clinical practice. In doing this, potentially significant gaps in the standard of care for animals being anaesthetised for research purposes were identified as well as multiple protocols that contained the use of specific drugs or techniques that may have a major confounding effect on the ability to successfully and accurately record visually evoked potentials.

Following this review multiple principles around the minimisation of the undesired effects of anaesthesia were incorporated into the decision-making tool.

The selection tool was developed with attempts to mirror current best practice standards in both human and veterinary practice. These standards represent the current pinnacle of anaesthetic practice and can be reasonably be assumed to provide the best possible conditions to successfully generate visually evoked potentials in a research setting. At the heart of these changes is an attempt to include balanced anaesthetic options wherever possible for both small and large animals research models.

By providing balanced anaesthesia, animals benefit from both the provision of analgesia and reducing the amount of anaesthetic agent required to maintain immobility for both surgical procedures as well as cortical recording sessions. This is important as it will help to maintain physiologic stability throughout the experimental period, hence reducing confounding factors, while providing optimal conditions for recording cortical potentials. Researchers planning anaesthetic events should at the forefront consider that all anaesthetic agents depress all major body systems in a dose dependent manner, therefore minimising the amount of anaesthesia needed, via employing balanced techniques will help to maximise the outcome of any experimental session. By incorporating these techniques, experiments will also closely mirror human practice which aims to maintain a healthy brain and maintain cortical activity as fully as possible during anaesthesia.

Effects on cortical recordings

Electrophysiology is often used to assess the functionality of devices such as visual prostheses, or the ability of techniques to evoke cortical activity. In such studies, there is a real risk that the anaesthetic agents' effects on cortical activity may lead to erroneous conclusions about the effectiveness of a device. Negative or unconclusive studies, as defined by the absence of reliable recordings from the brain may also cause an increase in the number of animals that are used, as the researchers may need to repeat experiments. As an example, Gekeler *et al*. listed anaesthetics amongst factors that may have decreased the success rate of detecting electrically evoked cortical potentials [134]. Similarly, Ryu *et al*. reported that "[…] it is possible that the anesthesia protocols used here may have contributed to the high threshold levels" [210].

Because all drugs will cause a dose-dependent depression/alteration of the cortical activity, even when using refined anaesthetic protocols specifically for electrophysiology, experiments should be designed to be as immune as possible to anaesthetic-related changes to cortical activity. For example, comparison of two stimulation strategies in a single animal should minimise the bias caused by the anaesthetic protocol and variations of the anaesthetic depth. Furthermore, dedicated experiments could be useful to establish the relation between the duration and depth of anaesthesia, with cortical signals such as the VEP amplitude, prior to performing experiments that will rely on those values as a measure of an additional experimental parameter.

4.5 Conclusion

Following development of the anaesthesia refinement tool we were able to develop a suitable anaesthetic protocol that was used experimentally in two Dorper sheep, where measurements of visually evoked potentials in the cortex could be recorded.

The anaesthetic technique, monitoring recommendations, and supplied checklists enabled a smooth anaesthetic event with no problems or delays occurring due to equipment or drugs not being available as required. The selection tool resulted in stable anaesthetic event that required minimal intervention once the animal was anaesthetised throughout a prolonged recording period, including during invasive surgical procedures such as craniotomies. Beyond the emphasis on balanced anaesthesia, the present article supports and reiterates the benefits of taking a methodical and structured approach to animal experimentation. Through the extensive use of inventory and procedure checklists, researchers and operators can ensure their readiness for all predictable and unpredictable events, therefore maximising the chances of successful experiments, maintenance of animal welfare and robust scientific outcomes.

Due to the success of the anaesthetic refinement tool and the underlying principles of providing balanced, well monitored anaesthesia, further evaluation of this selection tool for anaesthetic events for other types of experimental protocols is warranted. Examples include the selection of balanced protocols for experiments on rodents, or for studies intending to record cortical activity outside the visual system. Additionally, objective comparisons between experiments performed under anaesthetic regimes defined with and without the current tool’s guidance, for example with regards to the number of adverse events, would be useful to formally validate its usefulness.

As anaesthesia is an essential requirement for invasive electrophysiology experiments, many researchers in the field will be familiar with some protocols. It is important to emphasize that the introduction of an opioid to 'balance’ a protocol, from which it was previously absent, is aimed to produce a significant reduction in the required dose of anaesthetic (inhalant or injectable) and thus dose-dependent adverse effects. Researchers adopting a balanced anaesthetic protocol must be very mindful of this reduced requirement of the primary anaesthetic agent, for example isoflurane. Otherwise, ignorance of this change in requirements may lead to the animal reaching a deeper plane of anaesthesia than expected, that can increase risk of mortality of the animal or preventing successful electrophysiological measurements.

Although the prospect to alter a protocol that may have been long-established in a laboratory may seem daunting, it is important to highlight that the skills required to execute balanced protocols may not differ significantly from unbalanced techniques (e.g., the addition of an injectable component to a protocol is no major modification), and that the scientific and welfare benefits may be significant. Nonetheless, because of the effectiveness of the balanced protocols in reducing the required dose of anaesthetic agent, transitioning towards balanced protocols should therefore be done with adequate training.

This tool was designed to help improve the reasoning, planning, execution, and reporting of the anaesthetic protocols, therefore improving research outcome and reproducibility, according to the principles presented in the ARRIVE guidelines [185, 186]. In their book "The principles of humane experimental technique", Russell and Burch described anaesthetics as "[…] the greatest single advance in humane technique, [which] has at the same time been virtually indispensable for the advance of experimental biology" [211]. The intention behind the present paper is therefore to assist in the refinement of animal research, which in turn may lead to a reduction of the number of animals used for research purposes.

The present anaesthesia and monitoring refinement tool is not an exhaustive list of effective protocols for cortical neurophysiology experiments. Similarly, the tool isn't intended to provide the required technical training. It is rather a source of information to generate and facilitate discussions around the topic of modern anaesthetic techniques, particularly with veterinary and anaesthesia professional advice, for the purpose of ensuring that the scientific endeavours are of the highest quality and accuracy as currently achievable.

5 SUPRACHOROIDAL RECORDINGS

IN VIVO RETINAL RESPONSE DURING VISUAL AND ELECTRICAL STIMULATION

5.1 Introduction

Many excitable cells, neurons, and muscle cells, generate action potentials when placed in the appropriate conditions.[8] This sudden change of the cell's resting membrane potential can propagate along the length of a cell [212] and, in the case of neurons, triggers the release of neurotransmitter molecules at the interface between two cells – the synapse [213]. At the synapses, information about the arrival of an action potential in one neuron is picked up by the second cell, which sees its behaviour influenced and becomes either more or less excitable depending on the type of junction. Neurons typically share synapses with multiple other excitable cells and can generate actions potentials based on their summed inputs. In other words, action potentials convey information over a distance via the axon of neurons and communicate with other cells which use the inputs for conduction and computation [214]. For example, some axons of the neurons that compose the sciatic nerve transmit signals from the lower back, and all the way to the tip of the toes while other axons transmit signals from the toes to the lower back. In the visual system, the retinal ganglion cells (RGC) extend their axons from the eye to the lateral geniculate nucleus, which serves at a relay centre within the brain for the visual information captured by the photoreceptors [215].

[8] Note that this isn't the only conduction mechanism. For example, inside the retina, most of the processing is performed using passive conduction without action potentials being generated. In this case, graded potentials elicit the release of neurotransmitter. (Hetling, J.R., *Electrophysiology of Natural and Artificial Vision*, in *Artificial Sight: Basic Research, Biomedical Engineering, and Clinical Advances*, M.S. Humayun, et al., Editors. 2007, Springer New York: New York, NY. p. 355-380)

In natural vision, multiple levels of image processing – neural computation – take place simultaneously in the retinal layers until the signals are sent down RGC axons towards the cortex [74]. This process involves more than 60 different types of specialised neurons, including large "families" of so-called horizontal cells, bipolar cells, amacrine cells, as well as the RGCs. These neurons all respond differently depending on the properties of the incident light which has been transduced by the photoreceptors, including the coding of complex information such as colour, contrast, or movement [74].

By measuring the local changes in electrical potential caused by the neural activity, electroretinography (ERG) can be used to assess the function of the eye. During ERG, which is a common diagnostic tool, the electrical response of retinal neurons is recorded during and after visual stimuli, such as flashes are delivered. By using different test conditions information about the retinal health can be obtained. For example, the cone pathway can be assessed by light adapting the eye before the test. Exposing the eye to a constant source of light decreases sensitivity of the rods due to a process called 'bleaching'. The response of the rods during subsequent bright flashes is therefore minimised compared to the cones, which are less sensitive to light, and allows one to isolate the electrical activity of the cone-associated network [216]. As AMD affects mostly the central retina, which is characterised by a high cone density, light adapted ERG can therefore be used as part of the diagnostic of the disease [217].

When the photoreceptors degenerate, as is the case in RP and AMD, the retinal neurons, reorganise and degenerate as well due to sensory deprivation [3, 4, 149]. Fortunately, it has been shown that even after many years of blindness, the retinal neural network may maintain functional levels of connectivity with the brain, although there are strong interindividual variations [4, 150]. The clinical successes obtained with retinal implants indeed appear to confirm that many patients maintain at least some level of connectivity [14, 45, 46, 84, 99, 116]. The observed retinal remodelling nonetheless has important effects on the vision restoration strategies, the way the cells may be recruited during electrical stimulation and the appearance of the elicited phosphenes [4].

Electrical stimulation of the retina blindly[9] stimulates many cell types which find themselves within the volume of neural tissue that is in the presence of adequate

[9] Pun intended

conditions. This may also include "passing" axons of RGCs which correspond to an area of the visual field that is unrelated to the location of the stimulation. Both in healthy and degenerate retinas, this can cause possibly contradicting fragments of information to be processed in parallel and delivered to the brain, which may therefore struggle to interpret them [56]. As part of the ongoing refinement of the stimulation strategies to improve the acuity and functionality of the restored vision, researchers would therefore benefit from detailed information about the type of cells that are being recruited and the timing of their activation. It would provide important missing links between the stimuli and the percepts described by implant recipients.

There are three reports of corneal electrodes designed for ERG being used successfully to measure the electrically evoked electroretinogram (eERG) in humans [218] and in rats [219, 220]. The reports share limitations such as small signal and low signal to noise ratio. As an attempt to overcome the low signal amplitude issue, Stronks, Barry and Dagnelie stimulated all available electrodes on the Argus II simultaneously and delivered a total current of 3.0 mA (1.38 μC per stimulus phase).[10] Despite this large stimulus, they concluded that "recording capability from the electrodes in the array … [is] essential" [218], like the technology deployed in cochlear implants, in which it provides objective feedback of device functionality. Because the neural activity elicited by electrical stimulation which may be captured by suprachoroidal electrodes is likely to stem from many neurons and their axons, and to use the wording commonly used in cochlear implants, we will henceforth refer to the electrically evoked activity measured from the stimulating array as compound action potentials (eCAP). The present chapter describes the "hunt" for the elusive eCAP in a sheep model and attempts to establish a correlation between the measured signals and the cortical response.

Like in cochlear implants, an in depth understanding of the eCAP could present numerous benefits for bionic eyes in the clinic. On one side, it could help diagnose malfunctions and tune stimulation parameters intraoperatively while the recipient is anaesthetised. It could also give researchers objective information that can be compared to the subject's

[10] In the original article cited here, it is said that "the total injected current at maximal current level was 3.0 A in all subjects, and the total charge injected during the 0.46 ms stimulus phase was 1.38 mC". This is inconsistent with the reported number of electrodes and the per-electrode current (which are consistent with other papers on the Argus II). Doing the math yields a total current of *3.0 mA*, which is the value used here.

subjective description of the percepts and used to refine the stimulation. On the way towards clinical trials, it could also help to refine the design of the final preclinical experiments with the Phoenix[99]. Not only could retinal recordings provide a better understanding of the perceptual thresholds, but they may also allow continuous monitoring of the responses during long-term studies, as they do not require a craniotomy to acquire cortical signals in response to the stimuli. Incidentally, the electronics of the Phoenix[99] already include a recording and reverse telemetry technology which may be usable to measure retinal responses, but it is yet to be tested *in vivo*.

What is likely the main challenge of such recordings is readily being addressed in the current design: the presence of a very large electrical artefact due to the stimulus. The stimulation pulses, delivered in close proximity to the recording sites, cause the amplifiers to saturate, and the microvolt neural signals to be distorted and "lost" in the high amplitude artefacts [12]. To address this issue, the Phoenix[99] implements a technique described by Wheatley and Lehmann, which effectively avoids amplifier saturation and reduces the amplitude of the artefact in the recordings [12]. While the details of the implementation are out of scope for this dissertation, it is interesting to highlight its biggest limitation: it allows only one datapoint to be acquired after each stimulus, therefore requiring long recording sessions. While this may not be an issue after typical successful and unsuccessful stimuli have been characterised in detail, because recordings will then be focussed on a short, representative post stimulus time window, it may not be practical in the exploratory phase in which we currently find ourselves. Figure 5-1 shows an example of what a "targeted" recording using the Phoenix[99] may look like. Provided that the latency, duration and frequency spectrum of the response of interest are known, a small number of stimuli/recordings events can be used to detect the presence of a response, or even plot a waveform. Nonetheless, even in this ideal case, multiple samples at each post-stimulus timepoints may be required to minimise the effects of noise on the recordings. Depending on the stimulation frequency, the duration of recordings may rapidly become unpractical in the exploratory phase, where the parameters of the response are unknown.

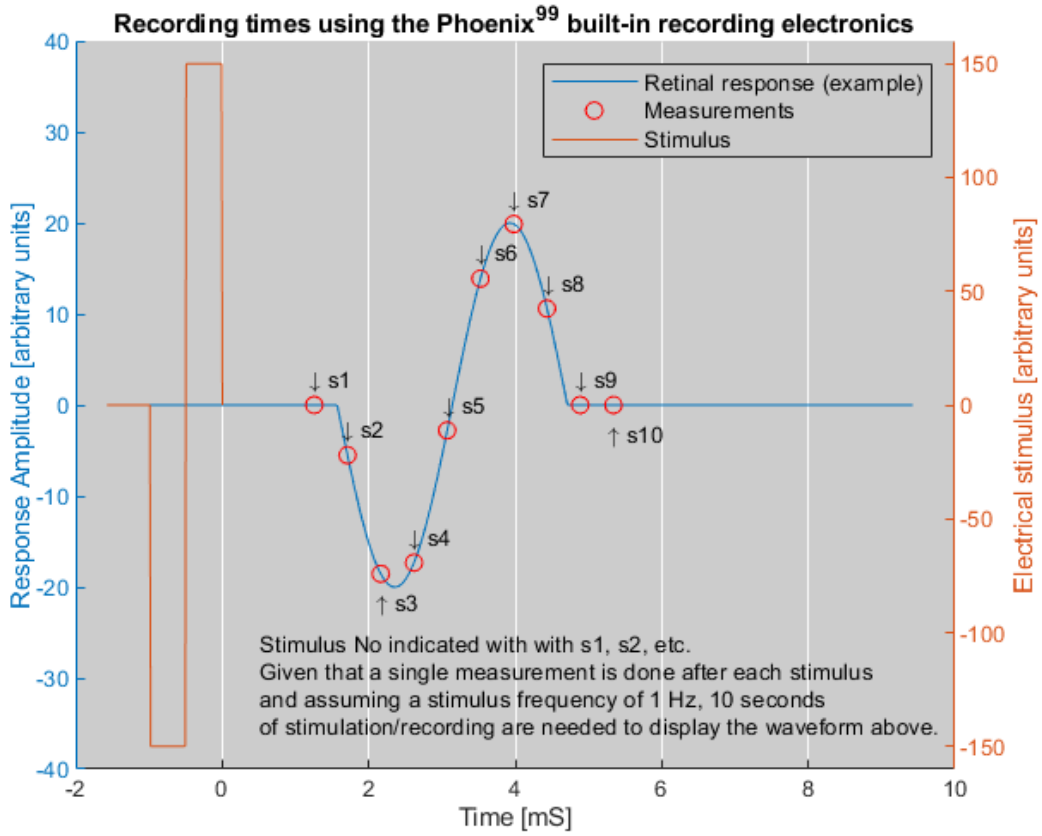

Figure 5-1 Targeted recording using the Phoenix[99] built-in electronics. Provided that the latency and duration of the response of interest are known, a small number of stimuli/recordings events can be used to detect the presence of a response, or even plot a waveform. In this example, a stimulation frequency of 1 Hz is assumed. Because a single measurement can be performed after each stimulus, it takes 10 seconds to collect 10 data points. Samples collected after stimuli s1, s2, s3, etc. are marked with a red circle. In the presence of noise, multiple datapoints would be required at each timepoint. Similarly, if the latency, duration, and frequency spectrum of the response are unknown, long recordings and over-sampling are required to capture the waveforms.

Little is known about what the retinal eCAPs may look like. *In vitro* electrophysiology with retinal preparations provide detailed information about the response of a wide variety of cells to light and electrical stimulation [65], the attempts at *in vivo* recording of the eERG have shown very different temporal behaviour [218]. In the present context, a system with continuous recording capability is therefore preferable to provide more flexibility. In this chapter, we explore retinal response recordings using the Intan technologies RHS stimulation/recording controller (Intan Technologies, Los Angeles,

California, USA), rather than the application-specific integrated circuit designed to be implemented in the Phoenix^{99}.

Because little information is currently available about what the eERG may look like, we began this exploratory experiment by characterising the retinal response from the suprachoroidal space during visual stimulation. Although ERG is typically measured from the cornea, the signal has been studied extensively and the influence of many types of cells on the signal has been characterised. Using this information, we explored novel ways to use the suprachoroidal ERG (sERG) to determine the location of the electrode array with regards to the high acuity areas of the retina. In the sheep and in the human alike, areas of high cone photoreceptor density dedicated to high acuity vision in high light levels are clearly defined [221]. Accordingly, we hypothesised that bright flashes in the light adapted eye of the sheep could cause sERG signals of higher amplitude in electrodes located in areas of higher cone densities, hence providing information about the type of functional network that electrical stimulation may subsequently recruit.

In the context of bionic eye research, particularly using normally sighted animals, the novel concept of sERG may become a useful tool to identify the type of photoreceptor network (e.g. rod or cone) with which the individual stimulation electrodes are in most direct contact. This may be useful to study the correlation between the primary type of recruited network, for example neurons specialised in high acuity, photopic vision, and cortical responses and thresholds. Obviously, its application to blind eyes with degenerate retinas and only few surviving photoreceptors may yield results that are difficult to interpret. Nonetheless, as the Phoenix^{99} and other suprachoroidal devices may be compatible with residual vision [123], one might foresee an application for sERG in precisely identifying the position of the array with regards to health areas of the retina. With this information, stimulation of the areas of remaining light sensitivity could be avoided to minimise the disturbance of the surviving natural vision.

In the present chapter, hypothesis-generating experiments are presented. As such all conclusions call for confirmation using specifically designed experimental protocols. Nevertheless, even with a small sample size, interesting observations could be made, that will impact how research on retinal recordings and around the Phoenix^{99} is conducted.

5.2 Methods

5.2.1 Electrode array

For this acute, terminal experiment, there were no requirements for the device to be fully implantable. As such the experimental set-up was adapted to include a suprachoroidal array for stimulation and recording, with wired connections to the externalised electronics.

5.2.1.1 Features

The electrode array was designed to resemble the array of the Phoenix[99]. As such, despite featuring 15 electrodes and one large diameter return instead of 98 and one in the fully implantable design, the electrode array used in this acute experiment was built using the same materials. The acute arrays included 15, 600 µm diameter stimulation/recording electrodes organised in a hexagonal pattern with a centre-centre distance of 1 mm (Figure 5-9), like the electrodes of the Phoenix[99] and a Ø4.2 mm monopolar electrode. Each hexagon, composed of seven electrodes, received a number and each electrode was numbered from zero to six with electrode zero at the centre of the hexagon. The array featured two full hexagons, named Hex1 and Hex2 and one additional electrode named H5E1 as it corresponds to the fifth hexagon of the Phoenix[99] design [11]. See Figure 5-2 for an overview of the electrode names on the acute array.

[11] Electrode organisation, nomenclature and connectivity were maintained from the Phoenix[99] to allow for straightforward use of the custom application-specific integrated circuit for stimulation and recording experiments in the future, using same electronics as the fully-implantable device.

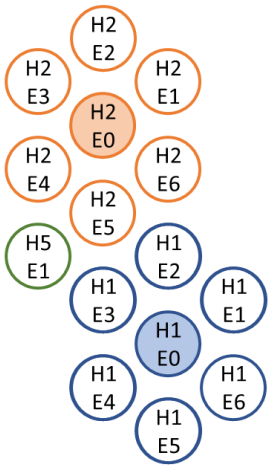

Figure 5-2 Electrode names on the acute electrode array. The naming convention follows that used in the electronics of the Phoenix[99].

The position of the monopolar return was adapted in a way that the electrode is located *inside* the suprachoroidal space, instead of on the sclera. This was done to avoid issues due to unreliable electrical contact. Indeed, in the Phoenix[99], the monopolar return electrode is located at the bottom of the VS capsule that is sutured directly to the sclera [1] and is therefore tightly pressed against the tissue. Additionally, the device is designed for long term implantation and during the postoperative period, fluids will infiltrate any available space and improve conductivity in case of gaps. During an acute procedure, the presence of fluid can't be guaranteed, and it may lead to poor conductivity, hence the decision to move the return inside the scleral incision. As seen in Figure 5-3, this change nonetheless resulting in a very similar distance between the stimulation electrodes and the return (13.7 mm in the Phoenix[99] versus 15 mm in the acute array). A notable difference which is the result of this design is that using the acute array, the return electrode is located under the sclera. The electrical path for the current may therefore be significantly different from the Phoenix[99] where the current will need to flow through the sclera.

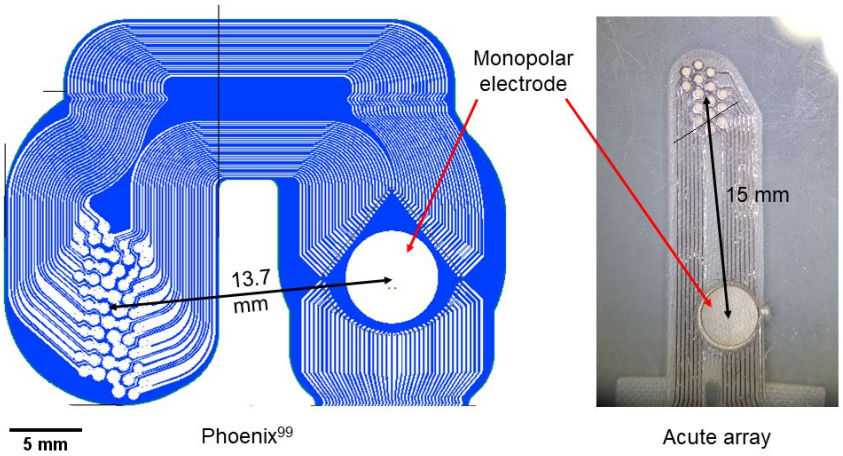

Figure 5-3 Monopolar return position comparison between the Phoenix^{99} and the acute array. In the acute device, the monopolar return is located 15 mm from the centre of the group of electrodes, versus 13.7 mm in the Phoenix^{99}. Note that the monopolar return in the acute array is located under the sclera, where the sclera separates the stimulating and return electrodes in the design of the Phoenix^{99}.

Other defining features of the acute array were the use of a fine grade nylon mesh backing to increase the electrode rigidity. This was required to compensate for the fact that the Phoenix^{99} is built by folding two silicone-platinum-silicone "sandwiches" onto each other to get the 98-electrode array [222]. Finally, the array uses an additional patch of nylon mesh covered in medical grade silicone and glued perpendicular to the array to (1) provide a physical guide to the adequate insertion depth, and (2) allow for safely suturing the array in position at the scleral incision. An oblong hole was also added at the centre of the array to be used to place a third suture to ensure adequate array stability and help with wound closure (Figure 5-4). Figure 5-5 shows the entire electrode array, including a custom-made copper-polyimide ribbon cable used to reliably connect the electrode array to the stimulation/recording electronics using commercially available zero insertion force connectors.

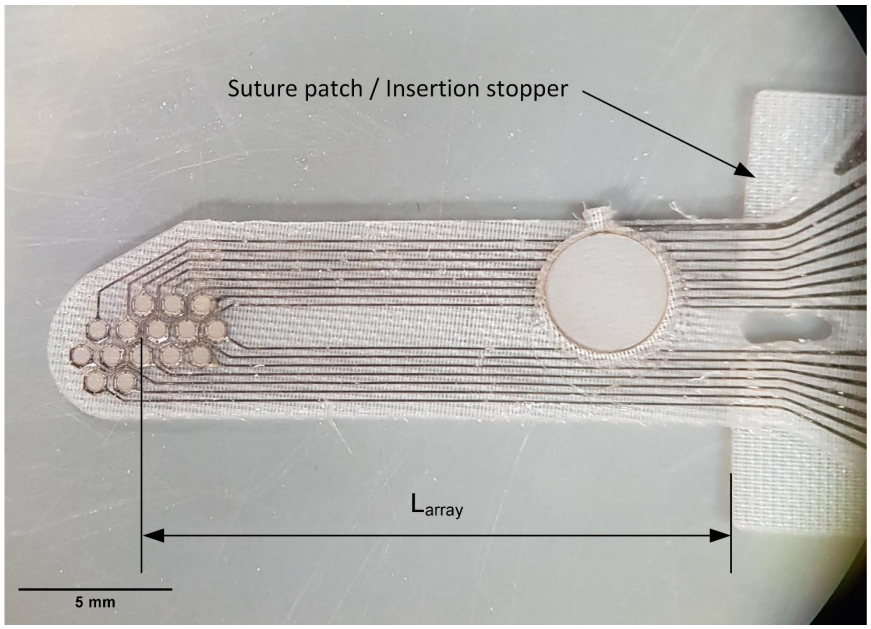

Figure 5-4 Electrode array with return electrode, monopolar return and suture patch, which also serves to limit the maximum insertion depth. The oblong hole on the right provides an additional location to position a suture. The nylon mesh is visible under the platinum structures, through the silicone.

Figure 5-5 Whole array with custom made, copper-polyimide ribbon cable for connection to the stimulation/recording electronics.

5.2.1.2 Dimensions

Sheep eyes have similar dimensions to the human and are therefore an adequate model for surgical training and experimentation with implants designed for humans [162]. There

are nevertheless differences which should be accounted for when dimensioning arrays specifically for this animal model.

The sheep cornea is oval with the vertical corneal diameter (VCD) is smaller than the horizontal corneal diameter (HCD) [223]. This difference, as well as the incision location during surgery should be considered when dimensioning devices. Although this may not always be possible, for example if a device in its final form is to be tested in animals. In the present experiment, electrode arrays were designed specifically for the sheep and hence dimensioned to maximise the number of electrodes positioned close to the centre of the visual field (*area centralis*). Note that the sheep retina is lacking the fovea – which is responsible for high acuity vision in humans [224] – but the *area centralis* is nonetheless responsible for high acuity vision in the frontal field of vision [221].

Without specific information on the dimensions of the globe in the Dorper breed, the following dimensioning exercise was performed based on the measurements made by Mohammadi [162] on Afshar sheep. Afshar and Dorper sheep have similar adult weights (Adult Dorper Ewes: 50-80kg [225] VS Adult Afshar ewes: average 70.52 kg. [226] and the eye dimensions were therefore also assumed to be similar.

The electrode array length (L_{array}) required to centre the array as close as possible to the *area centralis* was defined as the distance between the location of the suture patch – which also sets the insertion depth – and the geometric centre of the group of electrodes (Figure 5-4). Knowing the exterior radius of the globe (R_{globe}), the position of the incision with regards to the corneal limbus (IP) and the thickness of the sclera (T_{sclera}), L_{array} can be calculated as the length of arc under the sclera between IP and the *area centralis*, as per Equation (2). Note that for the sake of simplicity, the eyeball geometry was simplified to a sphere Figure 5-6 shows a cross-section through the centre of the sphere and intersects the centres of the *area centralis* and the iris.

$$L^{array} = R_{sc} \cdot \theta \quad \textbf{(2)}$$

With θ, the angle covered by array and R_{sc}, the radius at the implant location in the suprachoroidal space:

$$R_{sc} = R_{globe} - T_{sclera} \quad \textbf{(3)}$$

From Figure 5-6, we see that

$$\theta = 180 - \alpha - \beta$$

(4)

With

$$\alpha = \sin^{-1}\left(\frac{VCD/2}{R_{globe}}\right)$$

(5)

Similarly, noting that IP is measured with callipers during surgery and therefore as a straight line across the globe we get

$$\beta = 2 \cdot \sin^{-1}\left(\frac{IP/2}{R_{globe}}\right)$$

(6)

A numerical application with the variables from Table 5-1 leads to L_{array} = 19.3 mm, which was implemented in the electrode array design used in the present experiment.

Table 5-1 Eye size and incision position to determine electrode array dimensions.

Variable	**Value [mm]**	
R_{globe}	12.89	[162]
T_{sclera}	1	[227]
VCD	17	[162]
IP	10	[1]
L_{array}	19.3	

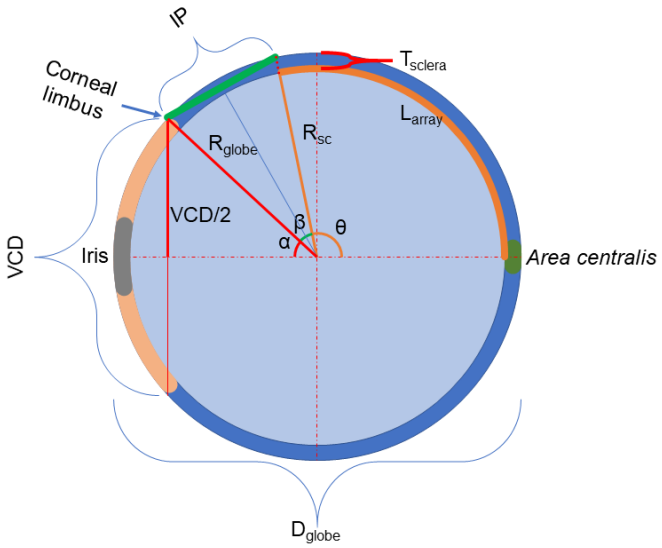

Figure 5-6 Determination of electrode array dimensions. Cross-section through the centre of the sphere and intersects the centres of the *area centralis* and the iris. VCD: vertical corneal diameter; D_{globe} and R_{globe}: globe diameter and radius, respectively; IP: position of the incision; R_{sc}: radius at the implant location in the suprachoroidal space; T_{sclera}: scleral thickness; L_{array}: electrode insertion depth, between the insertion stopper and the centre of the group of electrodes.

5.2.1.3 Manufacturing

Electrode array manufacturing was adapted from a technique previously reported [122]. Briefly, medical grade silicone (MED-1000, NuSil Technology LLC, Carpinteria, California, USA) was thinned with n-Heptane (1:1 volume ratio) and squeegeed into fine-mesh nylon fabric, directly on a glass slide covered with a release layer (Type 4124, Tesa, Eastern Creek, NSW, Australia). The nylon-reinforced electrode base was then cured at 80°C for 10 minutes. Silicone mixed with n-Heptane (1:1 volume ratio) was then spin-coated on top of this layer and pre-cured at 80°C for 10 minutes before laminating a plasma activated platinum foil (Zepto, Diener electronic GmbH & Co. KG, Ebhausen, Germany, power 75%, oxygen flow 0.5-1L/min, time 20mins).

The metal foil was then patterned using femtosecond laser cutting with 540 nm wavelength (µFAB-L, Newport Corporation, Irvine, California, USA). Metal dust from the ablation process was then wiped off with a clean room wipe soaked with ethanol before peeling off the extra foil, leaving behind a network of tracks and electrodes, attached to the substrate (Figure 5-7). The assembly was then plasma activated as per

procedure above to promote adherence for the final layer of spin-coated, thinned silicone and cured 10 minutes at 80°C.

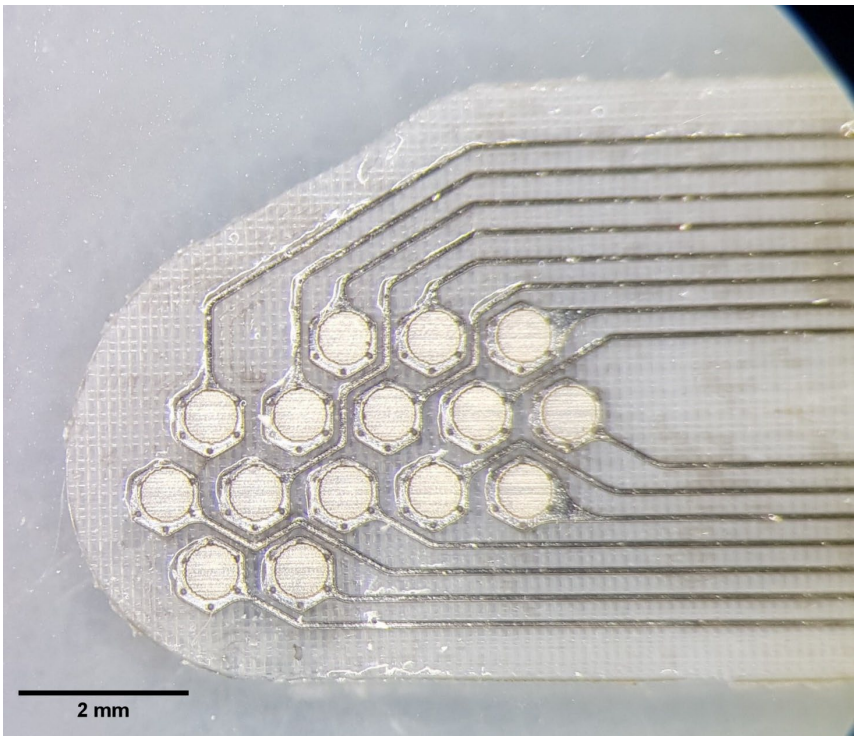

Figure 5-7 Electrode close-up. Fifteen, microroughened, platinum electrodes organised in a hexagonal structure. The design choice provides three "full" hexagons, featuring seven electrodes (one central electrode and six 'guards').

The contour of the array was then cut with the Femtosecond laser system. The surface of the electrodes, except for the monopolar, were exposed by ablation of the silicone. The process was designed to simultaneously micro roughen the metal surface and increase the real surface area available for charge injection, similar to the method described by Green et al. [228] (Figure 5-9 and Figure 5-10). The monopolar return was carefully lifted off the substrate, folded over tracks of the array and glued in place using a drop of pure MED-1000 (Figure 5-4), which was cured for 10 minutes at 80°C. After ablating the silicone off the monopolar following the same technique as for the electrodes, the array was lifted from the substrate using ethanol 90% as release medium.

The suture patch was prepared by diluting MED-1000 with n-Heptane (1:1 volume) a using a squeegee to saturate the cloth on a Tesa tape release layer and curing as described above. The patch was then laser cut according to the process described above, glued in place with silicone and cured (Figure 5-8).

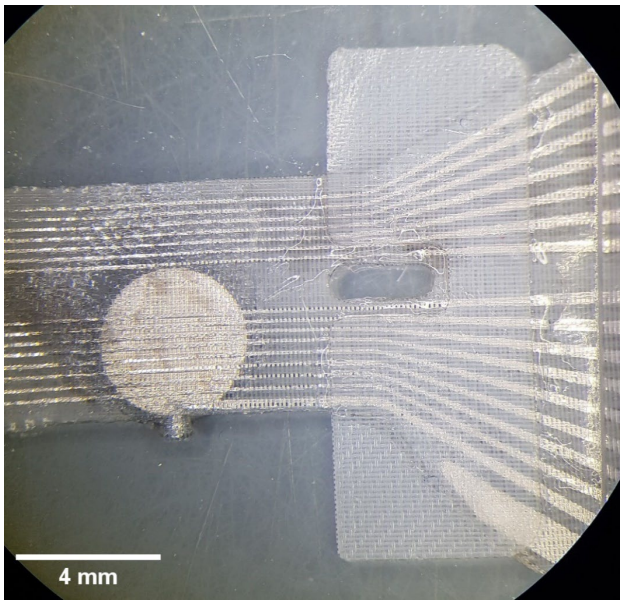

Figure 5-8 Bottom view of the electrode array and suture patch showing the oblong opening to secure the array to the sclera.

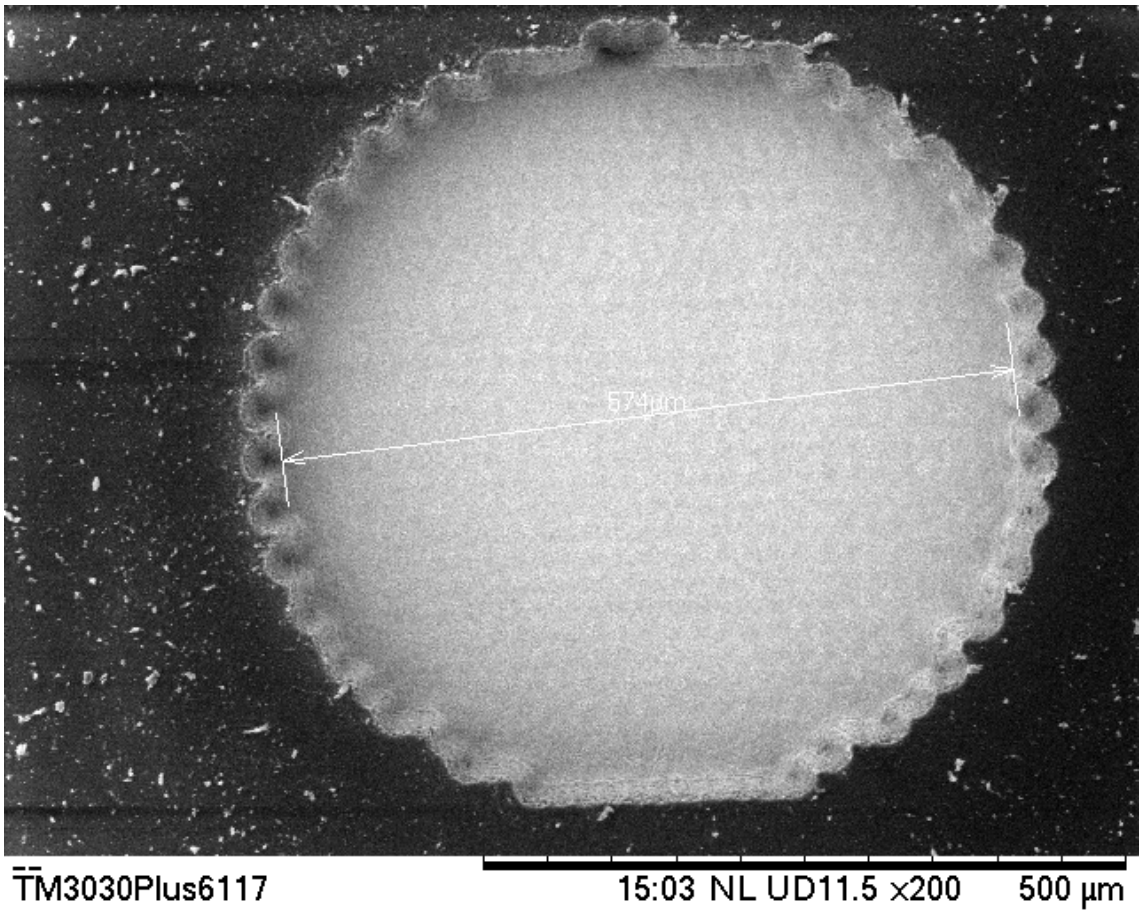

Figure 5-9 Laser-microroughened platinum electrode. The effective diameter of fully exposed platinum is 574 µm, marginally smaller (surface area reduction smaller than 8.5%, calculated by simplifying the electrode geometry as a circle of Ø574 µm) than the specified value of 600 µm. The measurement, which included only the surface area of platinum completely exposed nonetheless underestimated the total surface area of metal available for charge delivery. For the sake of simplicity, the electrode diameter was therefore considered to be 600 µm. Using the laser control software, the beam path was defined automatically inside a circle, leading to the minor asymmetricity of the result.

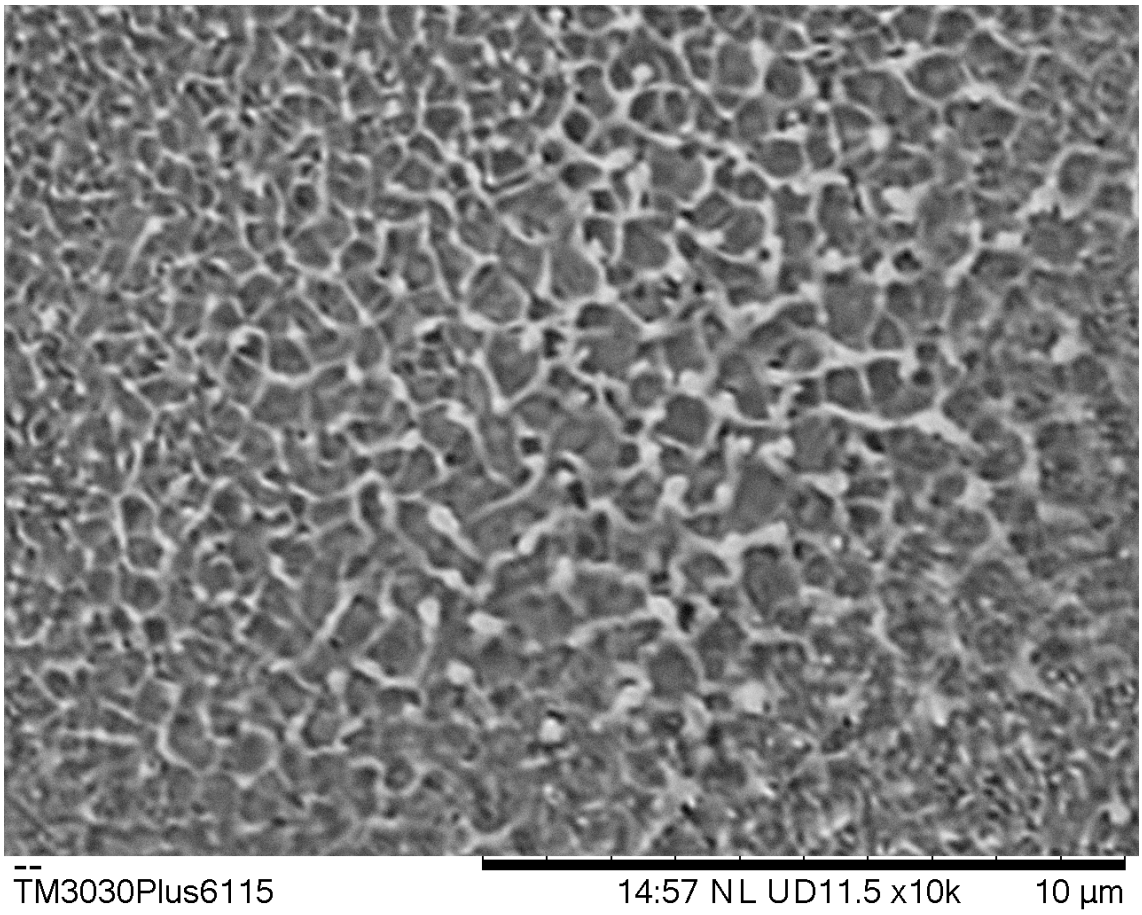

Figure 5-10 Microroughened platinum electrode surface (x10000 magnification).

5.2.2 Animal model, cohort, and care

Model selection for long-term implantation studies is an extremely important process, as it may strongly affect the validity of the results with regards to translation to human subjects. Furthermore, chronic studies should consider practical factors, such as the size of the animals, which will impact the ease with which the experiments can be performed over the months of the study.

To increase coherence and continuity between studies related to the same device it is very beneficial to use the same animal model for all experiments. As a pilot for long-term studies of the Phoenix[99], the experiment described in this chapter uses the same model to ensure reproducibility of the results and applicability of the conclusions.

As described in details in Chapter 3 [1], an appropriate model has been identified in the Ovis aries (sheep). The sheep – and the human – have a relatively large volume of fatty media in the space separating the eye from the orbit. This is particularly true in the lateral and temporal areas of the orbit where the device is intended for implantation.

In particular, the Dorper breed was selected because of the suitability of the neck tissue for tunnelling and communications with the telemetry unit in future studies. Dorper sheep do not have the folds of fleece around the neck associated with sheep bred for wool production. The relatively small size of the Dorper breed also makes the handling of the animals easier. But most importantly, the size and shape of the orbit are a good match with human anatomy [1, 162].

Two ewes of the Dorper breed, aged between one and two years old and weighing 50 and 51 kg, were used for this acute, terminal experiments. During the preoperative acclimation period (minimum two weeks), the animals were held together in a modular pen system (9 m^2) with straw as bedding material and artificial night/day cycles (13 hours of light per day). Temperature was maintained between 20 and 24°C and relative humidity kept in the range 40-60%. Hay and water were provided *ad-libitum* and the sheep received small amounts of lucerne hay and chaff on the ground to assist with acclimatisation. Environmental enrichment included mirrors, plastic toys and lick blocks, and novel food provided daily within the straw to encourage rooting behaviour.

A full exam was performed by a veterinarian on admission and visual health inspections were performed at least twice weekly. Due to the experiment being terminal, the second sheep was held alone for 48 hours before undergoing the procedure, according to the standard operating procedures in place (see Appendices). Frequent visits from the staff and additional enrichment were provided to minimise the effects of isolation.

5.2.3 Intraocular pressure

Intraocular pressure (IOP) was obtained as an indicator of eye health and to evaluate the effects of the intervention. It was measured using a TonoVet rebound tonometer (Icare Oy, Helsinki, Finland). Baseline pressure was measured in the pen using gentle restraint in a standing position on three different days during the last two weeks prior to the intervention.

Pre- and intraoperative IOP were obtained with the animal anaesthetised on the operating table and in position for surgery.

5.2.4 Anaesthesia and monitoring

Anaesthesia and monitoring were performed according to the protocol described in detail in Chapter 4.

5.2.5 Surgeries and electrical recordings

After dilating the pupils with Atropine 1% (Aspen Australia, St Leonards NSW, Australia) a staged protocol was used to acquire electrical recordings during visual and electrical stimulation. First, preoperative light adapted ERG (see 5.2.6 for details) was performed to establish a baseline using one custom, gold, corneal electrode (Figure 5-11) in each eye. The ERG signal electrodes were positioned as deep as possible under the lower eyelid and the wire was suture to the lid for increased stability. The eyelids were held open and the eyes regularly hydrated using eye ointment (Lacri Lube, Allergan Australia Pty. Ltd, North Sydney, NSW, Australia) throughout the experiments. All electrical recordings were performed using the Intan Technologies RHS multichannel stimulation/recording system driven by the associated RHS Data Acquisition Software (Intan Technologies, Los Angeles, California, USA). For ERG recordings, a needle electrode positioned on the nose at equal distance from both eyes was used as reference. A second needle electrode inserted in the skin of the scalp was used as a headstage ground (isolated from earth ground). As opposed to all other recordings, including from the suprachoroidal space and the cortex, a modified Intan headstage was used. The electronics ground and reference pads were insulated from each other to improve the common-mode rejection capability of the set-up in this particular case where only two channels were used.

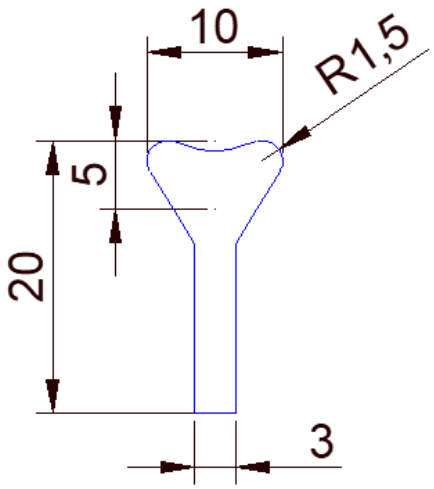

Figure 5-11 Corneal ERG electrode geometry. The shape of the "whale tail" was tested in sheep cadavers and provided good stability under the lower lid of the sheep. A wire was soldered directly to the 25 µm gold foil and the solder joint was covered with medical grade silicone (MED-1000, Nusil). Two corneal electrodes were used simultaneously in each animal, one in each eye.

After establishing the preoperative ERG baseline, the suprachoroidal electrode array was implanted in the right eye of both animals according to a technique adapted from the procedure described in Chapter 3. Briefly, a lateral canthotomy was performed after blanching the tissue from the lateral canthus with haemostats to reduce bleeding. A corneal stay suture was used to manipulate the globe. The conjunctiva and tenon's capsule were dissected and a seven-millimetre incision of the sclera was made ten millimetres posterior to the limbus (Figure 5-6). Array insertion was simplified by the creation of a suprachoroidal pocket by blunt dissection using a polyester insertion guide with the same dimensions as the array. The array was sutured to the sclera at the insertion site using three 6-0 Vicryl sutures (Ethicon, Raritan, New Jersey, USA) located on either sides and in the centre of the scleral incision. For all recordings from the suprachoroidal space, the ground of the amplifier headstage was connected to the monopolar electrode of the electrode array visible in Figure 5-4.

Craniotomy

The posterior segment of the skull was exposed using full-thickness, midline incision of the skin. A 30 by 30 mm craniotomy, centred 20 mm rostral and 10 mm lateral to the lambdoid suture [200], allowed access to the cortex. Bone haemorrhages were stopped

by massaging sterile bone wax (W31G, Ethicon, Raritan, New Jersey, USA) into the pores. A durotomy was performed by carefully lifting the dura with tweezers and incising it with an ophthalmic knife (Alcon, Geneva, Switzerland) around the craniotomy.

After preliminary probing of the cortex with a platinum ball-electrode manipulated by a KUKA lbr med robotic arm (KUKA, Augsburg Germany), and with a needle-electrode as ground/reference in the scalp dorsal from the incision, a penetrating Utah array (Blackrock Microsystems, Salt Lake City, Utah, USA) was inserted in the visual cortex. A custom-built, 3D printed Utah pneumatic inserted holder was assembled on the KUKA robotic arm. The pneumatic inserter was then used to impact the Utah array into the cortex. Ground/reference electrodes from the Utah array were positioned under the scalp and the Utah connected to the Intan system via a custom-made adapter printed circuit board.

Up to four RHS 32-channel headstages were used simultaneously to record the biological signals: one for ERG; one to record from the electrode array implanted in the suprachoroidal space; and one (platinum ball-electrode) or three (Utah array) headstages were used to record from the cortex. The Intan system was also used to deliver electrical stimulation and trigger the delivery of visual stimuli.

5.2.6 Light stimulation

Full-field illumination, where all the photosensitive retina is exposed to the light, maximises the response and, if of interest, allows for the functional evaluation of the whole retina. For the present experiment, custom made full-field flash stimulators were designed and 3D-printed out of white thermoplastic (polylactic acid). The design feature a spherical cavity to maximise the surface area of retina exposed to light. A single, circular cavity which is positioned directly in front of the eye was opened in the reflective sphere. Two white (approximately 6740 Kelvin) light emitting diodes with wide viewing angle (NSDW570GS-K1-B-P9-P11, Nichia Corporation, Anan, Tokushima, Japan) were positioned inside the sphere and oriented towards the portion of the sphere facing the eye (indirect illumination of the retina).

One LED was constantly switched on and used to adapt the eye with dim light (72 lm/m2, 12.7 cd/m2). The second LED was used to deliver bright flashes (1778 lm/m2, 422 cd/m2) lasting 50 ms while the adaptation light was kept on. The Intan system was used to trigger the flashes via one of the digital outputs. Figure 5-12 and Figure 5-13 show a photograph of the device and a rendered view of the 3D model, including the position and angle of

the LEDs. Note that the homogeneity of the illumination at the viewing hole was not characterised.

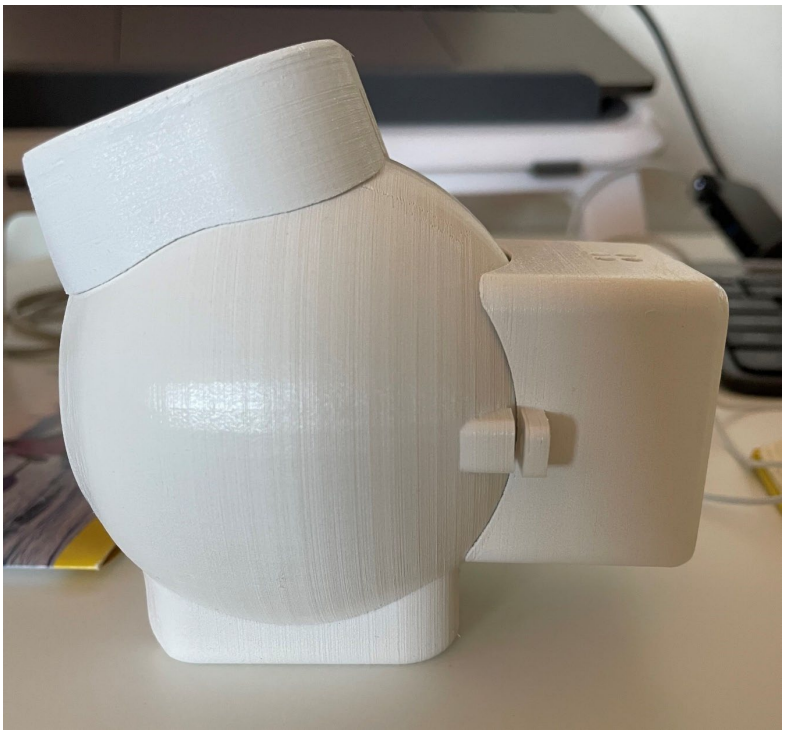

Figure 5-12 Full-field light stimulator. Photograph

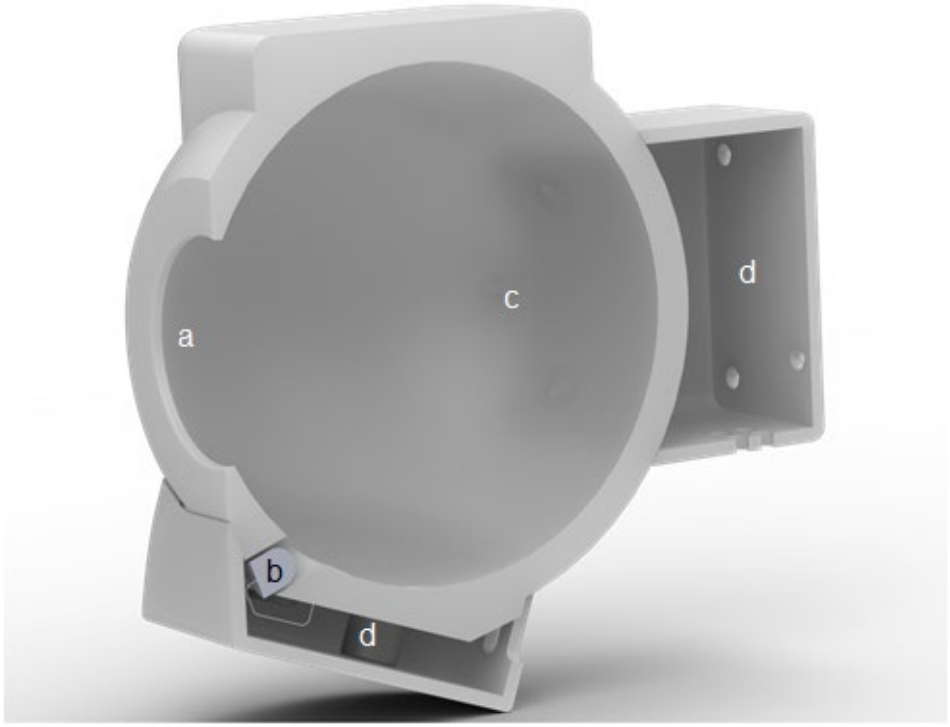

Figure 5-13 Three-dimensional rendering of the light source showing the viewing hole (a), one of the two LEDs used for light adaptation and flash stimulation (b), the spherical reflective screen (c), and the cavities for the power and control electronics (d).

5.2.7 Electrical stimulation

Square, biphasic, cathodic-first pulses of constant amplitude (400 µA, 500 µS) with no inter-phase gaps were delivered on one, two, three or four suprachoroidal electrodes simultaneously (see stimulation configurations in Figure 5-14), with reference to a monopolar electrode located in the suprachoroidal space, close to the incision site. Series of 25 pulses were delivered at 1.01 Hz using the Intan RHS stimulation/recording system.

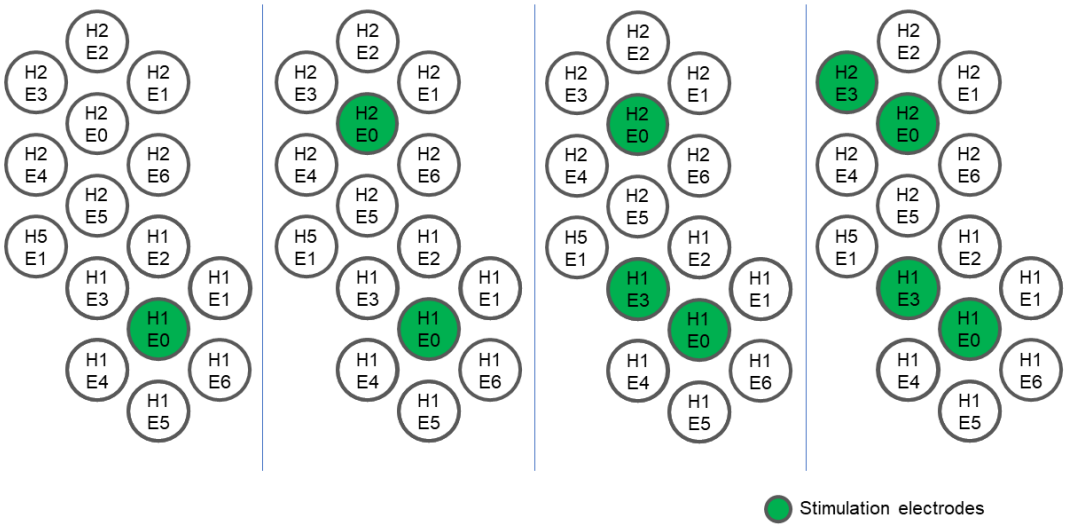

Figure 5-14 Stimulation configurations overview. Up to four stimulation electrodes (green) were used to deliver pulses simultaneously. On each active electrode, the stimulation consisted in a biphasic pulse with an amplitude of 400 µA and a phase duration of 500 µS.

5.2.8 Data processing

All data were processed in Matlab R2021b (Update 1, MathWorks, Natick, Massachusetts, USA) using custom scripts. ERG and sERG signals were notch filtered using Butterworth band-stop filters at 50, 100, 150, 200 and 250 Hz to remove peaks at the harmonic frequencies, then high-pass filtered (0.8 Hz) and low-pass filtered (300 Hz). Because of the very large stimulation artefact, filtering caused large oscillations before and after the stimulus in the suprachoroidal recordings with electrical stimulations. Filters were therefore not applied for these recordings.

Ensemble average was performed on all recordings. For each stimulation configuration, all available data was included by grouping recordings with identical parameters. The number of recording sessions with a given set of parameters was not scripted, which lead to variable numbers of recordings being performed. As a result, between 25 and 150 repeats of each configuration, unless specified otherwise, were averaged together to minimise the effects of random noise. Artefact minimisation techniques were applied to the suprachoroidal recordings with electrical stimulation, including subtraction of post-mortem recordings, digital referencing to neighbouring electrodes with similar artefacts, and subtraction of runs with fewer stimulating electrodes.

5.3 Results

5.3.1 Electroretinography

Corneal, full-field ERG (ffERG, henceforth termed ERG for the sake of simplicity) of the two normally sighted sheep presented three well defined main peaks shown in Figure 5-15. During the 50 ms stimuli, a rapid, negative peak (n1) was quickly followed by a positive peak (p1). Timing and sequence of the peaks suggest that n1 and p1 correspond to the commonly reported a-wave and b-wave, respectively [216]. In the light adapted, healthy eye as in the present setting, the ERG waveform is dominated by the response from the cone network. The a-wave, measured from the signal baseline to the peak, reflects the activity of the cone photoreceptors and cone Off-bipolar cells. The b-wave, which is measured between the peaks of the a-wave and b-wave, represents the response from the On- and Off-cone bipolar cells [216]. The latencies for both peaks, measured pre- and postoperatively in both eyes of the two animals, were consistent with values reported by Regnier et al. for light adapted ERG in the sheep (a-wave: 12.94 ± 0.67 ms *vs* 13.01 ± 0.7 ms, b-wave: 28.26 ± 4.07 ms *vs* 29.6 ± 0.9 ms [229]).

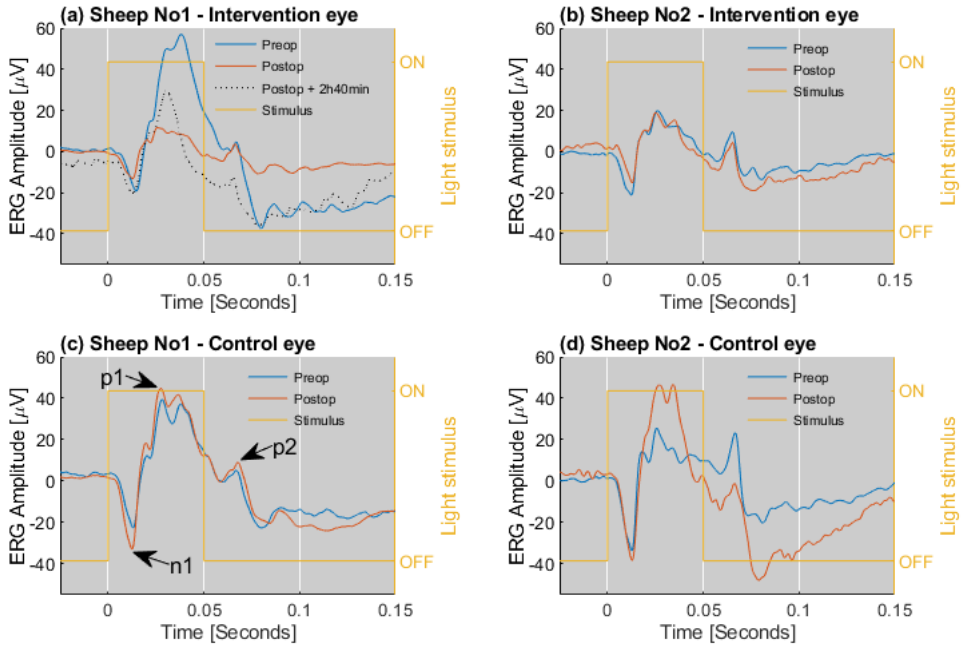

Figure 5-15 Corneal electroretinogram. In each panel, pre- (blue) and postoperative (orange) ERG recordings showing three main peaks related to the stimulus switch-on and switch-off. Magnitude variations between the pre- and postoperative settings were seen in one operated eye and one control eye. In Sheep No1, the intervention eye (a) presented reduced b-wave magnitude (p1-n1) postoperatively, which partially recovered over time and after tapping the anterior chamber to reduce IOP which was elevated after array implantation (additional trace in black). In Sheep No2, the ERG amplitude was larger postoperatively for the a-wave (baseline – n1) and b-wave (b). The eye aperture was difficult to verify after positioning the light source and some of the ERG variations may be explained by the surface area of retina illuminated by the stimuli. In all eyes, the latency of n1 (12.94 ± 0.67), p1 (28.26 ± 4.07 ms) and p2 (66.29 ± 0.86 ms) were consistent pre- and postoperatively. Additionally, the peak latencies for the a- and b-waves were consistent between both animals and with the literature [229]. The secondary peaks and oscillations visible in the traces were not further analysed, due to the uncertainties related to their origin and interpretation.

Upon light switch-off, a fast, positive peak (p2) was observed which appears consistent with the d-wave described by the International Society for Clinical Electrophysiology of Vision (ISCEV) in an extended protocol developed to assess the On- and Off-systems. It is a complex response which involves Off-bipolar cells, as well as cone photoreceptors and On-bipolar cells [230]. Although further characterisation of the d-wave in sheep is

out of scope for the present dissertation, it is worth noting that the d-wave may not have been measured in the ovine model before with Sustar et al. claiming that "positive On- and Off-responses, as those in humans, can only be recorded in some non-human primates" [230]. Further experiments in the sheep, particularly with varying stimulus lengths, would be required to demonstrate that the waveform highlighted as p1 in Figure 5-15 is indeed an example of d-wave. Due to the uncertain biological interpretation of 'd-wave' in the ovine, the a- and b-waves will be the centre of attention in the remainder of this section. Similarly, the secondary peaks and oscillations visible in the traces were not further analysed, due to the uncertainties related to their origin and interpretation.

ERG amplitudes were consistent pre- and postoperatively in the control eye of Sheep No1 and in the operated eye of Sheep No2. The control eye of No2 presented an increased b-wave and overall noticeably different waveform, compared to the preoperative signal. The IOP was consistent during both recordings and didn't influence the measurements. Because light adaptation was performed using an LED positioned inside the light sources, they had to be kept in place during all adaptation and test sequences. Consequently, it was difficult to access the eyes to verify that they were adequately open. It is presumed that the eye lids may have been partially closed during the preoperative measurements. The corneal electrode may also have moved slightly, changing the surface area of gold in contact with the tissue.

The operated eye of Sheep No1 presented reduced ERG amplitudes after electrode array insertion. Similar to Sheep No2, the eye lids may have been partially closed during the postoperative trials. Alternatively, the gold corneal electrode may have been only partially in contact with the cornea. The differences between the signals may also have been the result of accidental trauma to the eye. During initial array insertion, bipolar cautery was used to control bleeding of a scleral blood vessel at the incision site. This operation may have weakened the tissue, possibly causing a local perforation which subsequently led to a tear during array insertion, exposing the vitreous humour. Array insertion at that location was aborted, and the wound was carefully sutured. Secondary array insertion, approximately 7 mm further nasal from the initial insertion site was completed without incident. Although this event is unlikely to have caused direct retinal damage, it can't be excluded that the additional eye trauma due to a secondary insertion participated in the ERG changes measured.

Additionally, IOP was elevated postoperatively (44 mm Hg *vs* preoperative 13 mm Hg), which may have depressed the ERG. The signal only partially recovered (black trace in

quadrant (a) of Figure 5-15) after tapping the anterior chamber to reduce the IOP (0.53 ml tap resulting in 10 mm Hg IOP). In Sheep No2, tapping was performed before the postoperative ERG recordings and pressure was maintained in the preoperative range (9 and 4 mmHg pre- and postoperatively, respectively). The cone-driven a- and b-waves could nonetheless always be identified adequately in both animals.

5.3.2 Suprachoroidal electroretinography

Compared to the ERG, the averaged signal from 15 suprachoroidal electrodes yielded very similar patterns despite overall increased signal amplitude and increased secondary peak amplitudes. The three main peaks (n1, p1 and p2) were clearly identifiable in both animals. Interestingly, an unexpected signal inversion (positive a-wave, negative b- and d-waves) was seen in Sheep No2 (panel (b) in Figure 5-16). Sheep No2 also presented a markedly increased sERG amplitude compared to Sheep No1.

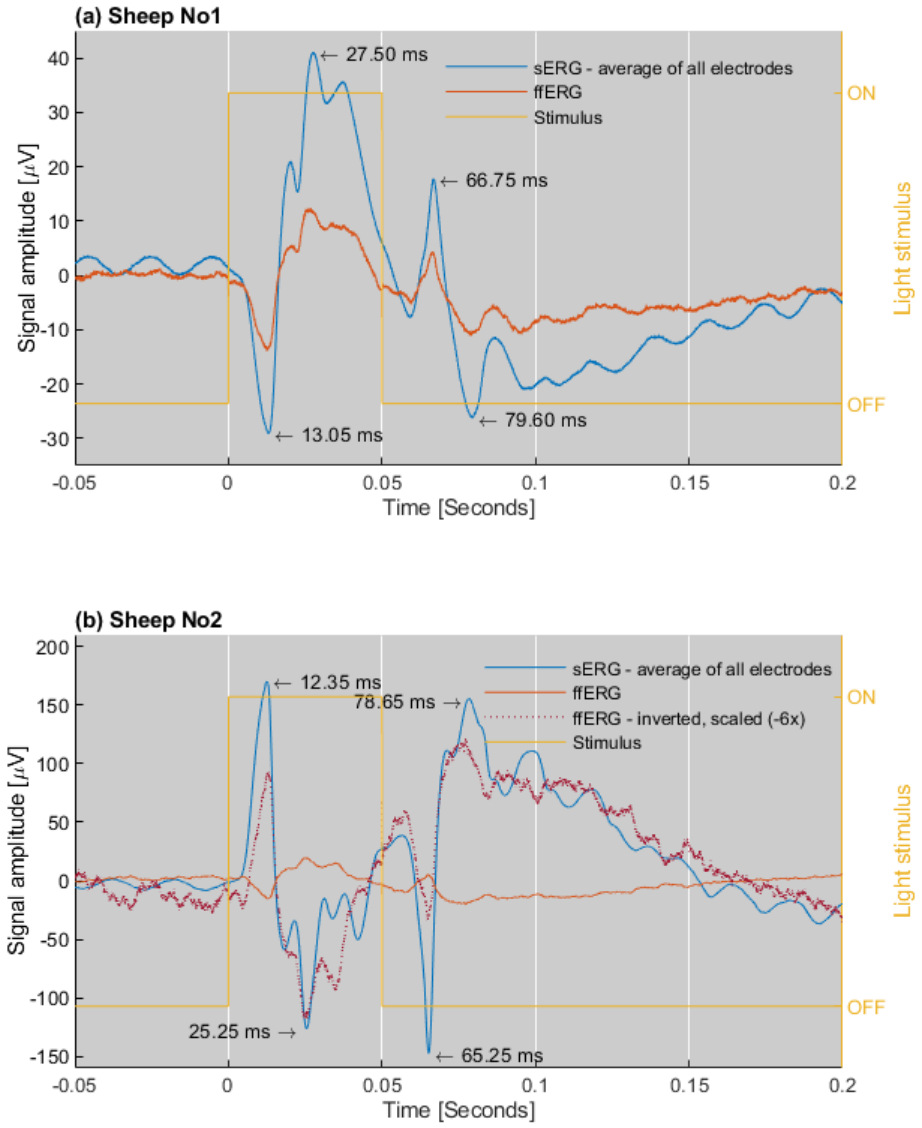

Figure 5-16 Full-field ERG and suprachoroidal ERG comparison.

In each animal, signals acquired on all 15 suprachoroidal electrodes were consistent with regards to the latency of the main a-, b- and d-waves, as well as the overall waveforms. The main difference between all sERG traces is the magnitude of each wave. A representative example is show in Figure 5-17, in which a selection of channels is shown, as well as their relative position on the electrode array.

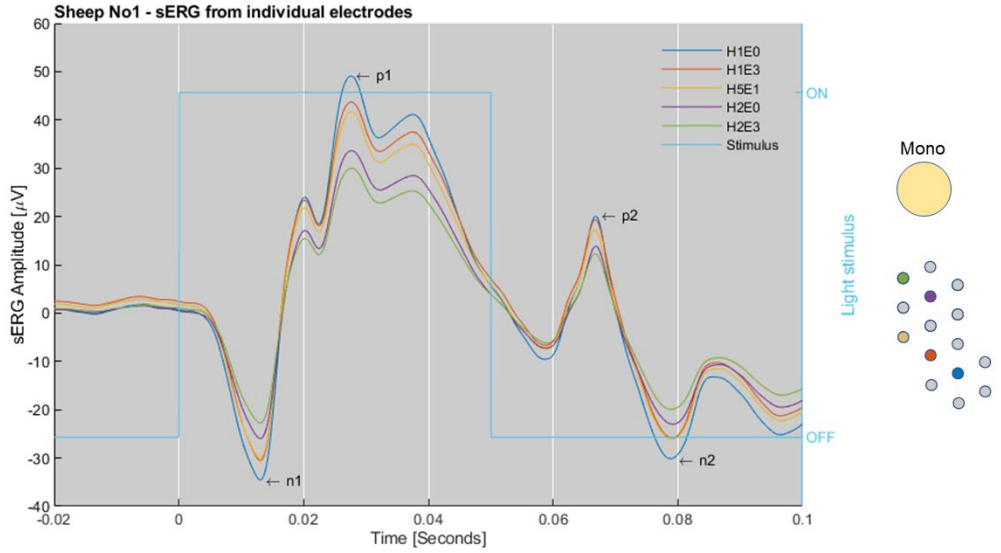

Figure 5-17 Representative sERG from individual electrodes shows amplitude differences (electrodes omitted for clarity). Note that the distance to the monopolar electrode (reference) is not to scale in this figure.

5.3.2.1 Localisation of photoreceptor populations

To identify whether the position of electrodes relative to the retina influenced the recorded signals, the magnitude (unsigned) of the a- and b-waves were mapped on the electrode array layout. Figure 5-18 clearly shows two different trends between animals. In Sheep No1, the magnitude of the sERG waves increased towards the tip of the array (marked with a black arrow) while the magnitude of the signal decreased towards the tip of the array in Sheep No2.

In the present experiment, the eyes were light adapted for at least 10 minutes [209] before the recordings. This would effectively have bleached the rod photoreceptors, meaning that the measured response was dominated by the cone network. By design, the arrays in both animals should have been centred close to the *area centralis* (refer to 5.2.1.2). The electrodes at the tip would have therefore been placed in presence of a higher density of cones than the rest of the array [221]. While the observations in Sheep No1 are compatible with this position, the results in Sheep No2 are not consistent, suggesting the influence of confounding factors.

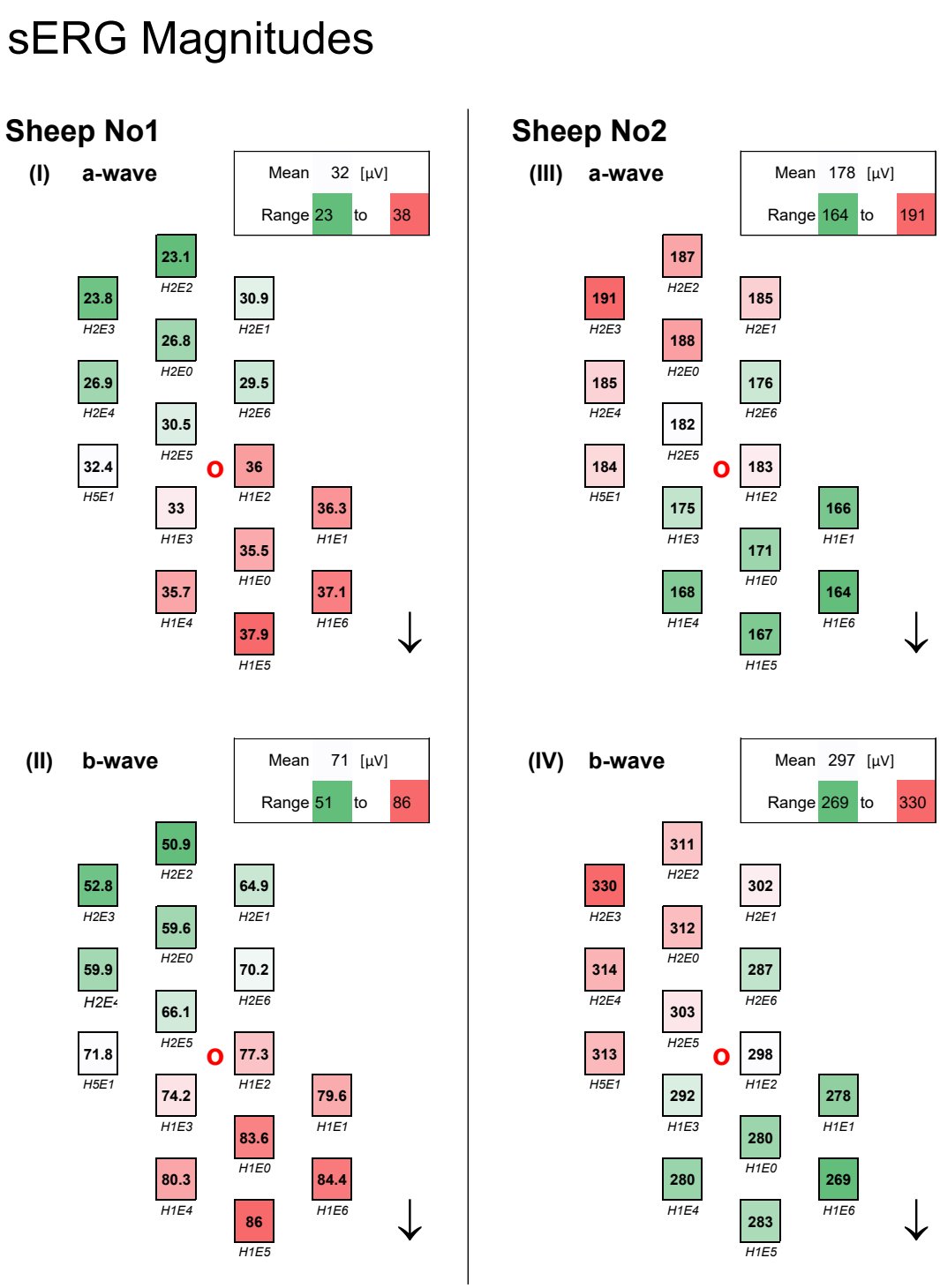

Figure 5-18 sERG magnitudes at the corresponding location on the electrode array. In each quadrant, the red circle indicates the theoretical centre of the visual field and the black arrow points towards the tip of the array, away from the monopolar electrode. In both animals, clear trends with regards to sERG waves magnitude. In Sheep No1, the magnitude of both a- and b-waves increases towards the tip of the array. In Sheep No2, an opposite trend is visible.

To understand the differences in signal sign (Figure 5-16), magnitude, and magnitude trend along the electrode array (Figure 5-18) observed between the two animals, a deeper understanding of the specific sheep retinal anatomy is necessary. Shinozaki, Hosaka, Imagawa and Uehara used histological methods to establish a functional map of the sheep retina, including the density of RGCs, rods and *cones*. The sheep retina features two main zones with high cone photoreceptor densities. The 'horizontal visual streak', which is common to many land animals, allows to scan the horizon [221], possibly for predators and the other sheep in the flock. The second, located in the dorsotemporal quadrant (Figure 5-19), is "probably involved in perception of the binocular anteroinferior visual field" [221].

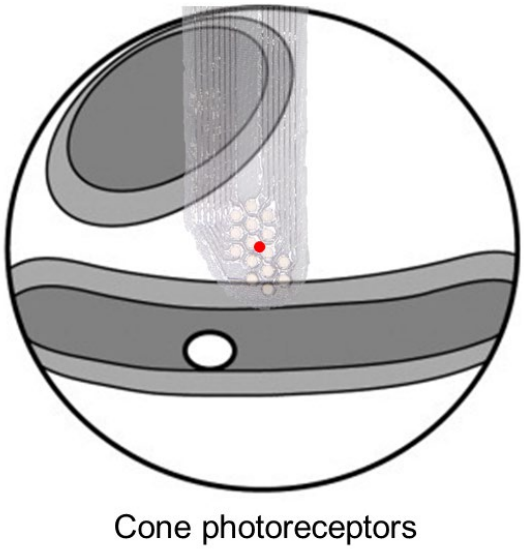

Figure 5-19 Qualitative view of the cone density in the retina of the right eye of the sheep. Areas marked in dark grey present the highest cone density, followed by light grey and white areas. An electrode array tip was overlaid to show the theoretical position of the electrodes with regards to the areas of high cone density, namely the horizontal visual streak and the dorsotemporal region. Note that due to uncertainties in scaling due to the 2-dimensional representation of a 3D object, dimensions are only an approximation. The red dot shows the centre of the eye. Adapted with permission from Shinozaki et al. including mirroring of the image to show the anatomy of the right eye, as used in the present experiment.

As described in section 5.2.1, the electrode array for this study was designed mainly with electrical stimulation in mind, and a particular focus was placed on maintaining features and geometries of the Phoenix[99]. As such the importance of the dorsotemporal high cone density area with regards to the sERG properties was underestimated.

When the array was inserted in its target location, as it was the case in sheep No2, the monopolar return electrode – which was used as reference electrode for the measurements (and as return during electrical stimulation) – finds itself near many cones and associated neurons. Because of the size of the monopolar contact, the reference electrode of the system sums the activity of a very large number of cells, which results in a large, negative change of electrical potential. Meanwhile the electrodes of the array, while they may also be in presence of a dense cone population, integrate the potential of fewer cells. Because the recording system effectively measures the potential *difference* between a signal electrode and the reference, the signal electrodes appeared to present a *positive* a-wave. Effectively, the electrical potential at the signal electrodes were only "less negative" than the reference.

In sheep No1, the array had to be inserted significantly further nasally, compared to Sheep No2. As such, the monopolar/reference electrode was located far away from the dorsotemporal cone population. Accordingly, the potential measured at the reference may still have been influenced by some cones, but the potential at the signal electrodes were even "more negative", therefore causing the measured signal to present the expected negative a-wave and positive b-wave. The relatively low amplitude of the traces in Sheep No1, compared to Sheep No2 (average a-wave on the array: -32 µV and 178 µV, respectively), may be attributed to the size difference between the signal and reference electrodes. Indeed, even in the presence of a small negative cone response, the reference would have summed the potential from many cells, leading to a small negative signal being measured with regards to even the best responding signal electrodes. A qualitative, 3D representation of the differences in array position in both animals, with regards to the cone density map described by Shinozaki et al. [221] is shown in Figure 5-20.

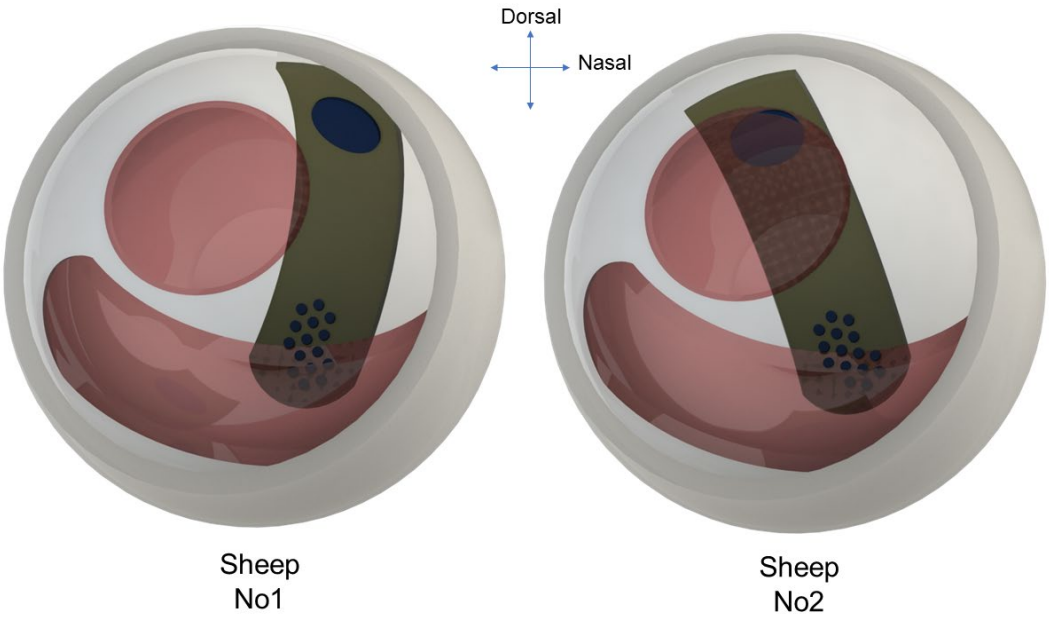

Figure 5-20 Qualitative representation of the electrode array position in both sheep, including the monopolar return/reference electrode, with regards to the cone densities described by Shinozaki et al. [221]. In sheep No1, the array was inserted approximately 7 mm further nasal compared to sheep No2, in which it was inserted at the planned position. As a result, the reference electrode in No1 was positioned in an area of low cone density, where the electrode in No2 would have been in zone with a dense cone population.

In both animals, the tip of the array may have been located close, or inside the horizontal visual streak. Given the highlighted influence of the reference electrode in determining the polarity of the signal, the trends seen in Figure 5-18 are consistent with the signal electrodes on the end of the array being exposed to the response of a denser cone population. In Sheep No1, the whole array was likely exposed to changes in local electric potential that would have been higher than those affecting the reference. Because the response grew towards the cone-dense areas, the magnitude of the a- and b-wave would have increased further as the distance to the visual streak decreased. In Sheep No2, like in Sheep No1, the magnitude of the local electric potential changes after light flashes at the signal electrodes were likely larger in electrodes located closer to dense cone areas. As such, the voltage at the tip electrodes presented a peak amplitude that was more comparable – similarly negative – to the reference, yielding an apparent decrease in signal amplitude close to the horizontal visual streak. The apparently opposed trends seen in Figure 5-18 may effectively reflect a similar position of both arrays with regards to an area with a dense cone population. The effects observed here, including the influence of

the position of a 'monopolar' reference electrode located close to electrically active cells has been described in depth by Fehmi and Sundor [231] and future work in the characterisation of the localisation capabilities of sERG should carefully consider this.

5.3.3 Electrically evoked retinal activity

Electrical stimulation of the retina from the suprachoroidal space has been shown to cause visual percepts in people with severe visual impairment due to end-stage retinitis pigmentosa [45, 46]. In most subjects, the phosphenes were retinotopically organised (reflected the spatial position of the electrode that delivered the stimulus on the retina), suggesting that the stimulation triggered neural activity close to the electrode, which was then transmitted towards the brain. In the present experiment, all 15 electrodes of the array were used to record the electrical activity of the retina during and after stimulation using a monopolar stimulation paradigm with the intention to record the elicited eCAPs. Unfortunately, in Sheep No1, an unexplained outcome with the recording headstage dedicated to the suprachoroidal array caused a large, decaying, oscillatory noise after each stimulus. The amplitude of the noise steadily decreased over the first 150 ms, after which it was barely noticeable. Because of its frequency (50 Hz), the oscillatory noise may have been attributed to powerline noise but, interestingly, the latency of the peaks after the stimulus were consistent between all recordings. This excludes powerline noise because the separate recording sessions were triggered manually, therefore rendering a repeated, accidental "synchronisation" on the 50 Hz of the mains highly unlikely. Despite all the attempts to minimise the impact of this artefact, no conclusive, objective observations could be made from these recordings and all results presented in this section were obtained from Sheep No2.

5.3.3.1 Raw recordings

As expected, electrical stimuli caused a large artefact on all suprachoroidal and corneal (ERG) electrodes. The artefact saturated the amplifier of all channels. The recorded signals then slowly recovered with individual time functions. At first, notch filtering at 50 Hz was used to reduce the observed powerline noise. Because of the extremely sharp changes the signal around the stimulus, notch filtering caused large signal distortions around the stimulus. Additionally, in most cases, the powerline noise was comparatively small and therefore filtering was deemed to be more disruptive than beneficial. The unfiltered, raw data was therefore used for the following analysis and only ensemble average over multiple stimuli was used for denoising. Figure 5-21 shows an example of

the distortion caused by notch filtering (IIR notch filter: Matlab 'iirnotch(wo, bw)' with wo = 50 [Hz] / (sampling frequency / 2), and bw = wo/2) compared to the raw signal.

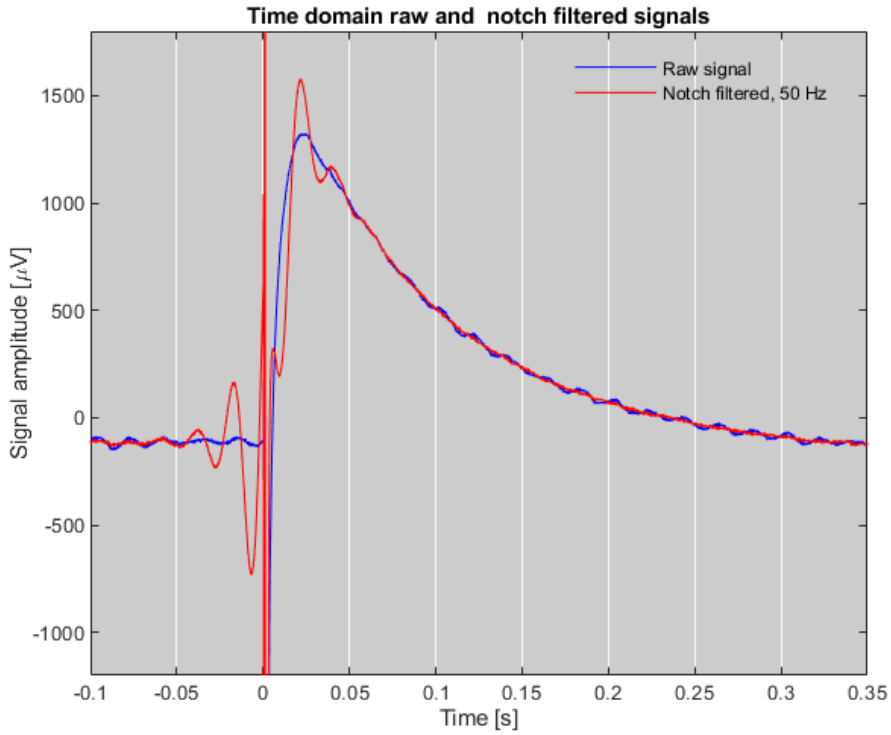

Figure 5-21 Notch filtering artefact on eCAP recordings in Sheep No2 (representative example, electrode H2E6 during stimulation on H1E0). Although the filter was effective in reducing the amplitude of the 50 Hz powerline noise, it caused a high amplitude artefact (red trace). Other notch filters were also investigated, which either led to similar disruptions or were not as effective in reducing the noise. Ensemble averaging over multiple stimuli was therefore used as sole denoising strategy.

Despite the large artefact, a retinal response was clearly identifiable at 40 ms after stimulus on-set, on some of the electrodes located closest to the stimulation electrode (H1E0: central electrode on the hexagon located at the tip of the array). Due to the variable artefact amplitude and latencies on different electrodes, the response was often strongly distorted, even obscured. Figure 5-22 show a representative subset of traces during monopolar stimulation with biphasic pulses on H1E0 (400 µA, 500 µs per phase).

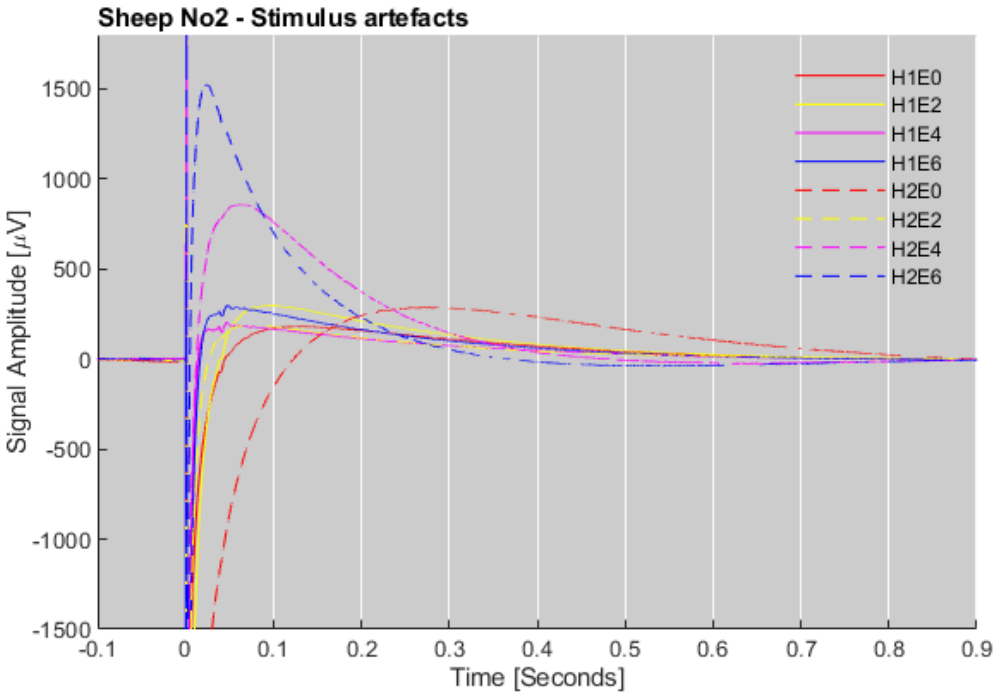

Figure 5-22 Electrical stimulation artefacts (stimulation delivered on H1E0). Despite the large artefact, a retinal response was clearly identifiable at 40 ms after stimulus on-set, on some of the electrodes located closest to the stimulation electrode. Due to the variable artefact amplitude and latencies on different electrodes, the response was often strongly distorted, even obscured such as on the pink trace, where a "dip" in the trace is visible but doesn't reflect the shape of the response seen on other channels with smaller artefacts.

Up to four electrodes (H1E0, H1E0 and H2E0, H1E0, H1E3and H2E0 or H1E0, H1E3, H2E0 and H2E3, see Figure 5-14) were used simultaneously to deliver stimulation to the retina. Increasing the number of stimulating electrodes increased the number of channels on which a response was identifiable. In Figure 5-23, panels (a1) and (a2) present details of a representative subset of traces recorded during stimulation on H1E0, specifically from electrodes in Hex1 and Hex2, respectively. Although a subtle deflection can be seen in the traces in (a2) at the same time as the response seen in (a1), the amplitude of the response waveform is small. When stimulation was delivered on H1E0 and H2E0 simultaneously, all channels on the array presented a strong response as seen in (b1) and (b2).

The main response was characterised by a positive peak (p1), followed by a negative peak (n1). Finally. a second, slower, positive peak (p2) was also visible after the first positive to negative inflection. Because of the artefact-related signal distortion, quantification of

the response magnitude was difficult. Evaluation from the channels with comparatively small artefacts and large decay time constants, showed that the peak-to-peak magnitude (p1-p2) of the response was in the range of 30 μV on the best responding channels when one or two stimulating electrodes were used. The amplitude of the response on the electrodes of Hex1 didn't appear to be significantly affected by the simultaneous stimuli on H1E0 and H2E0, compared to stimulus on H1E0 only. Interestingly, the response amplitude did appear to increase when three or four electrodes were used to stimulate simultaneously with a peak-to-peak magnitude between 190 and 195 μV measured in the electrode closest to all three stimulating electrodes (Figure 5-24). Similar to one and two stimulation electrodes, there were no significant differences between the response amplitudes measured with three and four electrodes. Before and after the main response, some smaller peaks are visible (for example between 25 and 30 ms), which may be part of the response. Their scale is small compared to the overall magnitude of the signals. In all recordings no response amplitude can be precisely measured due to the artefact-related distortion.

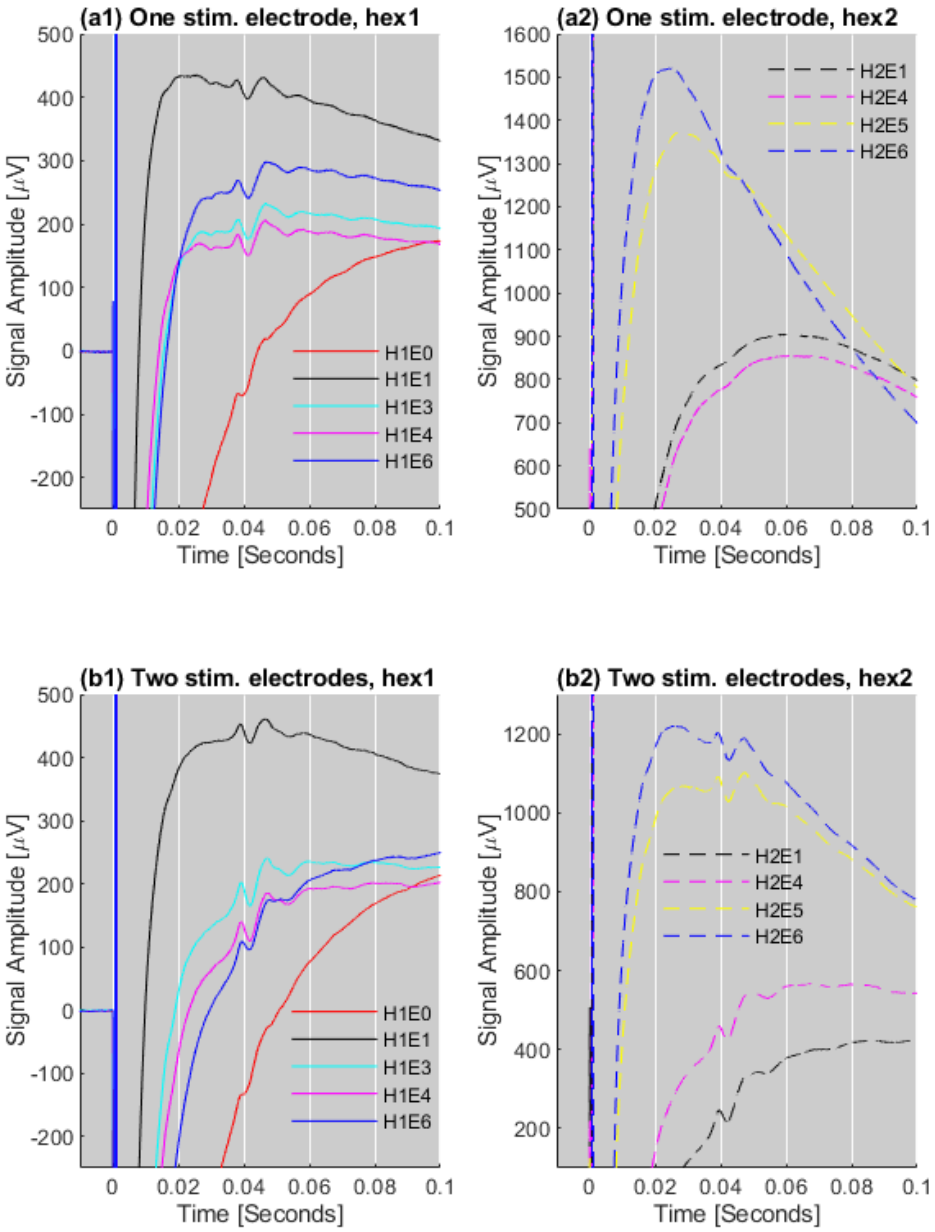

Figure 5-23 Retinal response to stimulation on multiple electrodes. Top: Traces obtained during and after stimulation on one electrode (H1E0). Panel (a1) and (a2) show representative recordings on Hex1 (close to the stimulation) and Hex2, respectively. Bottom: Recordings on the same electrodes as in the top panels during and after stimulation on two electrodes (H1E0 and H2E0). During stimulation with H1E0, the amplitude of the response on Hex2 is smaller than on Hex1, probably due to the increased distance to the stimulation site. During stimulation with two electrodes, there appears to be no major increase in response amplitude in Hex1, yet the response measured from Hex2 is significantly larger.

In a subset of recordings, an Intan-specific functions called ‘amplifier settle’ was used as an attempt to speed up amplifier recovery and minimise the duration of the artefact. While it appears to be efficacious to shorten the ‘tail’ of the artefact and stabilize the recordings, the chosen amplifier settle duration must be tuned carefully to provide benefits while avoiding unnecessary obscuration of early signals. Figure 5-24 shows the effects of the amplifier settle. The tail of the artefacts was effectively shortened, providing more stable and comparable recordings after releasing the amplifier. The artefact was reduced, not suppressed, and a slow voltage drift was still visible as soon as the amplifier came out of settle. In Figure 5-24, the amplifiers were kept in ‘settle’ for 25 ms, which provided satisfactory artefact reduction but obscured any potential early retinal response which may have occurred before 25 ms. Peaks visible during amplifier settle (earlier than 25 ms) are most likely remnants of the reduced artefact. On the traces for H2E1 and H2E6, the artefact appeared to be more effectively reduced than on other electrodes (peaks cropped out in Figure 5-24 to improve visibility), possibly highlighting the need for individual tuning of the settle parameters for each electrode. Panel (b) presents post-mortem recordings, including three channels using the amplifier settle function for comparison.

Most importantly, as shown in Figure 5-24, there was no measurable retinal response in the post-mortem recordings, supporting the hypothesis of the neural origin of the response described above.

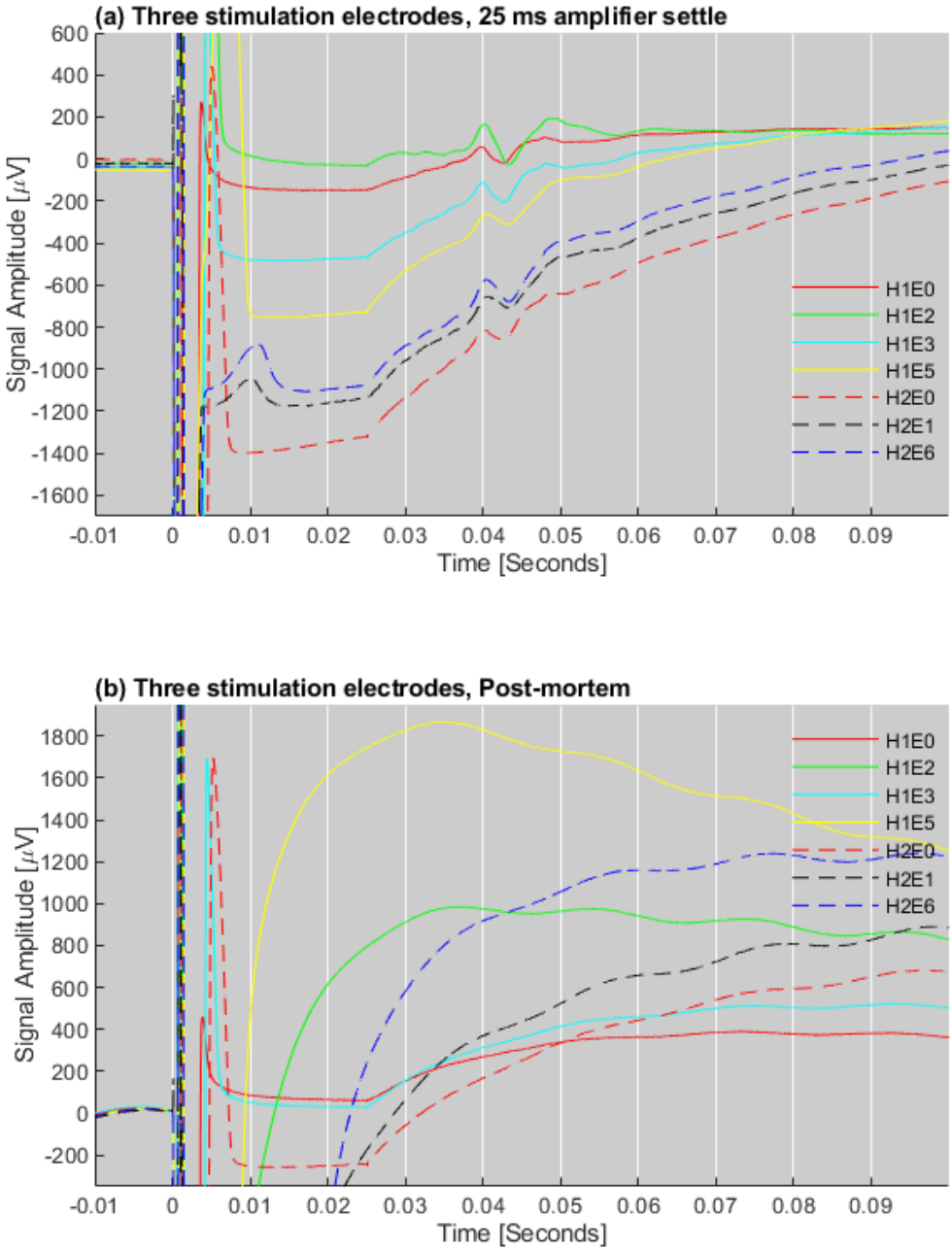

Figure 5-24 Response to stimulation on three electrodes (a) and postmortem recordings with the same stimulation configuration (b). During the postmortem recording, amplifier settle was applied only to a subset of electrodes (all three stimulation electrodes: cyan, red, and dashed red traces), whereas amplifier settle was applied on all channels in (a). The effects of amplifier settle can be compared to the non-settled channels. In (a), a large response can be seen on H1E2 (green trace) which is the closest to all three stimulation electrodes.

Peak latency

Because the location of peaks can be more readily identified, compared to the amplitude of small responses, even in a distorted signal, quantitative analysis could be performed on the peak latency. Although it could not be measured on all channels for stimulation with one and two electrodes, peak latency presented small but statistically significant variations between the stimulation conditions (one to four stimulation electrodes) as shown in Figure 5-25. Because the measurements taken on each electrode are paired (repeated measurements), and because there were missing values which are incompatible with a traditional "repeated measures ANOVA", the data was analysed by fitting a mixed-effects model, as implemented in GraphPad Prism version 9.3.1 for Windows (GraphPad Software, San Diego, California USA). The analysis assumes that the missing values occurred truly randomly. In this case, the missing values were due largely to the presence of artefact-related distortions combined with small response amplitudes, which made accurate measurements of the latency impossible. Even where the latency of the peaks could not be determined, a response may have existed. Indeed, deflections from the traces around 40 ms were visible in most cases. Missing datapoints were therefore considered to have occurred "truly randomly" because the factors that influence the ability to measure were independent of the existence values themselves (latency of a small or distorted peak exists, even if it can't be measured). The mixed-model analysis was therefore considered to be reliable.

The analysis revealed that the number of stimulation electrodes had a significant effect on the mean latency for both p1 and n1 ($P = 0.002$ and $P < 0.0001$). A Tukey's multiple comparison test was performed as confirmation, to evaluate the difference between the means between all pairs of groups. All means were significantly different ($P<0.05$) for p1 and n1 with two exceptions. The mean p1 latency for two and four ($P=0.0525$) electrodes and the n1 latency for three and four electrodes ($P=0.0538$) were not significantly different to each other (marked ns in Figure 5-25). The proximity of both P-values to the arbitrary cut-off of 95% confidence level is nonetheless noteworthy. The number of stimulation electrodes didn't influence the average inversion speed – the time between p1 and n1 (2.77 ms ± 0.56 ms) – as revealed by a mixed-model analysis ($P = 0.3806$).

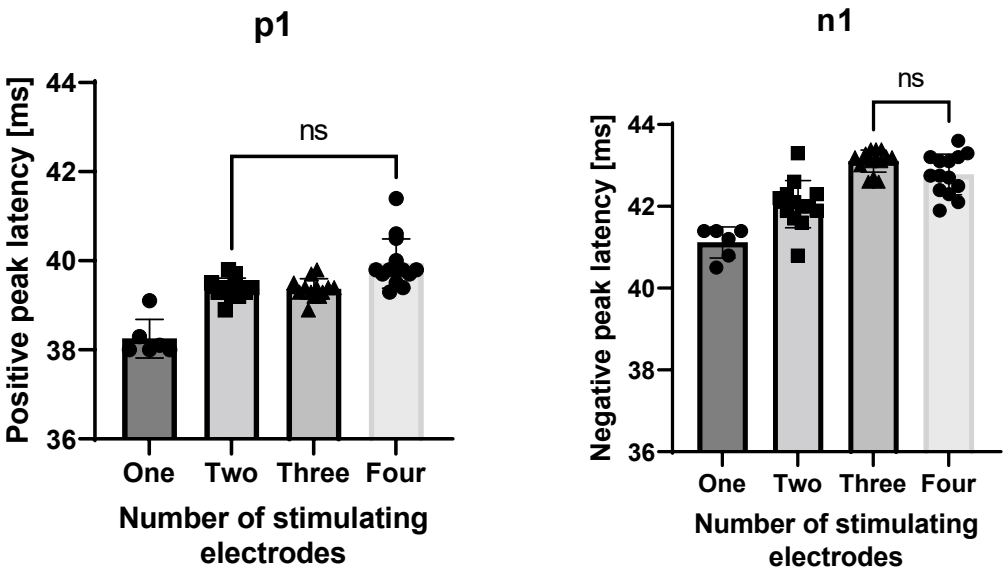

Figure 5-25 eCAP peak latency. A trend may exist, were the latency of the recorded eCAP peaks (p1 and n1) increases with the number of electrodes used for stimulation, within a given region of the retina. Data fitted to a mixed-effect model (P = 0.002 and P < 0.0001 for p1 and n1, respectively).

In the case where three electrodes were used simultaneously for stimulation, and where the amplifier settle was applied, all latencies for p1 and n1 could be measured. They were mapped onto the array to observe potential local trends. A single recording was available which met all criteria, and the following observations should therefore be considered as hypothesis-generating, rather than conclusive.

Figure 5-26 shows the latencies for p1 and n1 in their respective positions on the array. For both peaks, it appears that the stimulating electrodes (marked in orange in the figure) recorded peaks earlier than their direct neighbours. This is particularly clear for H1E0 and H2E0 where all of their hexagonally organised ‘guards’ presented a delayed peak. The third stimulating electrode (H1E3) responded earlier than most of its neighbours, except H1E0 (stimulating) and H1E4, which were expected to be involved in the response to H1E0. The use of two neighbouring electrodes for stimulation may have influenced this measurement.

Interestingly, the p1 peaks on the stimulating electrodes were not synchronised, with H2E0 lagging 0.2 ms behind H2E1. On the contrary, the negative peaks happened simultaneously on all stimulating electrodes (within 0.1 ms from each other) and significantly earlier than on all the passive electrodes. To exclude that the delays between

channels may have been related to the recording electronics rather than the physiology, the traces obtained from eight cortical electrodes which had been electrically connected to each-other (shorted) were observed. Based on the peaks of the stimulation artefact, there were no observable delays on shorted electrodes. This suggesting that the asynchronous nature of the eCAP peaks may have been of neural origin.

Except for n1 on the stimulating electrodes (which were synchronised), there appears to be a trend with shorter latencies on the tip electrodes – presumably located close to areas with high cone densities (see 5.3.2.1) – for both positive and negative peaks. Overall, the differences in latency between the sites were short and confirmatory experiments are warranted before the trends observed here can be confirmed.

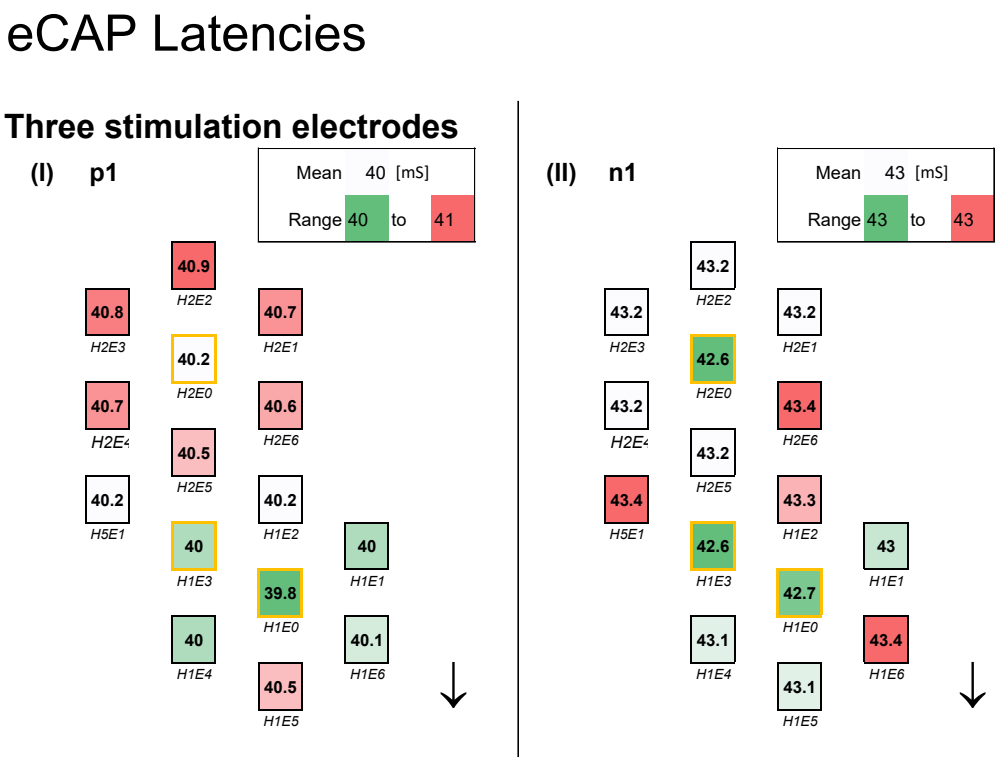

Figure 5-26 eCAP latency during stimulation with three electrodes. The stimulation electrodes (orange borders) generally responded quicker than their direct neighbours. Secondly, there appears to be a trend for p1 and n1, where the electrodes of hexagon 1, at the tip of the array and therefore closer to a cone-dense retinal zone (tip of the array marked with an arrow), responded faster than the rest of the array. Note nonetheless that n1 was synchronised on all stimulating electrodes and that some exceptions are obvious, particularly close to the areas that would have been under the influence of multiple stimulating electrodes.

As visible in Figure 5-25, a trend may exist, where the peak latencies increase with the increasing number of stimulation electrodes. Note that the missing values – should the shorter peak latencies at the tip electrodes be real – may have biased the data. Indeed, for this stimulation condition, the latency could be measured mainly at the electrodes of hexagon 1 and would therefore skew the average towards shorter latencies when a single electrode was used for stimulation.

5.3.3.2 Artefact compensation

In post-processing, attempts were made to minimise the stimulation artefact in the hope to identify other components of the retinal response. Indeed, it would be particularly interesting to isolate the early retinal response, which most likely starts within the first milliseconds after the stimulus [65].

First digital referencing was applied, where the recording on an electrode of the array with a similar artefact as the chosen 'signal' electrode is subtracted from the main electrode. In theory, should the artefact be sufficiently similar, this operation should leave behind the components of the neural response that are unique to either of the electrodes, similar to the case where two electrodes are located sufficiently close to each-other [231].

Due to the high variability of the artefact between electrodes when the 'amplifier settle' function was not used, the technique yielded its best results in the recordings during which this function was applied. After a small number of tests with different durations, an amplifier settle of 25 ms appeared to yield promising results, although it obscured the first 25 ms of potential responses. During recordings without amplifier settle enabled, the channels with most comparable artefacts were chosen manually but, except for the readily visible p1-n1-p2 inflections, no patterns emerged that were repeatable between recordings. Figure 5-27 shows the results of digital referencing applied to a recording with three stimulation electrodes. In panel (a), the signal from electrode H1E2 was subtracted from a representative selection of channels. The resulting trace contains the main response (at 40 ms) but with an inversion due to the amplitude difference between the signal and digital reference electrode. Due to its position close to all three stimulation electrodes, the amplitude of the response measured on H1E2 was larger than on the other electrodes, resulting in the difference between the signals showing a negative peak first, followed by a positive peak. In (b), an opposite case is shown, where H2E0 (also used as stimulation site) had a smaller response amplitude than its neighbours. Note that differences in latencies, or phase shifts, could also have caused signal inversions as seen

here if the response on different channels had presented a shift close to 180 degrees (although it doesn't appear to be the case here, as visible in Figure 5-24).

In the traces in (a), minor peaks at 31 and 34 ms are visible, which may be part of the response (marked with stars on a representative trace). Although small in amplitude, compared to the main response, they are shared with varying amplitudes in multiple traces. Due to the use of electrode H1E2 as reference, one of the best responding electrodes for this specific stimulation configuration, they may reflect neural activity that was detected mostly on the reference (and of negative polarity, visible in (a), Figure 5-24) with smaller echoes on the signal electrodes. Although the secondary peaks in Figure 5-27 (a) were readily visible before digital referencing, positive-negative-positive inflections with similar latencies were only made visible after digitally subtracting a reference in panel (b).

Using this newfound information, it is interesting to try and identify the location from which the signal originated. If the signal seen in hexagon 1 is of the same type as seen in hexagon 2, it can be interpreted that the amplitude of the secondary peaks on the reference of hexagon 2 (H2E0) was higher than on its neighbours. Interestingly, this is despite the amplitude of the main response being smaller on the reference than on the signal electrodes (no signal inversion compared with the raw trace in Figure 5-24).

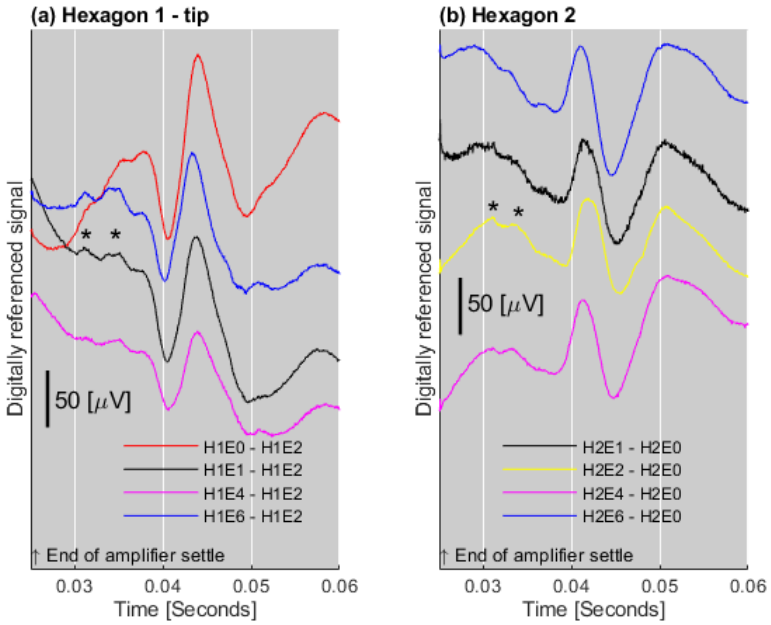

Figure 5-27 Digital referencing from neighbouring electrodes with similar stimulation artefacts. Two positive peaks are visible on multiple traces. Vertical position of the traces was changed manually to improve visibility.

In acute experiments, a reliable way to minimise the stimulus artefact is to record a "pure" stimulus artefact – in the absence of all biological response – after sacrificing the animal. This recording, can then be subtracted from the *in vivo* data, leaving behind only the neural activity [12]. Unfortunately, miscommunication within the team led to many stimulation electrode combinations and amplifier settle configurations trialled *in vivo* to be omitted during the postmortem recording session. The number of usable postmortems was therefore limited.

Nonetheless, artefact minimisation could be performed on all stimulating electrodes of the three-electrode stimulation data presented above, using postmortem signal subtraction (Figure 5-24). Due to the use of the amplifier settle function, the first 25 ms of the recordings were obscured. Although some residual distortion of the signal is visible, including due to an unexplainedly high 50 Hz noise (compared to the *in vivo* recordings), some of the finer details of the retinal response are revealed. Particularly noteworthy is the visibility of the negative peaks at 31 and 34 ms on H2E0, the presence and polarity of which were postulated using digital referencing (marked with stars in Figure 5-28).

[12] Provided that the amplifier was not saturated.

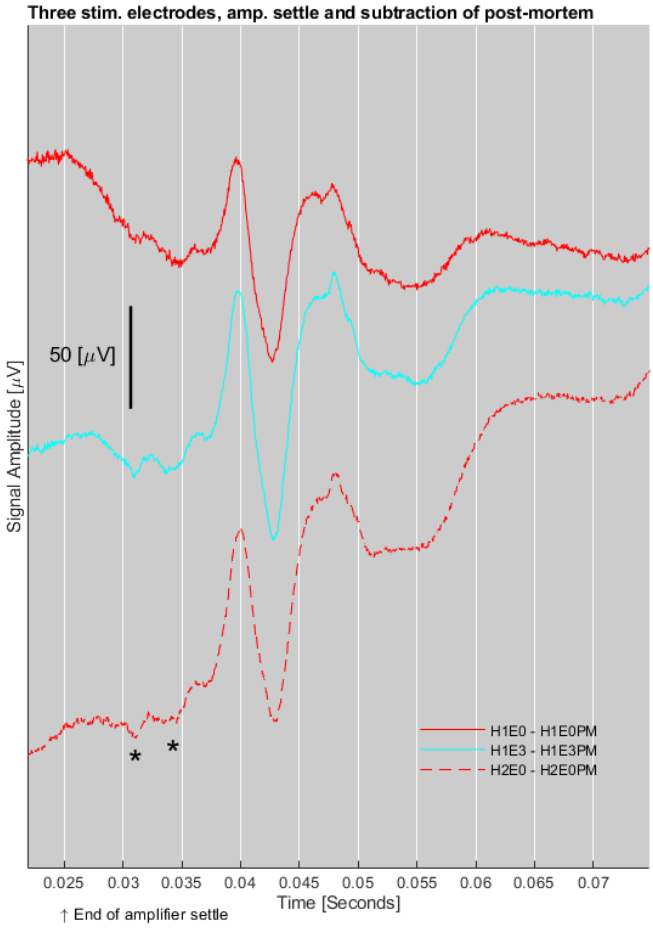

Figure 5-28 Post-mortem artefact subtraction. After artefact reduction by subtraction of the postmortem recordings from the three stimulation electrodes, early, negative sub-peaks (stars show representative examples) were made visible in all traces at 31 and 34 ms. Vertical position of the traces was changed manually to improve visibility.

The most promising artefact minimisation process was based on the observation that despite the large differences in the charge delivered during stimulation with one, two, three or four electrodes, the recorded artefacts themselves on each electrode presented moderate variations. In the absence of corresponding post-mortem recordings, artefacts were partially removed by subtracting the signal recorded during stimulation with a single electrode from the recordings with two electrodes, for each recording side.

Due to the similarities between the artefacts between recordings, the result was traces in which the rapid artefact decay was flattened from 10 ms after stimulus on-set, and which

revealed some responses visible in Figure 5-29, including one with the first positive peak at 16ms.

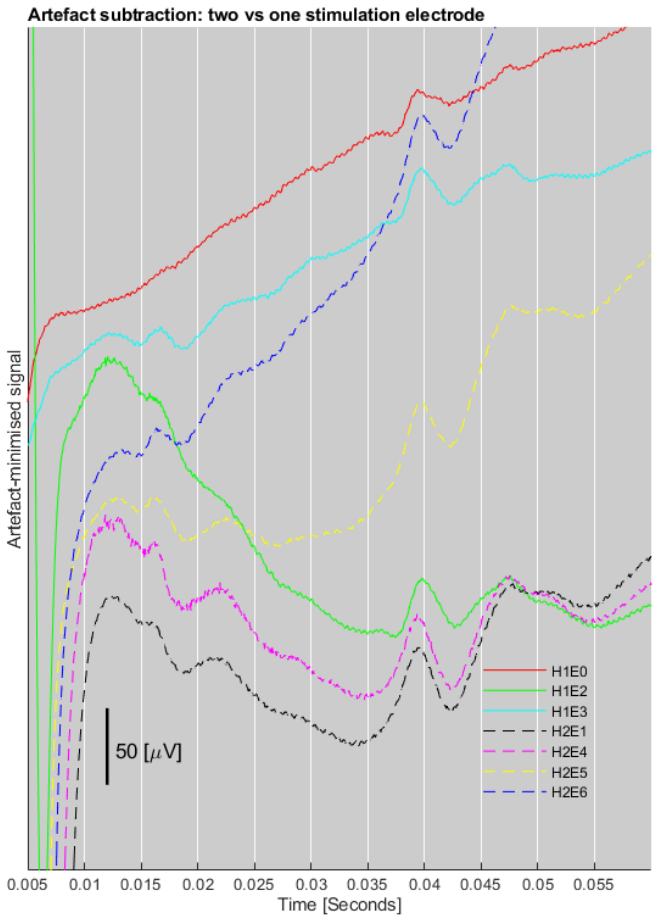

Figure 5-29 Artefact minimisation. Subtraction of recordings with different stimulation electrode configurations allowed to reduce the amplitude of the stimulation artefact. It revealed response peaks as early as 16 ms. Interestingly, the negative peaks made visible by postmortem recording subtraction (31 and 34 ms in Figure 5-28) do not appear clearly. They may have been very similar in amplitude during stimulation with varying numbers of electrodes, leading to their disappearance because of the subtraction process. Vertical position of the traces was changed manually to improve visibility.

Because in theory, artefacts should follow an exponential decay function, any high frequency signal could be either noise or biological signals. Specifically, the resulting traces represent the difference between the amplitude of the response caused by two stimulating electrodes and the response due to one electrode. This is confirmed by

observing the behaviour of the main response (20 ms). Although in the raw traces there was no noticeable differences in the peak-to-peak amplitude of the response between one and two electrodes (Figure 5-23), a clear change is visible after minimisation of the artefact by subtraction. Indeed, the signal still presents the same response with corresponding polarity. Of course, some of the differences in amplitudes are due to the differences in latencies previously detailed in this section, which causes a phase shift and, in this case, accentuates the signal amplitude. Nevertheless, it appears that stimulation of two electrodes caused a neural response of higher amplitude and included detectable components as early as 16 ms.

The same alternating peaks were also clearly visible in all other comparisons, including comparing three-electrode and four-electrode stimulation to single-electrode measurements, subtraction of two-electrode traces from three- and four-electrode recordings, and finally subtraction of three-electrode recordings from four-electrode traces. With the increasing number of stimulating electrodes, the duration of the artefact did increase noticeably, to the point that in the comparisons using the four electrodes, the very early components appeared distorted. (Supplementary figures in the Appendices).

The presence of the responses, including those at 16 and 40 ms, as well as other final peaks, like the 31 and 34 ms peaks in multiple subtracted traces (Figure 5-29 and Appendix), with increasing amplitude at increasing charge delivery – through multiple electrodes – overall suggest that the responses were biological, rather than artefactual.

5.3.4 Electrically evoked cortical potentials

Unfortunately, the cortical recordings during the experiments in both sheep were strongly contaminated by noise. Some of the sources of noise could be identified, including respiration and brain movements due to heart beats and respiration. Attempts were made to minimise their impact, yet another source caused very large (hundreds to thousands of mV), irregularly timed (between 0.5 to 3 seconds apart) peaks which were only identified during postprocessing after both experiments.[13]

[13] According to the ethics protocol, a sheep could not remain alone for more than 48 hours. Because of the Covid-19 restrictions, no companion sheep were available and therefore both experiments were performed within 48 hours.

During the experiment, the cortical mapping process included the visualisation of the ensemble average for a specific recording, which was supposed to lead to the identification of the highest response peak, and therefore the best-responding site in the visual cortex. In the ensemble-averaged traces, the large peaks of noise caused local skewing of the data, which led to recurrent misinterpretation of the recordings. This interfered with the cortical mapping process. As a result, recordings were made from a suboptimal cortical area which responded only to stimulation with high charge (900 μA, 3ms) and was most likely not located withing the primary visual cortex. The high currents required to get a cortical signal caused an exceptionally large stimulus artefacts in the retinal recordings, which still caused significant signal distortion after 150 ms. Therefore, the interpretation of the eCAP difficult and a correlation between the measured retinal and cortical responses could not be established.

5.4 Discussion

Vision is complex. It involves a large variety of highly specialised, strongly interconnected neurons that, compared to any of the other senses, provide the brain with the finest details about a person's environment[14]. Examples of the capabilities of the visual system include conveying information about movement, colour, brightness, and contrast. And it all starts with a local change of membrane potential in the photoreceptors, as a result of a photon being absorbed [232]. When the photoreceptor function is lost, retinal visual prostheses attempt to evoke intelligible neural activity by stimulating the surviving cell network but, to date, there is still a significant mismatch between the refinement of the neural system and the technologies available to interface it [157]. Despite this, very encouraging results have been obtained in blind patients with retinal prostheses [45, 46, 84, 116] and further improvements are not out of reach.

In this process, detailed information and feedback about the activity elicited in the retina of implant recipients would be very beneficial. In the clinic, objective assessments of stimulation efficacy could assist with implant tuning and patient training, and with intraoperative device functionality testing. In research, including safety and efficacy testing in animal models, intimate knowledge of the retinal cells' responses could guide

[14] Some animals rely on other senses to understand, navigate and interact with their environment.

the development of the stimulation strategies to improve the restored vision. Not having to rely on cortical recordings, which are generally invasive and may be less sensitive to subtle changes in the stimulation due to the high levels of information processing involved before the signals reach the brain, the researchers may also be able to more accurately determine the stimulation amplitudes which cause a perceptual response. This information could then be used to refine the safety testing protocols by more accurately defining clinically relevant stimulation levels.

Because retinal stimulation requires arrays of electrodes to be positioned as close as possible to the retina, an opportunity exists to attempt to use these electrodes to record the neural activity and explore ways to capture and understand the retinal activity *in vivo*. Due to the novelty of the approach, little information was available to guide these attempts. In the process of developing our understanding of the suprachoroidal recording techniques, we began with measuring the retinal response to visual stimulation, allowing to refer to the vast body of knowledge on ERG.

5.4.1 Array localisation by sERG

Using the suprachoroidal arrays implanted in two sheep, the novel sERG was recorded during light adapted, bright flash stimulation. The signal presented the same peak latency characteristics as the ERG for both animals and, may have therefore originated from the same cells. Because multiple electrodes were available for recording, which were spread over different regions of the retina, we then investigated whether the local response may be usable to locate the electrode array with regards to retinal regions.

Light adaptation and bright flash stimulus minimised the rod and rod-associated network and the observed response was therefore driven by the cone photoreceptors and their associated neurons. It was hypothesized that electrodes located close to areas with a stronger response to the visual stimuli would record a larger signal amplitude. By design, and despite a shifted array insertion site between the two animals, the tip of the electrodes were located close to the cone-dense area of the sheep called the horizontal visual streak [221], and were therefore expected to display a stronger response.

Result interpretation using the specific retinal anatomy of the sheep, demonstrated that indeed, the tip electrodes recorded an a-wave that was more negative than their neighbours outside the retinal visual streak and a b-wave that was more positive. Since the wave polarity and magnitude matched the ERG, the sERG signals of the tip electrodes, it confirms that the tip electrodes were in presence of cells that contributed to a greater

extent to the ERG signal, thus that the tip electrodes were closer to the cone-dense region. To further confirm this theory, different types of test conditions could be applied, such as dark-adapted dim flashes. Adaptation and stimuli can effectively be used to isolate specific cell networks [216, 230] and could help locate these populations accurately with sERG.

Although this technique is only applicable in eyes with sufficient residual photoreceptor populations, it could be beneficial to the bionic vision research. In allowing identification of the type of cells located close to each individual electrode *in vivo*, the sERG would also provide information about the type of cells that are primarily stimulated by electrical impulses in subsequent experiments. As such, the sERG combined with electrical recordings from the retina and visual cortex may lead to a better understanding of cell-specific responses to electrical stimulation.

This study was obviously limited by the sample size. Additional experiments are required to confirm the effects observed here. In particular, special care should be taken to minimise the effects of the reference electrode placement on the recordings. For example, a reference electrode located on the nose or at the base of the ear (common reference location for ERG) would be more immune to the disruption observed in Sheep No2 and which was probably due to the reference being located too close to excitable tissue which responded to the stimuli [231]. The effects of the return/reference electrode position should also be carefully considered for retinal stimulation and recording during stimulation. Indeed, most current prostheses feature similar return locations as the Phoenix^{99}, and while this doesn't appear to have caused major disruption, the present findings invite to further investigation. Some of the retinal recordings presented in this chapter may already have shown cues with regards to the importance of the return/reference configuration.

5.4.2 Electrically evoked retinal response

Although the data was strongly contaminated by the stimulus artefact, this study allowed the first-ever recording of the electrically evoked retinal response from implanted electrodes. The response was dominated by a positive-negative-positive inflection occurring at 40 ms after the stimulus on-set and lasted for approximately 10 ms.

The latency of the response, although relatively long compared to expectations from *in vitro* retinal preparations [65], is consistent with some of the previous reports where the electrical response of the retina was recorded using corneal electrodes. In rats, Hetling

measured the first electrically evoked peaks at 35 ms, which is consistent with the present data [220]. Furthermore, the timing of the response is compatible with the peak latency of the electrically evoked potentials (EEP) in the cortex measured by Barriga-Rivera et al. in a sheep model (62 ms [200]). Unfortunately, noise in the recordings led to difficulties with the identification of the best-responding cortical area in the primary visual cortex. As a result, the latency of the EEP couldn't be determined in the present experiment and values from the literature had to be used. With regards to the latency of the retinal peaks, an interesting and unexpected result suggested that the latency of the peaks may become longer with increasing number of stimulating electrodes (Figure 5-25). Further investigation is warranted to propose explanations for this effect, including the identification of the cell types responsible for the response.

Hetling used pharmacological dissection to identify the origin of the components of the so-called electrically evoked ERG (eERG) [220]. The technique uses pharmacological agents to selectively suppress the response from chosen cell types. By sequentially altering the response of specific cell types and repeating the stimulation-recording sequences, the origin of each peak can be determined. Hetling attributed the first observed peak (negative, 35 ms) to the off-bipolar cells [220]. The retinas of the different species, and therefore probably the timing and characteristics of the cell responses, differ significantly. Note also that Hetling used subretinal electrodes to stimulate the retina. Due to the proximity of the electrodes to the retina and the lower current spread, the responses to suprachoroidal stimulation may differ significantly. Comparison to the rat experiment nonetheless suggests that the 40 ms response could be related to the off-pathway bipolar cells. Obviously, this should be confirmed in the sheep, for example by applying pharmacological dissection.

Another response of apparently smaller amplitude was measured at around 16 ms using a technique of recording subtraction between multiple recordings with variable numbers of stimulating electrodes. Similar to all other measured responses, the origin of these responses is unknown and further investigation is warranted. Again, pharmacological dissection could provide insights into the origin of the responses, independent of their latency. Hetling also described other strategies such as using pairs of stimuli on wisely designed pairs of electrodes, to gain further insights into the kinetics of the response and which would deserve further investigation [220].

As they are the messengers that finally convey the result of stimulation towards the brain, it would be particularly interesting to identify the RGC response. Indeed, knowledge

about the RGC response could be used to discriminate an effective stimulation – one that would have caused a perceptual threshold – compared to one that caused activity localised to the retina. Using simultaneous intraocular RGC activity recordings using tungsten wires, as described by Baig-Silva, Hathcock and Hetling, could provide the required insights, which could then be compared to the eCAP recordings to isolate the RGC response latency and characteristics [219].

Besides the very small number of samples, the main limitation of the present data is the very large stimulation artefact that affected all readings. While post-processing techniques could be successfully applied to observe the early retinal response, it calls for additional measures to limit the effects of the artefact. For example, the reference electrode of the array was used both as stimulation return and as reference for the measurement. During stimulation, the current delivered spreads "laterally" as it flows between the stimulation electrode and the return. Because the reference electrode is the site at which all the current exists or enters the electronics, while the signal electrodes find themselves at locations where only a portion of the current flows, it creates a large potential difference and a large artefact [233]. Based on this observation, the stimulus artefact would be beneficially impacted if the return and the reference were separated.

Furthermore, the distance between the return and the reference, as well as the distance between the signal electrodes and the reference should be reviewed critically. The variability of the stimulation artefact between the electrodes appeared to be influenced by more than the distance to the stimulating electrode. This suggests that the monopolar return may not behave as a "true" monopolar which requires the electrode to be sufficiently far away as to be considered "at infinity", causing asymmetrical current spread in the tissue. Figure 5-30 shows a map of the distances between the individual electrodes and the monopolar/reference electrode. Significant differences exist between the sites, which may influence the shape and size of the stimulus artefacts [233] and amplitude of the measured responses.

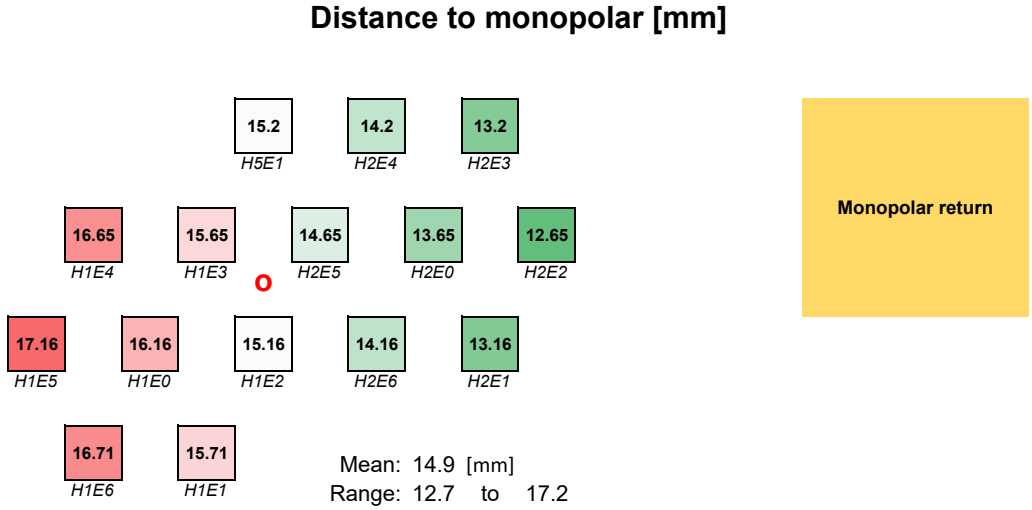

Figure 5-30 Distance between the monopolar return and the electrodes. Significant differences can be seen between all electrodes. This may influence the way the current spreads during stimulation, as well as the stimulus artefact shape, or even the amplitude of the measured response.

Future experiments should also include measurements during subthreshold electrical stimulation and increasing stimulus amplitude. This would not only allow the evaluation of the actual stimulation thresholds, but it would also allow for the modelling of the artefact at suprathreshold amplitudes for subtraction from the signal. Furthermore, the saturation of the response – the stimulation amplitude above which no increase of the response is seen, despite increasing stimulation – should also be determined [220].

Other artefact-blanking mechanisms have been shown to be efficacious in other locations, such as forward masking in cochlear implants [234]. Although due to the very different dynamics between the cochlear nerve and the retina, which presents much longer lasting responses, the forward masking may not be as promising in the eye [218]. Sequences of cathodic-first and anodic-first stimuli – which, in theory, average to a net zero signa – have also been proposed to minimised the stimulation artefacts [218].

Finally, establishing the correlation between the stimulation threshold in the retina and in the cortex simultaneously would be a game changer in the way electrophysiology of the retina is performed. Reliably establishing this correlation would allow for all future studies to be performed with the "less invasive" retinal recording technique while being able to refer to a solid database of their corresponding brain responses.

5.4.3 eCAPs and sERG localisation

Although hypothetical, due to the very low sample size, some interesting observations were made by comparing the measured latency of the 40 ms response in sheep, with the sERG data. The latency of the eCAP measured during stimulation on three electrodes "spread out" on the suprachoroidal array, appeared to be shorter close to the tip of the array, which may have been located close to the cone-dense horizontal visual streak (Figure 5-26). This may represent one of the key utilities of the sERG for bionic vision in sighted animals as it may enable *in vivo* characterisation of the photoreceptor-specific (e.g. cone pathway) differences in the response to electrical stimulation.

Suprachoroidal arrays are not readily visible using fundoscopy and require the use of dedicated equipment, such as infrared fundus imaging or OCT, to be visualised [1]. Should sERG provide reliable information with regards to the location of the array with regards to cell sub-populations, it may open the door to long term *in vivo* studies of the photoreceptor-network specific effects of electrical stimulation, because there is no need to sacrifice the animals.

5.5 Conclusion

Bionic vision research will benefit from every piece of information that is available with regards to the effects of the stimulation, its ability to cause a response, the selectivity of the stimuli to cell sub-types (e.g., ON- versus OFF-pathways), or the retinal area affected by a single stimulus. In this chapter, we have explored novel methods to record the retinal activity *in vivo*.

The sERG, the recording of the visually evoked retinal activity from the suprachoroidal space may provide insights about the type of cells that are close to individual electrodes. Because it relies on the presence of functional photoreceptors, it will be mostly useful for bionic vision research with sighted animals, but it may also serve a clinical purpose in the future. Unlike other types of retinal prostheses such as epiretinal arrays, suprachoroidal devices are, at least theoretically, compatible with residual vision. Because they reside in a space that is physically isolated from the neural tissue by the choroid, and because they do not impair the blood supply to the retina, they present a lesser risk of damage to the tissue responsible for natural vision (Chapter 3 [1]). Should the safety of suprachoroidal electrode arrays be deemed sufficient to be implanted in people with residual vision, the sERG could be used to accurately identify the electrodes that are located close to healthy retina. These electrodes could then be deactivated to avoid disrupting the surviving

natural vision, therefore maximising the benefits of the prosthesis as complement to the recipients residual vision, as envisioned by Zapf, Boon, Lovell and Suaning [235].

In this study, we have also recorded the retinal response to electrical stimulation from an implanted electrode array, demonstrating the potential of this type of recordings to gather deeper insights into the effects of retinal stimulation *in vivo*. This includes the ability to objectively measure the perceptual thresholds without the need to rely on invasive and complex cortical recordings, which are also sensitive to biases such as the use of anaesthetic agents.

Finally, this exploratory study generated many hypotheses which are all deserving of focused attention, as they may represent key steps towards improved performance of existing and future prostheses. Results from future studies will most likely fuel the development of accurate computer models, helping our field move forward in confidence.

> *"A major objective is to learn enough about the input–output relationship of the prosthesis-diseased retina system to support detailed computational models, which will ease the experimental burden, and facilitate rapid prosthesis design."* *John R. Hetling*

6 SIMULATION OF STIMULATION

TOWARDS CALIBRATED COMPUTER MODELS FOR THE OPTIMIZATION OF PARALLEL STIMULATION

6.1 Introduction

Clinical trials have shown that patterns of visual percepts can be created in patients blinded by retinal degenerative diseases such as retinitis pigmentosa, using electrical stimulation of the surviving retinal neurons. Challenges to further improve the quality of the restored vision to paint meaningful "pictures" include the ability to control the number, size and shape of the percepts and the rate at which they can be delivered.

Multi-electrode, parallel stimulation could allow for an increase in the number of images delivered per second, as well as it has the potential to be perceived as more "natural" [11]. Unfortunately, there are concerns over electrical crosstalk and the way it may affect the restored vision when multiple electrodes are used simultaneously [236]. The shape and size of percepts caused by two or more parallel stimuli may vary significantly from the percepts caused by each individual stimulus.

Varying current return configurations, such as surrounding each stimulating site with "guard" return-electrodes can be used to insulate neighbours from each-other, at the cost of increased current amplitudes to cause percepts. Quasimonopolar (QMP) stimulation, where the stimulation current is returned partially through a distant, monopolar return electrode and through hexapolar guards can be used effectively to stimulate the retina while limiting the current spread and therefore minimize crosstalk. But during simultaneous stimulation from multiple sites, the monopolar component of the current is – again – available to influence the thresholds of its neighbours [31]. Matteucci et al. observed that the presence of a simultaneous, monopolar stimulus had beneficial effects on the stimulation thresholds on a primary site located several millimetres away (at least 2.19 mm), even if the secondary stimulus was subthreshold. As such, during simultaneous QMP stimulation, the monopolar current delivered by each site can be expected to *lower*

the thresholds on all other sites. But quantification of this effect isn't available for stimulation from more than two sites.

6.1.1 Worst case, but not too much

As we move towards chronic safety tests of simultaneous stimulation, the complexity of defining clinically relevant test parameters has been discussed under multiple perspectives in this dissertation. Regarding simultaneous stimulation, an idea for a clinically relevant 'worst case' case is relatively straight forward: stimulate on all available electrodes in parallel. Of course, because a white picture conveys just as few details about a scene as a black one, it is unlikely to be used in the clinic, but that is precisely what one understands by clinically relevant worst case.

Because it can't be completely excluded that a stimulus corresponding to a "white picture" (all or the majority of all electrodes used simultaneously) will be delivered[15], and because it is the stimulus with the highest associate risks, it therefore matches the definition of clinically relevant worst case perfectly. But what about the amplitude of the stimulation? Haven't we just highlighted how electrodes lower the stimulation thresholds of their neighbours, at least when monopolar current is used? Here's an additional layer of complexity in establishing the "right" test parameters: the number of combinations that may need to be tested in an *in vivo* pilot study is immense. But computer models can fuel our understanding of crosstalk in this context, lower the need for experimental data and refine the experiments where they are still required.

6.1.2 *In vivo*, *in silico* and *in vivo*, again

During *in vivo* electrophysiology experiments, where perceptual thresholds are difficult to evaluate precisely, researchers must identify a way to measure the efficacy of stimulation paradigms. The 'P50', defined as the current which causes 50% of the maximum firing rate at the visual cortex is a widely used threshold definition. This reduces the nonlinear current/excitation curves, which often exhibit sigmoidal behaviours (Figure 6-1), to a single representative value, which is useful to compare stimulation paradigms, for example.

[15] Unless this is done explicitly in the hardware and/or software.

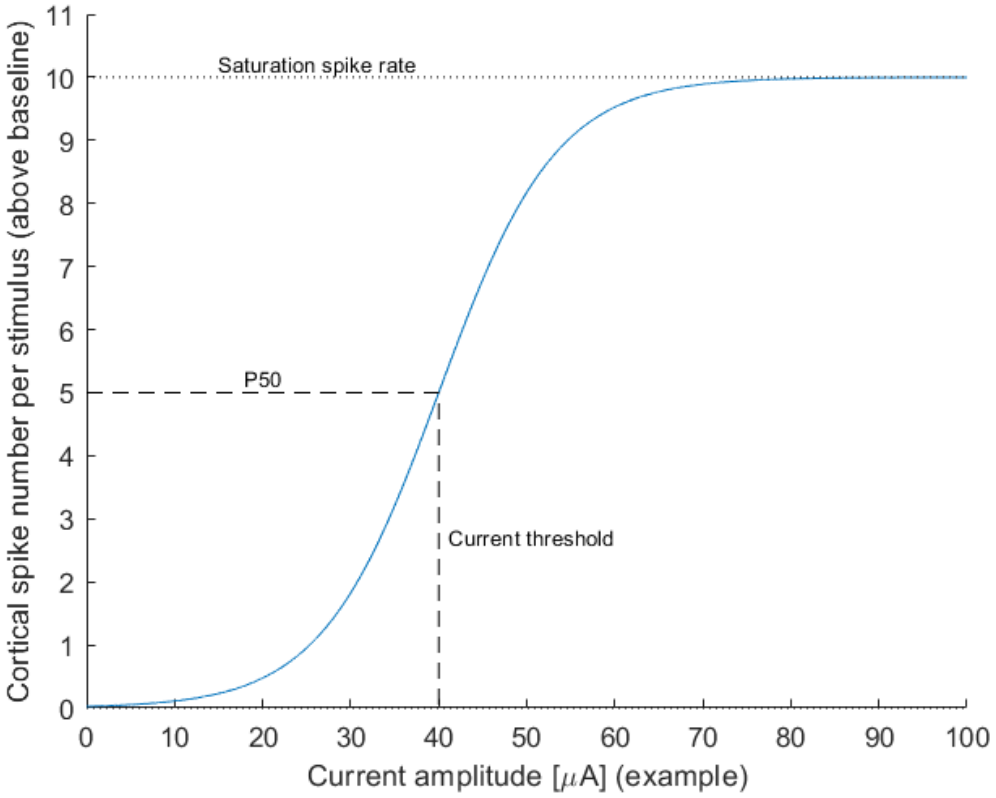

Figure 6-1 Sigmoidal behaviour of the cortical spike rate with increasing stimulation current amplitude. From baseline, the cortical spike rate increases gradually until it reaches saturation. The current threshold is the stimulation amplitude which causes 50% of the maximum spike rate (P50).

As one seeks to use computer simulation to further understand the complex processes at work in the visual system during electrical stimulation of the retina and, to propose and test new strategies *in silico*, the limitations of the reported arbitrary threshold become evident. As these do not reflect the gradual nature of the excitation curves, the use of this empirical data to calibrate computer models is not straightforward. Similarly, the complexity and variability of the empirical excitation curves, even within a single animal, would require complex models to be built, which could be difficult to validate.

The ongoing research presented here endeavours to provide a computer model based on the electric field (E-field) distribution in the neural tissue, which can easily be calibrated on empirical P50 values. Previously, other quantitative models of retinal stimulation used the E-field to predict interference and crosstalk but did not calibrate the activation thresholds on empirical cortical data [236-238]. This model could be used to predict the effects of spatial interference during multi-site, simultaneous stimulation of the retina on the thresholds, and therefore define the clinically relevant worst-case stimulation for any

combination of electrodes. Used as test parameters for a chronic safety test *in vivo*, they would likely increase the significance of the results.

The peak electric field value by itself is a poor predictor of neuronal spiking rate in the visual cortex, although E-field summation has commonly been used to explain crosstalk [61, 239]. As an example, Matteucci et al. evaluated the monopolar and hexapolar currents required to elicit the cortical spike rate corresponding to the cortical P50 threshold. Using Gauss's law and the empirical values for monopolar and hexapolar thresholds published by Matteucci et al. [61], the E-field amplitudes in the RGC layer during stimulation at the thresholds with both paradigms could be calculated. Figure 6-2 shows the calculated E-field for both cases. Since both curves represent an electric field distribution that caused the same *level of cortical response* (spike rate), but because the peak values don't match, it is obvious that the peak amplitude is not correlated with the spike rate.

In the present chapter, as a first attempt to predict cortical P50 thresholds using a calibrated model, the surface area of retinal ganglion cell layer exposed to an E-field above a threshold was hypothesised as being a predictor for experimentally reported cortical thresholds.

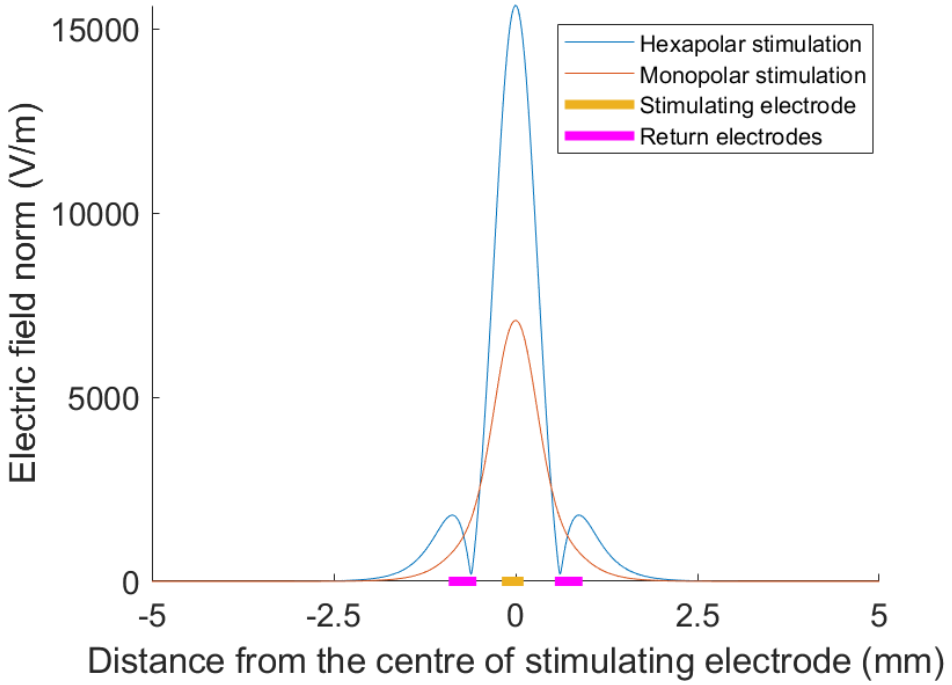

Figure 6-2 Electric field norm in the RGC layer above a suprachoroidal electrode during two stimuli (monopolar, red and hexapolar, blue), which caused the same cortical spike frequency (P50) *in vivo*. It is obvious that the peak E-field value is not a good predictor of cortical activity. E-field norm was calculated using the model presented in this chapter.

Given an electrode geometry, electrode-neuron distance, and tissue electrical properties (conductivity), the surface area above an arbitrary threshold can be calculated using a relatively simple model of the E-field. To test the hypothesis that the surface area of suprathreshold retina is a predictor of cortical activation, a model was built in COMSOL Multiphysics (Burlington, Massachusetts, USA), which was calibrated on the experimental thresholds reported by Matteucci et al. for a single electrode used for monopolar, hexapolar and QMP [61]. As we show that a correlation may exist, we therefore establish the potential of this parameter and explore its ability to predict multi-site crosstalk. In the future, the model may lead to a better understanding of the effects of parallel stimulation and to the refinement of the stimulation strategies. The outcome of the research done *in silico* could therefore lead to *in vivo* stimulation safety studies that are more representative of the clinical application, effectively straightening the path towards human recipients.

6.2 Methods

6.2.1 Model

Similar to previous work [61, 238], the electrostatics module of COMSOL Multiphysics was used to build a model of the E-field distribution in the eye according to Gauss's law in Equation (7) with V, the electric potential, ρ the volume charge density and ϵ_0 the permittivity of free space [236-238].

$$-\nabla \cdot \nabla V = \frac{\rho}{\epsilon_0} \quad \textbf{(7)}$$

Retinal thickness and conductivity values from published sources were used to construct a realistic model of the cat retina (Table 6-1). Fourteen electrodes (Ø380 µm, corresponding to the dimensions used by Matteucci et al. [61]) organised in two hexagons were positioned in the suprachoroidal space and allowed to simulate stimuli delivered with current returning independently to six guard electrodes or to a distant return positioned across 5 mm of vitreous (Figure 6-3). The ratio of the current returned to the guards, to the total can be defined (0%: pure monopolar stimulation, 100%: pure hexapolar stimulation). The model then calculated the electric field distribution in the eye and the field norm in a surface located 290 µm [240] away from the electrodes – corresponding to the RGC layer – was used to predict cortical activity.

Table 6-1 Retinal thickness and electrical properties applied to the finite element model.

Layer	Thickness [µm]	Conductivity [mS/m]
Choroid	82 [241]	43.48 [240]
Retinal pigmented epithelium	10 [242]	0.813 [240]
Outer segment	52.34 [242]	78.7 [240]
Outer nuclear layer	57.49 [242]	16.7 [240]
Outer plexiform layer	22.22 [242]	16.7 [240]
Inner nuclear layer	19.51 [242]	16.7 [240]
Inner plexiform layer	35.45 [242]	54.9 [240]
RGC layer	22.97 [242]	14 [240]
Retinal nerve fibre layer	20.19 [242]	14 [240]
Vitreous	5000	1000 [240]

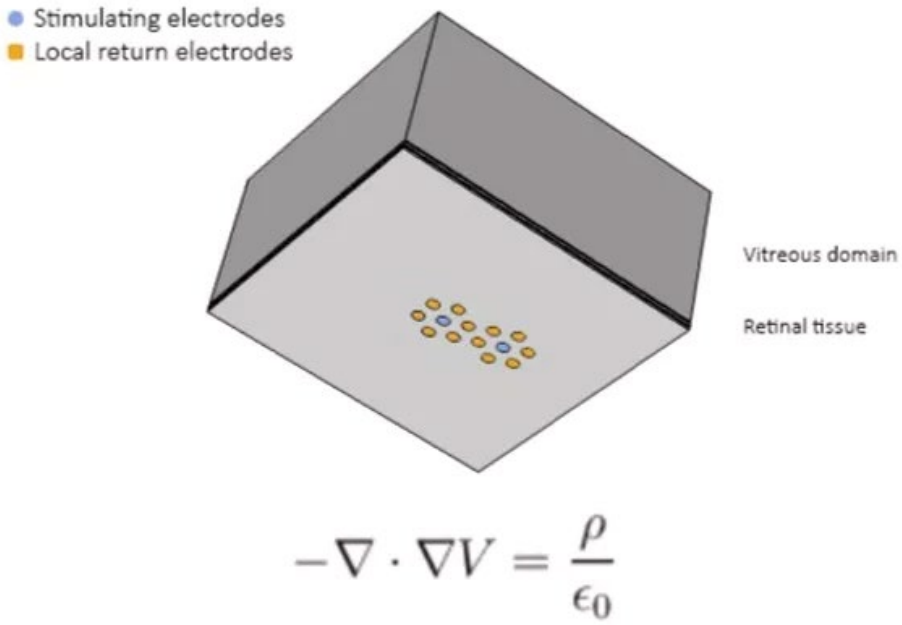

$$-\nabla \cdot \nabla V = \frac{\rho}{\epsilon_0}$$

Figure 6-3 Finite element model and governing equation. The model implemented eye tissue thickness and electrical properties, including all the retinal layers, from published sources. Fourteen electrodes were organised in two hexagons and "directed" to the hexapolar guards to a distant monopolar across the vitreous. The ratio of the current returned to the guards, to the total can be defined (0%: pure monopolar stimulation, 100%: pure hexapolar stimulation). The model then calculated the electric field distribution in the eye and the field norm in a surface located 290 µm away from the electrodes – corresponding to the RGC layer – was used to predict cortical activity.

6.2.2 Calibration: single electrode

Matteucci et al. reported the efficacy of monopolar, hexapolar and two different QMP configurations by comparing the cortical P50 [61]. In their study, five cats were implanted with a suprachoroidal electrode array for stimulation and a 96-channel cortical array for recording purposes. Each available electrode was then stimulated using either a monopolar or quasimonopolar stimulation paradigm with increasing current amplitudes while the resulting cortical spikes were counted. Quasimonopolar stimulation was performed using a range of hexapolar current for each monopolar current value tested. The cortical stimulation thresholds, the P50, for monopolar and quasimonopolar

stimulation, and for each available electrode, were calculated by fitting a sigmoid to resulting spike count data. The numbers were then used to calculate the average monopolar and hexapolar thresholds between all animals and electrodes.

Extending this experiment, the purpose of the present computational model was to quantify the *additive* effects of stimulation from multiple electrodes with regards to the cortical thresholds. In this sense, QMP can be considered as a singular case of interference between two electrodes, where two co-located electrodes (separated by a distance of 0) are used to deliver hexapolar and monopolar stimulation simultaneously.

To calibrate the model, the reported P50 values for pure monopolar and pure hexapolar stimulation were used. Building upon the knowledge of these two empirical values, the model aimed to predict the cortical thresholds for cases where monopolar and hexapolar are combined, also known as QMP.

For monopolar and hexapolar stimulation, the surface area of the RGC layer in the presence of an E-field norm above an arbitrary value E_{th} was computed at the mean current threshold value reported by Matteucci et al. Figure 6-4 shows an example of the variation of surface area above an E-field threshold for varying stimulation current values.

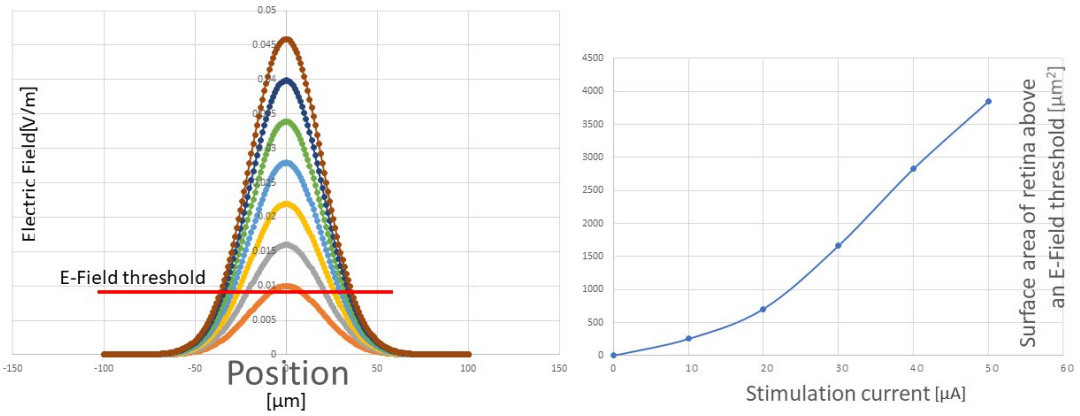

Figure 6-4 Calculation of the surface area exposed to an E-field above an arbitrary threshold . Left: E-field norm in the RGC layer as a function of position around the stimulation electrode, for varying monopolar stimulation current values (coloured curves). Assuming isotropic properties the two-dimensional plot represents a section of a 3D "cone" or "bell" (visualised by rotating the cone around the vertical axis). The intersection of the cone with the plane of the E-field threshold (red horizontal line) defines a disc with a surface area S, which is the total surface area of the RGC layer presented to an E-field above threshold. Right: Surface area of the RGC layer exposed to an E-field above threshold (S) as a function of the stimulation current. Curves are for illustration purposes and do not reflect experimental data.

To calibrate the model, the surface area (S) was plotted as a function of E_{th} for monopolar and hexapolar stimulation at their respective current thresholds. Because all stimulation strategies presented the same saturation spiking frequency [61], it was assumed that the P50 current caused a similar cortical activity, independent of the paradigm, including QMP combinations. It was therefore hypothesised that a pair of values (E_{th} and S) must exist, which are common to all paradigms. The calibration step therefore consisted in establishing what surface area S_{th} was exposed to the same minimum E-field E_{th} with both strategies. The field threshold E_{th} and surface threshold S_{th} were therefore determined as the intersection of the monopolar and hexapolar curves. Effectively, this intersection was hypothesised to identify the E-field to which the RGC layer must be exposed to be stimulated, and the surface area which needs to be activated to cause the P50 spike count, independent of the stimulation paradigm chosen (monopolar, hexapolar or QMP).

6.2.3 QMP predictions

For given values of monopolar currents, the value of hexapolar current required to cause the same S_{th} and E_{th} combination in the RGC layer was sought. A binary search algorithm was used to reduce the computational load. Indeed, the model needs to be run for each value of hexapolar current.

The QMP P50 thresholds reported by Matteucci et al. for a concurrent injection of 36 and 76 µA [61] monopolar current were visually compared to the model predictions with equivalent current values after plotting.

6.2.4 Crosstalk prediction

To evaluate the generalisability of the model to multi-site crosstalk, which is the end-goal of this research, the output of the calibrated model was compared to the results of another experiment reported by Matteucci et al. in 2016, in which the effects of interference from a second electrode were studied. In this configuration, an electrode located 2.19 mm away from the main site [31] was used to deliver simultaneous current relative to a monopolar return electrode. The monopolar current on the main electrode was set and the interfering current, which caused S_{th}, the threshold surface area above the field thresholds E_{th}, was calculated. A qualitative comparison to the empirical data evaluated whether the amplitude of crosstalk matched.

6.3 Results

6.3.1 Calibrated model

The model was calibrated by evaluating the electric field threshold and corresponding surface area which are common to both stimulation types. The surface area threshold S_{th} and the E-field threshold E_{th} were determined as the pair of values common to both stimulation paradigms. For all further stimulations, a stimulus was defined as successful if it caused at least S_{th} (0.77 $mm^2 \pm 2.8\%$ at 95% CI) of RGC layer to be exposed to a field above E_{th} (2463 V/m). Figure 6-5 shows the calibration curves used to establish S_{th} and E_{th}.

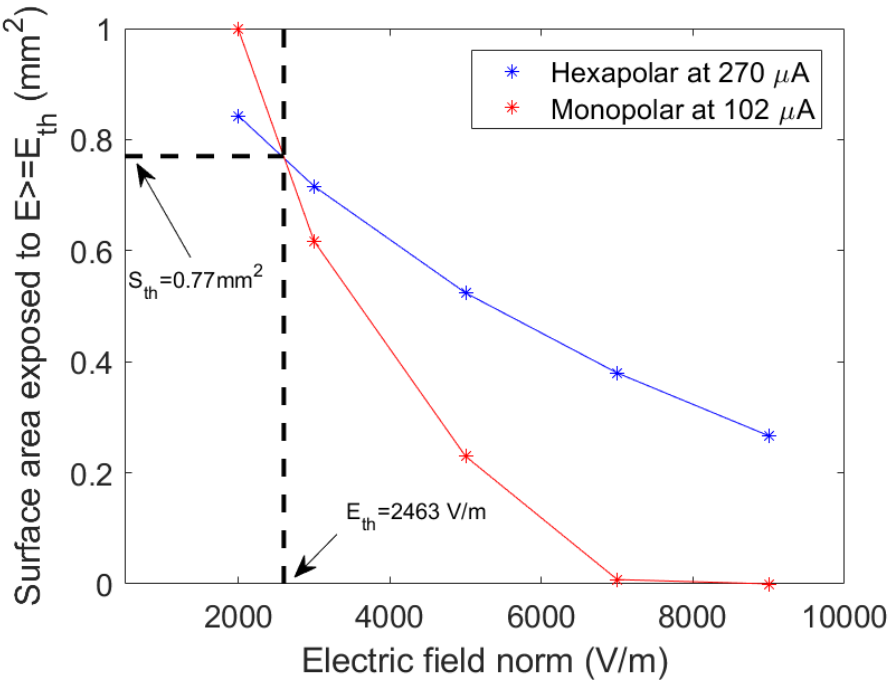

Figure 6-5 Activated surface and E-field threshold calibration for pure monopolar and pure hexapolar stimulation. The surface area of RGC layer exposed an E-field above an arbitrary threshold was plotted as a function of that threshold for experimentally determined current threshold values which caused the same spike rate in cats (P50) [61]. The surface area threshold S_{th} and the E-field threshold E_{th} were determined as the pair of values common to both stimulation paradigms. For all further stimulations, a stimulus was defined as successful if it caused at least S_{th} (0.77 mm^2) of RGC layer to be exposed to a field above E_{th} (2463 V/m).

Note that E_{th} was significantly higher than the value for E-field threshold previously reported in the literature on similar computation models (1116 V/m) [243]. In other models, E-field threshold was defined as the E-field norm which causes an RGC to fire. In the present study, E_{th} is the E-field norm which will cause half of the maximum spike rate in the cortex (P50). Assuming that the cortical P50 requires a multitude of RGCs to respond together to a single stimulus, the difference in E-field thresholds may be expected. Indeed, given the location of the array during the Matteucci et al. *in vivo* experiment [61] and RGC density map established by Hughes [244], a surface area of 0.77 mm^2 may have caused the activation of hundreds, if not thousands, of RGCs depending on the precise location of the electrodes.

Note that the surface area of activated RGC layer is 6.8 times the surface area of the electrode used for stimulation (0.11 mm^2), which suggests that a considerable amount of

current spreading occurs, even during hexapolar stimulation. It is inevitable since the current spread is only limited by the guard electrodes, which are comparatively far from the centre electrode (730 µm, centre to centre). This is clearly visible in Figure 6-2.

6.3.2 Prediction of QMP current thresholds

Using the calibrated model, the required hexapolar current required to excite S_{th} of the RGC layer was determined for two values of monopolar current which had been reported. Figure 6-6 overlays the experimental data used for calibration, as well as the predicted and experimental QMP thresholds. The calibration values S_{th} and E_{th} allowed for a good prediction of the experimental value, suggesting that the cortical activation is correlated with surface area of the recruited RGC layer.

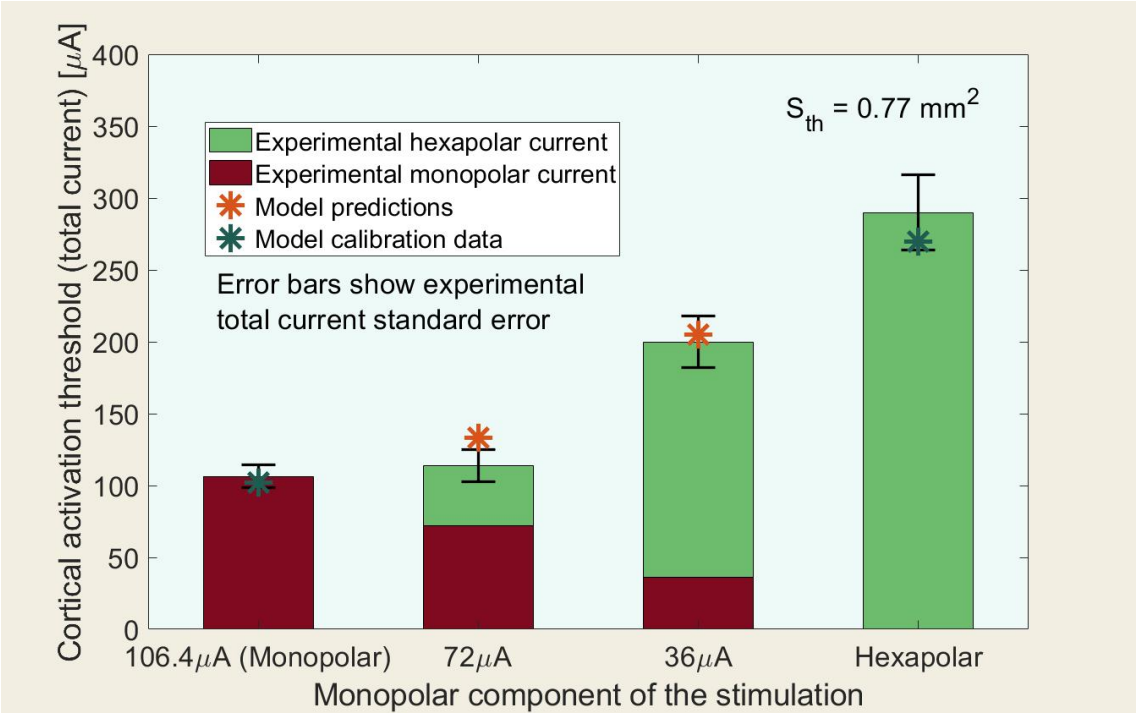

Figure 6-6 Quasimonopolar threshold prediction using a calibrated model of E-field norm in the cat retina. The model was calibrated using the pure monopolar (right) and pure hexapolar (left) current values required to cause 50% of the saturation spike rate in the feline cortex [61]. Using the model, the required hexapolar current needed to reach the P50 for two QMP combinations were predicted and compared to the empirical results. There is a good match between the predictions and the experimental results, suggesting that the surface area of RGC layer above a defined E-field threshold is a strong predictor of cortical activation. (Adapted from Matteucci et al. [61])

6.3.3 Multi-site crosstalk

In 2016, Matteucci et al. reported a development of the QMP experiment used so far, in which the influence of a distant electrode on the cortical thresholds was evaluated. They found that a distant (at least 2.19 mm away) electrode caused a significant drop in the current threshold of the primary when it was used to deliver current with regards to a monopolar electrode. This effect was independent of the type of stimulation used at the primary site (monopolar or hexapolar) and was significant even when the secondary site delivered stimulation at subthreshold amplitudes [31].

In an attempt at generalisation, the model presented here was used to test the hypothesis that E-field summation, which contributes to the surface area of the RGC layer exposed to a field above E_{th}, accounts for the decrease in stimulation threshold reported by Matteucci et al. [31]. The preliminary results (Figure 6-7) were unable to replicate the strength of the interference. Effectively, the addition of a second electrode lowers the amount of current required to reach S_{th}, but the effect is mostly due to the surface area activated directly by the interfering electrode, not because of E-field summation. Indeed, even at subthreshold current values at the interfering site, a significant surface area of RGC layer may already be exposed to a field above E_{th}. Because this surface area is expected to participate to the cortical response, the current model doesn't exclude the direct activation at the interfering site.

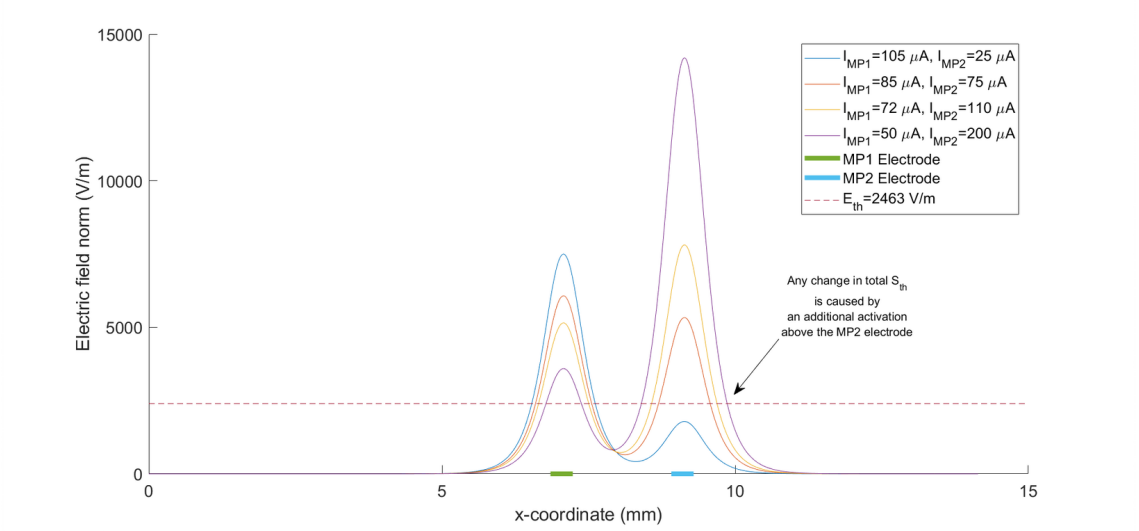

Figure 6-7 Electric field summation during simultaneous monopolar stimulation from multiple electrodes. The model prediction of E-field summation was unable to predict the effects of field summation reported by Matteucci et al. [31] When two electrodes are used simultaneously, lower current amplitudes are needed on the primary to reach S_{th}, as observed experimentally (decreased stimulation threshold on the primary). Nonetheless, the interference electrode appears to contribute to the surface area above threshold S mostly by creating a second zone where the RGC layer is exposed to a suprathreshold E-field (E_{th} shown as a dotted red line). It therefore appears that field summation may not be the primary driver of the interference reported by Matteucci et al. [31]

6.4 Discussion

Computer simulations are remarkable tools to explore and study the effects of electrical stimulation of the retina. The use of computational models gives researchers the opportunity to test many strategies and configurations in a controlled environment, without sacrificing animals, and with reduced time and financial costs. Yet the validation and verification of the models – the demonstration that a model is "correct" and adequately accurate for its intended use [245] – requires special care. Where little experimental data is available to tune the models, such as the electric field distribution in the retina, this process can be challenging.

Previous studies have explored various strategies to estimate the current amplitude required to cause an RGC response, including the Hodgkin-Huxley model of neuronal conduction [240] or an E-field norm threshold [236-238, 243]. In the present chapter, we explored a novel approach by calibrating the model of retinal stimulation on cortical

recordings. Because of the sigmoidal behaviour of the cortical response to increasing retinal stimulus amplitude, which leads to researchers reporting current thresholds as the arbitrary P50 [60], a single E-field value could not be used as threshold. Instead, we tested the hypothesis that the surface area of retina above the threshold determined the cortical P50.

Using the empirical, cortical thresholds for monopolar and hexapolar stimulation in cats, the model of E-field distribution could be calibrated to accurately predict the experimental P50 of QMP stimulation in the same animals. Model generalisation for the prediction of the cortical, and ideally perceptual, thresholds in the case of parallel stimulation from many electrodes would be very useful to define and refine the test parameters for safety studies. Unfortunately, at this stage, the current model was unable to predict the amplitudes of crosstalk measured experimentally and further refinement of the model may be required. Besides the distance between electrodes, the degree of electric field interaction depends on the conductivity of the retinal tissue layers. Hence, future refinement of the model might include adjusting the material conductivity to include anisotropy, the geometry of the model, or modification of the boundary conditions used in the model.

Because the computational model suggests that direct activation of the retina from the interfering site may occur even at subthreshold stimulus amplitude, and because this direct activation would participate to the cortical response, one could hypothesise that the interfering effects seen by Matteucci et al. were mostly due to the direct activation above the second electrode. Yet it is incompatible with their experimental results using a hexapolar interfering electrode. Indeed, hexapolar interference cause a mild *increase* of the current threshold at the primary [31]. This discrepancy highlights some limitations of the current model, as well as they raise questions about the universality of the cortical recording experiments. Since the recording electrodes cover a finite portion of the visual cortex, the results may be strongly biased by the location of the primary and the secondary with regards to the cortical area mapped by the recording array. Further investigation is therefore warranted, ideally including the reproduction of the experiment reported by Matteucci et al., to refine our understanding of the E-field interference and validity of the model for the prediction of multisite crosstalk.

6.5 Conclusion

Using a simple model of E-field distribution in the retina, we were able to predict empirical QMP thresholds by applying a novel calibration technique. Although still in exploratory phase and in need for further calibration, validation and verification, the model may become a useful tool for the quantification of cortical thresholds in the case of multi-electrode interference.

In the present example, the cortical P50 current values were used as calibration and predictions were therefore made for this specific parameter. Yet this proof of concept could be adapted to any other form of threshold, such as retinal (Chapter 5) or perceptual (clinical) thresholds. In the latter case, one can envision accelerated tuning procedures where the computational model is calibrated “on-line” based on the percepts caused by a small number of representative stimuli. An optimisation algorithm could then suggest adequate stimulation amplitudes for parallel stimulation, which will cause minimal crosstalk while conveying the visual information. After final tuning, the implant may then be able to adapt the stimulation parameters “on the fly” to match each and any combination of electrodes.

Finally, the present chapter represents a small but significant step towards the building of a model which could be used to define clinically relevant, worst case sets of parameters for the safety study of parallel stimulation using hexapolar and QMP paradigms (Chapter 8). As we move closer and closer to the long-term use of active devices, we will also need to maximise the lifetime of the devices in the harsh environment of the body.

7 *IN VITRO* DEVICE AGING

POLYMER INSULATION TESTING AND DESIGN OPTIMIZATION

7.1 Introduction

Every surgical intervention includes risks, anaesthesia, haemorrhage, injury and scarring. An effective strategy to minimise the risks is to minimise the number of interventions. Because all devices have a finite lifetime, one ground for secondary surgeries is to replace a medical implant that has failed or has become obsolete. Therefore, devices should ideally be designed to allow for upgrades, and they should be built for long-term reliability.

Electronic vision prostheses require positioning close to neural tissue, which is sensitive to disruptions and has limited ability to heal after injury, compared to other organs such as the skin or bones, for example. Although surgical and device safety are therefore paramount in protecting the cells that are required for vision restoration, yet the benefits of long-lasting devices shouldn't be underestimated[16]. Devices with a lifespan longer than the recipients' life expectancy would, under normal circumstances, require no secondary surgery, therefore minimising all surgery-related risks. Devices should therefore be built to remain functional for decades.

[16] There have been at least two reports on the safety of replacing retinal implants (subretinal and suprachoroidal devices) *in vivo*, both with encouraging results. The is nonetheless no denying that it would be best to avoid these secondary surgeries, unless absolutely necessary.

- Gekeler, F., et al., Repeated transchoroidal implantation and explantation of compound subretinal prostheses: An exploratory study in rabbits. Japanese Journal of Ophthalmology, 2010. **54**(5): p. 467-475.)
- Leung, R.T., et al., Safety and efficacy of explanting or replacing suprachoroidal electrode arrays in a feline model. Clinical and Experimental Ophthalmology, 2015. **43**(3): p. 247-258.

7.1.1 A big bath of salt water

Implanted electrical stimulators are subject to multiple sources of stress, which may cause failure. Some are due to the environment – the body is essentially a big bath of salt water (amongst many other things) at 36.9°C– and some are due to the job they do in this environment. Hermetic capsules are commonly built around the most sensitive components of the devices to slow down the ingress of water molecules[17], therefore delaying the formation of liquid droplets that may cause corrosion, among other possible failure modes [246].

The stimulation itself, is another source of stress for the device and the materials used to build it: voltage stress. Constant-current electrical stimulators, such as the system designed for the Phoenix[99] apply a current between two electrodes. The resulting voltage difference between the electrodes is a function of the applied current and the impedance of the circuit, as given by Ohm's law.[18] The resistance of the circuit includes multiple components, including: the tissue-electrode interfaces; the resistance of the tissue itself; and the resistance of the wires/tracks/conductors that connect the stimulator to the electrodes. During current-driven stimulation, as used in the majority of retinal prostheses [157] including the Phoenix[99], the higher the resistance of the circuit, the higher the voltage delivered by the electronics, for a defined current value. And the higher the voltage applied between electrodes, the higher the stress on the insulator that separates the tracks.

All insulators have an upper limit of electric field that they can withstand before undergoing electrical breakdown – suddenly becoming conductive and hence failing as an insulator. This limit is called the dielectric strength of the insulator. For two electrodes

[17] Hermeticity is not a requirement *per se*, only a mean to achieve the goal of protecting the electronics. There are successful examples of non-hermetic encapsulation techniques which provide long-term survival of implantable electrodes and that have recently been the subject of a review by Chong et al. (Chong, H., et al., *Non-hermetic packaging of biomedical microsystems from a materials perspective: A review.* MEDICAL DEVICES & SENSORS, 2020. **3**(6): p. e10082.)

[18] Note that this isn't applicable to purely capacitive capacitors, in which the current in the tissue is a function of the change in voltage applied to the capacitor (Schoen, I. and P. Fromherz, *The Mechanism of Extracellular Stimulation of Nerve Cells on an Electrolyte-Oxide-Semiconductor Capacitor*. Biophysical Journal, 2007. 92(3): p. 1096-1111).

separated by a defined insulator, the maximum voltage that can be applied between them before the insulator fails depends on the geometry of the system. It is a function of the distance between the electrodes, or the length of the insulator. For plate electrodes separated by a flat sheet of insulator, the breakdown voltage increases linearly with increasing distance between the electrodes. It follows that in any configuration, increasing the distance between two electrodes would increase the breakdown voltage of a particular electrode pair. Unfortunately, due to the needs for miniaturisation of devices and implants, tracks/electrodes of opposite polarity often find themselves packed tightly together, hence possibly pushing the insulator towards its limits.

Let's take the example of an electrode array where all tracks are located in a 2D plane, such as obtained by laser patterning of platinum foil [228], as used in the Phoenix^{99} (Figure 7-1). When the stimulator delivers current to the tissue by applying a voltage (V) between a monopolar return electrode (a) and a stimulating electrode (b). The insulator between the tracks that lead to the monopolar and the stimulating electrodes is exposed to V. Because the distance between the tracks may be very small, the electric field across the insulator may be very high, potentially close or above the dielectric strength of the material.

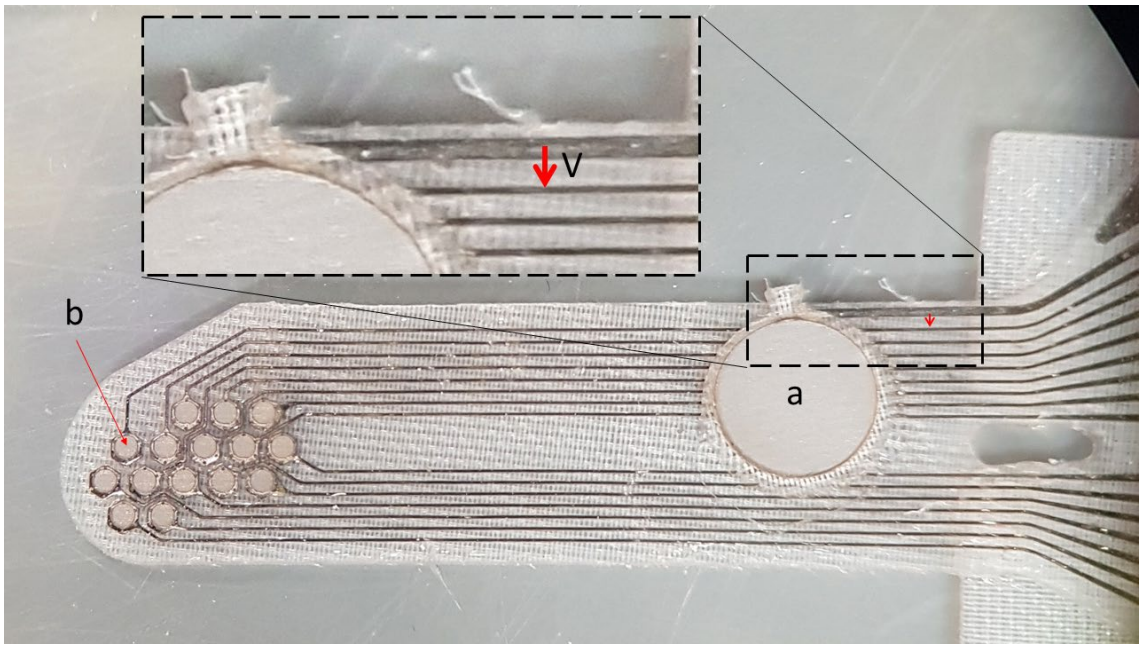

Figure 7-1 Voltage stress in electrode arrays. When the stimulator delivers current to the tissue between the monopolar return electrode (a) and a stimulating electrode (b), a voltage (V) is applied between the sites. The insulator between the tracks that lead to the monopolar and the stimulating electrodes is exposed to V. Because the distance between the tracks may be very small, the electric field across the insulator may be very high, potentially close or above the dielectric strength of the material.

In the Phoenix[99], the material used to insulate the tracks is medical grade silicone rubber (MED-1000, NuSil Technology LLC, Carpinteria, California, USA), which has a dielectric strength of 20 kV/mm when dry. But silicone is not hermetic, it is actually highly permeable to water vapour [247] and absorbs approximately 1% water when placed in a wet environment such as the body. The dielectric strength of the insulator therefore finds itself reduced to 2 kV/mm [248]. Henle, Schuettler, Ordonez and Stieglitz established that even in this condition, an insulator thickness as small as 12 µm should allow for applying 24 V. In Phoenix[99] the tracks are separated by 15 µm at a minimum and the compliance voltage of the current sources (the maximum voltage that the stimulator can apply to attempt to deliver a defined current value through a resistor) is approximately 18 V. Given these theoretical considerations, the design should therefore be adequate.

7.1.2 Contaminants, channels, and corrosion

In reality, the behaviour of the system may be strongly influenced by parameters other than the dielectric strength of the insulator such as the presence of contaminants on the

surface before encapsulation. Anderson, Markovac and Troyk described how contaminated surfaces lead to early circuit failure. Due to the permeability of the polymers to vapour, water diffuses through the encapsulant and condenses primarily at the sites of contamination. Due to the high osmotic pressure, the bond between the substrate and the insulator can be destroyed. This phenomenon can cause the formation of water-filled channels between tracks. Because the water dissolves some of the impurities, the solution then becomes conductive and causes leakage currents between the tracks as well as corrosion of the metals, eventually leading to device failure [249].

Based on the presented failure modes of polymer encapsulated electronics, we hypothesised that (a) insulator failure probability increases with increasing chronic stress voltage and (b) insulator failure probability decreases with increasing distance between tracks. We present a simple investigation designed to test these hypotheses with the Phoenix^{99}. Insulation testing and optimisation for implantable electronics has been the focus of much work since the 1970's, including the development of a sophisticated apparatus to test large numbers of samples in parallel by Donaldson et al. and aimed at evaluating the expected device lifetime of devices [250]. The present investigation is not an attempt to estimate the device lifetime, but rather to propose design optimisation and strategies to maximise it until more rigorous testing can be performed. The results from formal performance and longevity testing, for example according to the guidelines published by Boehler, Carli, Fadiga, Stieglitz and Asplund [251], will then determine the need for further design and process optimisation to meet the target device lifespan of several decades. For example, the optimisation of the cleaning processes prior to deposition of the insulator layer may increase device lifetime.

In the present study, one Phoenix^{99} delivered stimulation equally on 98 electrodes in saline. Because the implant is designed to deliver current-driven stimulation, stimulation voltage can't be readily modulated. Instead, the impedance of the circuit for each electrode was controlled (the higher the circuit impedance, the higher the applied voltage). The test electrodes were effectively insulated from the saline using silicone. The last step of manufacturing was omitted, where the electrode pads are exposed by laser ablation of the silicone. By applying a current (460 µA) to a high impedance circuit (>33.7 kΩ), the stimulator reached its compliance voltage and stressed the insulator with 15.5 V. A subset of electrodes served as controls: their pads were exposed to the saline to lower the resistance of the circuit therefore reducing the stress voltage. The controls were effectively in the "normal" condition which would be used for stimulation. While this

may be counter-intuitive, this approach allowed for the use of the device's own stimulation electronics to stress the dielectric, rather than relying on external electronics with voltage-control capability. Indeed, due to the miniaturisation of the devices, connecting the 98 tracks of the electrode array to external electronics would have been considerably more challenging while possibly introducing other biases.

Using the visual stimulator electronics dedicated reverse telemetry function, the resistance of the circuit was measured for each electrode. Insulator failure was defined as a significant drop in circuit resistance, an apparent short-circuit between the stimulating electrode and the return. Statistical methods were used to test the effects of track distance on failure probability at a given stress voltage. As a result of this investigation, recommendations were made with regards to the design of the implant, as well as the management of non-functional electrodes.

7.2 Methods

7.2.1 Device aging under electrical stress

One hermetically sealed Phoenix[99] Bionic Eye similar in all aspects to the passive devices presented in Chapter 3 underwent lifetime testing. The electronics were energised and driven by a dedicated set of external electronics and using radiofrequency, wireless communication.

The visual stimulator included 14 monopolar current sources used for stimulation. Each current source is capable of being connected to one of seven electrodes. Stimulation can therefore be delivered to seven groups of 14 electrodes in parallel. Sequentially switching between groups allows all 98 electrodes to be used in stimulation. All current sources were connected to a large, platinum return electrode located at the bottom of the visual stimulator capsule. The polarity of the sources could be reversed and used to deliver square, charge balanced biphasic pulses.

Prior to the electrical fatigue tests, the functionality of the device was tested by performing sequential electrode impedance measurements on all electrodes in air (open circuit) and then in saline. The impedance measurement system built into the stimulator application specific integrating circuit provides readings of the voltage at the electrode and at the monopolar return. If the current source is used within its compliance voltage, the difference between electrode and return voltages and the knowledge of the injected current magnitude allows for the calculation of the impedance.

The device was rated as functional if the open circuit measurements all showed values corresponding to the compliance voltage of the current sources. To compare device aging under normal and worst-case electrical stress, a subset of 18, randomly selected electrodes were mechanically exposed by laser ablation of the silicone insulation (diameter 600 µm) (Optec Laser Systems, Frameries, Belgium). Saline impedance measurements were used to confirm the conductivity of the mechanically exposed electrode pads. Electrodes with a measured impedance below 15 kΩ (reading below 7 V) were included.

For the sake of simplicity, the device was immersed in saline at room temperature (21°C), rather than body temperature (36.9°C). It was programmed to deliver biphasic pulses with an amplitude of 460 µA, a phase duration of 500 µs, and an inter-phase gap of 250 µs at a frequency of 30 Hz on each electrode. During each stimulation event, all 14 current sources were used simultaneously to deliver the charge to 14 electrodes. After two weeks (approximately 36 million pulses), a second impedance measurement in saline was performed. Because the measurement showed that a significant number of electrodes had failed at that stage, the experiment (which did not have a scheduled end-date) was interrupted and the data was analysed. The final (two weeks) impedances in saline were compared to the initial measurements to identify changes. Electrodes were categorized as 'shorted' to the monopolar return if the voltage difference measured was equal to zero and as 'open' if the measurement corresponded to the current source compliance voltage. Shorted electrodes were considered to have failed. Failure rates were calculated for both groups of electrodes, exposed and insulated.

Where short-circuits are a possible failure mode, these most likely to occur at the locations where two conductors are the closest. The worst-case distance between the tracks of all individual electrodes and the return was identified at the visual stimulator capsule, where the conductive platinum/alumina feedthroughs are connected to the platinum/silicone electrode array (Figure 7-2). For each electrode, the shortest distance to the return pad was measured in the design file used for the laser micromachining of the electrode array.

The device was inspected visually under an optical microscope to identify possible failure modes and locations.

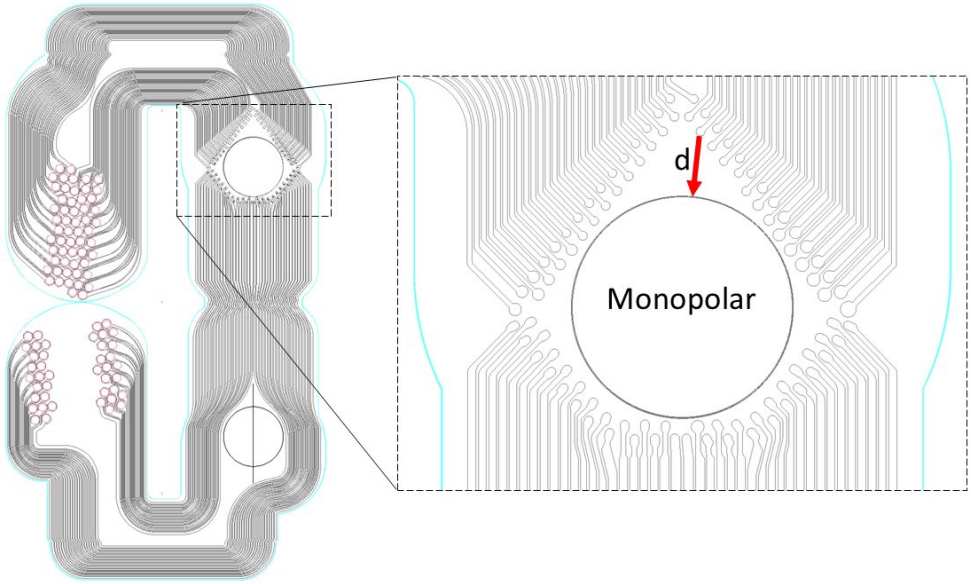

Figure 7-2 Distance between electrode tracks and the monopolar return electrode. Details of the electrode track design of the Phoenix[99] and measured distance (d) between electrode tracks and the monopolar electrode. The monopolar electrode is a large platinum disc at the bottom of the hermetic capsule that contains the stimulating electronics. Each electrode track exists the capsule around the monopolar and connects the stimulator to the electrodes (red on the left picture). The distance d varies between electrodes (mean: 0.7434, range: 0.204 to 1.98 mm)

7.2.2 Statistical methods

For each group of electrodes (exposed, low stress voltage and insulated, maximum stress voltage) an unpaired Mann-Whitney U test was performed to compare distance between failed (or 'shorted') electrodes and functional electrodes. Note that the Mann-Whitney U test was used because the distances to monopolar are not normally distributed. Additionally, to verify the random allocation of the controls and test electrodes – to exclude that the measured effect was due to all controls being positioned further to the monopolar than the test channels – a Mann-Whitney U test was performed and the distance between each group and the monopolar return was compared.

7.3 Results

The purpose of the test was to observe failure modes during lifetime aging of a hermetically sealed 'fully implantable' device during chronic stimulation and test the hypotheses that (a) lower stress voltage leads to lower failure rates and that (b) increasing

the distance between the stimulation poles decreases the rate of failure. In particular, the device was subjected to worst-case electrical stresses caused by using insulated electrodes, thus stressing the insulation to the full magnitude of the devices compliance voltage. The insulated (unexposed) electrodes have a high impedance path to the saline which leads to the current sources delivering pulses at their compliance voltage (15.5 ± 0.5 V). On the control electrodes, the insulation was removed from the pads, exposing the electrodes to the conductive saline, and thus lowering the circuit impedance and therefore the applied voltage. Because of inter-electrode differences, the resulting low-voltage stress varied between sites, but it was consistently under 2 V (corresponding to an impedance < 4.35 kΩ) except for one electrode which received pulses with 5 V due to a measured impedance of 10.9 kΩ (range 0.8 to 5 V or 1.74 to 10.9 kΩ).

Impedance measurements were performed in air prior to the addition of the saline and the device was considered fully functional based on the open circuit test. One exposed electrode was excluded from further analysis after the preliminary saline test because it presented a high impedance corresponding to an open circuit, possibly due to the presence of air bubbles on the electrode pad. Ten further electrodes were excluded because of noisy, unconclusive final impedance measurements. Unfortunately, the measurements were not repeated on the last day of experiments, offering few clues with regards to the cause of the unconclusive data. Another type of failure, possibly with the electronics, may have caused this issue, although this is pure speculation. Optical microscopy did not provide conclusive results on the location of the suspected insulation failure, but the use of statistical methods provided more detailed information.

7.3.1 Electrical stress and insulation failure

Over the duration of the test, none (0/17) of the exposed electrodes failed while 58.6% (41/70) of the insulated electrodes were shorted to the monopolar return after two weeks (Figure 7-3).

The effectiveness of the random allocation of the controls out of all available electrodes was verified by comparing the position of the tracks of the exposed and unexposed electrodes with regards to the monopolar return electrode. There was no statistical difference (P = 0.4539) between the distance of the exposed electrodes to the return (0.7401 ± 0.4242 mm, mean ± standard deviation) and the distance of the insulated electrodes to the return pad (0.7499 ± 0.3152 mm). The randomisation was therefore considered effective. Post hoc power calculation (G*Power Version 3.1.9.6 [252])

showed that the achieved power of the Mann-Whitney U test was 6.04%. The test therefore presented a low risk of failing to reject the null hypothesis if it was false (false negative). Given the null hypothesis that the means of both groups were equal, it can be concluded that the means of both groups were most likely equal.

As a result, the difference of failure rate between the controls (low voltage) and the test electrodes (high stress voltage) were attributed to the amplitude of the stress voltage. It confirmed the hypothesis that voltage stress is a primary cause of electrode failure. Yet in the absence of visual cues, the location of the failure remained to be confirmed.

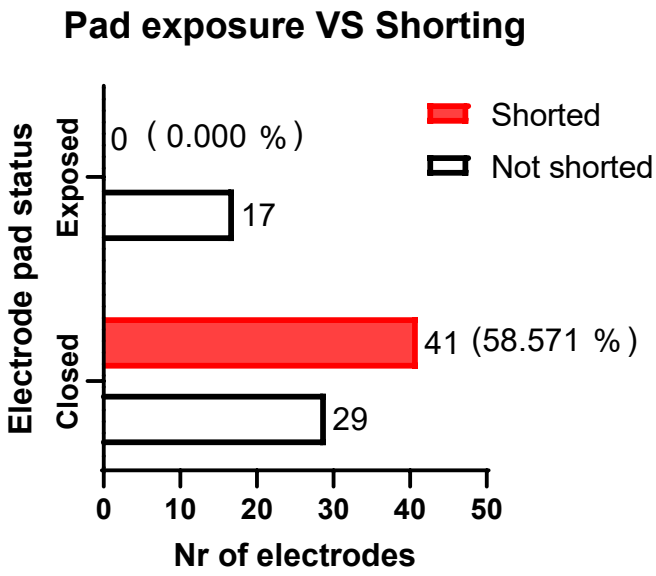

Figure 7-3 Saline aging. Failure rates between low (exposed) and high (closed) stress voltage electrodes. In the low stress voltage group, which may correspond to the clinical usage of the system, no failures (shorting to the monopolar return) were observed (0/17). The failure rate was 58.6% (41/70) in the group subjected to biphasic pulses with a stress voltage of 15.5 V.

7.3.2 Failure and track location

Since insulation failure increased at higher stress voltage, a weak point exists at the location where conductors of opposed polarity are closest to each other. Assuming small resistance values of the tracks, it can be assumed that the whole metallic component of an electrode bears the same electrical potential. Where the tracks are closest, the insulator is therefore exposed to the highest electric field. For all electrodes, in the case of the monopolar paradigm used in this test, this area of interest was located at the bottom of

the hermetic capsule. The electrode tracks exit the capsule, organised in two rows in a diamond shape around the monopolar return disc.

To test the hypothesis that this site was the location of the failure, the test group, where the tracks were subjected to 15.5 V biphasic pulses, was further divided into two subgroups: those that failed (became shorted to the monopolar) and those that were functional after two weeks of testing. A Mann-Whitney U test found that the populations were significantly different between the failed and the functional electrodes (P = 0.0473), demonstrating that the electrodes tracks located closer to the monopolar were more likely to fail under the same cyclic voltage aging conditions (Figure 7-4). Additionally, this also supports the hypothesis that the failures occurred where the electrode tracks are closest to the monopolar (Figure 7-2). Indeed, if the parameter 'distance to monopolar' had been measured in an incorrect location, the statistical test would not likely yield a significant result.

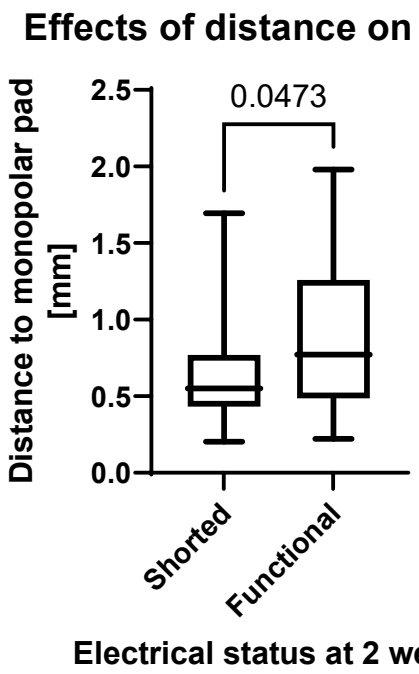

Figure 7-4 Effects of distance to the monopolar return on failure probability. Box and whiskers plot showing the minimum, maximum, median, lower and upper quartiles of the distance between functional and failed (shorted) electrodes and the monopolar return. A Mann-Whitley U test showed that the functional electrodes belong to a population with significantly larger distances P = 0.0473.

7.4 Discussion

Insulation failure under electrical, voltage stress is a known challenge for medical devices [249, 250, 253]. Accurately estimating a device's lifetime using accelerated aging demands rigorous experiments with large sample sizes and specialised equipment [250]. It is therefore worth going through an optimisation process before, or in parallel to, this lifetime testing to ensure only the most promising designs and techniques are put through this time-consuming investigation.

The present experiment is an example of relatively simple test, which can be used to identify the most likely failure modes and locations and serve as basis for design optimisation. While saline may not represent a worst-case medium for testing, due to the absence of biologically relevant aggressive chemical agents such as reactive oxygen ions [254], it allowed for the identification for likely faire modes and mechanisms Using this test set-up, it was demonstrated that the device is likely to survive at least two weeks at 21 degrees (36 million stimuli) when monopolar stimulation is applied to electrodes that have been exposed (normal operation, low voltage stress). On the other hand, the probability of failure increased significantly in the presence of a high impedance circuit, which leads to high stress voltages. For example, a high electrode-tissue impedance may lead to electrical failure as quickly as two weeks. Although some studies have found that the impedance of the electrode-tissue interface may decrease over months or years after implantation [45, 255], it should be closely monitored throughout the lifetime of the prosthesis. Since current-driven stimulators will increase the applied voltage until the defined current flows, or they reach compliance, high circuit resistance may lead to early failures. By design and through monitoring, electrode impedance should be minimised as far as practical and failed electrodes, particularly those presenting an open circuit (high voltage) should be excluded from stimulation to avoid large voltages applied across the insulator.

In the present experiment, only the monopolar stimulation paradigm was tested. Similar evaluation would be beneficial using hexapolar stimulation. In this case, the impedance may be lower than for monopolar because of the proximity between the stimulation and return electrodes, but the tracks are also much closer together, sometimes separated by as little as 15 microns. Additionally, the tracks follow parallel paths over long distances (several centimetres), which increases the probability of a contamination-related local insulation failure [249], compared to the single, worst-case location seen tested here (Figure 7-2).

Independent of the stimulation strategy used (monopolar, hexapolar, quasimonopolar), it is recommended to design devices to maximise the distance of tracks that may carry opposite polarities, within practical limits. In the case of monopolar stimulation, increasing the distance between the stimulation tracks and the monopolar electrode. In devices where a many of tracks must coexist within a tight space, such as the Phoenix[99], this may require an optimisation process between electrode track width and maximising space between tracks. Indeed, decreasing the track width will cause an increase in circuit resistance, but simultaneously allow for larger distances between conductors and hence decrease the failure probability.

Based on the results from this experiment, a design change to the design of the Phoenix[99] was implemented. The geometry of the monopolar electrode was modified to match the diamond organisation of the stimulation tracks, while maintaining the same surface area (Figure 7-5).

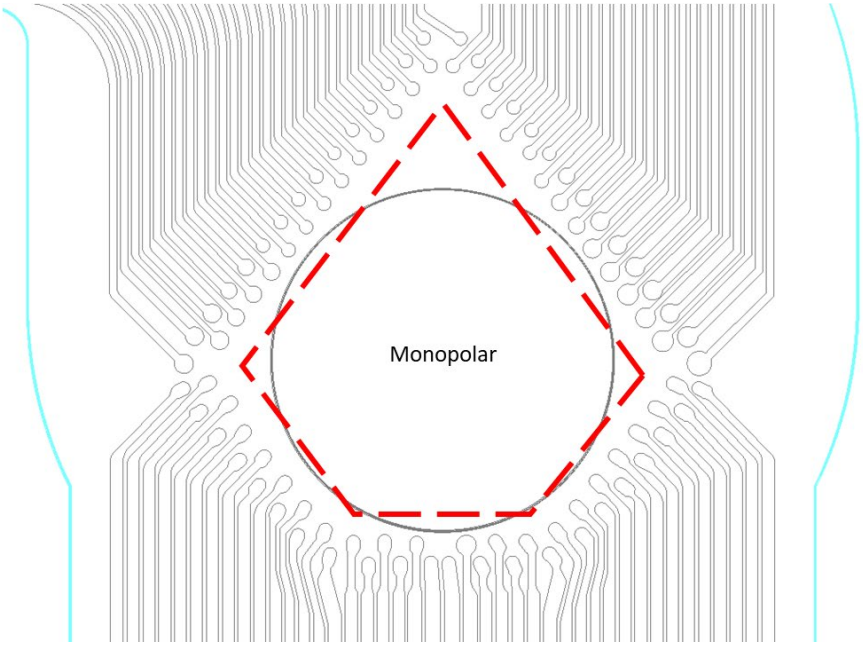

Figure 7-5 Modified monopolar electrode design. The new geometry of the monopolar electrode maintains the total surface area available for charge exchange while maximising the average distance between the stimulation electrode tracks and the monopolar return. The design change represented a very minor change in the design yet may bring about significant lifetime improvements. Geometry for illustration purposes only.

Contamination of the substrate before coating with the insulation material, in this case silicone rubber, has been shown to significantly reduce device lifetime [249].

Manufacturing techniques that minimise contamination should be favoured. For example, peeling away the platinum foil after laser micropatterning a technique called shadow masking [248], instead of ablation of large amounts of materials may minimise the amount of debris on the substrate. Cleaning is obviously paramount to maximise the device lifetime and will required extensive optimisation. Finally, improving the adhesion between the substrate and the insulator may provide some benefits, although the osmotic pressure due to the presence of contaminants in solution in the channels may limit the effectiveness of adhesion promotion [249].

7.5 Conclusion

Device lifetime optimisation is a critical task moving forward towards clinical trials. Pre-clinical studies as well will benefit from the confidence that devices will survive the duration of the study, ensuring that the planned outcome of the safety studies can be achieved without unexpected device failure.

In the present chapter, we have presented some of the known failure modes of implantable devices due to the nature of the stresses associated with electrical stimulation from miniature devices in the harsh environment of the body. Insulator failure under cyclic voltage stress occurred at the location where conductors with opposed polarities were the closest. From the literature, it appears that the failure may have been caused by contamination-related formation of water channels made conduction by dissolution of the contaminants into the water.

Under normal use conditions, where the applied voltages don't exceed 2 V, the current design of the Phoenix^{99} may allow for electrodes to remain functional after at least 36 million cycles. It is noteworthy that this study was not designed to predict the device lifetime. This crucial next step in the development will require determination of adequate worst-case conditions for accelerated aging, possibly including exposing the devices to reactive oxygen species [254] at elevated temperatures [251]. Nonetheless, the low level of complexity of the method presented here (saline at room temperature, using increased voltage as stress factor) allowed to rapidly perform the experiment and identify potential failure modes and locations. As a result, simple yet effective changes to the Phoenix^{99} bionic eye were implemented based on the conclusions of this investigation; effectively optimising the expected device performance and allowing the confident progression towards *in vivo* trials with electrically active devices.

8 THE FUTURE OF THE PHOENIX^{99}

STIMULATION SAFETY IN ANIMALS AND SURGICAL EFFICACY IN HUMANS

8.1 Introduction

As we build ever stronger evidence of the Phoenix^{99} potential as a vision prosthesis and as a tool to deepen our understanding of electrical stimulation of the retina, the sophistication of the experiments increases. More than two decades of multidisciplinary research have been brought together into a device, which is yet to face its biggest challenge: being used in human patients to finally demonstrate its true potential.

More often than not, and with the obvious benefit of isolating the parameters being investigated, subparts of the device or its working principles have been tested separately. Notable examples of this separation include:

- Electrical properties of the microroughened platinum electrodes [228]
- Efficacy of hexapolar stimulation to limit electric crosstalk during parallel stimulation [31]
- Hermeticity requirements for long-term implantation of electronics [246]
- Stimulation electronics design, fabrication and characterisation [256]

On the path towards the clinic, the Phoenix^{99} now stands at a point where all this partitioned evidence needs to be combined to serve as irrefutable proof that the device is safe and ready for long-term trials in humans, including delivery of electrical stimulation using promising novel paradigms. Consolidating this evidence could take multiple forms, including reviewing the literature and establishing practical and theoretical equivalence between the published data and the device, or performing unifying experiments. An example of such a study has been presented in Chapter 3, in which the safety of the devices in their final form was tested.

Using biocompatible materials to build an implantable prosthesis is a requirement. *Per se*, this doesn't constitute evidence that the devices will be biocompatible since the manufacturing techniques, thermal treatments and other laser micromachining processes, could yield devices that cause an unacceptable host response. As such, the experiment in Chapter 3, demonstrated the biocompatibility of the Phoenix^{99} and all its components in an animal model.

As the device progresses towards the ultimate unifying experiment, where it'll be used actively in humans to restore sight, two critical tasks remain. Firstly, the safety of the novel stimulation paradigms which can be delivered by the Phoenix^{99} must be assessed. Secondly, the safety of the surgical technique, previously evaluated in an animal model (Chapter 3), must be confirmed in humans.

The present chapter details study protocols intended to secure the required evidence and lead the Phoenix^{99} towards clinical trials, starting with the context in which investigation fits. The hypotheses and proposed methodology to answer the research questions are presented, as well as the significance of the expected outcome with regards to future, long-term studies in human patients.

8.2 Safety of parallel stimulation paradigms

8.2.1 Introduction

Simultaneous delivery of stimuli from multiple electrodes on a two-dimensional array causes electrical crosstalk, where the signals coming from neighbouring sites fuse into one larger phosphene [31, 236]. Although it can be used advantageously to reduce the stimulation threshold [11] or elicit the perception of simple patterns [257], this effect strongly limits the acuity of the restored vision and therefore the ability to convey complex, meaningful images.

Hexapolar stimulation, where the stimulating electrode is surrounded by a "ring" of six return electrodes, has been shown to effectively limit the amount of electrical crosstalk at the expense of higher stimulation thresholds. This limitation can be partially overcome by the concurrent delivery of subthreshold, monopolar stimuli [31]. This paradigm, called "quasimonopolar (QMP) stimulation" [61] could be used to elicit spatially discrete phosphenes simultaneously, thus getting the best of simultaneous stimulation, which is closer to natural vision, and sequential stimulation, which also limits crosstalk [236]. To the best of the author's knowledge, the long-term safety of stimulation using the

quasimonopolar and hexapolar paradigms has not been studied in an animal model, in particular with regards to the increased current delivery related to the parallel stimulation on multiple electrodes (also called simultaneous stimulation). As an example, at the same stimulation frequency and the same charge delivery on each electrode, two electrodes used simultaneously will deliver twice the charge to the retina. As the number of electrodes used in parallel increases, and as the distance that separates them decreases, the effects of the combinations may become significant.

The Phoenix^{99} Bionic Eye is a fully implantable system, designed to deliver electrical stimuli to the retina from the suprachoroidal space to restore vision. The electrode array was optimized for the use of the quasimonopolar paradigm described above but the dedicated electronics were built to provide maximum flexibility in the type of stimuli, allowing the use of any stimulation pattern from pure hexapolar to sequential monopolar stimulation, and all combinations thereof.

The primary aim of the proposed study is to compare the safety profiles of the simultaneous hexapolar, simultaneous quasimonopolar and sequential monopolar stimulation using a sheep model. The effects of long-term stimulation will be compared using histological methods, as well as *in vivo* imaging techniques. Furthermore, the effects of the different stimulation paradigms on the cortical activation thresholds, measured during terminal electrophysiology experiments at the end of the study, will be studied as an indicator of neuronal damage.

The secondary aim is to establish the safety of the Phoenix^{99} as a retinal stimulator and serve as a steppingstone towards a clinical trial of the device. Focus will be placed on the host response to the implant (to confirm and extend the outcome of the study with electrically inactive devices detailed in Chapter 3) and the effects of electrical stimulation as delivered by the device. We will further investigate the safety of the wireless communication technique used to deliver power and data to the implant through the skin and the ability of the device to elicit responses in the brain of the animal. Finally, animal behaviour, as well as the activity of the visual cortex in response to electrical stimuli will be studied.

This study builds upon the encouraging results from the surgical safety and biocompatibility study of the Phoenix^{99} implant realised in a sheep model (Chapter 3 [1]).

8.2.2 Methods

The proposed study was approved by the University of Sydney (Australia) Animal Research Ethics Committee (2020/1773) to be conducted at the Charles Perkins Centre, The University of Sydney (Sydney, Australia). Unfortunately, study development, animal sourcing and device manufacturing where severely impaired by the Covid-19 pandemic and related lockdowns. Restriction of access to the Hybrid Theatre at the Charles Perkins centre and the sydneyBIONICS Laboratory at the University of Sydney, as well as the laboratory of the Graduate School of Biomedical Engineering, University of New South Wales caused such delays that the entire study had to be postponed. The detailed protocol is provided in the Appendices.

8.2.2.1 Animal model, statistical methods and cohort size

Model selection for long-term studies is an extremely important parameter, as may strongly affect the validity of the results with regards to translation to human subjects. Furthermore, long-term studies should consider practical factors, such as the size of the animals, which will impact the ease with which the experiments can be performed over the duration of the study. For reasons previously detailed in Chapters 3 and Chapter 5 normally sighted Dorper ewes will be used in this experiment.

The effects of chronic (several months), sequential (one electrode at a time), monopolar (current flows between the stimulation electrode and a distant return) stimulation of the retina from the suprachoroidal space have been previously reported in humans [45, 46] as well as in the feline [35] and rabbit [44, 258] models. The effects of the delivery of current to the tissue on all parameters were shown to be mild, including the retinal thickness, the pathology score of the tissue and the cortical stimulation thresholds [35]. The purpose of the experiment proposed here is to compare the safety profile of two novel stimulation paradigms to the established sequential monopolar stimulation. For two of the paradigms, namely hexapolar and quasimonopolar parallel stimulation of the retina, no safety data has been published. Without prior data, power calculation isn't possible as the effect size is unknown.

The secondary aim of this study is the evaluation of the safety of the Phoenix^{99}. The adequate number of animals was determined by adapting the ISO Standard for Biological evaluation of medical devices — Part 6: Tests for local effects after implantation (ISO10993-6) [259]. This standard recommends that an implantable device be tested in a minimum of three animals and at a minimum of ten implant sites. In this experiment, a

single representative implantation site (eye) can be used in each animal, because an intervention to both eyes may cause unacceptable welfare issues. To obtain a total of ten implantation sites, a minimum of ten animals is therefore required. The protocol proposes the comparison of the local effects of three stimulation paradigms in three experimental groups and a total of 12 animals (equal number of four animals per experimental group) was therefore chosen.

Because the differences between the stimulation paradigms are expected to have localized effects only, it is considered as an acceptable compromise. In effect, this limits the number of animals required to obtain significant results regarding the safety of the device. Additionally, the suitability of three groups of four animals to fulfil the main aim of the study was verified using a statistical analysis.

Two parameters have been selected as the main indicators of the health of the tissue after chronic stimulation: the retinal thickness and the cortical stimulation thresholds. For both parameters, the average of each group will be compared to the two other groups using a one-way analysis of variance (ANOVA). Since the effect sizes (loss of retinal thickness and shift in stimulation thresholds) of the intervention are unknown, the influence of this variable on the power of the statistical method was analysed.

In practice, the G*Power software [252] was used to display the statistical power as a function of the observed effect size, for a total of 12 animals (see Figure 8-1). This showed that to obtain a power of 80% with a significance level of 0.05, an effect size of approximately 1.1 will be needed (Figure 8-1). If an effect size of this magnitude isn't reached for either of the parameters the relatively low power of the statistical analysis will be a limitation of the study.

Nevertheless, the experiment was designed to be robust to such eventuality. By comparing new stimulation paradigms to a widely used and tested paradigm, a small effect size will be an encouraging sign. In practice, the function of a visual prosthesis depends on the ability of the neural tissue to detect stimulation and transmit it to the brain. Small differences to an established stimulation pattern would likely imply that the new paradigm could be used to restore vision.

This study is designed as a steppingstone towards human trials and if a limited increase of tissue damage or cortical activation threshold was suggested, a risk/benefit analysis could be performed to establish whether the benefits of the new paradigms outweigh the hypothetically increased risks suggested by the present protocol. Therefore, the chosen

number of animals for this protocol is adequate in providing statistically relevant information to be used to advance the Phoenix[99] as potential candidate to restore vision in blind people.

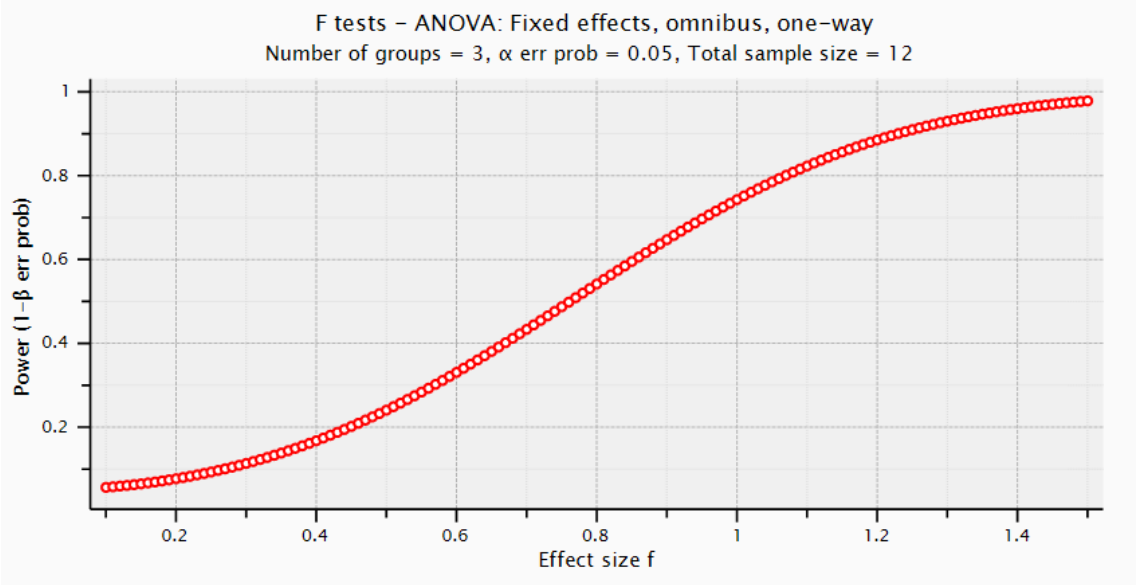

Figure 8-1 Power calculation as a function of effect size for three groups of four animals using analysis of variance (ANOVA). As the effect size of hexapolar and quasimonopolar stimulation, compared to monopolar stimulation can't be estimated based on previous studies or pilots, the present graph shows that an effect size of 1.1 would yield an acceptable study power of 80%.

8.2.2.2 Pre- and postoperative health and device position monitoring

Animal weight will be monitored at regular intervals as proxy indicator of general health and wellbeing.

Intraocular pressure will be measured in both eyes using a rebound tonometer throughout the experiment, including during the acclimatisation period (at least two weeks). Similarly, imaging techniques (ophthalmoscopy and infrared ophthalmoscopy, radiography/computed tomography, ultrasound, optical coherence tomography) will be used to monitor the healing process, observe potential movements of the implants and effects of the device's presence and stimulation on the eye tissue *in vivo*.

Electroretinography (ERG) will provide information about the retinal function. It is noteworthy that suprachoroidal devices, such as the Phoenix[99] may present a significant advantage compared to epi- and subretinal implants. Indeed, suprachoroidal implants sit in a pocket which is physically separated from the retina, doesn't block the path of light to the photoreceptors and may not impair the supply of nutrients to the outer retina by the

choroid. As such, suprachoroidal implants may be compatible with residual vision. ERG data will be used to obtain preliminary data regarding this compatibility.

8.2.2.3 Eye surgery and anaesthesia

Active Phoenix[99] Bionic Eyes will be implanted in the left eye of deeply anaesthetised animals, using sterile procedures. Briefly, two skin incisions will be made, one behind the ear and one at the lateral canthus (corner of the eye) to allow for implanting the telemetry implant and access the globe, respectively.

The eye surgery will be conducted by a specialist vitreoretinal (eye) surgeon. After appropriate dissection, an L-shaped scleral incision will be made to allow insertion of the electrode array (see 3.2.6 for details). The visual stimulator capsule will then be sutured to the globe and all wounds closed with sutures.

8.2.2.4 Postoperative recovery and long-term stimulation

Animals will be closely monitored during the recovery period. After 30 days, the devices will be activated and deliver sequential monopolar, parallel hexapolar, or parallel quasimonopolar stimulation (subjects randomly allocated to one of the three experimental groups) to the eyes of the animals, every day for 14-18 hours over two months. Stimulation amplitudes will be determined by further extending the work presenting in Chapters 5 and 6.

8.2.2.5 Acute electrophysiology

Cortical electrophysiology recordings will be performed during terminal procedures during postoperative weeks 13 or 14.

As previously explained, the effects of anaesthesia on cortical activity and overall physiological stability may represent confounding variables during electrophysiology experiments. As such, the refined propofol-morphine-isoflurane protocol selected in Chapter 4 will be used.

After gaining access to the primary visual cortex, it will be mapped electrically before inserting the penetrating electrode array (Utah array, Blackrock Microsystems, Salt Lake City, Utah, USA).

Visual and electrical stimuli delivered via the implanted stimulator will be delivered in all animals according to the three stimulation paradigms. The cortical responses will be recorded with a multichannel amplification and recording system (RHS

Stimulation/Recording System, Intan Technologies, Los Angeles, California, USA) and stored for offline analysis.

The animals will then be humanely sacrificed, the eyes will be collected, fixed and processed for histological and immunochemical analysis, as per the methods described in Chapter 3 [1]. Additionally, the location of individual electrodes will be identified to allow for a detailed analysis as per the protocol described by Nayagam et al. [260]

8.2.2.6 Data analysis

Acquired data will be deidentified (to blind the operator to the intervention) and analysed to extract the stimulation threshold at which the cortical firing rate reaches 50% of its saturation value (P50) [31]. The P50 for each stimulation paradigm will be compared between the three experimental units (three groups of four sheep) using ANOVA statistics to determine whether chronic hexapolar or quasimonopolar stimulation influenced the stimulation thresholds.

For each animal, the P50 for each of the three stimulation paradigms will also be compared to provide further insights into the differences between stimulation strategies [31, 60, 61].

Histological and immunohistochemical analysis will be performed according to the methods developed in Chapter 3 [1]. Tissue grading will be used to compare the effects of the three stimulation strategies on the health of the eye tissue, in particular the retina. The retinal thickness will be measured to serve during quantitative comparison between study groups. Finally, the histology results will be compared to the electrophysiology recordings to establish whether a correlation exists between the data.

8.2.3 Study significance

The hexapolar and quasimonopolar stimulation paradigms were specifically designed to minimise or avoid electrical crosstalk during multi-electrode, parallel stimulation. As such, they may provide means to restore vision with faster [31], possibly more natural frame rates [257], or with decreased flicker sensation [261]. Some of the consequences of parallel stimulation are intuitive. Because multiple electrodes can be stimulated simultaneously, the amount of electrical current that is delivered to the tissue may be increased, possibly causing long-term damage to the cells. Similarly, the number of stimuli delivered through the electrodes during each unit of time are higher. This could lead to faster aging of the electrode surface and electrode arrays. Finally, hexapolar and

quasimonopolar stimulation, which aim to minimise electrical crosstalk, have been shown to require higher current amplitudes to elicit cortical responses in animals [31, 60, 61]. This may also lead to increased tissue damage, compared to the widely used sequential, monopolar stimulation.

As previously described, the primary aim of this study is to understand the long-term effects of different stimulation paradigms, and the ability of the electrode arrays to deliver the stimulation. Effects of the delivery of current to the retina during extended periods of time can have an influence on the number of cells adjacent to the electrodes, their morphology or their function. The crucial factor which defines whether a type of stimulus is safe for chronic use cannot be defined solely by the local effects. It is the ability of the neural network to be stimulated by the implant and to trigger activity in the brain which determines whether the observed effects on the retina are appropriate. In this sense, it is the complex interconnection between the retina and the brain that is the focus of this study.

It is noteworthy that fully implantable devices are not formally required to study this relationship. Although it would be beneficial to acquire evidence of the safety of the complete Phoenix^{99} Bionic Eye, it is important to highlight that it may come at the costs of much higher experimental and technical complexity. It may also introduce confounding factors and reduce the strength of the conclusions which can be drawn.

Independent of the use of fully implantable devices, the long-term study will serve as a key steppingstone by gathering valuable evidence of stimulation safety and shedding light on the applicability of promising, novel stimulation paradigms.

8.3 Surgical safety in humans

8.3.1 Introduction

As shown throughout the present dissertation, the Phoenix^{99} is a mature device which implements key scientific findings of more than two decades of intense research. The present protocol describes a critical step on the path towards the clinical application of the device to demonstrate and study its vision restoration capabilities in humans. By providing evidence of the efficacy of the surgical protocol to position the device at the adequate location, it will feed directly into the application for the clinical trial of electrically active devices.

Despite extensive studies in human cadavers and live animals, before a chronic application of active implants can be realized, it is necessary to demonstrate that the surgical procedure for implantation is safe and effective in humans. Despite the apparent similarity between the Phoenix^{99} and its close cousin developed under the Bionic Vision Australia consortium (see 2.2.4), particularly with regards to the devices' materials or site of stimulation, there are significant differences between the ocular and orbital components of the suprachoroidal implant already tested in humans by Ayton et al. [45] and those of the present device. The main difference is the geometry of the scleral incision to provide access to the suprachoroidal space and the need to fixate a hermetic capsule to the sclera [1, 45]. These differences call for a demonstration that all the surgical procedure development work carried out to date in human and animal cadavers as well as in the living feline, rabbit and sheep has led to a mature procedure that is applicable and appropriate in living humans with, among others, pulsating blood pressure.

Some patients need the surgical removal of the eyes (enucleation procedure); for example to alleviate the pain that sometimes occurs in blind eyes [262] or due to cosmetic considerations. This represents an ideal model to test the surgical procedure because it minimizes the possibility of causing harm to the subject. Since the eye will be removed after the acute implantation, the most critical part of the experimental procedure has very limited chance of damaging any critical structures. More specifically, this study will focus exclusively on the part of the surgery that is located within the orbit of the eye and include the placement of the electrode array and stimulator hermetic capsule.

8.3.2 Methods

The Phoenix^{99} includes five main components (Figure 3-1). The electrode array is placed between two layers of the eye, namely the choroid and the sclera, and the visual stimulator capsule sits on the globe. The part of the implant responsible for the wireless communication with the outside world is designed to be implanted behind the ear and to mimic closely existing devices (specifically, cochlear implants) from geometrical, surgical site and procedure perspectives. Thanks to the existing clinical knowledge and experience with the implantation procedure of the behind-the-ear components and leads used to connect the different parts of the implants, this part of the procedure can be excluded from the present trial as it is virtually identical to that of routine cochlear implant surgeries.

During the implantation procedure, a scleral incision will be performed. The electrode array will be introduced between the choroid and the sclera. The incision will then be sutured closed before fixating an electronics capsule to the sclera by way of sutures. Owing to the delicacy of the device, manipulation carries a risk of damage to the device that could compromise functionality of active devices intended for future implantation. The physical integrity of the devices will be verified, using X-ray microtomography or similar non-destructive imaging techniques. For comparison purposes, these imaging techniques will be conducted both prior to and after the procedure to isolate any damage that may be caused during surgery.

Apart from additional intraocular pressure measurements and supplementary images (ophthalmoscopy, optical coherence tomography) for the purpose of the study, the intervention has no apparent effects on the participants' safety and well-being; besides an expected prolonged surgery/anaesthesia duration. The studied intervention is insulated within the orbit and on the globe which is being removed as the primary objective of the surgery. There is therefore a very beneficial ratio between the risks of the intervention and the potential benefits of the study. Even though the participants enrolled to undergo acute implantation of a bionic eye will have no benefits for themselves, this study will contribute significantly towards the clinical application of a novel implant for the blind. See Appendices for more details about inclusion and exclusion criteria, and detailed protocol in the filled-out SPIRIT check list (Standard Protocol Items: Recommendations for Interventional Trials) [263, 264].

8.3.3 Study significance and outcomes

The primary objectives of the study are to determine whether the surgical procedure is safe and effective when applied *in vivo* and, ideally, whether it preserves the tissue structures required for the elicitation of visual percepts using suprachoroidal electrical stimulation. Due to the pre-existing condition(s) that caused – or resulted from – the blindness, it may not always be possible to identify the specific effects of the intervention on intraocular structures.

The study will also allow to confirm that the surgical procedure results in the appropriate positioning of the electrode array when using the procedure *in vivo*. Furthermore, it will allow for the evaluation of the effects of the implantation procedure on the physical integrity (macroscopic or microscopic damage) and mechanical stability of the device after implantation.

The research hypotheses are listed in order of importance:

- The surgical procedure to implant the Phoenix^{99} bionic eye is safe and effective.
- The intervention does not cause serious adverse events or cause any material damage to critical structures required for electrical stimulation of the retina to be effective (e.g. nerve fibre layer or optic nerve).
- It allows the positioning of the electrode array in the adequate location in the suprachoroidal space without causing material damage to the device.
- It allows the visual stimulator capsule to be secured to the sclera via dedicated eyelets to prevent capsule and electrode array displacement or damage.

The proposed experiment also represents an opportunity to gather information with regards to efficacy and efficiency of custom and standard surgical tools and equipment and to propose refinements if required. Furthermore, confirmation that any intraocular pressure changes caused by the implantation procedure are safe will be sought.

Outcomes

The primary outcomes of the study are related to the intrinsic properties of the surgical procedure and its effects on the patient and the device. Failure on the following critical points would question the safety and efficacy of the intervention.

The safety of the intervention can be quantified as the number and severity of the adverse events recorded (adverse events will be documented and rated by the operating surgeon on a scale typically used for ocular surgery, for example the Common Terminology for Adverse Events (CTCAE) [265]). An independent expert will review the adverse events and provide scoring. that are related directly or indirectly to the implant or the implantation procedure. Adverse events will be considered as related to the implant or implantation procedure if they occur before or during closure of the scleral incision or if they involve any of the tissue that was dissected, transected or resected as part of the implantation procedure. Any adverse event involving the retina, as observed using intraoperative or post-operative fundus imaging (e.g. retinal detachment, or retinal, subretinal or suprachoroidal haemorrhage) will be considered to be implant related.

The functionality of passive implants can’t be evaluated directly since the devices do not contain electronics. Therefore, the evaluation of the device integrity will be done using high-definition imaging on the explanted devices. The surgical procedure will be considered a success if it doesn’t damage the implant in a way that may compromise its

functional longevity. Device inspection will consider macroscopic damage (bare eye inspection) or microscopic (optical microscope, micro-CT or other) to the silicone encapsulation, the conductive platinum tracks, the electrodes or any other part of the implant such as the eyelets used to secure the capsule to the globe.

This study will also be used to form recommendations and propose refinements for future surgeries. If required, small technique updates that would increase the likeliness of long-term success of the intervention will also be proposed.

Surgery duration provides information about the complexity of the procedure as well as it determines the minimal duration of the anaesthesia. Primary surgery duration will be measured from the first cut incision until the last suture of the scleral incision is placed. Surgery duration will be compared to the published values obtained for other visual prosthesis using electrical retinal stimulation.

Implantation of the device in the suprachoroidal space may cause changes in the intraocular pressure because of the incision made to the sclera and the insertion of a foreign body into the globe. Intraocular pressure measurement will be taken after suturing the scleral incision and before enucleating the eye. The intraoperative measurement will be compared to the baseline value obtained preoperatively to give recommendations about active, intraoperative IOP management during surgeries subsequent to this study.

The surgical procedure should allow for the device to be centred around the macula while avoiding interference with the optic nerve. Using intraoperative fundus images, the macula and the optic disc are clearly visible and used as landmarks for the evaluation of the implant position. Static intraoperative fundus images will be acquired for offline analyses and measurement of the distances of interest. Micro-CT will be use post-operatively to obtain quantitative data about implant position relative to the optic disc.

Significance

All the information which will be gathered during this experiment will play a vital role in the success of the interventions, when active devices will be implanted in patients which may benefit from them. At that stage, the stakes will be even higher as any adverse occurrence which compromises the tissue required for vision restoration (surviving neurons of the retina) or the implant itself, could have catastrophic consequences.

The development of this study therefore represents a vital element in the lifecycle of the Phoenix[99]. As it can be seen in the Appendices, protocol development is well underway.

Due to the Covid-19 pandemic and the pressure it put on the hospitals, it was nonetheless decided that the study shall be postponed until more favourable times, when the safety of all stakeholders can be guaranteed and when bottlenecks in the hospitals can be excluded.

8.4 Towards long-term trials in humans

Evidence of safety and efficacy is without any doubts the most critical component in the complex development process of a biomedical device. In the risk-averse society in which we live and where trial and commercialisation of biomedical devices has become incredibly challenging, engineers and researchers are bound to provide the best possible demonstration that the benefits of any intervention outweigh the risks.

In the case of the Phoenix^{99} Bionic Eye, much safety data can already be used to build the device's case, either directly – studies using the implant itself in its final form [1] – or indirectly, such as in studies having been performed on subcomponents of the implant [266] or on similar devices [35, 45, 133, 142, 145]. Nevertheless, there are aspects of the system's implementation which will benefit from additional evidence.

In the present chapter, two studies have been proposed and described, which will allow for the acquisition of critical safety data. This data is very likely to constitute the best evidence of safety and efficacy of the Phoenix^{99} to date and bring the whole system a giant step closer to the people who may benefit from it.

9 GENERAL DISCUSSION

Restoring vision using implantable electronics is no easy feat. Due to the nature of the work being performed, where high-tech devices are used for a therapeutic purpose, researchers in the field face challenges that combine human-machine interfaces; biology; neurology; miniaturisation; ethics; engineering; manufacturing; and regulatory affairs. Navigating this labyrinth is as arduous as it is fascinating. In this context, multidisciplinary teams need to work together consistently over many years, if not decades. Such an endeavour will strongly benefit from clear long-term goals, and a shared vision of the steps needing to be taken to achieve them, so that team members can work at their own level, knowing the role they must play.

Retinal vision prostheses – at least in their current form – may currently find themselves at a turning point in their history. Indeed, all three devices that had, at some point, received a regulatory clearance to be marketed have now been discontinued by their manufacturers for failing to meet expectations. Using the experience of these implants and identifying their shortcomings, the goals for the Phoenix^{99} may be reviewed to ensure that the research activities fit in the current context.

9.1 Benefits of the Phoenix^{99}

Many factors are likely to have influenced the fate of the other systems, including the size of the market, the complexity and costs of the devices, and most importantly: the relatively low quality of the restored vision. This last point, which correlates with the *efficacy* of the devices, is one that is difficult – if not impossible – to assess objectively in the preclinical setting. Given the novel technological features implemented in the Phoenix^{99} reviewed in Chapter 2, including current steering and crosstalk-limiting strategies for parallel stimulation, we established that this device is a promising candidate to improve the quality and intelligibility of the restored vision. As such, one of the goals for the Phoenix^{99} is to be used in a small cohort of blind patients to measure the efficacy of the device.

Even with the prospect of improved restored vision for the recipients, compared to previous implants, accessing the stage of clinical research requires a device to

demonstrate a *favourable risk-benefit ratio* [25]. On the path to a first efficacy trial in humans where its true benefits will be measured, a further goal for the Phoenix[99] is therefore to develop an adequate understanding of the risks associated with the device.

9.2 Safety of passive devices

In the ovine model, passive devices were well tolerated and did not cause unexpected disturbances of the retina beyond layers that would already be significantly damaged and remodelled in potential recipients. This study led to multiple significant findings with regards to the surgery- and device-associated risks. Device stability was improved over the course of the experiment, by making subtle yet efficacious alterations to the original surgical technique. Most importantly, beyond being usable as reference for all active device studies, the demonstrated safety and biocompatibility of the electrically inactive implants will be a key argument going forward. Using this result, switching off a device that is malfunctioning or is causing unforeseen adverse events when active can be presented as an effective remedial action. Because a passive device may be safe to remain in place while other solutions are sought, it could avoid immediate explant surgery. Even if it may be only a temporary solution, it is a good inclusion in a stimulation efficacy study protocol, complementing the active device and stimulation safety data which will have been acquired.

9.3 Safety and perceptual thresholds

Preclinical safety studies for devices such as retinal implants for vision restoration may aim to chronically apply clinically relevant, worst-case, stimuli to evaluate the effects of long-term device use on the tissue. This represents a major challenge as one would define “clinically relevant” as “stimulation which are likely to elicit visual percepts”, yet without feedback from a cooperating human, accurate determination of these values is difficult.

In animal research on vision prostheses, the methods commonly used to evaluate the ability of a specific stimulus to elicit phosphenes is to infer successful stimulation thresholds based on cortical recordings. Because of our limited ability to detect small changes in cortical activity, and because of the gradual increase measured with increasing electrical charge delivery to the retina, cortical thresholds may not be an accurate way to determine whether a specific stimulus elicited a response in the retina. It is obvious that any further confounding factors, such as an anaesthetics-related depression of the cortical

response in such trials would only draw the true perceptual thresholds and cortical thresholds further apart.

If cortical thresholds were used to determine the charge density values at which chronic tests should be performed, anaesthetic-related cortical depression could cause an unfavourable bias in long-term safety studies. Because one would have to interpret the absence of cortical response as resulting from subthreshold stimulation – stimulation that is below the minimum charge required to elicit a phosphene– one would define the 'clinically relevant' electrical charge above that of the true perceptual threshold. Used chronically, delivery of higher charges is likely to have a negative impact on the tissue or the devices, or both, which may not occur at the stimulation amplitudes required to elicit a response in the awake implant recipient.

Of course, anaesthesia is not the only parameter which make the evaluation of the perceptual thresholds difficult. In this context, a risk-based approach will guide the researchers to ensure that the stimulation levels during the safety trials are reasonably stronger – worse – than required to elicit a response. Should the stimulation levels be defined unrealistically high – not clinically relevant, for example because of the effects of anaesthesia – one might falsely conclude that a device isn't adequately safe and abandon a promising technique.

Beyond limiting the cortical depression that can be caused by anaesthesia, there are other advantages to carefully considering the anaesthetic protocols used for animal research. Adequate use of anaesthetic and analgesic regimes will also minimise fluctuations in recordings, which may be due to the varying physiological state of the subject (possibly including nociceptive inputs if analgesia in inadequate), and overall give confidence to the researchers moving ahead. In collaboration with a team of expert veterinarians and veterinary anaesthetists, we proposed a widely applicable method to guide researchers in the selection of adequate anaesthetic technique, drugs, and monitoring. Following our own selection criteria, we maintained two physiologically stable sheep for up to 14 hours while eye and brain surgeries were being performed, and while retinal and cortical recordings were acquired. At the time of submission of this dissertation, this "anaesthesia refinement tool" (Chapter 4) is undergoing a final review before being submitted as a methods journal article.

With the confidence of an optimised anaesthetic technique, which would minimise the drug-induced bias, we set out to establish a correlation between the retinal and cortical

responses in anaesthetised sheep. Had the cortical recordings been successful, this experiment should have permitted to evaluate the correlation that may exists between the different thresholds. Unfortunately, cortical recording electrodes were positioned in suboptimal locations in both animals as a result of intraoperative misinterpretation of noisy data. As a result, we were unable to establish the correlation, which remains an important task moving ahead, to better understand the significance of the novel recordings of the electrically evoked retinal activity, from the suprachoroidal space.

During this world-premiere, hypothesis-generating experiment, we could measure retinal activity from the electrode array of a retinal prosthesis during visual and electrical stimulation. Because of the proximity to the device-body interface, such recordings could be used to differentiate successful from unsuccessful stimulation without having to rely on cortical recordings, and therefore potentially get closer to the true perceptual threshold.

An obvious limitation of this experiment is the sample size. Due to the exploratory nature of the tests, and because this experiment was secondary in the protocol approved by the ethics authorities, only two animals were used out of a maximum of six. Additionally, issues with the retinal recordings in one of the sheep further reduced the amount of available data (5.3.3). The preliminary conclusions drawn from Chapter 5 will therefore need to be confirmed in further experiments and using specifically designed protocols.

Nonetheless, the technique could represent a technical solution to the absence of feedback in animals and anaesthetised humans alike. It could then be used in a similar fashion as done in cochlear implants where it provides objective feedback about device functionality and required stimulation amplitudes [54, 55]. It could also be used to define what ‘clinically-relevant’ stimuli is for safety studies because it is likely to be closer to the perceptual thresholds. Additionally, it would be a great research tool that may be more sensitive to the potentially subtle differences between the responses to different stimulation levels or paradigms. Regular recordings during chronic studies would also be facilitated using this technology.

9.4 Retinal recordings

For animal experiments involving recordings of the brain activity, technological developments including miniaturisation and wireless communication are allowing increasingly complex experiments in awake or even behaving animals. By eliminating the need for anaesthetic agents during cortical recordings, such experiments eliminate the

possible interference of anaesthesia on the cortical activity and therefore on the study results.

There is a technological challenge to the design and manufacture cortical recording apparatus that is compatible with recovery surgeries, including size and biocompatibility. Compromise in terms of measurement accuracy, frequency, resolution, or number of channels may be required, particularly in smaller animal models such as mice, rats, or rabbits.

Beyond the technical challenge, there are ethical concerns to be considered when considering recovery interventions. Due to the invasiveness of the surgical interventions and devices used, for example penetrating cortical multi-electrode arrays (MEA), the quality of life of the animals after the intervention may be impacted. To be ethically justifiable, the benefits of experiments in awake animals must outweigh the potential risks to animal welfare related to post-surgical pain and discomfort, even with the use of appropriate analgesics.

Retinal prostheses require the surgical implantation of a device in the eye. Studies which intend to use combined retinal stimulation and cortical recordings in the visual cortex must therefore consider the impact of two invasive interventions on the welfare of the animals, as well as solve the same technological challenges this time for a pair of devices. Such considerations will not only impact the study development costs and timelines, but also strongly influence the choice of animal model, with a strong orientation towards larger animals in which multiple devices can coexist, such as the sheep.

As previously discussed, the sheep model represents a good candidate for this type of research. First, anatomical similarities between the sheep and human allow for performing experiments with devices in their final (human) form-factor [1, 162]. Secondly, the relatively large size of the animals may allow for the implantation of complex recording apparatus, such as the system techniques developed by Perentos et al., which can be used for recordings in behaving animals [267]. But all these considerations may be simplified using retinal recordings. It is worth highlighting here that, to date, the majority of the electrophysiology experiments on the visual system use the feline or rabbit model. There is therefore scope for research aiming at comparing the different “historical” models with the sheep, specifically related to the electrophysiological responses to similar stimuli.

Once the correlation between the well-studied cortical responses, in sheep or other models, and the retinal recordings will be established, chronic experiments with close monitoring of the neural response may be possible without cortical recordings. In turn, the experiments, interventions, and equipment requirements would be simplified. Just as well, the animal welfare would be maximised. Because of the complexity and high costs of animal research – including the lives of sentient creatures – the outcome of each experiment should be maximised. The use of computer models to extend the scope of the *in vivo* results is only one examples of the work that can be undertaken to minimise the use of animals in research.

9.5 Simulations of stimulation

In the present work a relatively simple computer model was developed, which can be calibrated using *in vivo* cortical data. Even though cortical recordings may not allow for a straightforward quantification of the perceptual thresholds, cortical P50 values were used for two main reasons. First, this type of recording is the most used during *in vivo* animal experiments with bionic eyes and published data was therefore readily available for model calibration and therefore didn't require a new study. Secondly, the cortical P50 is a useful value to compare multiple stimulation paradigms with regards to their ability. A model calibrated based on these values would therefore allow for comparing further stimulation paradigms to those tested *in vivo*.

Using the 'surface area above an electric threshold' accurate cortical threshold predictions could be made in cases where monopolar and hexapolar return configurations were used simultaneously on a single electrode. This demonstrates the potential of the model and calibration technique. At this stage, more investigation is required to generalise the model to predict thresholds when multiple, distant electrodes are used concurrently. Once this model is available, it will be usable to fine tune the stimulation parameters for safety studies. Since concurrent stimulation at one site appears to lower the thresholds at distant electrodes [31], the clinically relevant stimulus amplitude on any electrode should be established based on the stimulation amplitudes at all sites used concurrently. Unless effects of interference can be quantified, one risks using stimulation amplitudes that are unnecessarily high. Further down the line, the ability to calculate the amplitude reduction required at site A to maintain the properties of a phosphene, given the stimulus amplitude at site B could be built directly into the image processing unit. In doing so, the consistency of the phosphenes at each electrode may be improved, therefore providing an overall more

intelligible set of sensations, even when displaying “real-life" images that may present an infinity of concurrent electrode combinations. Combining computer models of parallel stimulation calibrated using cortical data acquired in animals anaesthetised using an optimised protocol, retinal response recordings, as well as the safety data obtained using electrically inactive devices, we are building confidence that representative and meaningful stimulation safety data will be acquired during long-term studies. Device lifetime evaluation and optimisation to ensure that device failures do not interrupt these studies is yet another important task.

9.6 Long-term testing

In animals at first, and then in humans, the future of the Phoenix[99] will involve long studies where devices would be expected to work continuously for years. Device reliability testing and, if needed, improvement is therefore needed. Despite the small scale of the test presented in Chapter 7, a potential failure mode of the device could be identified and a simple design update with minor impact on the project timelines was implemented, which have a significant impact on future studies using this prosthesis. Obviously, more reliability testing is warranted before long-term testing is considered, which were not in scope of the present dissertation. Accelerated aging of the insulation should be considered to evaluate the expected device lifetime and ensure that it is longer than the duration of studies. Unless this can be demonstrated, device failures may prevent *in vivo* studies from reaching their scientific endpoints and leading to unnecessary animal sacrifices. The same applies obviously to future clinical studies as well.

9.7 Safety and efficacy

Medical devices such as vision prostheses should be safe and make a worthwhile contribution to improve the quality of life of the recipients. In this thesis, we have highlighted how the evaluation of efficacy without tests in human subjects may be difficult. Furthermore, we have discussed how the design of experiments for the sake of safety evaluation can be complex, particularly with regards to stimulation safety. As a result, the body of the work undertaken and reported here have had safety as a focus, for the purpose of accessing clinical trials and finally evaluate the true potential of the Phoenix[99] to restore a sense of vision. A study protocol to compare the effects of the novel stimulation techniques built into the prosthesis was proposed, which will benefit from the learnings described in Chapters 4 to 6. Additionally, a study was proposed, where the

safety of the surgical technique could be tested in humans while minimising any risks to the patients. Once these tests have been performed, and given that acceptable results are obtained, then the safety of the device will have been established with confidence and nothing should stand in the way of clinical trials. Because of its flexibility, the Phoenix[99] will most likely become a very useful research platform to study the restored vision and further develop the stimulation protocols and the image processing to maximise the efficacy of the prosthesis, using the feedback that the recipients will provide.

After safety and efficacy will have been demonstrated, we may imagine a future outside an academic structure and the device becoming available for a larger number of people who may benefit from it.

10 CONCLUSION

The intention of this thesis is to propose approaches to the safety and efficacy testing which align with the expectations from the regulatory bodies and hence streamline the process to gain ethics approval for human studies as a critical milestone towards wider availability of a retinal prosthesis for the blind.

Besides the long-term safety of implanting passive devices in an animal model, we endeavoured to get as close to the perceptual thresholds as possible, using this important transition from 'nothing to something' as a target to guide the research efforts. Whether in an anaesthetised human patient or in an animal who's unable to respond to questions, getting clear and unequivocal feedback about which specific stimulus caused a phosphene that wasn't there earlier is critical. It could be used to provide intraoperative feedback to a surgeon and technical team or, in a closer future, inform stimulation levels during chronic safety studies. As such, the knowledge of the true perceptual thresholds could play an important role in the future of retinal prostheses and their recipients.

Beyond the hypothesis that tests performed with stimuli that are clinically relevant – would have caused a percept – we considered, developed, and tested techniques which may one day be used to generate the data upon which an ethics approval for human studies may be granted.

After establishing the specific testing needs for active Phoenix[99], and building upon the publication of a long-term safety study in sheep in the peer reviewed journal Biomaterials, we focused on minimising the possible confounding factor in cortical recordings of the activity evoked by retinal stimulation. Together with veterinarians and laboratory animal anaesthetists, we developed guidelines for the selection of anaesthetic techniques and drugs, as well as recommendations with regards to animal monitoring, which will be submitted for publication as a methods paper. Secondly, investigated the electrical recordings of the retinal response to visual and electrical stimulation from the suprachoroidal space. Using this novel technique in a small cohort of sheep provided very encouraging results with regards to the ability of the techniques to identify surviving visual networks in people with residual vision after retinal degeneration. We also obtained the first recordings of the electrically evoked retinal response in vivo, gathering insights

into what may be used to accurately discriminate between sub- and suprathreshold stimuli.

To ensure that the data acquired from in vivo studies has a maximum impact, computer simulations are a very powerful tool. Indeed, provided that the right framework exists, the in vivo data can be used to refine or *calibrate* the models, leading to more accurate and meaningful simulations. In turn, the simulations may minimise the number of required in vivo experiments and therefore the number of animals used for research. Using published in vivo data, we successfully calibrated a computational model to predict the effects of parallel stimulation. Finally, a simple yet powerful device aging experiment was performed, which led to meaningful design upgrades and test recommendations. Along the way, the device and the body of knowledge that surrounds it were not the only things that evolved and grew.

The work presented here is the result of a long journey for me as an engineer and as a researcher. There is a long-term goal for everyone working with vision prostheses: allowing someone to see the world and navigate it more confidently.

When I first started – most likely like every other doctoral student before me – I imagined that I might be there when that promising prosthesis will be turned on for the first time in a person. The reality, as one should really expect in the field of medical devices, is that everything is more complex and lengthier than one would ever hope. As such, I realised that much was left to be done until that day that so many may have *seen* in dreams. Embracing the complexity of the task at hand, I focused my work and all my efforts on answering some questions that are relevant for the purpose of getting the Phoenix[99] to the clinic, where it'll be used to answer even more questions about visual prostheses.

All this time, I also tried to look even further ahead in the future of the device, and to keep an eye on what was happening around it a well. Having observed how the context of the work being undertaken, particularly in a world where things evolve so rapidly, may be as important as the work itself, I grew aware of the fate of other similar visual prostheses. In this context, where novel devices will be compared to their predecessors, it became obvious that the safety, reliability, and potential benefits of the prosthesis compared to previous ones will be scrutinised by the ethics committees and regulatory bodies when approvals for human studies are sought.

Through the study of the literature on retinal prostheses, I also became aware of the difficulties of getting representative safety and efficacy data in a system as complex as

the visual system and using high-tech stimulation paradigms such as quasimonopolar stimulation. For all these reasons, I dedicated my work to building evidence of safety and efficacy for the Pheonix^{99}.

The nature of the work, at the interface between science, engineering, veterinary science, regulatory and clinical affairs, led me to consider may aspects beyond the engineering feat that is the design and construction of a tiny implantable stimulator. For example, it took me on a fascinating "detour": to collaborated with veterinarians and veterinary anaesthetists to refine anaesthesia for *in vivo* experiments involving cortical recordings. The fruit of this collaboration will be submitted for publication because the knowledge that was acquired may impact how such experiments are performed and reported around the world.

The future of the Phoenix^{99} just like all the other retinal prostheses is uncertain. Given the importance of sight for people, a fantastic amount of work and resources are being dedicated to protecting and restoring vision. As such, one might hope that a universal solution might soon become available, which will cure blindness and render visual prostheses will one day become *useless*. But until this day comes, devices such as the Phoenix^{99} will have their role to play, should it be only to further study sight and blindness.

By any means, I hope that this modest contribution to the world of bionic eyes will have shortened the distance that separates this device from the people who may benefit from it.

11 REFERENCES

1. Eggenberger, S.C., et al., *Implantation and long-term assessment of the stability and biocompatibility of a novel 98 channel suprachoroidal visual prosthesis in sheep.* Biomaterials, 2021. **279**: p. 121191.
2. Brand, A., et al., *Beyond authorship: attribution, contribution, collaboration, and credit.* Learned Publishing, 2015. **28**(2): p. 151-155.
3. Stone, J.L., et al., *Morphometric analysis of macular photoreceptors and ganglion cells in retinas with retinitis pigmentosa.* Archives of Ophthalmology, 1992. **110**(11): p. 1634-1639.
4. Marc, R.E., et al., *Neural remodeling in retinal degeneration.* Prog Retin Eye Res, 2003. **22**(5): p. 607-55.
5. Hartong, D.T., E.L. Berson, and T.P. Dryja, *Retinitis pigmentosa.* The Lancet, 2006. **368**(9549): p. 1795-1809.
6. Al-Merjan, J.I., et al., *Registered Blindness and Low Vision in Kuwait.* Ophthalmic Epidemiology, 2005. **12**(4): p. 251-257.
7. Buch, H., et al., *Prevalence and causes of visual impairment and blindness among 9980 Scandinavian adults: The Copenhagen City Eye Study.* Ophthalmology, 2004. **111**(1): p. 53-61.
8. Berson, E.L., *Long-term visual prognoses in patients with retinitis pigmentosa: the Ludwig von Sallmann lecture.* Experimental eye research, 2007. **85**(1): p. 7-14.
9. Steinmetz, J.D., et al., *Causes of blindness and vision impairment in 2020 and trends over 30 years, and prevalence of avoidable blindness in relation to VISION 2020: the Right to Sight: an analysis for the Global Burden of Disease Study.* The Lancet Global Health, 2021. **9**(2): p. e144-e160.
10. Barriga-Rivera, A., et al., *Cortical responses following simultaneous and sequential retinal neurostimulation with different return configurations.* Conf Proc IEEE Eng Med Biol Soc, 2016. **2016**: p. 5435-5438.
11. Shivdasani, M.N., et al., *Visual cortex responses to single- and simultaneous multiple-electrode stimulation of the retina: Implications for retinal prostheses.* Investigative Ophthalmology and Visual Science, 2012. **53**(10): p. 6291-6300.
12. Wheatley, D. and T. Lehmann. *Electrically evoked compound action potential (ECAP) stimulus-artefact (SA) blanking low-power low-noise CMOS amplifier*. in *2007 50th Midwest Symposium on Circuits and Systems*. 2007. p. 41-44 DOI: 10.1109/MWSCAS.2007.4488536.
13. Ayton, L.N., et al., *An update on retinal prostheses.* Clinical Neurophysiology, 2020. **131**(6): p. 1383-1398.
14. Cehajic Kapetanovic, J., et al., *Highest reported visual acuity after electronic retinal implantation.* Acta Ophthalmologica, 2020. **98**(7): p. 736-740.

15. World Health Organization, *International Statistical Classification of Diseases and Related Health Problems*. 11th edition ed. 2019.

16. Troyk, P., et al., *A model for intracortical visual prosthesis research.* Artif Organs, 2003. **27**(11): p. 1005-15.

17. Wong, W.L., et al., *Global prevalence of age-related macular degeneration and disease burden projection for 2020 and 2040: a systematic review and meta-analysis.* The Lancet Global Health, 2014. **2**(2): p. e106-e116.

18. Jager, R.D., W.F. Mieler, and J.W. Miller, *Age-related macular degeneration.* N Engl J Med, 2008. **358**(24): p. 2606-17.

19. Niketeghad, S., et al., *Phosphene perceptions and safety of chronic visual cortex stimulation in a blind subject.* Journal of Neurosurgery JNS, 2020. **132**(6): p. 2000-2007.

20. Sahel, J.-A., et al., *Partial recovery of visual function in a blind patient after optogenetic therapy.* Nature Medicine, 2021. **27**(7): p. 1223-1229.

21. Karapanos, L., et al., *Functional Vision in the Real-World Environment With a Second-Generation (44-Channel) Suprachoroidal Retinal Prosthesis.* Translational Vision Science & Technology, 2021. **10**(10): p. 7-7.

22. National institute on deafness and other communication disorders. *Cochlear Implants*. 2019 [cited 2021 03.01]; Available from: https://www.nidcd.nih.gov/health/cochlear-implants.

23. Vaidya, A., et al., *The cost-effectiveness of the Argus II retinal prosthesis in Retinitis Pigmentosa patients.* BMC Ophthalmology, 2014. **14**(1): p. 49.

24. "Ethical." 2022. In *Merriam-Webster.com.* Retrieved 4 January, 2022, from https://www.merriam-webster.com/dictionary/ethical

25. Emanuel, E.J., D. Wendler, and C. Grady, *What Makes Clinical Research Ethical?* JAMA, 2000. **283**(20): p. 2701-2711.

26. Barriga-Rivera, A., et al., *High-amplitude electrical stimulation can reduce elicited neuronal activity in visual prosthesis.* Sci Rep, 2017. **7**: p. 42682.

27. Chang, Y.-C., et al., *Stimulation strategies for selective activation of retinal ganglion cell soma and threshold reduction.* Journal of neural engineering, 2019. **16**(2): p. 026017-026017.

28. Haji Ghaffari, D., et al., *The effect of waveform asymmetry on perception with epiretinal prostheses.* Journal of neural engineering, 2020. **17**(4): p. 045009-045009.

29. Agnew, W.F. and D.B. McCreery, *Considerations for safety with chronically implanted nerve electrodes.* Epilepsia, 1990. **31 Suppl 2**: p. S27-32.

30. Nayagam, D.A.X., et al., *A Pre-clinical Model for Safe Retinal Stimulation.* Investigative Ophthalmology & Visual Science, 2017. **58**(8): p. 4204-4204.

31. Matteucci, P.B., et al., *The effect of electric cross-talk in retinal neurostimulation.* Investigative Ophthalmology and Visual Science, 2016. **57**(3): p. 1031-1037.

32. Gonzalez-Calle, A. and J.D. Weiland, *Evaluation of Effects of Electrical Stimulation in the Retina with Optical Coherence Tomography.* Annual International Conference of the IEEE Engineering in Medicine and Biology

Society. IEEE Engineering in Medicine and Biology Society. Annual International Conference, 2016. **2016**: p. 6182-6185.

33. Colodetti, L., et al., *Pathology of damaging electrical stimulation in the retina.* Experimental Eye Research, 2007. **85**(1): p. 23-33.
34. Butterwick, A., et al., *Tissue Damage by Pulsed Electrical Stimulation.* IEEE Transactions on Biomedical Engineering, 2007. **54**(12): p. 2261-2267.
35. Nayagam, D.A.X., et al., *Chronic electrical stimulation with a suprachoroidal retinal prosthesis: A preclinical safety and efficacy study.* PLoS ONE, 2014. **9**(5).
36. Ahuja, A.K., et al., *Factors Affecting Perceptual Threshold in Argus II Retinal Prosthesis Subjects.* Translational Vision Science & Technology, 2013. **2**(4): p. 1-1.
37. Shivdasani, M.N., et al., *Factors affecting perceptual thresholds in a suprachoroidal retinal prosthesis.* Investigative Ophthalmology and Visual Science, 2014. **55**(10): p. 6467-6481.
38. de Balthasar, C., et al., *Factors Affecting Perceptual Thresholds in Epiretinal Prostheses.* Investigative Ophthalmology & Visual Science, 2008. **49**(6): p. 2303-2314.
39. Güven, D., et al., *Long-term stimulation by active epiretinal implants in normal and RCD1 dogs.* Journal of Neural Engineering, 2005. **2**(1): p. S65-S73.
40. Laube, T., et al., *Chronically implanted epidural electrodes in Göttinger minipigs allow function tests of epiretinal implants.* Graefe's Archive for Clinical and Experimental Ophthalmology, 2003. **241**(12): p. 1013-1019.
41. Morimoto, T., et al., *Chronic implantation of newly developed suprachoroidal-transretinal stimulation prosthesis in dogs.* Invest Ophthalmol Vis Sci, 2011. **52**(9): p. 6785-92.
42. Terasawa, Y., et al. *Safety assessment of semichronic suprachoroidal electrical stimulation to rabbit retina*. in *2013 35th Annual International Conference of the IEEE Engineering in Medicine and Biology Society (EMBC)*. 2013. p. 3567-3570 DOI: 10.1109/EMBC.2013.6610313.
43. Gekeler, F., et al., *Compound subretinal prostheses with extra-ocular parts designed for human trials: successful long-term implantation in pigs.* Graefe's Archive for Clinical and Experimental Ophthalmology, 2007. **245**(2): p. 230-241.
44. Zhou, J.A., et al., *A Suprachoroidal Electrical Retinal Stimulator Design for Long-Term Animal Experiments and In Vivo Assessment of Its Feasibility and Biocompatibility in Rabbits.* Journal of Biomedicine and Biotechnology, 2008. **2008**: p. 547428.
45. Ayton, L.N., et al., *First-in-Human Trial of a Novel Suprachoroidal Retinal Prosthesis.* PLOS ONE, 2014. **9**(12): p. e115239.
46. Petoe, M.A., et al., *A Second-Generation (44-Channel) Suprachoroidal Retinal Prosthesis: Interim Clinical Trial Results.* Translational Vision Science & Technology, 2021. **10**(10): p. 12-12.
47. Eng, J.G., et al., *Morphometric Analysis of Optic Nerves and Retina from an End-Stage Retinitis Pigmentosa Patient with an Implanted Active Epiretinal*

Array. Investigative Ophthalmology & Visual Science, 2011. **52**(7): p. 4610-4616.

48. Kitiratschky, V.B.D., et al., *Safety evaluation of "retina implant alpha IMS"—a prospective clinical trial.* Graefe's Archive for Clinical and Experimental Ophthalmology, 2015. **253**(3): p. 381-387.
49. U.S. Food and Drug Administration, *Recommended Content and Format of Non-Clinical Bench Performance Testing Information in Premarket Submissions*, December 20, 2019, U.S. Department of Health and Human Services, 2019.
50. Grill, E., et al., *Comparing the clinical effectiveness of different new-born hearing screening strategies. A decision analysis.* BMC public health, 2005. **5**: p. 12-12.
51. Gifford, R.H., et al., *Evidence for the expansion of adult cochlear implant candidacy.* Ear and hearing, 2010. **31**(2): p. 186-194.
52. Peixoto, M.C., et al., *Effectiveness of cochlear implants in children: Long term results.* International Journal of Pediatric Otorhinolaryngology, 2013. **77**(4): p. 462-468.
53. Lohmann, A.R., M.L. Carlson, and D.P. Sladen, *Intraoperative Cochlear Implant Device Testing Utilizing an Automated Remote System: A Prospective Pilot Study.* Otology & Neurotology, 2018. **39**(3).
54. Carlson, M.L., et al., *Prevalence and Timing of Individual Cochlear Implant Electrode Failures.* Otology & Neurotology, 2010. **31**(6).
55. Cosetti, M.K., et al., *An evidence-based algorithm for intraoperative monitoring during cochlear implantation.* Otol Neurotol, 2012. **33**(2): p. 169-76.
56. Fine, I. and G.M. Boynton, *Pulse trains to percepts: the challenge of creating a perceptually intelligible world with sight recovery technologies.* Philos Trans R Soc Lond B Biol Sci, 2015. **370**(1677): p. 20140208.
57. Prévot, P.-H., et al., *Behavioural responses to a photovoltaic subretinal prosthesis implanted in non-human primates.* Nature Biomedical Engineering, 2020. **4**(2): p. 172-180.
58. Halupka, K.J., et al., *Neural responses to multielectrode stimulation of healthy and degenerate retina.* Investigative Ophthalmology and Visual Science, 2017. **58**(9): p. 3770-3784.
59. Wong, Y.T., et al., *Spectral distribution of local field potential responses to electrical stimulation of the retina.* Journal of Neural Engineering, 2016. **13**(3).
60. Matteucci, P.B., et al., *Threshold analysis of a quasimonopolar stimulation paradigm in visual prosthesis.* Conf Proc IEEE Eng Med Biol Soc, 2012. **2012**: p. 2997-3000.
61. Matteucci, P.B., et al., *Current steering in retinal stimulation via a quasimonopolar stimulation paradigm.* Invest Ophthalmol Vis Sci, 2013. **54**(6): p. 4307-20.
62. Cicione, R., et al., *Spatiotemporal interactions in the visual cortex following paired electrical stimulation of the retina.* Investigative Ophthalmology and Visual Science, 2014. **55**(12): p. 7726-7738.

63. Spencer, T.C., J.B. Fallon, and M.N. Shivdasani, *Creating virtual electrodes with 2D current steering.* Journal of Neural Engineering, 2018. **15**(3).

64. Twyford, P., C. Cai, and S. Fried, *Differential responses to high-frequency electrical stimulation in ON and OFF retinal ganglion cells.* J Neural Eng, 2014. **11**(2): p. 025001.

65. Tsai, D., et al., *Survey of electrically evoked responses in the retina - stimulus preferences and oscillation among neurons.* Sci Rep, 2017. **7**(1): p. 13802.

66. Sorrenti, V., et al., *Understanding the Effects of Anesthesia on Cortical Electrophysiological Recordings: A Scoping Review.* Int J Mol Sci, 2021. **22**(3).

67. Villeneuve, M.Y. and C. Casanova, *On the use of isoflurane versus halothane in the study of visual response properties of single cells in the primary visual cortex.* J Neurosci Methods, 2003. **129**(1): p. 19-31.

68. Lissek, T., et al., *General Anesthetic Conditions Induce Network Synchrony and Disrupt Sensory Processing in the Cortex.* Frontiers in Cellular Neuroscience, 2016. **10**(64).

69. Burmedi, D., et al., *Emotional and social consequences of age-related low vision.* Visual Impairment Research, 2002. **4**(1): p. 47-71.

70. Nyman, S.R., M.A. Gosney, and C.R. Victor, *Psychosocial impact of visual impairment in working-age adults.* Br J Ophthalmol, 2010. **94**(11): p. 1427-31.

71. Taylor, H.R., M.L. Pezzullo, and J.E. Keeffe, *The economic impact and cost of visual impairment in Australia.* Br J Ophthalmol, 2006. **90**(3): p. 272-5.

72. Lighthouse, I., et al., *The Lighthouse national survey on vision loss : the experience, attitudes and knowledge of middle-aged and older Americans*. 1995, New York, NY: Lighthouse Inc.

73. Flaxman, S.R., et al., *Global causes of blindness and distance vision impairment 1990-2020: a systematic review and meta-analysis.* Lancet Glob Health, 2017. **5**(12): p. e1221-e1234.

74. Masland, R.H., *The neuronal organization of the retina.* Neuron, 2012. **76**(2): p. 266-80.

75. Gray, H., *Anatomy of the Human Body*. 20th ed. 1918, Philadelphia: Lea & Febiger.

76. Fine, I. and J.M. Park, *Blindness and human brain plasticity.* Annual Review of Vision Science, 2018. **4**: p. 337-356.

77. Merabet, L.B., et al., *Rapid and Reversible Recruitment of Early Visual Cortex for Touch.* PLOS ONE, 2008. **3**(8): p. e3046.

78. Chow, A.Y., et al., *The artificial silicon retina microchip for the treatment of vision loss from retinitis pigmentosa.* Arch Ophthalmol, 2004. **122**(4): p. 460-9.

79. Pardue, M.T., et al., *Possible sources of neuroprotection following subretinal silicon chip implantation in RCS rats.* J Neural Eng, 2005. **2**(1): p. S39-47.

80. Rosenfeld, P.J., et al., *Ranibizumab for neovascular age-related macular degeneration.* New England Journal of Medicine, 2006. **355**(14): p. 1419-1431.

81. Martin, D.F., et al., *Ranibizumab and Bevacizumab for Treatment of Neovascular Age-related Macular Degeneration: Two-Year Results.* Ophthalmology, 2012. **119**(7): p. 1388-1398.

82. Heier, J.S., et al., *Intravitreal aflibercept (VEGF trap-eye) in wet age-related macular degeneration.* Ophthalmology, 2012. **119**(12): p. 2537-48.

83. Pennesi, M.E., et al., *Results at 5 Years After Gene Therapy for RPE65-Deficient Retinal Dystrophy.* Hum Gene Ther, 2018.

84. da Cruz, L., et al., *Five-Year Safety and Performance Results from the Argus II Retinal Prosthesis System Clinical Trial.* Ophthalmology, 2016. **123**(10): p. 2248-2254.

85. Dahlmann-Noor, A., et al., *Current approaches and future prospects for stem cell rescue and regeneration of the retina and optic nerve.* Can J Ophthalmol, 2010. **45**(4): p. 333-41.

86. Busskamp, V., et al., *Optogenetic therapy for retinitis pigmentosa.* Gene Ther, 2012. **19**(2): p. 169-75.

87. Brindley, G.S. and W.S. Lewin, *The sensations produced by electrical stimulation of the visual cortex.* J Physiol, 1968. **196**(2): p. 479-93.

88. Allison-Walker, T.J., et al. *Local field potential phase modulates neural responses to intracortical electrical stimulation*. in *Proceedings of the Annual International Conference of the IEEE Engineering in Medicine and Biology Society, EMBS*. 2020. p. 3521-3524 DOI: 10.1109/EMBC44109.2020.9176186.

89. Rosenfeld, J.V., et al., *Tissue response to a chronically implantable wireless intracortical visual prosthesis (Gennaris array).* Journal of Neural Engineering, 2020. **17**(4).

90. Troyk, P.R., et al., *Intracortical visual prosthesis research - approach and progress.* Conf Proc IEEE Eng Med Biol Soc, 2005. **7**: p. 7376-9.

91. Pezaris, J.S. and R.C. Reid, *Demonstration of artificial visual percepts generated through thalamic microstimulation.* Proc Natl Acad Sci U S A, 2007. **104**(18): p. 7670-5.

92. Durand, S., et al., *A Comparison of Visual Response Properties in the Lateral Geniculate Nucleus and Primary Visual Cortex of Awake and Anesthetized Mice.* The Journal of Neuroscience, 2016. **36**(48): p. 12144-12156.

93. Veraart, C., et al., *Visual sensations produced by optic nerve stimulation using an implanted self-sizing spiral cuff electrode.* Brain Res, 1998. **813**(1): p. 181-6.

94. Veraart, C., et al., *Vision rehabilitation with the optic nerve visual prosthesis.* Conf Proc IEEE Eng Med Biol Soc, 2004. **6**: p. 4163-4.

95. Wang, K., et al., *Efficacy and reliability of long-term implantation of multi-channel microelectrode arrays in the optical nerve sheath of rabbit eyes.* Vision Research, 2011. **51**(17): p. 1897-1906.

96. Yan, Y., et al., *Electrically evoked responses in the rabbit cortex induced by current steering with penetrating optic nerve electrodes.* Investigative Ophthalmology and Visual Science, 2016. **57**(14): p. 6327-6338.

97. Gaillet, V., et al., *Spatially selective activation of the visual cortex via intraneural stimulation of the optic nerve.* Nature Biomedical Engineering, 2020. **4**(2): p. 181-194.

98. Humayun, M.S., et al., *Visual perception elicited by electrical stimulation of retina in blind humans.* Arch Ophthalmol, 1996. **114**(1): p. 40-6.

99. Yue, L., et al., *Ten-Year Follow-up of a Blind Patient Chronically Implanted with Epiretinal Prosthesis Argus I.* Ophthalmology, 2015. **122**(12): p. 2545-2552.e1.

100. Sinclair, N.C., et al., *The Appearance of Phosphenes Elicited Using a Suprachoroidal Retinal Prosthesis.* Investigative ophthalmology & visual science, 2016. **57**(11): p. 4948-4961.

101. Nimmagadda, K. and J.D. Weiland, *Retinotopic responses in the visual cortex elicited by epiretinal electrical stimulation in normal and retinal degenerate rats.* Translational Vision Science and Technology, 2018. **7**(5).

102. Caspi, A., et al., *Retinotopic to Spatiotopic Mapping in Blind Patients Implanted With the Argus II Retinal Prosthesis.* Invest Ophthalmol Vis Sci, 2017. **58**(1): p. 119-127.

103. Hornig, R., et al., *Pixium Vision: First Clinical Results and Innovative Developments*, in *Artificial Vision: A Clinical Guide*, V.P. Gabel, Editor. 2017, Springer International Publishing: Cham. p. 99-113.

104. Daschner, R., et al., *Functionality and Performance of the Subretinal Implant Chip Alpha AMS.* Sensors & Materials, 2018. **30**(2): p. 179-192.

105. Stingl, K., et al., *Subretinal Visual Implant Alpha IMS – Clinical trial interim report.* Vision Research, 2015. **111**: p. 149-160.

106. Villalobos, J., et al., *Development of a surgical approach for a wide-view suprachoroidal retinal prosthesis: evaluation of implantation trauma.* Graefe's Archive for Clinical and Experimental Ophthalmology, 2012. **250**(3): p. 399-407.

107. Finn, A.P., D.S. Grewal, and L. Vajzovic, *Argus II retinal prosthesis system: a review of patient selection criteria, surgical considerations, and post-operative outcomes.* Clinical ophthalmology (Auckland, N.Z.), 2018. **12**: p. 1089-1097.

108. Stronks, H.C. and G. Dagnelie, *The functional performance of the Argus II retinal prosthesis.* Expert review of medical devices, 2014. **11**(1): p. 23-30.

109. Second Sight. [cited 2022 06.01]; Available from: https://secondsight.com/.

110. Humayun, M.S., et al., *Interim results from the international trial of Second Sight's visual prosthesis.* Ophthalmology, 2012. **119**(4): p. 779-88.

111. Stronks, H.C., M.P. Barry, and G. Dagnelie, *Electrically elicited visual evoked potentials in Argus II retinal implant wearers.* Invest Ophthalmol Vis Sci, 2013. **54**(6): p. 3891-901.

112. Geruschat, D.R., et al., *An analysis of observer-rated functional vision in patients implanted with the Argus II Retinal Prosthesis System at three years.* Clin Exp Optom, 2016. **99**(3): p. 227-32.

113. Durand, M.L., *Endophthalmitis.* Clinical microbiology and infection : the official publication of the European Society of Clinical Microbiology and Infectious Diseases, 2013. **19**(3): p. 227-234.

114. Delyfer, M.-N., et al., *Improved performance and safety from Argus II retinal prosthesis post-approval study in France.* Acta Ophthalmologica, 2021. **99**(7): p. e1212-e1221.

115. Edwards, T.L., *Assessment of the Electronic Retinal Implant Alpha AMS in Restoring Vision to Blind Patients with End-Stage Retinitis Pigmentosa.* Ophthalmology., 2018. **125**(3): p. 432-443.

116. Stingl, K., et al., *Interim results of a multicenter trial with the new electronic subretinal implant alpha AMS in 15 patients blind from inherited retinal degenerations.* Frontiers in Neuroscience, 2017. **11**(AUG): p. 445.

117. Stingl, K., et al., *Artificial vision with wirelessly powered subretinal electronic implant alpha-IMS.* Proc Biol Sci, 2013. **280**(1757): p. 20130077.

118. Bloch, E., Y. Luo, and L. da Cruz, *Advances in retinal prosthesis systems.* Therapeutic advances in ophthalmology, 2019. **11**: p. 2515841418817501-2515841418817501.

119. Muqit, M.M.K., et al., *Six-Month Safety and Efficacy of the Intelligent Retinal Implant System II Device in Retinitis Pigmentosa.* Ophthalmology, 2019. **126**(4): p. 637-639.

120. Shim, S., et al., *Retinal Prosthetic Approaches to Enhance Visual Perception for Blind Patients.* Micromachines, 2020. **11**: p. 535.

121. Cheng, D.L., P.B. Greenberg, and D.A. Borton, *Advances in Retinal Prosthetic Research: A Systematic Review of Engineering and Clinical Characteristics of Current Prosthetic Initiatives.* Current Eye Research, 2017. **42**(3): p. 334-347.

122. Schuettler, M., et al., *Fabrication of implantable microelectrode arrays by laser cutting of silicone rubber and platinum foil.* J Neural Eng, 2005. **2**(1): p. S121-8.

123. Bareket, L., et al., *Progress in artificial vision through suprachoroidal retinal implants.* J Neural Eng, 2017. **14**(4): p. 045002.

124. Bach, M., et al., *Basic quantitative assessment of visual performance in patients with very low vision.* Invest Ophthalmol Vis Sci, 2010. **51**(2): p. 1255-60.

125. Pixium Vision. *Dry AMD PRIMA feasibility studies*. [cited 2022 01.06.]; Available from: https://www.pixium-vision.com/dry-amd-prima/.

126. Endo, T., et al., *Light localization with low-contrast targets in a patient implanted with a suprachoroidal-transretinal stimulation retinal prosthesis.* Graefes Arch Clin Exp Ophthalmol, 2018. **256**(9): p. 1723-1729.

127. Suaning, G.J., et al., *An efficient multiplexing method for addressing large numbers of electrodes in a visual neuroprosthesis.* Conf Proc IEEE Eng Med Biol Soc, 2004. **6**: p. 4174-7.

128. Suaning, G.J., N.H. Lovell, and T. Lehmann. *Neuromodulation of the retina from the suprachoroidal space: The Phoenix 99 implant*. in *2014 IEEE Biomedical Circuits and Systems Conference (BioCAS) Proceedings*. 2014. p. 256-259 DOI: 10.1109/BioCAS.2014.6981711.

129. Green, R.A., et al., *Integrated electrode and high density feedthrough system for chip-scale implantable devices.* Biomaterials, 2013. **34**(26): p. 6109-18.

130. Dommel, N.B., et al., *A CMOS retinal neurostimulator capable of focussed, simultaneous stimulation.* J Neural Eng, 2009. **6**(3): p. 035006.

131. Seo, J.-M., et al., *Biocompatibility of polyimide microelectrode array for retinal stimulation.* Materials Science and Engineering: C, 2004. **24**(1): p. 185-189.

132. Abbott, C.J., et al., *Safety Studies for a 44-Channel Suprachoroidal Retinal Prosthesis: A Chronic Passive StudySuprachoroidal Retinal Prosthesis Passive Safety.* Investigative Ophthalmology & Visual Science, 2018. **59**(3): p. 1410-1424.

133. Leung, R.T., et al., *Safety and efficacy of explanting or replacing suprachoroidal electrode arrays in a feline model.* Clinical and Experimental Ophthalmology, 2015. **43**(3): p. 247-258.

134. Gekeler, F., et al., *Repeated transchoroidal implantation and explantation of compound subretinal prostheses: An exploratory study in rabbits.* Japanese Journal of Ophthalmology, 2010. **54**(5): p. 467-475.

135. Güven, D., et al., *Implantation of an inactive epiretinal poly(dimethyl siloxane) electrode array in dogs.* Experimental Eye Research, 2006. **82**(1): p. 81-90.

136. Majji, A.B., et al., *Long-term histological and electrophysiological results of an inactive epiretinal electrode array implantation in dogs.* Invest Ophthalmol Vis Sci, 1999. **40**(9): p. 2073-81.

137. Barriga-Rivera, A., et al., *Long-term anesthetic protocol in rats: feasibility in electrophysiology studies in visual prosthesis.* Vet Ophthalmol, 2018. **21**(3): p. 290-297.

138. Sachs, H.G., et al., *Implantation of stimulation electrodes in the subretinal space to demonstrate cortical responses in Yucatan minipig in the course of visual prosthesis development.* Eur J Ophthalmol, 2005. **15**(4): p. 493-499.

139. Schwahn, H.N., et al., *Studies on the feasibility of a subretinal visual prosthesis: data from Yucatan micropig and rabbit.* Graefes Arch Clin Exp Ophthalmol, 2001. **239**(12): p. 961-7.

140. Völker, M., et al., *In vivo assessment of subretinally implanted microphotodiode arrays in cats by optical coherence tomography and fluorescein angiography.* Graefe's Archive for Clinical and Experimental Ophthalmology, 2004. **242**(9): p. 792-9.

141. Suaning, G.J., et al., *Discrete cortical responses from multi-site supra-choroidal electrical stimulation in the feline retina.* Conf Proc IEEE Eng Med Biol Soc, 2010. **2010**: p. 5879-82.

142. Villalobos, J., et al., *A wide-field suprachoroidal retinal prosthesis is stable and well tolerated following chronic implantation.* Invest Ophthalmol Vis Sci, 2013. **54**(5): p. 3751-62.

143. Granit, R., *The components of the retinal action potential in mammals and their relation to the discharge in the optic nerve.* The Journal of Physiology, 1933. **77**(3): p. 207-239.

144. Maya-Vetencourt, J.F., et al., *Biocompatibility of a Conjugated Polymer Retinal Prosthesis in the Domestic Pig.* Frontiers in Bioengineering and Biotechnology, 2020. **8**(1188).

145. Villalobos, J., et al., *Cortical activation following chronic passive implantation of a wide- Field suprachoroidal retinal prosthesis.* Journal of Neural Engineering, 2014. **11**(4).

146. Suaning, G.J., et al. *Discrete cortical responses from multi-site supra-choroidal electrical stimulation in the feline retina*. in *2010 Annual International*

Conference of the IEEE Engineering in Medicine and Biology Society, EMBC'10. 2010. p. 5879-5882 DOI: 10.1109/IEMBS.2010.5627527.

147. Eggenberger, S.C., et al., *Safety and biocompatibility of a bionic eye: Imaging, intraocular pressure, and histology data.* Data in Brief, 2021. **39**: p. 107634.
148. Mantravadi, A.V. and N. Vadhar, *Glaucoma.* Primary Care, 2015. **42**(3): p. 437-+.
149. Milam, A.H., Z.Y. Li, and R.N. Fariss, *Histopathology of the human retina in retinitis pigmentosa.* Prog Retin Eye Res, 1998. **17**(2): p. 175-205.
150. Santos, A., et al., *Preservation of the inner retina in retinitis pigmentosa. A morphometric analysis.* Arch Ophthalmol, 1997. **115**(4): p. 511-5.
151. Fariss, R.N., Z.Y. Li, and A.H. Milam, *Abnormalities in rod photoreceptors, amacrine cells, and horizontal cells in human retinas with retinitis pigmentosa.* Am J Ophthalmol, 2000. **129**(2): p. 215-23.
152. Moore, D.R. and R.V. Shannon, *Beyond cochlear implants: awakening the deafened brain.* Nature Neuroscience, 2009. **12**: p. 686.
153. Humayun, M.S., et al., *Visual perception in a blind subject with a chronic microelectronic retinal prosthesis.* Vision Res, 2003. **43**(24): p. 2573-81.
154. Weiland, J.D., W. Liu, and M.S. Humayun, *Retinal Prosthesis.* Annual Review of Biomedical Engineering, 2005. **7**(1): p. 361-401.
155. Eiber, C.D., N.H. Lovell, and G.J. Suaning, *Attaining higher resolution visual prosthetics: a review of the factors and limitations.* J Neural Eng, 2013. **10**(1): p. 011002.
156. Lewis, P.M., et al., *Advances in implantable bionic devices for blindness: a review.* ANZ J Surg, 2016. **86**(9): p. 654-9.
157. Barriga-Rivera, A., et al., *Visual Prosthesis: Interfacing Stimulating Electrodes with Retinal Neurons to Restore Vision.* Front Neurosci, 2017. **11**: p. 620.
158. Damle, S., Y.H. Lo, and W.R. Freeman, *High Visual Acuity Retinal Prosthesis: Understanding Limitations and Advancements Toward Functional Prosthetic Vision.* Retina, 2017. **37**(8): p. 1423-1427.
159. Nanduri, D., et al., *Retinal prosthesis phosphene shape analysis.* Conf Proc IEEE Eng Med Biol Soc, 2008. **2008**: p. 1785-8.
160. Ang, G.S., et al., *Comparison of standard trabeculectomy versus microtrabeculectomy as a surgical treatment for glaucoma: a randomized clinical trial.* Clin Exp Ophthalmol, 2011. **39**(7): p. 648-57.
161. Rososinski, A., D. Wechsler, and J. Grigg, *Retrospective review of pars plana versus anterior chamber placement of Baerveldt glaucoma drainage device.* J Glaucoma, 2015. **24**(2): p. 95-9.
162. Mohammadi, S.F., et al., *Sheep practice eye for ophthalmic surgery training in skills laboratory.* Journal of Cataract & Refractive Surgery, 2011. **37**(6): p. 987-991.
163. Gow, B.S. and G.J. Suaning. *A method to assess the location and positional stability of supra-choroidal retinal neuroprostheses*. in *2016 38th Annual International Conference of the IEEE Engineering in Medicine and Biology Society (EMBC)*. 2016. p. 4723-4726 DOI: 10.1109/EMBC.2016.7591782.

164. Schindelin, J., et al., *Fiji: an open-source platform for biological-image analysis.* Nature Methods, 2012. **9**(7): p. 676-682.

165. Rueden, C.T., et al., *ImageJ2: ImageJ for the next generation of scientific image data.* BMC Bioinformatics, 2017. **18**(1): p. 529.

166. Schindelin, J., *Align Image by line ROI*, in *Fiji*. 2006: GitHub.

167. Eamegdool, S.S., et al., *Extracellular matrix and oxidative stress regulate human retinal pigment epithelium growth.* Free Radical Biology and Medicine, 2020. **146**: p. 357-371.

168. Mohan, S., et al., *Genetic Deletion of PGF(2α)-FP Receptor Exacerbates Brain Injury Following Experimental Intracerebral Hemorrhage.* Frontiers in neuroscience, 2018. **12**: p. 556-556.

169. Pradhan, S., et al., *Shiga Toxin Mediated Neurologic Changes in Murine Model of Disease.* Frontiers in Cellular and Infection Microbiology, 2016. **6**(114).

170. Kendall, M.G., *Rank correlation methods*. 1970, London: Griffin.

171. Pigatto, J.A.T., et al., *Intraocular pressure measurement in sheep using an applanation tonometer.* Revista Ceres, 2011. **58**: p. 685-689.

172. Ringvold, A., *Evidence that hypotony in retinal detachment is due to subretinal juxtapapillary fluid drainage.* Acta Ophthalmol (Copenh), 1980. **58**(4): p. 652-8.

173. Kucukerdonmez, C., et al., *Treatment of chronic ocular hypotony with intraocular application of sodium hyaluronate.* Br J Ophthalmol, 2009. **93**(2): p. 235-9.

174. Shinozaki, A., et al., *Relationship between distribution of tapetum fibrosum and retinal pigment epithelium in the sheep eye.* J Vet Med Sci, 2010. **72**(2): p. 211-5.

175. [Dataset] Eggenberger, S.C., et al., *Stability and biocompatibility of a Bionic Eye - Histology and immunohistochemistry data*. v2, 2021, http://dx.doi.org/10.17632/8rzc45vp77.2

176. Saunders, A.L., et al., *Development of a surgical procedure for implantation of a prototype suprachoroidal retinal prosthesis.* Clin Exp Ophthalmol, 2014. **42**(7): p. 665-74.

177. Lewis, G.P., et al., *The Ability of Rapid Retinal Reattachment to Stop or Reverse the Cellular and Molecular Events Initiated by Detachment.* Investigative Ophthalmology & Visual Science, 2002. **43**(7): p. 2412-2420.

178. Kuner, R., *Central mechanisms of pathological pain.* Nat Med, 2010. **16**(11): p. 1258-66.

179. Clutton, R.E., *An Anglocentric History of Anaesthetics and Analgesics in the Refinement of Animal Experiments.* Animals, 2020. **10**(10): p. 1933.

180. Kumar Mishra, R., *Intravenous or inhalational anesthetics?*, in *Essentials of Evidence-Based practice of Neuroanesthesia and Neurocritical Care*, H. Prabhakar, Editor. 2021, Elsevier Science publishing.

181. Beloeil, H., et al., *Balanced Opioid-free Anesthesia with Dexmedetomidine versus Balanced Anesthesia with Remifentanil for Major or Intermediate Noncardiac Surgery.* Anesthesiology, 2021. **134**(4): p. 541-551.

182. Shafford, H.L., et al., *The effect of diazepam on isoflurane-fentanyl minimum alveolar concentration (MAC) in the dog.* Vet Anaesth Analg, 2000. **27**(2): p. 102.

183. Robbins, S., *Premedication and Sedation Drugs*, in *Anesthesia for Veterinary Technicians*, S. Bryant, Editor. 2010, Wiley-Blackwell.

184. McMillan, M., *Checklists in veterinary anaesthesia: why bother?* The Veterinary Record, 2014. **175**(22): p. 556.

185. Percie du Sert, N., et al., *Reporting animal research: Explanation and elaboration for the ARRIVE guidelines 2.0.* PLoS Biol, 2020. **18**(7): p. e3000411.

186. Percie du Sert, N., et al., *The ARRIVE guidelines 2.0: Updated guidelines for reporting animal research.* PLoS Biol, 2020. **18**(7): p. e3000410.

187. Serfontein, L., *Awareness in cardiac anesthesia.* Current Opinion in Anesthesiology, 2010. **23**(1): p. 103-108.

188. Flecknell, P., *Anesthesia of animals for biomedical research.* British journal of anaesthesia, 1994. **71**: p. 885-94.

189. Navarro, K.L., et al., *Mouse Anesthesia: The Art and Science.* ILAR J, 2021.

190. Fudickar, A., et al., *The effect of the WHO Surgical Safety Checklist on complication rate and communication.* Dtsch Arztebl Int, 2012. **109**(42): p. 695-701.

191. Simpson, D.P., *Prolonged (12 hours) intravenous anesthesia in the rat.* Lab Anim Sci, 1997. **47**(5): p. 519-23.

192. Fuehrer, L., *Induction Drugs*, in *Anesthesia for Veterinary Technicians*, S. Bryant, Editor. 2010, Wiley-Blackwell.

193. Adediran, S., Adetunji, A, *Comparison of cardiorespiratory and anaesthetic effect of alfaxalone or propofol in dogs premedicated with acepromazine buprenorphine.* Bulgarian Journal of Veterinary Medicine, 2021.

194. Murrell, J.C., et al., *Changes in the EEG during castration in horses and ponies anaesthetized with halothane.* Veterinary Anaesthesia and Analgesia, 2003. **30**(3): p. 138-146.

195. Ilkiw, J.E., et al., *The Cardiovascular Sparing Effect of Fentanyl and Atropine, Administered to Enflurane Anesthetized Dogs.* Canadian Journal of Veterinary Research-Revue Canadienne De Recherche Veterinaire, 1994. **58**(4): p. 248-253.

196. Steinbacher, R.M. and R. Dörfelt. *Anaesthesia in dogs and cats with cardiac disease@ An impossible endeavour or a challenge with manageable risk ?* 2013.

197. Ohad, D.G. *Sedation and Anaesthesia for Pets with Cardiac Disease*. in *World Small Animal Veterinary Association World Congress*. 2014. Cape Town: Veterinary Information Network, Inc

198. Flecknell, P., *Laboratory Animal Anaesthesia*. 4th ed. 2015, Cambridge, Massachusetts: Academic Press.

199. Doufas, A.G., *Consequences of inadvertent perioperative hypothermia.* Best Pract Res Clin Anaesthesiol, 2003. **17**(4): p. 535-49.

200. Barriga-Rivera, A., et al., *Electrically evoked potentials in an ovine model for the evaluation of visual prosthesis efficacy.* Conf Proc IEEE Eng Med Biol Soc, 2015. **2015**: p. 3359-62.

201. Mandel, Y., et al., *Cortical responses elicited by photovoltaic subretinal prostheses exhibit similarities to visually evoked potentials.* Nature Communications, 2013. **4**.

202. Kumar, R., et al., *Comparative evaluation of propofol and ketamine total intravenous anaesthesia (TIVA) with dexmedetomidine and butorphanol in goats.* Indian Journal of Animal Sciences, 2018. **88**(6): p. 667-671.

203. Dzikiti, B.T., et al., *Total intravenous anaesthesia (TIVA) with propofol-fentanyl and propofol-midazolam combinations in spontaneously-breathing goats.* Veterinary Anaesthesia and Analgesia, 2010. **37**(6): p. 519-525.

204. Sarotti, D., R. Rabozzi, and P. Franci, *Impact evaluation of two different general anesthesia protocols (TIVA with propofol vs isoflurane) on the total number of interventions to treat cardiovascular depression or arousa/movement episodes in dogs undergoing orthopedic surgery receiving an intrathecal anesthesia.* Journal of Veterinary Medical Science, 2016. **78**(10): p. 1549-1555.

205. Liu, M., He, E., Fu, X., Gong, S., Han, Y., Deng, F., *Cerebral blood flow self-regulation in depression.* Journal of Affective Disorders, 2022. **302**: p. 324-331.

206. Silva, A. and L. Antunes, *Electroencephalogram-based anaesthetic depth monitoring in laboratory animals.* Laboratory Animals, 2012. **46**(2): p. 85-94.

207. Association of Veterinary Anaesthetist. *Anaesthetic Safety Checklist*. 2022 [cited 2022; Available from: https://ava.eu.com/resources/checklists/.

208. National Health and Medical Research Council (Australia), A.R.C., *Australian code for the care and use of animals for scientific purposes*. 8th edition. ed. 2013, Canberra, ACT: National Health and Medical Research Council.

209. Ezra-Elia, R., et al., *Flicker cone function in normal and day blind sheep: a large animal model for human achromatopsia caused by CNGA3 mutation.* Doc Ophthalmol, 2014. **129**(3): p. 141-50.

210. Ryu, S.B., et al., *Spatially confined responses of mouse visual cortex to intracortical magnetic stimulation from micro-coils.* Journal of Neural Engineering, 2020. **17**(5).

211. Russell, W.M.S. and R.L. Burch, *The principles of humane experimental technique*. 1959, London: Methuen.

212. Hodgkin, A.L. and A.F. Huxley, *A quantitative description of membrane current and its application to conduction and excitation in nerve.* The Journal of Physiology, 1952. **117**(4): p. 500-544.

213. Cowan, W.M., T.C. Südhof, and C.F. Stevens, *Synapses*. 2001, Baltimore: Johns Hopkins University Press.

214. Abbott, L.F. and W.G. Regehr, *Synaptic computation.* Nature, 2004. **431**(7010): p. 796-803.

215. Wang, F., *Axon Guidance: Building Pathways with Molecular Cues in Vertebrate Sensory Systems*, in *Encyclopedia of Neuroscience*, L.R. Squire, Editor. 2009, Academic Press: Oxford. p. 1073-1079.

216. McCulloch, D.L., et al., *ISCEV Standard for full-field clinical electroretinography (2015 update).* Documenta Ophthalmologica, 2015. **130**(1): p. 1-12.

217. Forshaw, T.R.J., et al., *Full-field electroretinography in age-related macular degeneration: an overall retinal response.* Acta Ophthalmologica, 2021. **99**(2): p. e253-e259.

218. Stronks, H.C., M.P. Barry, and G. Dagnelie, *Electrically evoked electroretinograms and pupil responses in Argus II retinal implant wearers.* Doc Ophthalmol, 2016. **132**(1): p. 1-15.

219. Baig-Silva, M.S., C.D. Hathcock, and J.R. Hetling, *A preparation for studying electrical stimulation of the retinain vivoin rat.* Journal of Neural Engineering, 2005. **2**(1): p. S29-S38.

220. Hetling, J.R., *Electrophysiology of Natural and Artificial Vision*, in *Artificial Sight: Basic Research, Biomedical Engineering, and Clinical Advances*, M.S. Humayun, et al., Editors. 2007, Springer New York: New York, NY. p. 355-380.

221. Shinozaki, A., et al., *Topography of ganglion cells and photoreceptors in the sheep retina.* Journal of Comparative Neurology, 2010. **518**(12): p. 2305-2315.

222. Dodds, C.W.D., et al. *Advancements in electrode design and laser techniques for fabricating micro-electrode arrays as part of a retinal prosthesis*. in *2011 Annual International Conference of the IEEE Engineering in Medicine and Biology Society*. 2011. p. 636-639 DOI: 10.1109/IEMBS.2011.6090141.

223. Doughty, M.J., *Consideration of growth (age)-related effects on globe size and corneal thickness in ovine eyes for use in laboratory studies.* Clinical and Experimental Optometry, 2017. **100**(4): p. 380-384.

224. Provis, J.M., C.M. Diaz, and B. Dreher, *Ontogeny of the primate fovea:a central issue in retinal development.* Progress in Neurobiology, 1998. **54**(5): p. 549-581.

225. Cavrep. *Sheep Breeds*. [cited 2021 04.06.2021]; Available from: http://www.cavrep.com.au/S/SHEEPBREEDS.html.

226. Powerin. *From Shepard Afshar, we know more about the pure breed of the sheep of Iran*. [cited 2021 04.06.2021]; Available from: http://powerinfeed.com/index.php/en/news/110-from-shepard-afshar,-we-know-more-about-the-pure-breed-of-the-sheep-of-iran.

227. Unknown. *Sheep Eye Dissection*. Available from: https://jb004.k12.sd.us/my%20website%20info/human%20anatomy/CHAPTER%2015/SHEEP%20EYE%20DISSECTION/SHEEP%20EYE%20PAGE%201.htm.

228. Green, R.A., et al., *Laser patterning of platinum electrodes for safe neurostimulation.* J Neural Eng, 2014. **11**(5): p. 056017.

229. Regnier, A., et al., *Clinical, electroretinographic and histomorphometric evaluation of the retina in sheep with natural scrapie.* BMC Vet Res, 2011. **7**: p. 25.

230. Sustar, M., et al., *ISCEV extended protocol for the photopic On–Off ERG.* Documenta Ophthalmologica, 2018. **136**(3): p. 199-206.

231. Fehmi, L.G. and A. Sundor, *The effects of electrode placement upon EEG biofeedback training: the monopolar-bipolar controversy.* International journal

of psychosomatics : official publication of the International Psychosomatics Institute, 1989. **36 1-4**: p. 23-33.

232. Ebrey, T. and Y. Koutalos, *Vertebrate Photoreceptors.* Progress in Retinal and Eye Research, 2001. **20**(1): p. 49-94.

233. Scott, R.N., L. McLean, and P.A. Parker, *Stimulus artefact in somatosensory evoked potential measurement.* Med Biol Eng Comput, 1997. **35**(3): p. 211-5.

234. Miller, C.A., P.J. Abbas, and C.J. Brown, *An Improved Method of Reducing Stimulus Artifact in the Electrically Evoked Whole-Nerve Potential.* Ear and Hearing, 2000. **21**(4): p. 280-290.

235. Zapf, M.P., et al., *Assistive peripheral phosphene arrays deliver advantages in obstacle avoidance in simulated end-stage retinitis pigmentosa: a virtual-reality study.* J Neural Eng, 2016. **13**(2): p. 026022.

236. Wilke, R.G., et al., *Electric crosstalk impairs spatial resolution of multi-electrode arrays in retinal implants.* J Neural Eng, 2011. **8**(4): p. 046016.

237. Khalili Moghadam, G., et al., *Quasi-monopolar stimulation: a novel electrode design configuration for performance optimization of a retinal neuroprosthesis.* PLoS One, 2013. **8**(8): p. e73130.

238. Khalili Moghaddam, G., et al., *Performance optimization of current focusing and virtual electrode strategies in retinal implants.* Comput Methods Programs Biomed, 2014. **117**(2): p. 334-42.

239. Dumm, G., et al., *Virtual electrodes by current steering in retinal prostheses.* Investigative Ophthalmology and Visual Science, 2014. **55**(12): p. 8077-8085.

240. Joarder, S.A., et al., *A continuum model of retinal electrical stimulation.* J Neural Eng, 2011. **8**(6): p. 066006.

241. Shen, Q., et al., *Magnetic resonance imaging of tissue and vascular layers in the cat retina.* Journal of Magnetic Resonance Imaging, 2006. **23**(4): p. 465-472.

242. Noh, G.M., et al., *Analysis of Changes in Retinal Photoreceptors Using Optical Coherence Tomography in a Feline Model of Iodoacetic Acid-induced Retinal Degeneration.* Korean J Ophthalmol, 2019. **33**(6): p. 547-556.

243. Moghaddam, G.K., et al. *Electrode design to optimize ganglion cell activation in a retinal neuroprosthesis: A modeling study*. in *2011 5th International IEEE/EMBS Conference on Neural Engineering*. 2011. p. 542-545 DOI: 10.1109/NER.2011.5910605.

244. Hughes, A., *A quantitative analysis of the cat retinal ganglion cell topography.* Journal of Comparative Neurology, 1975. **163**(1): p. 107-128.

245. Sargent, R.G., *Verification and validation of simulation models.* Journal of Simulation, 2013. **7**(1): p. 12-24.

246. Schuettler, M., et al., *Fabrication and test of a hermetic miniature implant package with 360 electrical feedthroughs.* Conf Proc IEEE Eng Med Biol Soc, 2010. **2010**: p. 1585-8.

247. Bian, P., Y. Wang, and T.J. McCarthy, *Rediscovering Silicones: The Anomalous Water Permeability of "Hydrophobic" PDMS Suggests Nanostructure and Applications in Water Purification and Anti-Icing.* Macromol Rapid Commun, 2021. **42**(5): p. e2000682.

248. Henle, C., et al. *Scaling limitations of laser-fabricated nerve electrode arrays*. in *2008 30th Annual International Conference of the IEEE Engineering in Medicine and Biology Society*. 2008. p. 4208-4211 DOI: 10.1109/IEMBS.2008.4650137.

249. Anderson, J.E., V. Markovac, and P.R. Troyk, *Polymer encapsulants for microelectronics: mechanisms for protection and failure.* IEEE Transactions on Components, Hybrids, and Manufacturing Technology, 1988. **11**(1): p. 152-158.

250. Donaldson, N., et al., *Apparatus to investigate the insulation impedance and accelerated life-testing of neural interfaces.* Journal of neural engineering, 2018. **15**(6): p. 066034-066034.

251. Boehler, C., et al., *Tutorial: guidelines for standardized performance tests for electrodes intended for neural interfaces and bioelectronics.* Nature Protocols, 2020. **15**(11): p. 3557-3578.

252. Faul, F., et al., *Statistical power analyses using G*Power 3.1: Tests for correlation and regression analyses.* Behavior Research Methods, 2009. **41**(4): p. 1149-1160.

253. Troyk, J.P., R. Francovik, and J.E. Anderson, *Experimental techniques for electrical testing of microelectronics coatings.* IEEE Transactions on Components, Hybrids, and Manufacturing Technology, 1991. **14**(2): p. 428-435.

254. Takmakov, P., et al., *Rapid evaluation of the durability of cortical neural implants using accelerated aging with reactive oxygen species.* Journal of neural engineering, 2015. **12**(2): p. 026003-026003.

255. Yue, L., et al., *Retina-electrode interface properties and vision restoration by two generations of retinal prostheses in one patient-one in each eye.* J Neural Eng, 2020. **17**(2): p. 026020.

256. Jung, L.H., et al., *Towards a chip scale neurostimulator: system architecture of a current-driven 98 channel neurostimulator via a two-wire interface.* Conf Proc IEEE Eng Med Biol Soc, 2011. **2011**: p. 6737-40.

257. Wilke, R., et al., *Spatial Resolution and Perception of Patterns Mediated by a Subretinal 16-Electrode Array in Patients Blinded by Hereditary Retinal Dystrophies.* Investigative Ophthalmology & Visual Science, 2011. **52**(8): p. 5995-6003.

258. Nishida, K., et al., *Electrophysiological evaluation of a chronically implanted electrode for suprachoroidal transretinal stimulation in rabbit eyes.* Journal of Artificial Organs, 2019. **22**(3): p. 237-245.

259. The British Standards Institution, *Biological evaluation of medical devices - Part 6: Tests for local effects after implantation* (Standard Number: BS EN ISO 10993-6:2016), BSI Standards Limited. 2016, www.bsigroup.com.

260. Nayagam, D.A.X., et al., *Techniques for Processing Eyes Implanted With a Retinal Prosthesis for Localized Histopathological Analysis.* JoVE, 2013(78): p. e50411.

261. Humayun, M.S., et al., *Pattern electrical stimulation of the human retina.* Vision Research, 1999. **39**(15): p. 2569-2576.

262. Custer, P.L. and C.E. Reistad, *Enucleation of blind, painful eyes.* Ophthalmic Plast Reconstr Surg, 2000. **16**(5): p. 326-9.

263. Chan, A.-W., et al., *SPIRIT 2013 Statement: Defining Standard Protocol Items for Clinical Trials.* Annals of Internal Medicine, 2013. **158**(3): p. 200-207.

264. Chan, A.-W., et al., *SPIRIT 2013 explanation and elaboration: guidance for protocols of clinical trials.* BMJ : British Medical Journal, 2013. **346**: p. e7586.

265. National Cancer Institute, *Common terminology criteria for adverse events (CTCAE)*. Vol. 5.0. 2017, [Bethesda, Md.]: U.S. Dept. of Health and Human Services, National Institutes of Health, National Cancer Institute.

266. Green, R.A., et al., *Cytotoxicity of implantable microelectrode arrays produced by laser micromachining.* Biomaterials, 2010. **31**(5): p. 886-893.

267. Perentos, N., et al., *Techniques for chronic monitoring of brain activity in freely moving sheep using wireless EEG recording.* Journal of Neuroscience Methods, 2017. **279**: p. 87-100.

268. Arden, G.B., et al., *Gold Foil Electrode - Extending the Horizons for Clinical Electroretinography.* Investigative Ophthalmology & Visual Science, 1979. **18**(4): p. 421-426.

269. McAllan, A., J. Sinn, and G.W. Aylward, *The effect of gold foil electrode position on the electroretinogram in human subjects.* Vision Res, 1989. **29**(9): p. 1085-7.

270. Szabó-Salfay, O., et al., *The electroretinogram and visual evoked potential of freely moving rats.* Brain Research Bulletin, 2001. **56**(1): p. 7-14.

271. Gélisse, P., et al., *How to carry out and interpret EEG recordings in COVID-19 patients in ICU?* Clin Neurophysiol, 2020. **131**(8): p. 2023-2031.

272. James, F.M., et al., *Investigation of the use of three electroencephalographic electrodes for long-term electroencephalographic recording in awake and sedated dogs.* Am J Vet Res, 2011. **72**(3): p. 384-90.

12 APPENDICES

APPENDIX 1 SURGICAL SAFETY AND BIOCOMPATIBILITY: IMMUNOHISTOCHEMISTRY

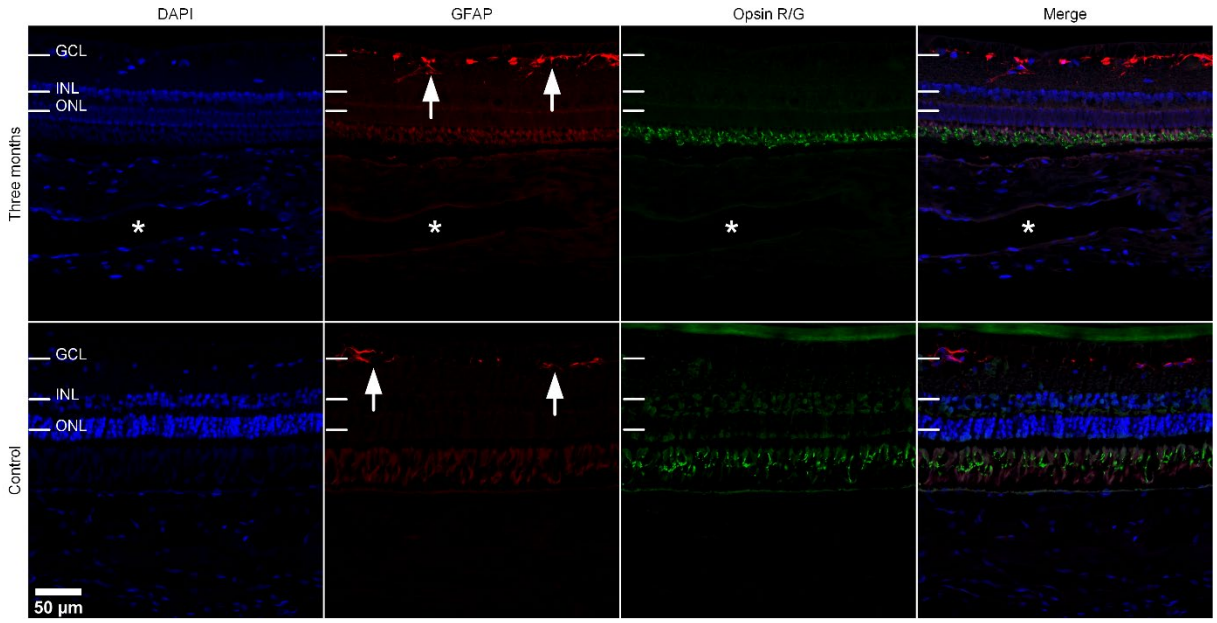

Appendix Figure 1 GFAP and Opsin R/G immunofluorescence. 3M#2 left (three months) and 3M#2 right eye (control). Up arrows indicate retinal astrocytes.

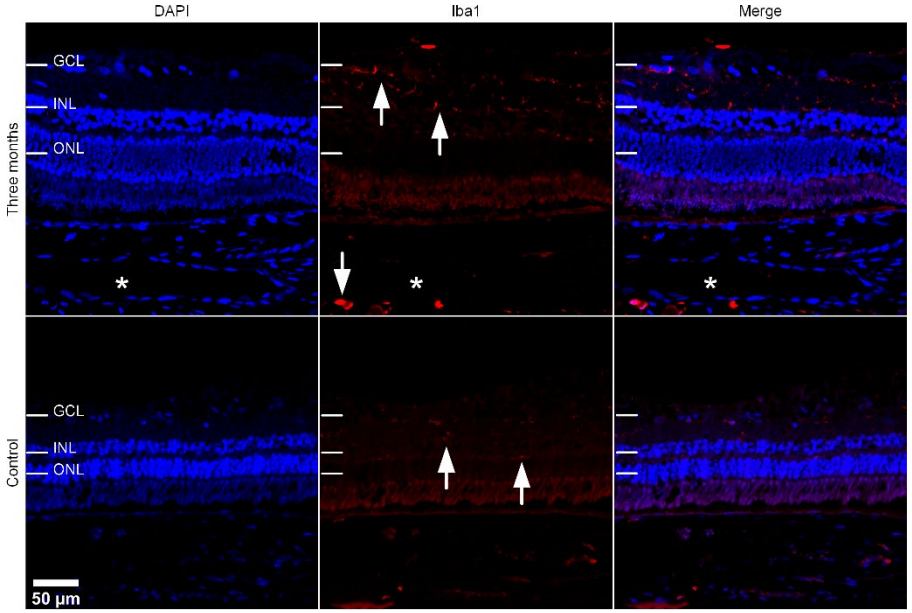

Appendix Figure 2 Iba1 immunofluorescence. 3M#2 left (three months) and 3M#2 right eye (control). Up arrows indicate retinal microglia and down arrow indicates a choroidal macrophage.

Supplementary Table A ImageScope Positive Pixel Count parameters

Hue Value	Hue Width	Colour Saturation Threshold	Intensity Threshold of Weak Positive Pixels upper limit Iwp	Intensity Threshold of Positive Pixels upper limit Ip	Intensity Threshold of Strong Positive Pixels upper limit Isp (high)	Intensity Threshold of Strong Positive Pixels lower limit Isp (low)	Intensity Threshold of Negative Pixels upper limit Inp
0	0.4	0.25	160	140	120	0	-1

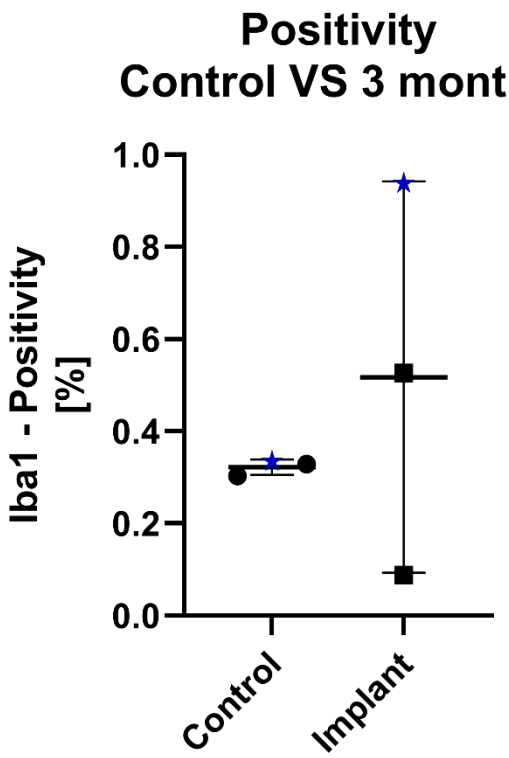

Appendix Figure 3 Iba1 Positivity in the retina – percentage of number of positive pixels to the number of positive and negative pixels counted using the ImageScope™ Positive Pixel Count algorithm – used as a measure of the Iba1+ macrophages/microglia (six eyes from 5 sheep). The mean value for each group is shown and error bars show the standard deviation (control: 0.3221 % ± 0.01681, three months: 0.5174 % ± 0.4249, mean ± standard deviation). The blue stars highlight the right (control) and left (3-months implant) eyes of animal 3M#2. The other measurements were obtained from four independent animals (controls N=2 and implant N=2). The positivity values for both eyes of 3M#2 are significantly different. Nonetheless, the Iba1 positive cells did not infiltrate the outer nuclear layer and there was no significant impact on the retinal anatomy. Note the comparatively large standard deviation in the 3-months group compared to the control group.

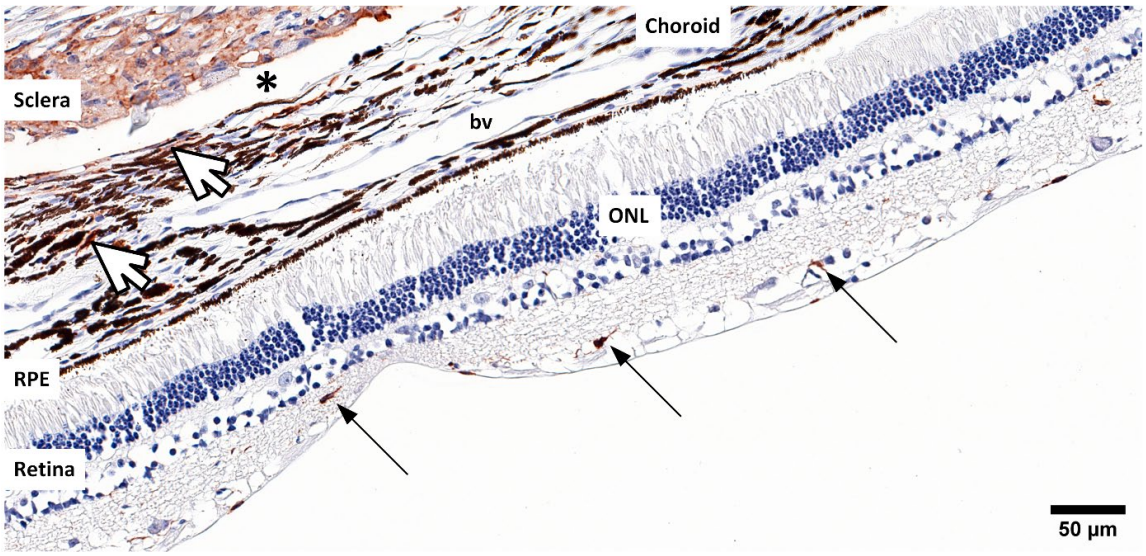

Appendix Figure 4 Representative micrograph showing a cross-section of the sclera, choroid, and retina in the region of the suprachoroidal implant (* indicates location of implant, removed before paraffin embedding). Iba1+ cells were visualised with immunoperoxidase (VectorRed chromogen, haematoxylin counterstain). In the retina, sparse Iba1+ cells in the inner retina ganglion cell layer/nerve fibre layer can be seen (black arrows); cells were not observed in outer retinal layers. Within the choroid, Iba1+ cells (white arrows) and numerous black/brown melanocytes (black-brown) were seen more often in the outer choroid, adjacent to the suprachoroidal space. (bv blood vessel; ONL outer retinal layer; RPE retinal pigment epithelium). ***A high-resolution version of this slide for use with the Virtual Microscope is available as eSlide: VM06308.***

APPENDIX 2 SURGICAL SAFETY AND BIOCOMPATIBILITY: DATA PAPER

Published in Open Access as:

Samuel C. Eggenberger, et al., *Safety and biocompatibility of a bionic eye: Imaging, intraocular pressure, and histology data*, Data in Brief, Volume 39, 2021, 107634, ISSN 2352-3409, https://doi.org/10.1016/j.dib.2021.107634.

Data in Brief 39 (2021) 107634

Contents lists available at ScienceDirect

Data in Brief

journal homepage: www.elsevier.com/locate/dib

Data Article

Safety and biocompatibility of a bionic eye: Imaging, intraocular pressure, and histology data

Samuel C. Eggenberger[a,*], Natalie L. James[b], Cherry Ho[b], Steven S. Eamegdool[c], Veronika Tatarinoff[b], Naomi A. Craig[b], Barry S. Gow[b], Susan Wan[d], Christopher W.D. Dodds[b], Donna La Hood[e,f], Aaron Gilmour[a,b], Shannon L. Donahoe[g], Mark Krockenberger[g], Krishna Tumuluri[c,h,i], Melville J. da Cruz[j,k], John R. Grigg[c,k], Peter McCluskey[c,k], Nigel H. Lovell[b], Michele C. Madigan[c,f], Adrian T. Fung[c,h,i], Gregg J. Suaning[a,b,*]

[a] School of Biomedical Engineering, Faculty of Engineering, University of Sydney, Sydney, Australia
[b] Graduate School of Biomedical Engineering, University of New South Wales (UNSW), Sydney, Australia
[c] Save Sight Institute, The University of Sydney, Specialty of Clinical Ophthalmology and Eye Health, Faculty of Medicine and Health
[d] The Westmead Institute for medical research, Westmead, Australia
[e] Brien Holden Vision Institute, Sydney, Australia
[f] School of Optometry and Vision Science, University of New South Wales (UNSW), Sydney, Australia
[g] Veterinary Pathology Diagnostic Services, Sydney School of Veterinary Science, University of Sydney, Sydney, Australia
[h] Westmead Clinical School, Specialty of Clinical Ophthalmology and Eye Health, Faculty of Medicine and Health, University of Sydney, Sydney, Australia
[i] Department of Ophthalmology, Faculty of Medicine and Health Sciences, Macquarie University, Sydney, Australia
[j] Department of Otolaryngology, Westmead Hospital, University of Sydney, Sydney, Australia
[k] Faculty of Medicine and Health, University of Sydney, Sydney, Australia

DOI of original article: 10.1016/j.biomaterials.2021.121191
* Corresponding authors.
E-mail addresses: samuel.eggenberger@sydney.edu.au (S.C. Eggenberger), gregg.suaning@sydney.edu.au (G.J. Suaning).

https://doi.org/10.1016/j.dib.2021.107634

ARTICLE INFO

Article history:
Received 25 October 2021
Revised 11 November 2021
Accepted 22 November 2021
Available online 26 November 2021

Keywords:
Visual prosthesis
Intraocular pressure
Opthalmoscopy
Biocompatibility
Histopathology
Retina

ABSTRACT

The data presented here are related and supplementary data to the research article "Implantation and long-term assessment of the stability and biocompatibility of a novel 98 channel suprachoroidal visual prosthesis in sheep" [1]. In Eggenberger et al., nine sheep of the Suffolk (N=2) and Dorper (N=7) breeds were implanted in the left eye with an electrically inactive, suprachoroidal retinal stimulator (Bionic Eye) for durations of up to 100 days. The surgical safety, implant stability and device biocompatibility were assessed. Intraocular pressure measurements, indirect and infrared ophthalmoscopy and optical coherence tomography were performed at fixed time points to evaluate the clinical effects of the surgery and device implantation. Post-mortem eye tissue collection and histology was performed to measure the effects of the intervention at the cellular level. The data, including a comprehensive collection of fundus, infrared, optical coherence tomography and histology images can be used as a reference for comparison with other research, for example, active retinal stimulators. Furthermore, these data can be used to evaluate the suitability of the sheep model, in particular Dorper sheep, for future research.

Specifications Table

Subject	Biomedical Engineering
Specific subject area	Intraocular pressure, clinical imaging, and histology: long-term effects of retinal implants in sheep
Type of data	Table Image Graph Figure
How data were acquired	Intraocular pressure: TonoVet rebound tonometer, Icare Oy, Helsinki, Finland, GraphPad Prism version 8.4.3 for Windows (GraphPad Software, San Diego, California USA) Indirect ophthalmoscopy: Super Quad 160 lens (Volk, Mentor OH, USA), video camera (Galaxy S3, Samsung, Seoul, South-Korea or XR500, Sony, Tokyo, Japan), OPMI operating microscope (Zeiss, Oberkochen, Germany), VLC Media Player software (Free Software Foundation, Inc., Boston, USA) Infrared fundus imaging: Wangiscope (Custom device as described in [2]), VLC Media Player software (Free Software Foundation, Inc., Boston, USA) Optical coherence tomography: Envisu 2300 system (BiOptigen, Morrisvile NC, USA) Histology: Aperio Versa 1.0.4, Leica Biosystems, Nussloch, Germany, ImageScope™ version 12.4.0.5043 (Leica Biosystems, Nussloch, Germany) Fluorescence immunohistochemistry: LSM 700 Meta Confocal microscope system and ZEN Blue software, Carl Zeiss, Germany. Iba1 immunoperoxidase and quantitative analysis: Aperio Versa 1.0.4, Leica Biosystems, Nussloch, Germany, ImageScope™ version 12.4.0.5043 (Leica Biosystems, Nussloch, Germany)
Data format	Raw Analysed Filtered
Parameters for data collection	Intraocular pressure was measured in awake sheep. Ophthalmoscopy and optical coherence tomography were performed in anaesthetised animals. Histology and immunohistochemistry was performed after fixing and paraffin embedding the tissues.
Description of data collection	Nine sheep were implanted with a suprachoroidal visual prosthesis comprising of a platinum-silicone electrode array. The animals were implanted for durations of between two days and three months.
Data source location	Institution: Graduate School of Biomedical Engineering, University of New South Wales City/Town/Region: Sydney, New South Wales Country: Australia
Data accessibility	Repository name: Mendeley Data Data identification number: Intraocular pressure, ophthalmoscopy, optical coherence tomography: DOI 10.17632/9hnz6c99py.2 Histology: DOI 10.17632/8rzc45vp77.2 Direct URL to data: Intraocular pressure, ophthalmoscopy, optical coherence tomography: http://dx.doi.org/10.17632/9hnz6c99py.2 Histology and immunohistochemistry: http://dx.doi.org/10.17632/8rzc45vp77.2
Related research article	Samuel C. Eggenberger, Natalie L. James, Cherry Ho, Steven S. Eamegdool, Veronika Tatarinoff, Naomi A. Craig, Barry S. Gow, Susan Wan, Christopher W.D. Dodds, Donna La Hood, Aaron Gilmour, Shannon L. Donahoe, Mark Krockenberger, Krishna Tumuluri, Melville J. da Cruz, John R. Grigg, Peter McCluskey, Nigel H. Lovell, Michele C. Madigan, Adrian T. Fung, Gregg J. Suaning Implantation and long-term assessment of the stability and biocompatibility of a novel 98 channel suprachoroidal visual prosthesis in sheep Biomaterials, Volume 279, 2021, 121191, ISSN 0142-9612 https://doi.org/10.1016/j.biomaterials.2021.121191. [1]

Value of the Data

- The sheep (*ovis aries*) is a promising model for eye surgery and visual neuroscience, due to the similarities in size and shape with the human ocular anatomy [3]. The extensive dataset can be used as a reference for research involving retinal and suprachoroidal devices or to evaluate the adequacy of the ovine model for future research, therefore helping to reduce the numbers of animals used for research purposes.
- Researchers developing and studying retinal implants, in particular devices positioned in the suprachoroidal space can benefit from the data by using it as reference. Other researchers in the field of ophthalmology can use the data to evaluate the adequacy of the ovine model for their research.
- The dataset establishes a reference to which research involving surgical interventions on the eye and/or implantation of devices can be compared.

1. Data Description

Note: Animals were identified according to the experimental group to which they were assigned (duration of experiment 2 days, 1 month, 2 months and 3 months). For instance, 2D#1 was the first animal in the group implanted for a duration of 2 Days. 3M#3 was the third animal in the group implanted for 3 Months. 2D#1 and 1M#1 were of the Suffolk Breed. All other animals were of the Dorper breed.

1.1. Intraocular pressure (IOP)

Fig. 1 shows the preoperative intraocular pressure (IOP) values for both eyes of four sheep. For each eye, multiple consecutive measurements were averaged together. A paired Student's t-test showed no statistical difference between the left and right eyes (P=0.0837). The average preoperative IOP in both eyes for this cohort was 16.8 ± 2.4 mmHg (mean ± SD), which is similar to reported values (16.36 ± 2.19 mmHg) [4].

Fig. 2 shows the changes in IOP in both eyes for seven animals implanted in the left eye for two days, one month, two months or three months respectively. When available, the pre-

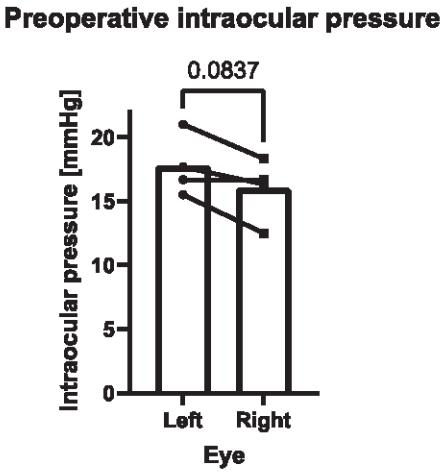

Fig. 1. Left and right eyes baseline (preoperative) intraocular pressure for four sheep. There was no significant difference between the left and right eyes (paired Student's t-test, P=0.0837).

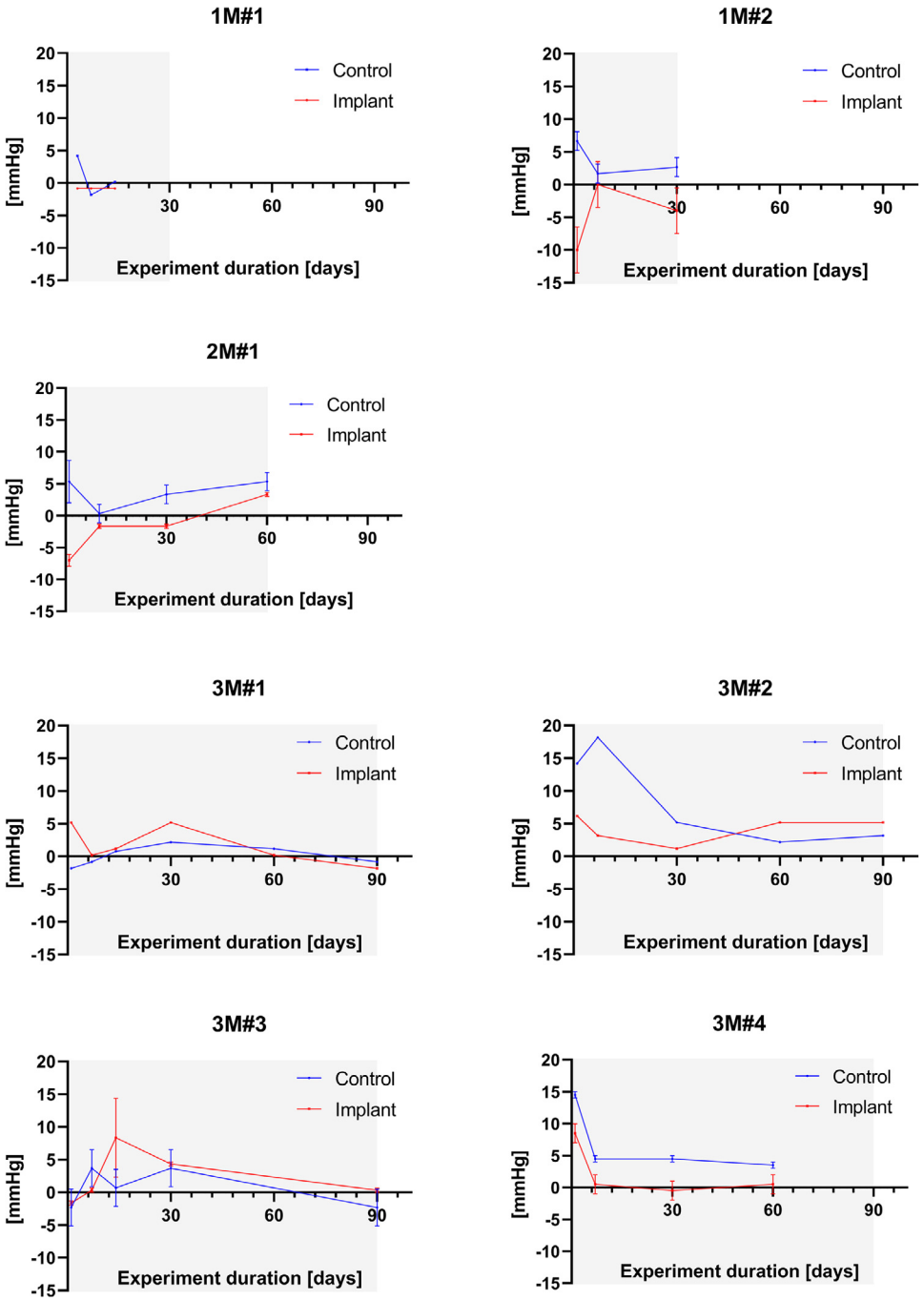

Fig. 2. Changes in IOP compared to baseline for seven animals. For 1M#1, 3M#1 and 3M #2, where no baseline value was available, the average baseline value from all other eyes in the study (16.8 mmHg) was used. Grey areas represent the experiment duration, allowing all plots to be displayed with the same horizontal axis. Error bars represent the standard error of the mean (SEM) where multiple values were obtained on the same day.

operative baseline for each eye was subtracted from the post-operative values. In three animals (1M#1, 3M#1, and 3M #2), no baseline was available. In these cases, the preoperative baseline of the other eight (right and left) eyes were averaged together and used as baseline substitute (16.8 mmHg). Variations to baseline were plotted against time over the duration of the trials.

The data shows that postoperative variations occurred in both eyes after surgery, mostly within the first seven days after surgery. The average day 1 absolute variation from baseline was 6.4 ± 2.9 mmHg (mean ± SD) for the operated eye and 7.6 ± 5.5 mmHg for the contralateral eye. Three operated eyes increased, two decreased and one remained stable (pressure difference ≤ 2 mmHg) while five and one non-operated eyes increased and decreased, respectively.

The whole dataset is available as supplementary data in [5].

1.2. Ophthalmoscopy – colour and infrared fundus images (raw and aligned data)

Colour, fundus images for nine sheep of the Dorper breed are presented in [5]. Images present the appearance of the retinas and blood vessels before and after a silicone-platinum electrode array was positioned into the suprachoroidal space, in individual eyes. The rotated and cropped image stacks provide direct comparison between time points. The data provides an overview of the surgery-related changes to the retinal appearance, including transient, localized reflectivity changes at the edges of the array allowing for identification of its position.

Postoperative infrared images obtained from the same cohort and presented in [5] provide further information on the location of the electrode array in the suprachoroidal space. Using blood vessels as landmarks, the device position can be tracked over time in each animal. The same landmarks can be used to combine images from multiple imaging modalities, such as indirect ophthalmoscopy. Thus, permitting electrode array position visualisation in images where this information is missing.

1.3. Optical coherence tomography (OCT)

Preoperative and postoperative optical coherence tomography (OCT) rasters for four sheep of the Dorper breed are presented [5]. These images show the retinal layers and compare the retinal anatomy before and after device positioning in the suprachoroidal space. The different scales between the scan depth and scan position accentuate the stepped appearance of the retina at the array edges. In some images, the individual 600 µm platinum electrodes of the array are visible in the suprachoroidal space. Data is unavailable for 3M#3 at two and three months, and for 3M#4 at three months due to technical difficulties. All images are available as supplementary material in [5].

1.4. Histology – raw images

Hematoxylin and eosin (H&E) stained slides of the sheep retina, choroid, and sclera are presented here. Five eyes had an electrode array surgically implanted in the suprachoroidal space for one (N=1), two (N=2), and three months (N=3). Control scans of the contralateral eyes are also presented (N=3). The microscopic images show the retinal layers, choroid and sclera as well as the host response to the foreign body (fibrosis and inflammation). The devices were removed prior to embedding and sectioning and the pocket vacated by the electrode array is clearly visible for all implant durations. The collection of micrographs allows comparison of the effects of the intervention and presence of the device between animals and implant durations, and between control sheep retinas obtained from the same animals.

The data shows segments of detached retina. Hypertrophied retinal pigmented epithelium (RPE) can be used to differentiate *in vivo* detachments from artefactual detachments secondary

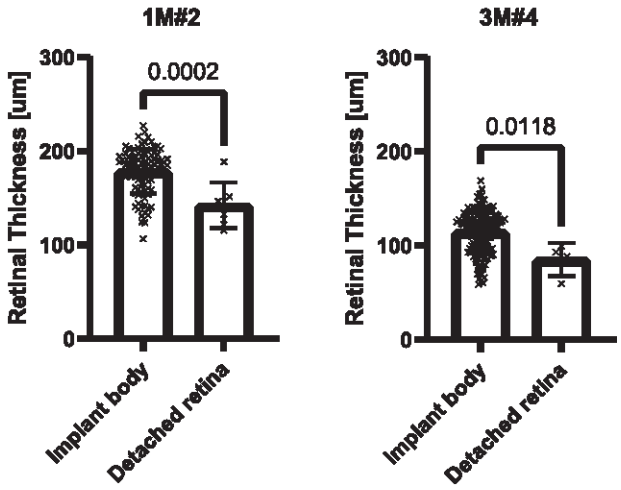

Fig. 3. Retinal thickness over segments of detached retina. Scatter plots with bar showing mean and standard deviation for the implanted eye of two animals. Significant thinning of the detached retinal segments was observed in both cases (P=0.0002 and P=0.0118).

Table 1
Mean retinal thickness values and standard deviation for detached segments and over the body of the implant.

	Retinal thickness Implant body		Detached segments	
Animal ID	Mean	SD	Mean	SD
1M#2	178.6	23.82	142.3	24.11
3M#4	114.5	22.83	85.15	17.6

to tissue processing. When present, device and/or surgery-related thinning and remodelling of the retina is visible in the scanned slides. The data shows the host response to the surgery and the silicone-platinum electrode array.

The micrographs are available as supplementary material in [6].

1.5. Histology - retinal thickness

Fig. 3 shows the measured total thickness of the sheep retina in two animals in which non-artefactual detachments were visible. In both cases, the detached retinal segments were significantly thinner (than the retina located above the implant body; two-tailed Student's t-test, P=0.002 and P=0.0118 respectively). Table 1 summarizes the average thicknesses and standard deviations for the two sheep.

Fig. 4 compares the retinal thickness measured over the implant body and the thickness measured adjacent to the edges of the electrode arrays. The difference was not significant in 3M#3 and 3M#4, P=0.3243 and P=0.0873, respectively). The retinas were significantly thinner adjacent to the device edges in three cases (3/5). Average retinal thicknesses, standard deviations and p-values are summarized in Table 2.

Samples were collected at variable distances from the *area centralis*, sometimes at the transition from visual to non-visual retina. Raw data is available as supplementary material in [6].

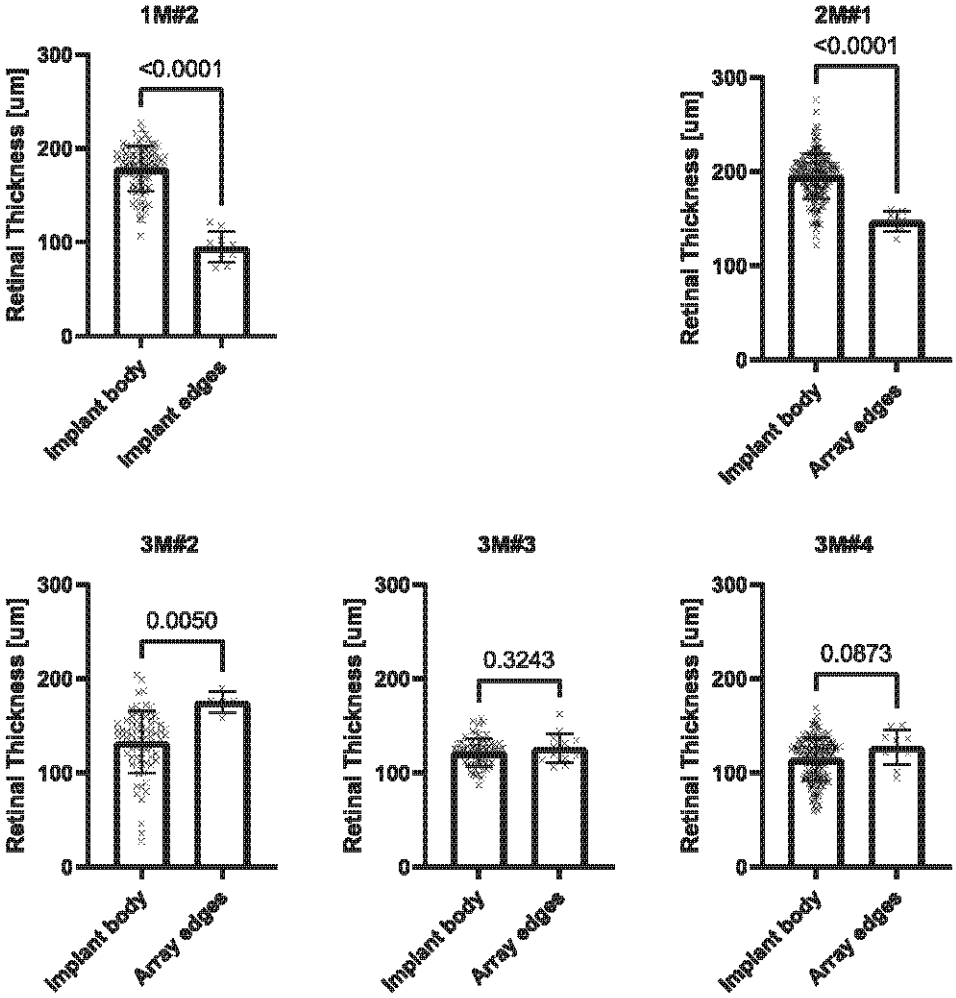

Fig. 4. Comparison of the retinal thickness measured over the implant body and the thickness measured adjacent to the edges of the electrode arrays. The difference was significant in 1M#2, 2M#1, and 3M#2.

Table 2
Retinal thickness values over the body of the implant and at the implant edges. P-values showing significant thinning in the retina close to the implant edges and calculated using an unpaired Student's t-test are shown.

	Retinal thickness [µm]				
Animal	Implant body		Implant edges		
ID	Mean	SD	Mean	SD	P
1M#2	178.6	23.82	94.73	16.42	<0.0001
2M#1	195.2	23.86	147.4	10.68	<0.0001
3M#2	132.3	32.99	175.3	11.05	0.005
3M#3	121.8	14.77	126.1	15.09	0.3243
3M#4	114.5	22.83	127.2	18.66	0.0873

1.6. Immunohistochemistry

The data present a collection of fluorescence micrographs obtained from sheep implanted for zero (control), one, two and three months with a suprachoroidal visual prosthesis. A combination of GFAP and LM-opsin immunostaining allow for the assessment of Muller glia activation and effects on the photoreceptor layer. Iba1 immunostaining allows for visualisation of the macrophage/microglia cells.

All fluorescence micrographs were imaged using confocal microscopy and are available as supplementary data in [6].

The data also present a collection of Iba1 immunoperoxidase micrographs for three control eyes and three eyes implanted for three months, as well as their corresponding negative controls. Quantitative analysis was performed using the Aperio ImageScope "Positive Pixel Count" algorithm on the retinas [7, 8]. The regions of interest were manually defined around the retinas. All micrographs and algorithm outputs are available as supplementary data in [6], including but not limited to the 'Positivity' (ratio of the number of Iba1-positive pixels to the total number of negative and positive pixels in the region of interest).

2. Experimental Design, Materials and Methods

2.1. Intraocular pressure

Preoperative intraocular pressure (IOP) was measured in four sheep (ovis aries) of the Dorper breed. Postoperative IOP measurements were obtained in seven animals (Suffolk breed N=1, Dorper breed N=6) on day one,

Intraocular pressure (IOP) measurements were made using a TonoVet rebound tonometer (Icare Oy, Helsinki, Finland), in the holding pen and without anaesthesia. Preoperative IOP was measured after the acclimatisation period in the animal facilities (Graduate School of Biomedical Engineering (GSBmE), UNSW Sydney, Australia) and at least two days prior to surgery. Individual baseline IOP was calculated, for each eye, as the mean of two readings for one animal or three measurements for a further three sheep. IOP values were obtained on days 1 and 7 post-surgery, then on days 30, 60 and 90, where applicable. One IOP value was obtained at day 3 instead of day 1 after surgery. One measurement was performed on day 10 instead of 7 because of a secondary surgical intervention. Similarly, no IOP values were obtained from 3M#3 at the two-month mark because of a secondary surgery. The 30-, and 90-day IOP measurements were not available on the last experimental day for 1M#1 and 3M#4, respectively. Additional measurements at 14 days were made in a subset of the cohort (N=3). Whenever possible, six successive readings were obtained, according to the device's mode of operation. The mean of consecutive measurements was used whenever sufficient consecutive values could not be obtained.

IOP values were recorded in GraphPad Prism version 8.4.3 for Windows (GraphPad Software, San Diego, California USA). Whenever multiple preoperative measurements were available for a single eye, these were averaged to obtain the IOP baseline for that eye. An unpaired, two-tailed Student's t-test was performed in GraphPad to compare the average IOP in the left and right eyes. Individual baselines were averaged together to serve as reference for the other eyes. IOP baseline values were subtracted from the postoperative measurements and plotted versus time.

2.2. Ophthalmoscopy – colour and infrared fundus images (raw and aligned data)

Indirect ophthalmoscopy was used to obtain colour fundus images before and after implantation of a suprachoroidal visual prosthesis in anaesthetised animals. The data was obtained as video files using a Super Quad 160 lens (Volk, Mentor OH, USA) and video camera (Galaxy S3, Samsung, Seoul, South-Korea or XR500, Sony, Tokyo, Japan), passed through the optics of

an OPMI operating microscope (Zeiss, Oberkochen, Germany). Infrared fundus imaging was performed postoperatively using a technique described in [2] and recorded as video files.

All video files were visualised frame by frame after deinterlacing (automatic) using VLC Media Player software (Free Software Foundation, Inc., Boston, USA). Visibility of the region of interest (whenever possible, centred around the location of the electrode array) and image focus were used as criteria to select the most representative frames. For each imaging technique and each eye (indirect ophthalmoscopy or infrared imaging), blood vessels visible in all images were identified and used as landmarks to rotate and scale the data in Fiji [9, 10] and using the "align image by line ROI" plug-in [11]. The resulting stacks were then cropped to the region of interest.

Both techniques were applied to obtain images directly after surgery and then monthly until the animal was sacrificed (up to three months). Additionally, preoperative colour fundus images were acquired as baseline.

2.3. Optical coherence tomography (OCT)

OCT imaging was performed in anaesthetised animals with an Envisu 2300 system (BiOptigen, Morrisvile NC, USA). Images were obtained from four sheep of the Dorper Breed before device implantation, directly postoperatively and then at the one-, two and three-month mark.

2.4. Histology and retinal thickness

Tissue was fixed and processed according to the methods described in the co-publication [1]. Micrographs were digitised using an Aperio Versa 1.0.4 (Leica Biosystems, Nussloch, Germany) slide scanner and viewed in ImageScope™ version 12.4.0.5043 (Leica Biosystems, Nussloch, Germany). All retinal detachments were identified visually. Artefactual detachments, characterised by non-hypertrophied retinal pigmented epithelium, were excluded. Retinal thickness measurements were performed by placing markers every 200 µm along the retinal pigmented epithelium and then measuring the thickness perpendicular to the retina with the ruler tool. The location of the implant edges was identified visually (location of the pocket left by the electrode array, which was removed prior to embedding and sectioning). Tissue located 600 µm on either side of end the pocket was categorized as "adjacent to the device edge". In instances where the retinal layers were separated due to processing artefacts, the ruler tool was used to measure each segment separately. The corresponding sub-layer thicknesses were then added to obtain the local total retinal thickness. Values were compiled in MS Excel (Microsoft Corporation, Redmond, Washington, USA) and analysed in GraphPad Prism version 8.4.3 for Windows (GraphPad Software, San Diego, California USA). When multiple slides were available for a single eye, all thickness values from the slides were combined into one dataset prior to analysis.

Mean thickness and standard deviation were calculated for each eye and each type of segment (body of the implant, implant edges and detached retina). Two-tailed, unpaired Student's t-tests were performed for each eye (where data was available) to compare the mean thickness over the implant body and one of the regions of interest (implant edge or detached retina). The test's assumptions (approximately normal distributions of the continuous dependent variables, the absence of outliers and independence between the observations) were considered fulfilled despite the low number of samples obtained from the regions of interests (due to their small size).

2.5. Fluorescence immunohistochemistry

Tissues were fixed and processed, and paraffin sections cut, according to the methods described in the co-publication [1]. Briefly, sections were incubated with primary antibodies:

GFAP-Cy3 conjugate (mouse IgG; 1:800); opsin-red/green (opsin R/G) (rabbit IgG; 1:500, 1:1000) (Merck Millipore) and Iba1 (goat IgG; 1:200) (Abcam, USA). Immune complexes were detected with secondary antibodies to goat IgG, mouse IgG, or rabbit IgG, conjugated with Alexa-Fluor 488, 555, or 647 (Invitrogen, USA). Nuclei were counterstained with Hoechst 33258 (1:10,000) prior to mounting in glycerol:PBS (80:20). Representative regions of the slides were captured using an LSM 700 Meta Confocal microscope system and ZEN Blue software (Carl Zeiss, Germany). The images were then assembled in Photoshop CS software (Adobe Corporation, USA).

2.6. Iba1 immunoperoxidase and quantitative analysis

Tissues were fixed and processed, and paraffin sections cut, according to the methods described in the co-publication [1]. Briefly, 4um sections were heat antigen retrieved in high pH buffer (Target Retrieval Solution, S2367, DAKO®). The following steps were performed with DAKO® Link Autostainer: blocking (Bloxall, SP6000, VectorLabs®), primary antibody (macrophage/microglia, clone Iba1, BioCare Medical®, rabbit polyclonal, 1:200), secondary (Envision K5007, DAKO®), chromogen ImmPACT Nova Red (SK4805, Vector Labs®), counterstained in haematoxylin (Whitlocks, VPDS Histo Lab Manual©, 2021), cleared and mounted. Primary antibody was omitted in the negative controls. Sections were scanned (40x magnification) with Aperio Versa (Leica Biosystems®, UK).

Retinas were manually outlined using the Pen Tool in ImageScope™. The retinal pigmented epithelium was carefully avoided to prevent melanin-related false positives. The following algorithm parameters were used: hue value = 0, hue width = 0.4, colour saturation threshold = 0.25, intensity threshold of weak positive pixels upper limit = 160, intensity threshold of positive pixels upper limit = 140, intensity threshold of strong positive pixels upper limit = 120, intensity threshold of strong positive pixels lower limit = 0, intensity threshold of negative pixels upper limit = -1.

Declaration of Competing Interest

The authors declare the following financial interests/personal relationships which may be considered as potential competing interests: Gregg Suaning reports financial support was provided by NH&MRC. Gregg Suaning has patent issued to New South Innovations.

Ethics Statement

The procedures for this study were approved by the Animal Care and Ethics Committee (ACEC) of UNSW Sydney (protocol number 14/155B) and were conducted in accordance with the Australian Code for the Care and Use of Animals for Experimental Purposes 8th edition (2013) and the ARVO standards for use of animals in ophthalmic research.

CRediT Author Statement

Samuel C. Eggenberger: Methodology, Formal analysis, Data curation, Writing – Original draft, Visualization **Adrian Fung:** Conceptualisation, Investigation, Methodology, **Cherry Ho:** Methodology, Investigation, Formal analysis, Data curation **Veronika Tatarinoff:** Methodology, Investigation, Resources, Supervision **Natalie L. James:** Conceptualisation, Investigation, Methodology, Project administration, Resources **Susan Wan:** Investigation **Steven Eamegdool:** Methodology, Investigation, Resources **Chris Dodds:** Methodology, Investigation, Resources **Donna la Hood:** Methodology, Investigation **Aaron Gilmour:** Investigation, Resources **Peter McCluskey:**

Visualisation, Supervision, Project administration **Shannon Donahoe:** Formal analysis, Investigation **Mark Krockenberger:** Formal analysis, Investigation **John R Grigg:** Conceptualisation, Methodology **Barry S. Gow:** Investigation, Validation, Resources, Methodology **Naomi A. Craig:** Investigation, Resources **Krishna Tumuluri:** Conceptualization, Methodology **Melville J. da Cruz:** Methodology, Investigation, Funding acquisition **Nigel H. Lovell:** Conceptualization, Methodology, Validation, Investigation, Resources, Supervision, Project administration, Funding acquisition **Michele C. Madigan:** Resources, Formal analysis, Writing – Review and editing **Gregg J. Suaning:** Conceptualization, Methodology, Investigation, Resources, Writing – Review and editing, Supervision, Project administration, Funding acquisition.

Acknowledgments

This research was supported by the Australian Research Council (ARC) through its Special Research Initiative (SRI) in Bionic Vision Science and Technology grant to Bionic Vision Australia (BVA) (2010-2015) and by the National Health and Medical Research Council (NH&MRC) grant numbers APP1109056 and APP1087224.

We thank Elaine Chew, Andrew Fortis, Karen Barnes and the Veterinary Pathology Diagnostic Services, Sydney School of Veterinary Science for the help with immunohistochemical staining and in slide scanning. We thank Dr. Orsolya Kekesi for the helpful discussions on quantitative analysis of immunostaining. The authors acknowledge the technical assistance of Dr. Kathrin Schemann of the Sydney Informatics Hub, a Core Research Facility of the University of Sydney.

References

[1] S.C. Eggenberger, et al., Implantation and long-term assessment of the stability and biocompatibility of a novel 98 channel suprachoroidal visual prosthesis in sheep, Biomaterials 279 (2021) 121191.
[2] B.S. Gow, G.J. Suaning, A method to assess the location and positional stability of supra-choroidal retinal neuroprostheses, in: 2016 38th Annual International Conference of the IEEE Engineering in Medicine and Biology Society (EMBC), 2016, pp. 4723–4726, doi:10.1109/EMBC.2016.7591782.
[3] S.F. Mohammadi, et al., Sheep practice eye for ophthalmic surgery training in skills laboratory, J. Cataract Refract. Surg. 37 (6) (2011) 987–991.
[4] J.A.T. Pigatto, et al., Intraocular pressure measurement in sheep using an applanation tonometer, Revista Ceres 58 (2011) 685–689.
[5] [Dataset] Eggenberger, S.C., et al., Stability and biocompatibility of a Bionic Eye - Ophthalmoscopy, intraocular pressure, optical coherence tomography and radiography data. v2, 2021, http://dx.doi.org/10.17632/9hnz6c99py.2
[6] [Dataset] Eggenberger, S.C., et al., Stability and biocompatibility of a Bionic Eye - Histology and immunohistochemistry data. v2, 2021, http://dx.doi.org/10.17632/8rzc45vp77.2
[7] S. Mohan, et al., Genetic Deletion of PGF(2α)-FP Receptor Exacerbates Brain Injury Following Experimental Intracerebral Hemorrhage, Front. Neurosci. 12 (2018) p. 556-556..
[8] S. Pradhan, et al., Shiga Toxin Mediated Neurologic Changes in Murine Model of Disease, Front. Cell. Infect. Microbiol. 6 (114) (2016).
[9] J. Schindelin, et al., Fiji: an open-source platform for biological-image analysis, Nat. Methods 9 (7) (2012) 676–682.
[10] C.T. Rueden, et al., ImageJ2: ImageJ for the next generation of scientific image data, BMC Bioinformatics 18 (1) (2017) 529.
[11] J. Schindelin, Align Image by line ROI, in Fiji, GitHub, 2006.

APPENDIX 3 BIOMATERIALS AND DATA IN BRIEF AUTHORS CONTRIBUTIONS

- Samuel C. Eggenberger
  - Methodology
  - Formal analysis
  - Data curation
  - Writing – Original draft
  - Visualization
- Adrian Fung
  - Conceptualisation
  - Investigation
  - Methodology
  - Writing- review and editing
- Cherry Ho
  - Methodology
  - Investigation
  - Formal analysis
  - Data curation
- Veronika Tatarinoff
  - Methodology
  - Investigation
  - Resources
  - Supervision
- Natalie L, James
  - Conceptualisation
  - Investigation
  - Methodology
  - Project administration
  - Resources
  - Writing - review and editing
- Susan Wan
- Shannon Donahoe
  - Formal analysis
  - Investigation
  - Writing – review and editing
- Mark Krockenberger
  - Formal analysis
  - Investigation
  - Writing – review and editing
- John R Grigg
  - Conceptualisation
  - Methodology
  - Writing – Review and editing
- Barry S. Gow
  - Investigation
  - Validation
  - Resources
  - Methodology
- Naomi A. Craig
  - Investigation
  - Resources
- Krishna Tumuluri
  - Conceptualization
  - Methodology
  - Writing – Review and editing
- Melville J. da Cruz
  - Methodology
  - Investigation

    - Investigation
- Steven Eamegdool
    - Methodology
    - Investigation
    - Resources
    - Writing – Review and Editing
- Chris Dodds
    - Methodology
    - Investigation
    - Resources
- Donna la Hood
    - Methodology
    - Investigation
- Aaron Gilmour
    - Investigation
- Resources Peter McCluskey
    - Writing – review & editing
    - Visualisation
    - Supervision
    - Project administration
    - Funding acquisition
- Nigel H. Lovell
    - Conceptualization
    - Methodology
    - Validation
    - Investigation
    - Resources
    - Writing - Review & Editing
    - Supervision
    - Project administration
    - Funding acquisition
- Michele C. Madigan
    - Resources
    - Writing – Review and editing
- Gregg J. Suaning
    - Conceptualization
    - Methodology
    - Investigation
    - Resources
    - Writing – Review and editing
    - Supervision
    - Project administration
    - Funding acquisition

APPENDIX 4 ANAESTHESIA INVENTORY CHECKLISTS

Following checklists should be used to verify that all equipment, consumables and skills are available to perform specific anaesthetic and monitoring techniques.

Anaesthesia and monitoring

Inventory 1 - **Large animals**

Inventory 1a. Essentials

Complete in Step B

- **Equipment**
  - ☐ Intubation kit (appropriate for animal)
    - ☐ Staff trained to intubate with the specific kit
  - ☐ Appropriately sized breathing circuit
    - ☐ Tubing
    - ☐ Reservoir bags
    - ☐ Oxygen mask
  - ☐ Sling to lift animals from the ground to lift tables
  - ☐ Portable lift table
  - ☐ Heating device (BAIR hugger / Heat mat / Other:……)
  - ☐ Electric clippers and size 40 blades (remove hair to place IV catheter)
  - ☐ Sharps container
  - ☐ Anaesthetic machine/oxygen source and appropriately sized mask

Anaesthesia and Monitoring Inventory

- **Consumables**
  - ☐ Swabs
  - ☐ Needles (appropriate size for animal)
  - ☐ Syringes (appropriate size for animal)
  - ☐ (Pig) Extension set and extra-long needles required for IM pig sedation
  - ☐ Cuffed endotracheal tubes of appropriate sizes
  - ☐ Endotracheal tube ties (secure endotracheal tube)
  - ☐ Intravenous catheters (appropriate size for animal)
    - Catheters
    - Catheter T-ports
  - ☐ Sticky tape (secure catheters)
  - ☐ Chlorhexidine and alcohol solutions (prep IV catheter site)
  - ☐ Intravenous fluid bags (1L bags of balanced crystalloid i.e. Lactated ringers, plasmalyte 148)
  - ☐ Giving sets and extension sets for IV fluids as required
  - ☐ Concentrated oxygen source
- **Monitoring**
  - ☐ Anaesthetic record and pen (if paper-based record)
  - ☐ Rectal thermometer
  - ☐ Pulse oximeter
    - ☐ Staff trained to interpret readings and react appropriately
  - ☐ Non-invasive blood pressure
    - ☐ Blood pressure monitor
    - ☐ Range of blood pressure cuffs
    - ☐ ECG and capnography measurement capability
    - ☐ Staff trained to interpret readings and react appropriately
- **Other**
  - ☐ Staff for restraint and movement of animals

Anaesthesia and Monitoring Inventory

- **Strongly recommended in case of craniotomy (strike through if not relevant)**
  - Mechanical ventilation
    - Ventilator
    - Staff trained to use and adapt ventilation to monitoring readings
    - Blood gas analysis capability
    - Invasive blood pressure measurement equipment

Technique-specific checklists: Strike through sections that aren't relevant.

Complete in Step B

Inventory 1b. TIVA (Total Intravenous Anaesthesia)

NOTE: It is recommended to have the capability to perform PIVA (partial intravenous anaesthesia) as back-up to TIVA. See Checklist 2c below for the additional requirements.

- **Equipment**
  - ☐ Continuous infusion pumps with adjustable rate of infusion
    - ☐ Staff trained to operate equipment
- **Consumables**
  - ☐ Maintenance drugs

Function	Drug Select from Table 2 (Fill out in Step D)	Dosage/Rate (Fill out in Step E)
MAC sparing Opioid		
Hypnotic		

Notes: ……

Inventory 1c. PIVA (Partial Intravenous Anaesthesia)

- **Equipment**
  - ☐ Anaesthetic machine with vaporiser attached to concentrated oxygen source
    - ☐ Staff trained to operate equipment
  - ☐ Continuous infusion pump/syringe driver with adjustable rate of infusion
    - ☐ Staff trained to operate equipment
- **Consumables**
  - ☐ Maintenance drugs

Function	**Drug** Select from Table 2 (Fill out in Step D)	**Dosage/Rate** (Fill out in Step E)
MAC sparing Opioid		
Hypnotic		
Inhalant		

Notes: ……

Inventory 1d. BInhA (Balanced Inhalant Anaesthesia)

NOTE: It is recommended to prioritise TIVA or PIVA over balanced inhalant anaesthesia. Consider securing additional equipment and training if required.

- **Equipment**
  - ☐ Anaesthetic machine with vaporiser attached to concentrated oxygen source
    - ☐ Staff trained to operate equipment
- **Consumables**
  - ☐ Maintenance drugs

Function	Drug Select from Table 2 (Fill out in Step D)	Dosage/rate (Fill out in Step E)
MAC sparing Opioid		
Inhalant		

Notes: ……..

Inventory 1e. Premedication and induction

Complete in Step C

- **Equipment**
  - ☐ Refer to 'Essentials' checklist 1a
- **Consumables**
  - ☐ Premedication/sedation drugs

Function	Drug Select from Table 2 (Fill out in Step C)	Dosage/Rate (Fill out in Step E)
Analgesic		
Sedative		
Induction agent		

Notes: ……..

Inventory 1f. Monitoring – Recommendations

Complete in Step F

Strike through items that are not relevant.

NOTE: Improved monitoring positively reflects on the physiological stability of the animal, depth of anaesthesia and animal welfare. Consequently, improved experimental result quality and reproducibility may be expected.

IMPORTANT NOTE: Monitoring equipment is ineffective unless the readings can be correctly interpreted and used to influence the care of the animal. Ensure staff is adequately trained. It is strongly recommended to involve staff with professional medical or veterinary training to assist with animal monitoring and maintenance.

- **Equipment**
  - ☐ Invasive blood pressure monitoring
  - ☐ End tidal CO2
  - ☐ ECG.
  - ☐ Blood gas analysis

Anaesthesia and monitoring

Inventory 2 - **Small animals**

Inventory 2a. Essentials

- **Equipment**
  - ☐ Anaesthetic machine and mask or alternative way to delivery supplemental oxygen
  - ☐ Warming pad
  - ☐ Fluid warmer
  - ☐ Scales
  - ☐ Sharps container
  - ☐ (Recovery) Recovery cage
- **Consumables**
  - ☐ Swabs
  - ☐ Needles (appropriate size for animal)
  - ☐ Syringes (appropriate size for animal)
  - ☐ Concentrated oxygen source
  - ☐ Fluids for subcutaneous injection (use fluid warmer at body temperature)
- **Monitoring**
  - ☐ Anaesthetic record / pen
  - ☐ Rectal thermometer
  - ☐ Pulse oximeter
    - ☐ Staff trained to interpret readings and react appropriately
  - ☐ Concentrated oxygen source
- **Mechanical ventilation (Recommended in case of craniotomy)**
  - ☐ Intubation kit (appropriate for animal)
    - ☐ Staff trained to intubate with the specific kit
  - ☐ Endotracheal tubes of appropriate sizes
  - ☐ Ventilator (appropriate for animal)

Technique-specific checklists: Strike through sections that aren't relevant.

Complete in Step B

NOTE: Constant rate intravenous infusion (CRI) is recommended for all injectables as it provides greater anaesthetic stability and is easier to control. CRI comes with additional requirements which may render the technique impractical, in very small animals. Literature about dosage and long-term effects for CRI may not be available for all models. Cross-out items if CRI will not be used.

Inventory 2b. BInhA (Balanced Inhalant Anaesthesia)

- **Equipment**
  - ☐ Anaesthetic machine with vaporiser
  - ☐ Anaesthetic mask
  - ☐ Waste anaesthetic gas removal system I.e., active scavenge or charcoal scavenge
  - ☐ (CRI) Continuous infusion pump/syringe driver with adjustable rate of infusion
  - ☐ (CRI) Surgical tools to position intravenous access
    - ☐ (CRI) Staff trained to surgically position and secure intravenous catheter
- **Consumables**
  - ☐ CRI) Intravenous catheters (appropriate size for animal)
    - ☐ (CRI) Catheters
    - ☐ (CRI) Catheter T-ports
  - ☐ (CRI) Sticky tape (secure catheters)
  - ☐ Maintenance drugs

Function	**Drug** Select from Table 2 (Fill out in Step D)	**Dosage/Rate** (Fill out in Step E)
MAC sparing Opioid		
Inhalant		

Notes: ……..

Anaesthesia and Monitoring Inventory

Inventory 2c. BInjA (Balanced Injectable Anaesthesia)

Complete in Step B

NOTE: Constant rate intravenous infusion (CRI) is recommended for all injectables as it provides greater stability and is easier to control. CRI comes with additional requirements which may render the technique impractical, in particular in very small animals. Literature about dosage and long-term effects for CRI may not be available for all models. Cross-out items if CRI will not be used.

- **Equipment**
  - ☐ (CRI) Continuous infusion pump/syringe driver with adjustable rate of infusion
  - ☐ (CRI) Surgical tools to position intravenous access
    - ☐ (CRI) Staff trained to surgically position and secure intravenous catheter
- **Consumables**
  - Maintenance drugs

Function	Drug Select from Table 2 (Fill out in Step D)	Dosage/Rate (Fill out in Step E)
MAC sparing Opioid		
Inhalant		

Notes: ……

- ☐ (CRI) Intravenous catheters (appropriate size for animal)
  - ☐ (CRI) Catheters
  - ☐ (CRI) Catheter T-ports
- ☐ (CRI) Sticky tape (secure catheters)

Inventory 2d. Premedication and induction

Complete it Step C

NOTE: Injectable premedication and induction (injectable) can be performed with items listed in Inventory 2a: **Essentials** only. Additional equipment is required to perform inhalant-based induction (inhalant).

- **Equipment**
  - ☐ (Inhalant) Anaesthetic machine with vaporiser attached to compressed oxygen source
  - ☐ (Inhalant) Induction chamber
  - ☐ (Inhalant) Face mask
  - ☐ (Inhalant) Waste anaesthetic gas scavenging system
- **Consumables**
  - (Inhalant) Premedication/sedation drugs

Function	Drug Select from Table 2 (Fill out in Step C)	Dosage (Fill out in Step E)
Analgesic		
Sedative		
Induction Inhalant		

Notes: ……..

☐ (Injectable) Premedication/sedation drugs

Function	Drug Select from Table 4 (Fill out in Step C)	Dosage (Fill out in Step E)
Analgesic		
Anaesthetic		

Notes: ……..

Inventory 2e. Monitoring – Recommendations

Strike through items that are not relevant.

NOTE: Improved monitoring positively reflects on the physiological stability of the animal, depth of anaesthesia and animal welfare. Consequently, improved result quality and reproducibility may be expected.

IMPORTANT NOTE: Equipment is ineffective unless the readings can be correctly interpreted and used to influence the care of the animal. Ensure staff is adequately trained. It is strongly recommended to involve staff with professional medical or veterinary training to assist with animal monitoring and maintenance.

- **Equipment**
  - Non-invasive blood pressure
    - Blood pressure monitor
    - Range of blood pressure cuffs
    - Staff trained to interpret readings and react appropriately
  - End tidal CO2

APPENDIX 5 RETINAL RECORDINGS, SUPPLEMENTARY DATA

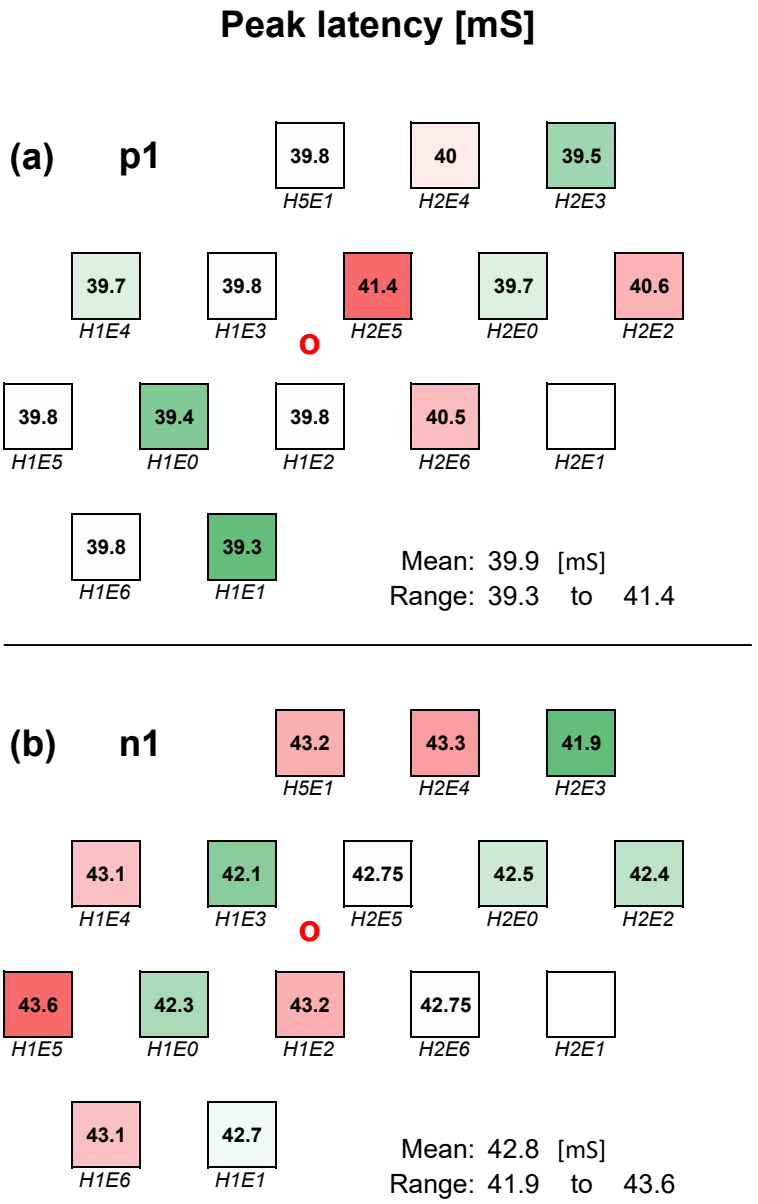

Appendix Figure 5 Latencies during recordings with simultaneous on four electrodes (H1E0, H1E3, H2E0 and H2E3). Stimulating electrodes peak earlier than their direct neighbours for p1 and n1. With the increasing number of stimulating electrodes, which are direct neighbours, it becomes more difficult to isolate the effects of each electrode on the latency of its neighbours.

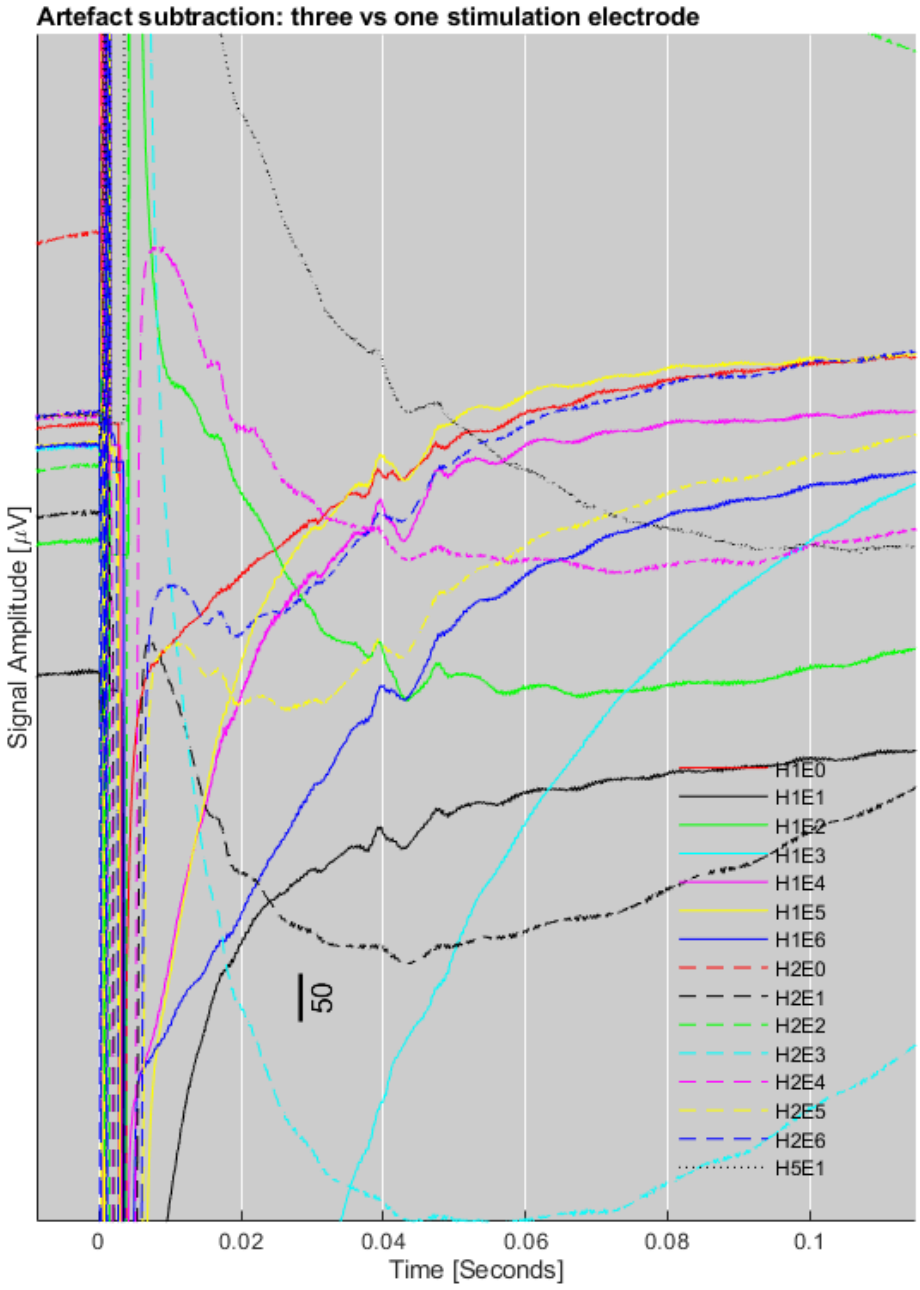

Appendix Figure 6 Artefact minimisation. Subtraction of recordings with different stimulation electrode configurations allowed to reduce the amplitude of the stimulation artefact.

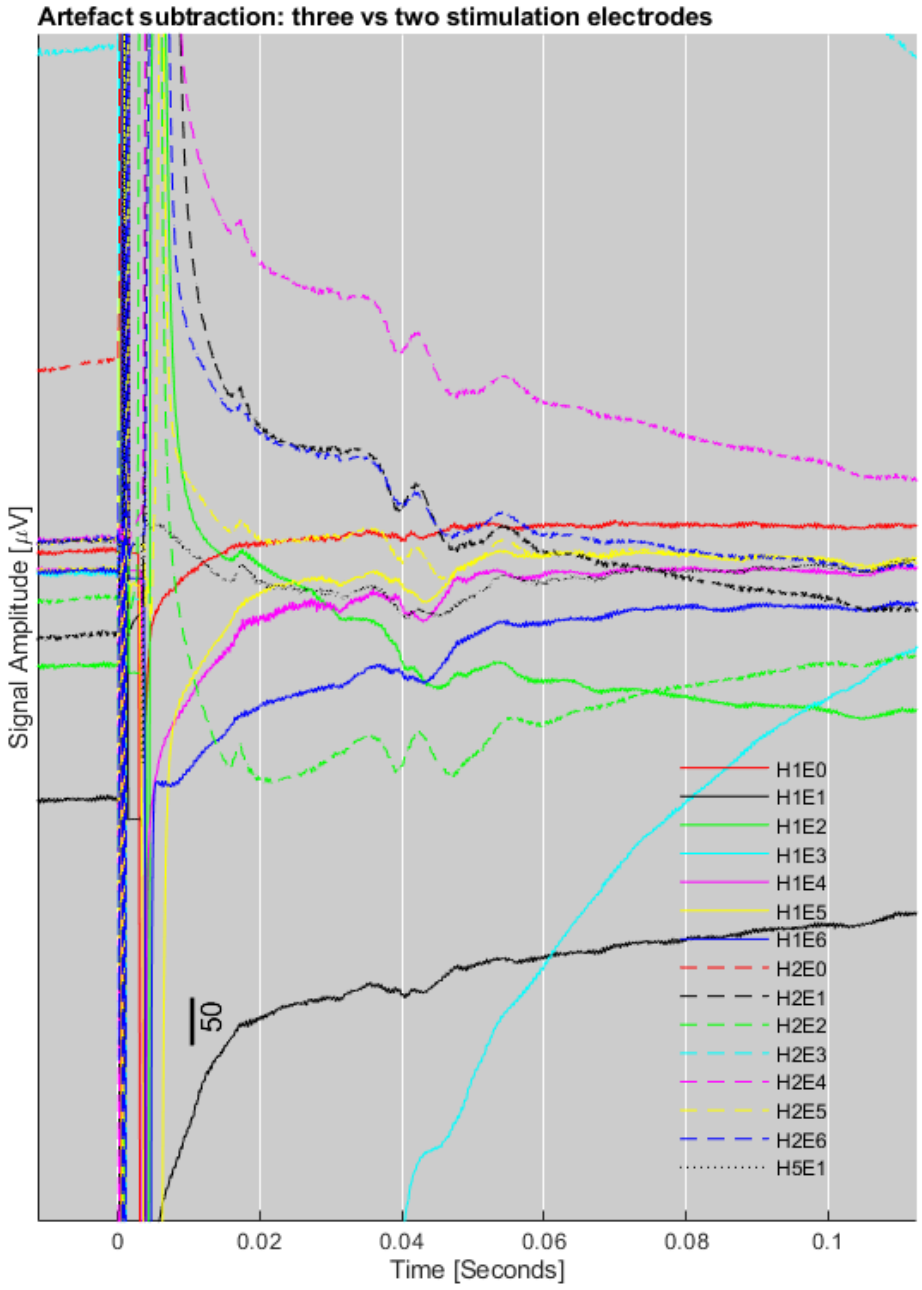

Appendix Figure 7 Artefact minimisation. Subtraction of recordings with different stimulation electrode configurations allowed to reduce the amplitude of the stimulation artefact.

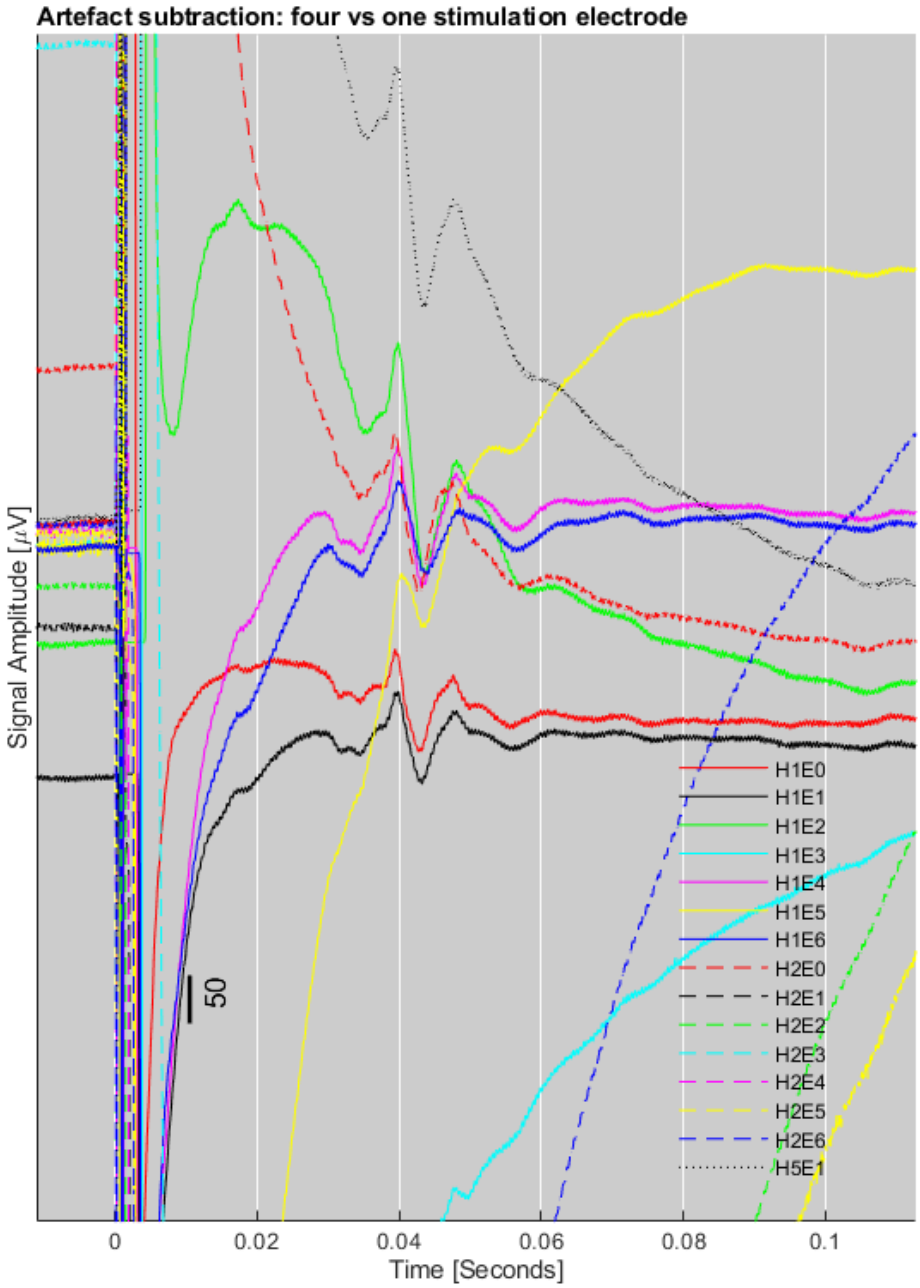

Appendix Figure 8 Artefact minimisation. Subtraction of recordings with different stimulation electrode configurations allowed to reduce the amplitude of the stimulation artefact.

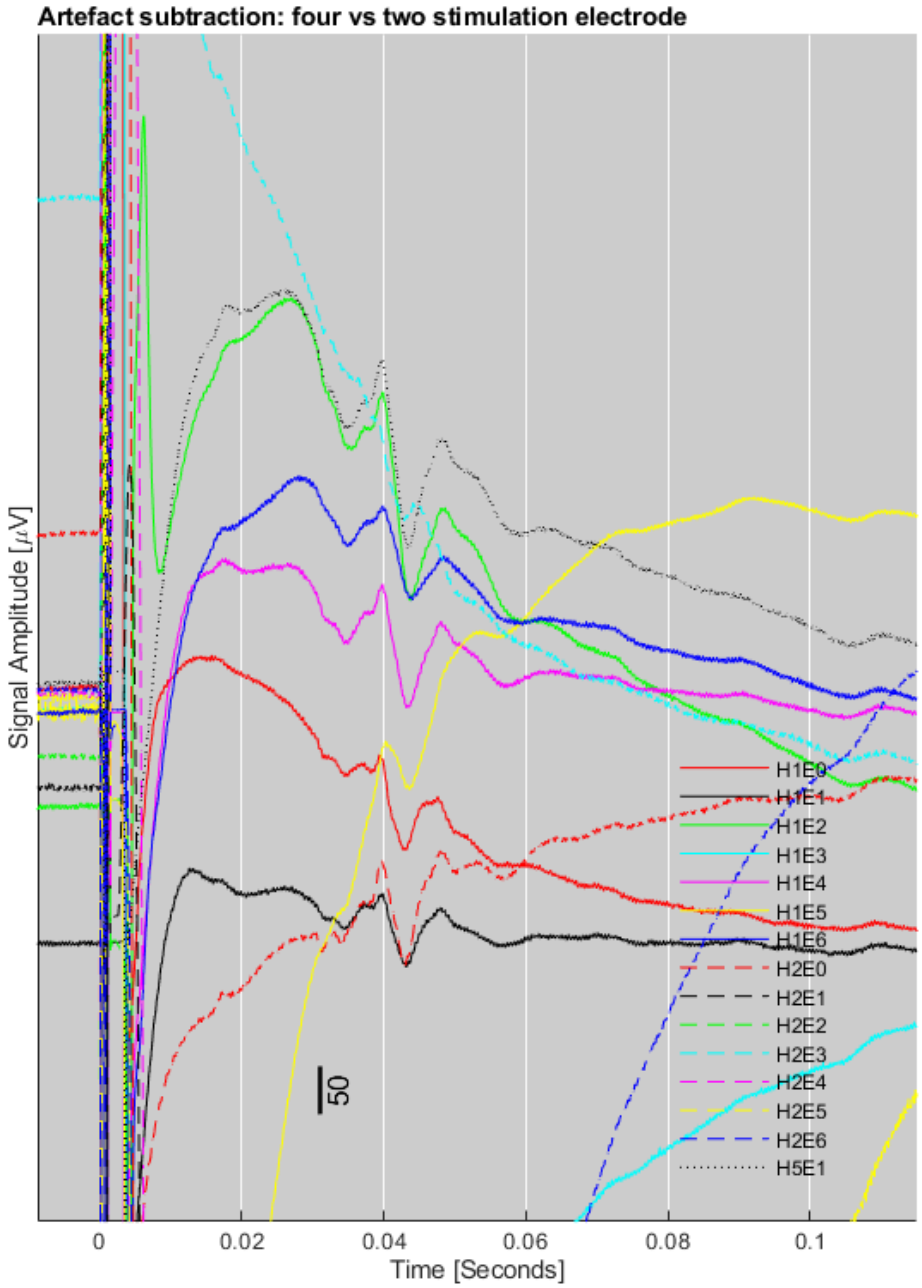

Appendix Figure 9 Artefact minimisation. Subtraction of recordings with different stimulation electrode configurations allowed to reduce the amplitude of the stimulation artefact.

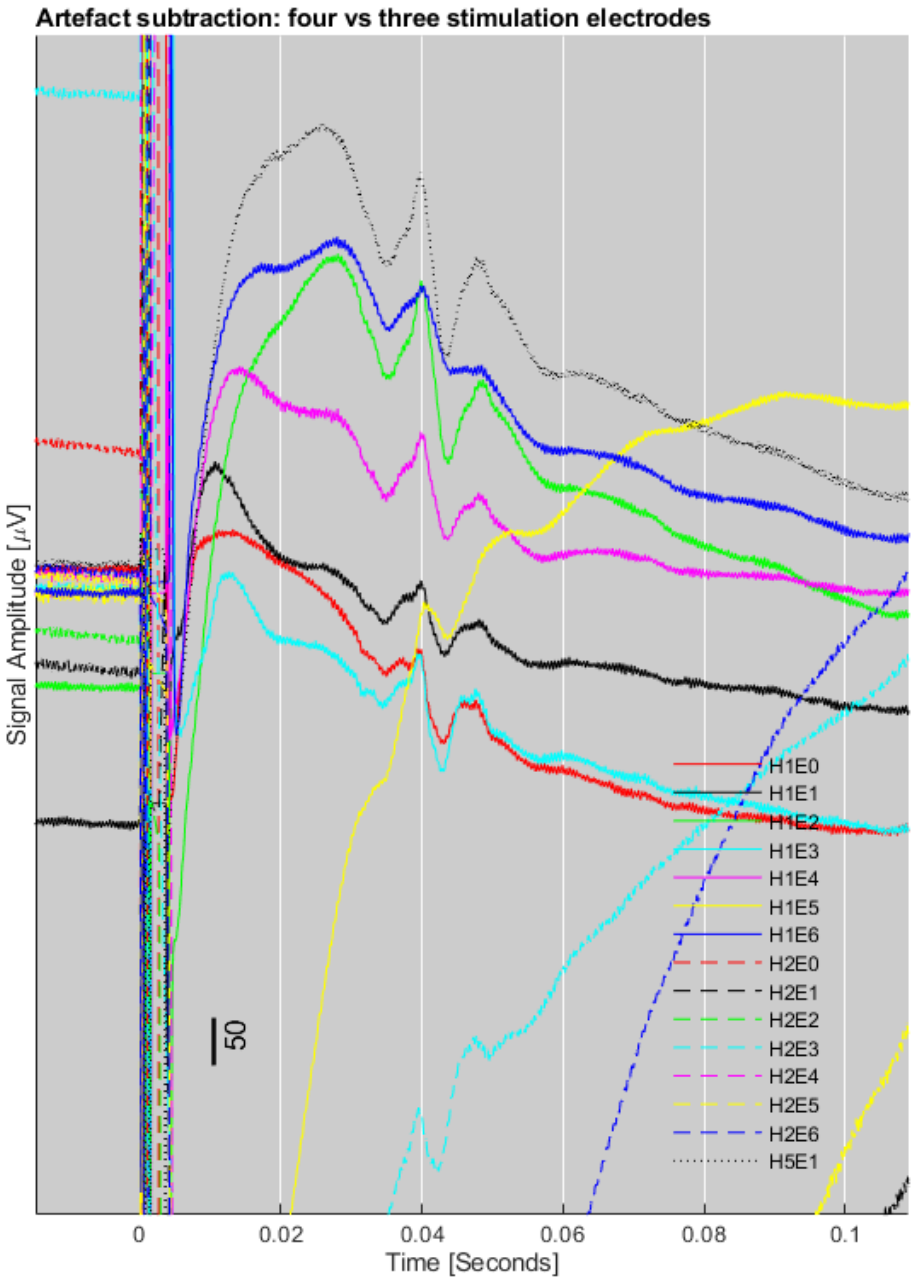

Appendix Figure 10 Artefact minimisation. Subtraction of recordings with different stimulation electrode configurations allowed to reduce the amplitude of the stimulation artefact.

APPENDIX 6 SIMULATION OF SIMULTANEOUS STIMULATION

Poster presented as

Eggenberger S.C., A.M. Pratiwi, G.J. Suaning (2021, October 3-5). "*Towards Calibrated Computer Models for the Optimization of Parallel Stimulation*". [Poster presentation] The Eye and the Chip: 12th World Research Congress on the Relationship between Neurobiology and Nano-Electronics Focusing on Artificial Vision (TEatC 2021), Detroit MI, USA, https://www.henryford.com/hcp/research/clinical-research/vision/research-congress/eye-chip

For the congress, a web page was prepared with more detailed information, to complement the poster:

https://samueleggenberger.wixsite.com/calibratedmodels

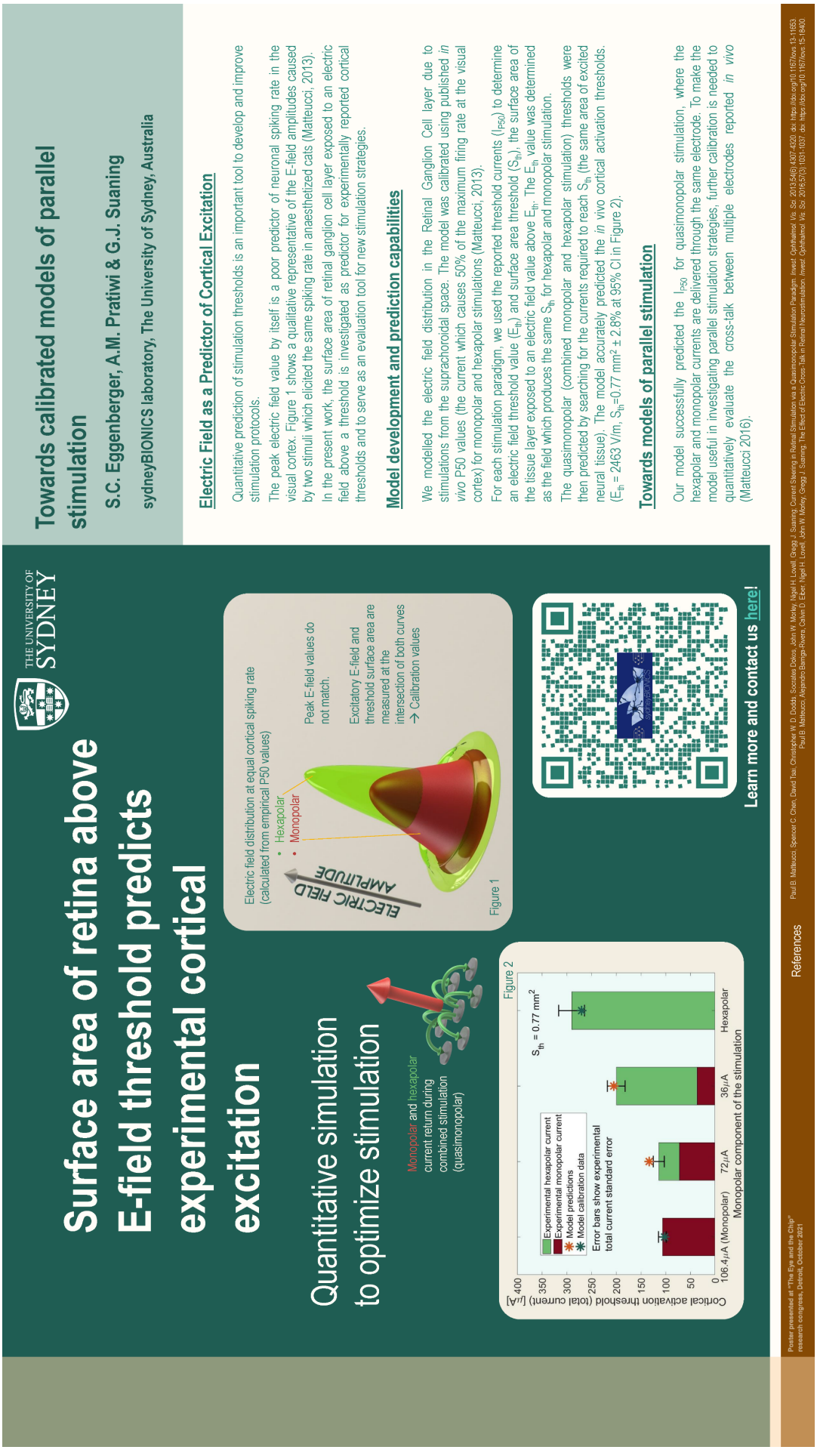
Surface area of retina above E-field threshold predicts experimental cortical excitation
THE UNIVERSITY OF SYDNEY
Quantitative simulation to optimize stimulation
Monopolar and hexapolar current return during combined stimulation (quasimonopolar)
Figure 2
Cortical activation threshold (total current) [μA]
Experimental hexapolar current
Experimental monopolar current
Model predictions
Model calibration data
Error bars show experimental total current standard error
S_{th} = 0.77 mm²
106.4μA (Monopolar)
72μA
36μA
Hexapolar
Monopolar component of the stimulation
Electric field distribution at equal cortical spiking rate (calculated from empirical P50 values)
Hexapolar
Monopolar
ELECTRIC FIELD AMPLITUDE
Peak E-field values do not match.
Excitatory E-field and threshold surface area are measured at the intersection of both curves → Calibration values
Figure 1
Learn more and contact us here!
Towards calibrated models of parallel stimulation
S.C. Eggenberger, A.M. Pratiwi & G.J. Suaning
sydneyBIONICS laboratory, The University of Sydney, Australia
Electric Field as a Predictor of Cortical Excitation
Quantitative prediction of stimulation thresholds is an important tool to develop and improve stimulation protocols.
The peak electric field value by itself is a poor predictor of neuronal spiking rate in the visual cortex. Figure 1 shows a qualitative representative of the E-field amplitudes caused by two stimuli which elicited the same spiking rate in anaesthetized cats (Matteucci, 2013).
In the present work, the surface area of retinal ganglion cell layer exposed to an electric field above a threshold is investigated as predictor for experimentally reported cortical thresholds and to serve as an evaluation tool for new stimulation strategies.
Model development and prediction capabilities
We modelled the electric field distribution in the Retinal Ganglion Cell layer due to stimulations from the suprachoroidal space. The model was calibrated using published *in vivo* P50 values (the current which causes 50% of the maximum firing rate at the visual cortex) for monopolar and hexapolar stimulations (Matteucci, 2013).
For each stimulation paradigm, we used the reported threshold currents (I_{P50}) to determine an electric field threshold value (E_{th}) and surface area threshold (S_{th}). the surface area of the tissue layer exposed to an electric field value above E_{th}. The E_{th} value was determined as the field which produces the same S_{th} for hexapolar and monopolar stimulation.
The quasimonopolar (combined monopolar and hexapolar stimulation) thresholds were then predicted by searching for the currents required to reach S_{th} (the same area of excited neural tissue). The model accurately predicted the *in vivo* cortical activation thresholds. (E_{th} = 2463 V/m; S_{th}=0.77 mm² ± 2.8% at 95% CI in Figure 2).
Towards models of parallel stimulation
Our model successfully predicted the I_{P50} for quasimonopolar stimulation, where the hexapolar and monopolar currents are delivered through the same electrode. To make the model useful in investigating parallel stimulation strategies, further calibration is needed to quantitatively evaluate the cross-talk between multiple electrodes reported *in vivo* (Matteucci 2016).
References
Paul B. Matteucci, Spencer C. Chen, David Tsai, Christopher W. D. Dodds, Socrates Dokos, John W. Morley, Nigel H. Lovell, Gregg J. Suaning. Current Steering in Retinal Stimulation via a Quasimonopolar Stimulation Paradigm. Invest Ophthalmol Vis Sci. 2013;54(6):4307–4320. doi: https://doi.org/10.1167/iovs.13-11953.
Paul B. Matteucci, Alejandro Barrigon-Rivera, Galvin D. Eiber, Nigel H. Lovell, John W. Morley, Gregg J. Suaning. The Effect of Electric Cross-Talk in Retinal Neurostimulation. Invest Ophthalmol Vis Sci. 2016;57(3):1031–1037. doi: https://doi.org/10.1167/iovs.15-18400
Poster presented at "The Eye and the Chip" research congress, Detroit, October 2021

APPENDIX 7 CHRONIC STIMULATION STUDY: DETAILED PROTOCOL

Delivery and acclimatisation

Sheep are obtained and acclimatised in group housing at CPC according to the LAS Sheep Husbandry SOP (SOP-HUS_07_LAS CPC Hybrid Theatre_sheep_20180506). Environmental enrichment and gentle handling are used as per the SOP to help optimise acclimatisation of the sheep. Any building emergencies during the time the sheep are in residence at CPC are managed according to the approved building emergencies SOP (SOP-HUS_20_LAS CPC Hybrid Theatre emergency procedures_20170929).

Sheep will be acclimatised using positive reinforcement methods to stand quietly while being restrained using a sheep head halter to allow the required postoperative care and ocular examinations, for example ophthalmoscopy. This training will be done at least once daily using highly appealing food, gentle tones of voice and gentle movements over a period of at least two weeks. Sheep that do not acclimatise to gentle restraint to allow ocular examinations within three weeks will be excluded from this study. The unacclimated sheep will be sent back to the supplier and transported in minimum of 2 sheep.

McMasters (long term housing)

SOP_HUS_31_LAS McMaster Annex husbandry_sheep_20180605. SOP-HUS_32_Transport of large animals between McMaster Annex & CPC_20180605

Intraocular pressure measurements

Intraocular pressure will be measured in both eyes using a rebound tonometer to establish the pressure baseline prior to surgery and then on postoperative days one, three, seven, 14, 30, 60 and 90. The procedure will take place while animals are awake and gently restrained using a sheep head halter. Tonometry measurements are painless. The sheep will need to be restrained for approximately 30 minutes to allow tonometry measurements.

Anaesthesia

For the implantation surgery, the sheep will be anaesthetised according to the LAS Sheep Anaesthesia and Analgesia SOP (SOP-ANA_02_LAS CPC Hybrid Theatre anaesthesia analgesia_sheep_20170921). And as per conclusions of the anaesthesia refinement process detailed in Chapter 4

Procedure Details (CI)

Weighing

Animals will be weighed on arrival at the facility and within 48 hours of the day of surgery. Animals will otherwise be weighed throughout the rest of the protocol only if unusual weight gain/loss is observed.

Imaging

Ophthalmoscopic and optical coherence tomography images of the retina will be acquired in the anaesthetised animals prior to commencing the surgical procedure and directly post-operatively. On post-operative days 28 and 60, the animals will be anaesthetised, and follow-up images will be acquired. Final images of the retina will be obtained in the anaesthetised animals prior to commencing acute electrophysiology tests on day 90. Pupils will be dilated using 1% Atropine drops for all imaging sessions.

X-ray images and/or CT scans will be obtained directly post-operatively and prior to commencing the acute electrophysiology tests.

Ultrasound imaging and/or fluoroscopy may be used during the implantation surgery to guide the insertion of the device.

Electroretinography

Electroretinographic (ERG) measurements require three electrodes to be placed on the animal: the signal electrode placed in direct contact with the globe, one reference and one ground electrode. The minimally invasive ERG measurements are performed by placing a thin, flexible gold foil recording electrode under the eyelid. The electrical contact formed by the flexible and light recording electrode is located at the inferior area of the cornea and is widely used in human and veterinarian clinical practice [268, 269]. Two more electrodes, a reference and a returning electrode are necessary for ERG measurements. Subcutaneous needle electrodes at the base of the ear and in the skin of the skull will be used as ground and reference electrodes. The use of subcutaneous needle electrodes is a commonly applied method in veterinary and human clinical practice [270-272].

Preoperative ERG measurements will be made in the anaesthetised animals on the day of surgery. ERG measurements will also be made during each imaging sessions during which animals will be anaesthetised.

Visual prosthesis implantation: Surgical procedure

For surgery, only sterile equipment and surgical tools will be used. The area around the operative site will be shaved and aseptically prepared. Immediately prior to surgery, the intravenous antibiotic cephazolin 20-30 mg/kg IV will be administered and repeated every 90 minutes during the surgical procedure.

The surgeon and the assistant will shave and scrub the implant sites below the ear on the neck and surrounding the eye thoroughly with chlorhexidine or povidone iodine using sterile gauze swab. The surface of the eye will be irrigated with 5% povidone iodine from a syringe by dripping 2 ml of solution over 1 minute (Ferguson, 2003). To facilitate cautery, a square (approximately 100 x 100 mm) will be shaved on the contralateral abdomen to interface with a monopolar plate electrode.

The surgical team will gown and glove as per standard sterile technique. The sites will be rinsed with sterile water, and the scrub procedures repeated twice more. Sterile drapes will be applied, leaving the sites clear but covering the outer edge of each site.

The position of the implanted telemetry unit will be marked on the neck of the animal below the ear, lateral to the spine. A full thickness skin incision will be made, and a subcutaneous pocket will be prepared adjacent to the incision by blunt dissection for placement of the telemetry unit.

A subcutaneous tunnel between the telemetry unit and the eye will be created by blunt dissection. The tunnel will extend to the lateral side of the orbital margin. The tunnel will be widened using a

12mm wide malleable brain retractor. An incision lateral to the orbital margin will be made to allow the malleable brain retractor to pass through. A 17mm, and then a 25mm wide malleable brain retractor, will be passed progressively through the tunnel to open a wide enough tunnel for a trocar to pass.

The implanted device will be delivered sterile to the surgery in a trocar. This trocar has been custom designed for this surgery, with detachable segments at each end that contain the visual stimulator with electrode array at one end and the telemetry unit at the other end. This trocar will be used to pass the visual stimulator and electrode array through the tunnel to the lateral side of the eye. When the end of the trocar containing the visual stimulator with electrode array is through the tunnel, the detachable segment of the trocar containing the visual stimulator with electrode array will be released from the trocar. At this point, the other end containing the telemetry unit will be released from the remaining

bridge section of the trocar. The trocar bridge will be dismantled, allowing its components to be passed forward or backward through the tunnel and removed.

A bone drill will be used to create a small groove (orbitotomy: approx. 2mm deep x 2mm wide) in the bone around the edge of the eye. A cutting guide, currently undergoing *in vitro* testing on bone simulation material, may be used to increase the speed and precision of the cuts. This orbitotomy is for stabilisation of the cable connected to the visual stimulator that will be implanted into the eye. A silicone grommet moulded onto the cable at this position along the lead will be inserted into the orbitotomy. Specifically, a flap of connective tissue will be raised from the bone and the orbitotomy will be created 2 mm above the zygomaticofrontal suture. The flap will be suture over the grommet for added stability.

The eye surgery will be conducted by a specialist vitreoretinal (eye) surgeon. The eye will be prepared by dilation with 1% tropicamide, 1% cyclopentolate and 2.5% phenylephrine. Gel artificial tears will be used throughout the surgery to maintain surface ocular hydration.

A lateral cantholysis will be performed with use of cutting/coagulation diathermy, using artery forceps to clamp the lateral canthus. The eyelid will be stabilized using 4-0 prolene traction sutures. A corneal traction suture will be placed at the superior limbus, using 6-0 prolene.

Conjunctival peritomy (removal of a strip of the conjunctiva of an eye) will be conducted with Westcott scissors and conjunctival forceps. It is important to ensure a pocket in the conjunctiva is made deep enough for visual stimulator insertion. The superior rectus muscle will be isolated with a muscle hook. The superior rectus will be sutured with double armed 6-0 vicryl. It will be cut and clamped at each end with an alligator clip. The superior oblique rectus muscle will be isolated and cut as described above.

An L-shaped wound will be measured with callipers (11 mm wide, 3.3 mm at one end), 10mm posterior to the limbus. The wound will be marked with a marking pen. The 10mm straight wound will be incised with a 15-degree crescent blade. If required, viscoelastic gel will be injected to separate the posterior edge of the scleral wound from the uvea.

A custom electrode-introducer made of silicone will be partially inserted in the incisions to create a pocket in the suprachoroidal space. The electrode array will be inserted into the pocket, using the introducer as a guide, and using with silicone covered Kelman

Mcpherson forceps. The introducer will be removed and the second part of the “L” (3.3 mm) will be carefully cut with the 15-degree blade.

The electrode array will be inserted fully into the pocket and the wound will be sutured closed using 7-0 prolene with 6 sutures as indicated in Appendix Figure 11.

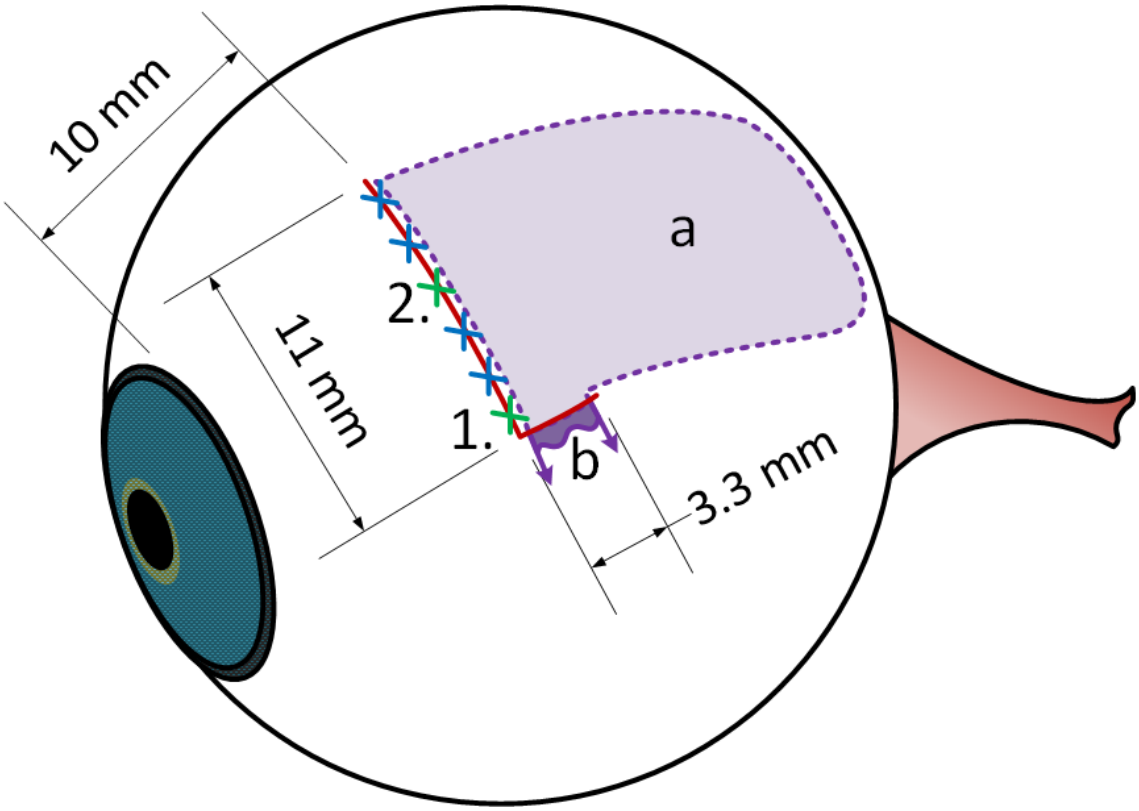

Appendix Figure 11 Scleral incision and sutures. (A) Schematic view of the globe and L-shaped incision. a) Location of the electrode array under the sclera, sutured scleral “L-shaped” incision (red line in A) and the remaining bridge (b) through which the conductors exit the globe. The short part of the L allows minimal residual scleral opening where the electrode array exits the eye and is connected to the VS via a bridge (b). After electrode array insertion in the suprachoroidal space, the long section of the L-shaped incision is sutured with 7-0 Prolene at the six locations indicated by crosses. The green sutures are placed first, following the numbering in the figure, before placing the remaining ones.

If required for control of the eye pressure, the anterior chamber will tapped with a 30-gauge needle and 1 ml syringe to draw 0.5 ml of fluid.

The eyelets for securing the capsule will be sutured with two loops of 7-0 prolene, each. The lateral rectus muscle will not be reattached as it has been observed that suturing of this muscle was correlated with reduced eye movements in a prior study (pending

publication). The tenons capsule and conjunctiva will be sutured with 7-0 vicryl. The canthotomy will be closed using 7-0 vicryl suture.

The telemetry unit will be placed into the subcutaneous pocket created previously and the incision

posterior to ear will be closed. Incision will be infiltrated with local anaesthetic at closure (Bupivicaine 0.25% at a maximum dose rate of 2 mg/kg)

Post-Op Recovery

Sheep will be returned to the holding area and recovered from anaesthesia as per the LAS Sheep anaesthetic recovery SOP-OTH_11_Anaesthetic recovery and post-op care_sheep_20180301.

A suitable NSAID will be administered daily for analgesia (E.g. Carprofen 4 mg/kg or meloxicam as per LAS SOP) for at least 7 days post-operatively and as per LAS veterinary staff's discretion after that. A transdermal fentanyl patch will be applied to a limb to deliver 2-4 mcg/kg/hr consistent opioid analgesia for the first 72 hours post-operatively. Pain assessment will occur three times daily by the LAS veterinary team or appropriately trained personnel (e.g. research team) using the pain scoring system (found in LAS Sheep anaesthetic recovery SOP-OTH_11_Anaesthetic recovery and post-op care_sheep_2018030). If the animal is considered to be painful to the degree that it is impeding normal behaviour, rescue analgesia (methadone) will be administered as required. Topical chloramphenicol antibiotic ointment, anti-inflammatory cortisone eye drops and artificial tears will be administered three times daily for 30 days, unless specified otherwise by the surgeon or LAS veterinary staff. Systemic antibiotics, ceftiofur 1 – 2 mg/kg intramuscularly once daily for at least three days post-operatively.

Sheep will be individually penned, but adjacent to other sheep, for the first 7 days postoperatively to allow the surgical site to heal. Sheep will be able to interact with other via, sight, sound, smell and nose-touching through the bars of the pen fencing. Following this recovery period, sheep will be housed in groups of at least two animals.

Animals will be assessed twice a day (morning and afternoon) by the LAS team and/or appropriately trained members of the research team (training and assessment of skills/knowledge at the discretion of the LAS team) during the first 7 days after the operation. The animals will be gently restrained with the sheep halter for up to 15 minutes to allow assessment using ophthalmoscopy using a hand-held equipment without

recording capability, temperature, wound appearance and eye health, behaviour and general wellbeing. Further eye health checks will be conducted using a hand-held indirect ophthalmoscope (hand-held device without recording capability) every 2-3 days for a minimum of 2 weeks post-surgery (duration: up to 15 minutes). Thereafter, where good health will be observed, ophthalmoscopy will be conducted weekly with daily general health assessments. Fluorescein staining, visualized with a Burton lamp, will be used as required to identify corneal damage. All assessments will be recorded in adequate forms (attachment: LAS - Large Animal Facility Hospitalsation Sheet - Bionic Eye Phoenix 99 AN IKW CB). Recording of ophthalmoscopic images will be done only on anaesthetised animals during the planned imaging sessions as described above during weeks 4, 8 and 13 (using an ophthalmoscopic set-up with recording capabilities).

In case of elevated intraocular pressure above 35 mmHg, medication against high intraocular pressure will be used under direction of surgeon, regular intraocular pressure measurements will be performed to assess if medication effective. Analgesia will be administered if required.

Long-term stimulation and behavioural testing

After a recovery period of 30 days, and provided that adequate healing is observed, the devices will be activated and deliver electrical stimuli to the eyes of the animals. A soft foam collar positioned around the neck of the sheep will contain a supply of batteries sufficient for 72 hours of operation, a radio transceiver, microcontroller, output amplifier and telemetry coil. It will weigh not more than 1 kg and will be positioned for even distribution of weight around the neck. The sheep will be familiarised with wearing the collar for at least 4 days before activation of the device. Every 2-3 days the batteries mounted in the collar around the neck of the sheep will be changed during the daily inspections.

The animals will be randomly allocated to one of three groups, to chronically receive one of three stimulation patterns. The first session of behavioural testing will be dedicated to identifying whether the stimulation parameters, defined as scientifically relevant by the investigators, cause any observable signs of pain or distress and to confirm whether the device is able to evoke artificial visual perception in the animal. The academic literature lacks behavioural studies relating to the delivery of electrical stimuli to the visual system in sheep. We have developed the following program to assess for behavioural responses to stimuli from the device.

The animal will be allowed to choose a comfortable position within an individual pen, but in the same room as its buddy. Animals will be acclimatised to this short-term separation before commencing the behavioural study to mitigate the stress from separation during the minimal time required to perform the study. A series of cameras will transmit video of the sheep from multiple angles in order to monitor behaviour and eye movements as well as to minimise interaction between the observer and the animal by allowing the observer to be in another room. Sheep being prey species invariably hide pain when humans/predators are present and therefore observation using cameras will ensure that pain can be observed if it occurs. A wireless link will be used to remotely control the implanted device. The implant tuning procedure is expected to last approximately two hours.

For each group, the specific type of stimulation will be applied with increased intensity within physiologically and electrochemically safe limits, one electrode at a time, while observing the animal's reactions. Should a negative reaction be observed for a specific electrode using the sheep pain scoring system (attached as part of the LAS post-operative SOP) (vocalisation, agitated movement, hiding), the intensity of the stimulation will be reduced back to a comfortable level. The value of maximal comfortable stimulation intensity will be stored and used during chronic stimulation.

After the mapping is complete for each electrode, the planned stimulation parameters will be altered to match the comfortable stimulation levels for single electrodes and the device will commence the stimulation over multiple electrodes. Again, the behaviour of the animals will be observed to identify any signs of discomfort. Should the animals show signs of distress or pain, the stimulation intensity on all electrodes will be scaled down by a specific factor and the experiment repeated until a comfortable level of stimulation is obtained.

Additionally, we aim to examine whether there are reflex-like eye movements in response to simulation of moving lines of stimuli, while observing eye movements for evidence of an optokinetic reflex. Based on responses reported in similar experiments in the feline by collaborators at the Bionics Institute in Melbourne, responses may take the form of eye movement or twitch, head movement, or posture changes coincident with the application of stimuli. If successful, this will become the standard test of functionality as it will not only show a response, but will further allow for the investigation of varied line movement frequencies, etc. This experiment will be performed during the second behavioural experiment after during the fourth week of chronic stimulation.

After defining comfortable stimulation parameters for each animal, chronic stimulation will be delivered 14-18 hours per day for 55-65 days. Animals will be observed daily for signs of pain or distress and stimulation will be interrupted if required. Sessions as described above during the 4 and 8th week of stimulation. If any signs of pain or distress are observed in the animal, which could be linked to uncomfortable stimulation parameters, the device will be switched off and the sheep behaviour observed. Should the observations suggest a correlation between the pain/distress an stimulation, the tuning procedure will be repeated to ensure that comfortable stimuli are delivered.

All sessions will be recorded with video cameras for off-line evaluation and assessment of outcomes.

If practical, behavioural studies will be done at McMasters to avoid stress to the animals and minimize transportation. Examples of limiting factors which would require the behavioural studies to be performed at CPC include, but are not limited to, the size of the pens and their modularity and light conditions.

A minimum of 48 hours will be respected between anaesthesia (for imaging purposes, for example) and other experiments such as behavioural testing.

Acute electrophysiology during terminal procedure during week 13 or 14

For the electrophysiology measurement procedure, an alfaxalone intravenous infusion will be utilised as the preferred anaesthetic technique. This technique has the least chance of causing cortical suppression that would proclude successful measurements by the research team. The anaesthetic protocol is based on current literature as listed below. Alfaxalone infusions in other species have also been successful for the purpose of electrophysiological measurements. The animals will still be attached to the anaesthetic machine to allow provision of oxygen supplementation and mechanical ventilation if required. All other aspects of the anaesthetic protocol will comply with the LAS Sheep Anaesthesia SOP. The procedure is terminal and the animals will not be recovered. The procedure is expected to take up to 12 hours.

Reference: Moll, X., et al. (2013) The effects on cardio-respiratory and acid-base variables of a constant rate infusion of alfaxalone-HPCD in sheep. The Veterinary Journal. 196, pp.209-212

The surgeon and the assistant will shave and scrub the head of the animal above the visual cortex with chlorhexidine or povidone iodine using sterile gauze swab. To facilitate

cautery, a square (approximately 100 x 100 mm) will be shaved on the contralateral abdomen to interface with a monopolar plate electrode.

The surgical team will gown and glove as per standard sterile technique. The sites will be rinsed with sterile water. Sterile drapes will be applied, leaving the sites clear but covering the outer edge of each site.

The scalp will be reflected and a craniotomy at the visual cortex will be performed on the contralateral side to that of the implanted eye, 10 mm lateral to the lambdoid suture (approximately 90 mm posterior to the coronal line formed between the ears). A 1–2 mm diameter platinum sphere electrode will be used to map the visual cortex while stimuli are delivered to the retina. After identifying the cortical area activated by the retinal stimuli, a perforating micro-electrode array will be inserted into the cortex.

An intravenous dose of dexamethasone will be administered pre-operatively to reduce the cortical inflammatory response; cephazolin intravenous antibiotics will be administered every 90 minutes to prevent infection.

A reference electrode will be placed within a small incision at the rostral end of the scalp incision.

Visual and electrical stimuli delivered via the implanted stimulator will be delivered to compare the cortical activity elicited by the different types of stimuli.

Response recording of neural activity in the cerebral cortex will be made with a multi-channel

amplification and recording system. In each animal, this recording procedure will be repeated over a range of electrical stimulation parameters corresponding to all three types of stimulation delivered chronically in the three groups. The purpose of this experiment is to compare whether the type of chronically delivered stimulation parameters influence the stimulation thresholds.

Further test using combinations of sequential and simultaneous stimulation using a range of parameters will be tested to evaluate the efficacy of the device and the different paradigms to elicit discrete visual percepts.

Euthanasia and tissue collection

Animals will be euthanised according to the LAS Large Animal Euthanasia SOP (SOP-EUTH_03_LAS Euthanasia and humane killing_sheep pigs_20170713). Tissue will be collected as per [1].

Histology and immunohistochemistry

As per [1] and electrode site identification as per [260]

Data analysis

Acquired cortical recording data will be deidentified to blind the operator to the intervention and analysed to extract the stimulation threshold at which the cortical firing rate reaches 50% of its saturation value (P50) [31]. The P50 for each stimulation paradigm will be compared between the three experimental units (three groups of four sheep) using ANOVA statistics to determine whether chronic hexapolar or quasimonopolar stimulation influenced the stimulation thresholds.

For each animal, the P50 for each of the three stimulation paradigms will also be compared to provide further insights into the differences between stimulation strategies [31, 60, 61].

Histological and immunohistochemical analysis will be performed according to the methods developed in [1]. Tissue grading will be used to compare the effects of the three stimulation strategies on the health of the eye tissue, in particular the retina.

Intervention timeline

A representative example of the timeline for a single animal is presented in Appendix Figure 12.

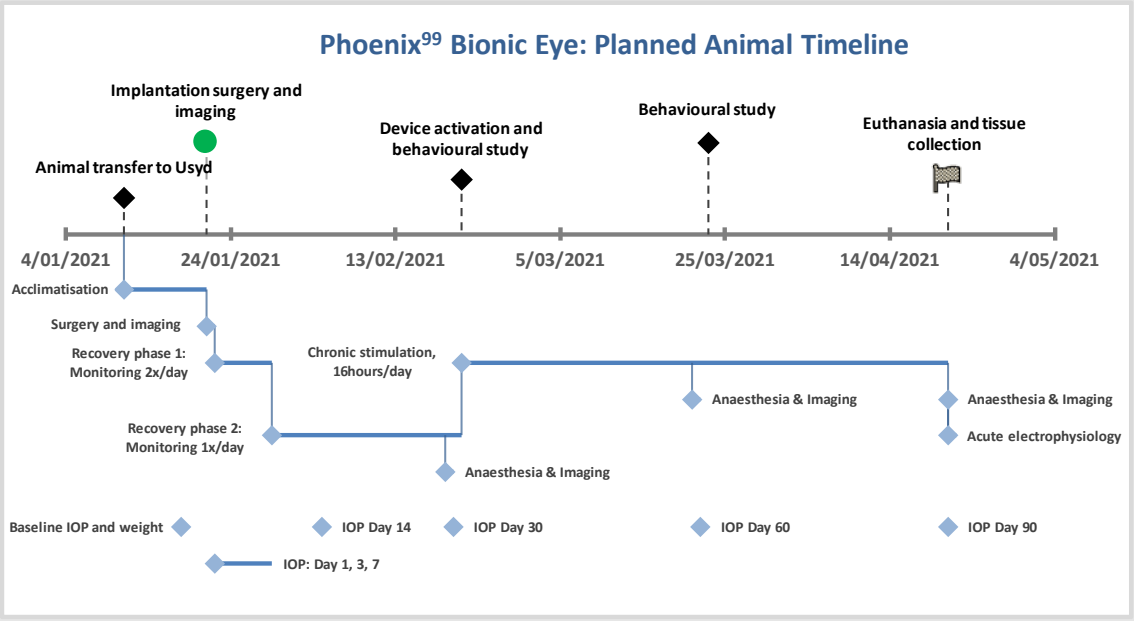

Appendix Figure 12 Overview of the intervention timeline for the safety study of parallel stimulation of the retina in sheep.

APPENDIX 8 SPIRIT CHECKLIST

Acute bionic eye implantation during an enucleation procedure

SPIRIT
STANDARD PROTOCOL ITEMS: RECOMMENDATIONS FOR INTERVENTIONAL TRIALS

SPIRIT 2013 Checklist: Recommended items to address in a clinical trial protocol and related documents*

Section/item	Item No	Description
Administrative information		
Title	1	Descriptive title identifying the study design, population, interventions, and, if applicable, trial acronym **Implantation procedure of a suproachoroidal retinal stimulator in two patients undergoing an enucleation procedure for non-cancerous reasons.**
Trial registration	2a	Trial identifier and registry name. If not yet registered, name of intended registry **Not registred. Will be registred with the Australian New Zealand Clinical Trials Registry (ANZCTR)**
	2b	All items from the World Health Organization Trial Registration Data Set **TBD**
Protocol version	3	Date and version identifier **TBD**
Funding	4	Sources and types of financial, material, and other support **TBD**
Roles and responsibilities		Names, affiliations, and roles of protocol contributors **TBD**
	5a 5b	Name and contact information for the trial sponsor **TBD**
	5c	Role of study sponsor and funders, if any, in study design; collection, management, analysis, and interpretation of data; writing of the report; and the decision to submit the report for publication, including whether they will have ultimate authority over any of these activities **TBD**
	5d	Composition, roles, and responsibilities of the coordinating centre, steering committee, endpoint adjudication committee, data management team, and other individuals or groups overseeing the trial, if applicable (see Item 21a for data monitoring committee) **TBD**
Introduction		
Background and rationale	6a	Description of research question and justification for undertaking the trial, including summary of relevant studies (published and unpublished) examining benefits and harms for each intervention **Background:**

1

Profound visual impairment is an extremely debilitating condition which can be caused by a variety of factors. Amongst the leading causes of blindness, retinal degenerative diseases such as Retinitis Pigmentosa (RP) and Age-Related Macular Degeneration (AMD) are known to cause or lead to the death of the photoreceptive cells in the eye (photoreceptors) [1, 2]. In the healthy eye, these cells are responsible for the transduction of light into patterns of neuronal activation (action potentials) that travel down the visual pathway to the visual cortex of the brain. The visual information transmitted by the eyes is then analysed and combined with many other inputs (e.g. memories) in deeper layers of the cortex before outputs are generated (e.g. movements). Without photoreceptors, information carried by the light isn't perceived, effectively depriving people from one of the most useful senses, e.g. for navigation or recognition. Indeed, visual impairment can be caused by pathologies that damage other critical elements of the neural network responsible for the delivery and interpretation of visual information. In glaucoma patients, for example, the optic nerve is compromised [3], therefore preventing any eventual signal coming from the eyes to reach the brain. Prosthetic solutions must account for the type of pathology which caused the impairment and act at the appropriate level.

The Phoenix^{99} bionic eye being developed in a collaboration between the University of Sydney, UNSW and clinicians at Westmead Hospital is intended to use electrical stimulation to replace the function of lost photoreceptors to restore functional vision in people suffering from end-stage retinal degeneration. In this population, the connectivity between the neurons located in the eye and the brain has been demonstrated to survive for extended periods, despite the neural remodelling processes caused by the lack of stimulation from the photoreceptors [4]. Profiting from the known excitability of neurons through electrical impulses, researchers have studied the visual percepts elicited during retinal stimulation [5, 6]. Different levels of prosthetic vision have been achieved clinically with several devices including three that have been cleared by regulatory bodies and made available as commercial products because they present the potential benefits to restore basic vision in the severely visually impaired ('Alpha AMS, Retina AG, Germany, IRIS II, Pixium Visa S.A., France and Argus II, Second Sight Medical Products, USA) [7-9].

The anatomy of the eye provides four main potential locations where a device can be positioned to deliver electrical stimulation to the retina. Epiretinal, subretinal, suprachoroidal and episcleral implants have been designed and tested in animals and/or humans [10, 11]. The Argus II and IRIS II both are examples of epiretinal implants in which the electrode array is positioned directly on the retina from the intraocular space. This approach provides proximity between the electrodes and target neurons but requires the vitreous humour (content of the eyeball) to be surgically removed to access the retina (vitrectomy) [8, 9]. The complexity of the surgery is further increased by the need to firmly anchor the electrode array as close as possible to the retinal surface [12]. Subretinal implants are positioned between the layers of retinal neurons and the choroid. Located very close to the surviving neurons and to the original position of the photoreceptors, subretinal devices such as the Alpha AMS are believed to, to some extent, recruit the image processing capabilities of the cell network and to provide percepts that are more easily interpreted by the brain[7]. The surgical procedure also involves a vitrectomy and associated

complexity in addition to the need for manipulation of the retinal tissue [12, 13].

Two suprachoroidal devices have been tested clinically [6, 14, 15]. The suprachoroidal space, located between the choroid and the sclera, provides relative ease of surgical access through a simple incision of the sclera and doesn't require retinal manipulation or vitrectomy [16, 17]. In that space, implants are in a "pocket" between two tissue layers which improves array stability without the use of retinal tacks commonly used in epiretinal implants [8, 9]. A potential limitation of this approach, the distance between the electrodes and the target neurons, is strongly linked to advantages provided by the said distance. The spatial resolution may indeed be decreased due to the current spreading in the tissue between the implant and the neurons, but it also represents a physical separation that may protect the cells from any stimulation biproduct.

Bareket et al. performed an in-depth comparison between the suprachoroidal approach and other locations for retinal stimulation [12].

The Phoenix^{99} bionic eye was developed in parallel to the device successfully tested by Ayton et al. The physical components of the implant, particularly the electrode array, are manufactured according to the same principles, and maintain similar shape and size. Compared to its sibling, which was connected to the outside world using a transcutaneous port that is prone to infection, the Phoenix^{99} incorporates stimulation electronics in a hermetic capsule as well as a telemetry unit (antenna and electronics) for wireless power and data transmission, thus making the device fully implantable. A fully implantable device is the obvious next step in the pathway to a clinically beneficial and safe bionic eye device.

The study performed by Ayton et al. represented the first human test of the suprachoroidal concept pioneered by Suaning and Lovell in collaboration with Korean research partners[18, 19]. This demonstrated the safety of the surgical procedure to position an electrode array in the suprachoroidal space It also showed that some level of functional vision can be restored using stimulation from this location [6]. The Phoenix^{99} builds on these results and implements novel, advanced stimulation strategies that allow better control over how the current is focussed into the retinal tissue to produce more meaningful visual percepts. These strategies aim to reduce interference between electrodes used simultaneously and minimise the stimulation threshold (quantity of electrical charge required to elicit a percept) [20-22]. Furthermore, the Phoenix^{99} was designed to allow comprehensively different and novel stimulation strategies to be tested, as opposed to simple variations of the stimulation parameters (e.g. current or frequency) offered by other devices, without the need for secondary surgery. The device also features 98 individual electrodes that have the potential to restore a wide visual field with adequate acuity to assist the patients in activities of daily life.

Apart from the extensive research related to the stimulation strategies (in-silico [23-25], in-vitro [26, 27] and in-vivo[20, 21, 28, 29]), the device also implements the advances in manufacturing (laser cut platinum electrodes [30, 31], and densely packed, hermetic feedthroughs [32]). Concluding the development and testing phase of the implant lifecycle, the safety of passive devices has been demonstrated during chronic implantation (up to 100 days) in sheep [publication pending]. This study demonstrated the appropriateness and maturity of the surgical procedure to safely and stably position the different parts of the implant in and on the eye of living animals, as well as the chronic biocompatibility of the device.

The Phoenix^{99} bionic eye is a mature device which implements key scientific findings of the last two decades of intensive research. The present protocol describes a critical step on the path towards the clinical application of the device to demonstrate and study its vision restoration capabilities.

Despite extensive studies in human cadavers and live animals, before a chronic application of active implants can be realized, it is necessary to demonstrate that the surgical procedure for implantation is safe and effective in a living human. Despite the apparent similarity between the two devices in terms of site of stimulation or manufacturing techniques, there are significant differences between the ocular and orbital components of the suprachoroidal implant already tested in humans by Ayton [Ayton, 2014] and those of the present device. The main difference is the geometry of the scleral incision to provide access to the suprachoroidal space and the need to fixate a hermetic capsule to the sclera. These differences call for a demonstration that all the surgical procedure development work carried out to date in human and animal cadavers as well as in the living feline, rabbit and sheep has led to a mature procedure that is applicable and appropriate in living humans with, among others, pulsating blood pressure.

Some patients need the surgical removal of the eyes (enucleation procedure) for example to alleviate the pain that sometimes occurs in blind eyes [33] or due to cosmetic considerations. This represents an ideal model to test the surgical procedure because it minimizes the possibility of causing harm to the subject. Since the eye will be removed after the acute implantation, the most critical part of the experimental procedure has very limited chance of generating harm to the patient. More specifically, this study will focus exclusively on the part of the surgery that is located within the orbit of the eye and include the placement of the electrode array and stimulator hermetic capsule. The Phoenix^{99} includes four main components. The electrode array is placed between two layers of the eye anatomy and the visual stimulator capsule sits on the globe. The part of the implant responsible for the communication with the outside world (via inductive telemetry so as to eliminate the need for infection-prone, percutaneous communication) is designed to be implanted behind the ear and to mimic closely existing devices (specifically, cochlear implants) from geometrical, surgical site and procedure perspectives. Thanks to the existing clinical knowledge and experience with the implantation procedure of the behind-the-ear components and leads used to connect the different parts of the implants, this part of the procedure can be excluded from the present trial as it is virtually identical to that of routine, cochlear implant surgeries.

During the implantation procedure, a scleral incision will be performed. A thin sheet comprising silicone rubber and platinum (an electrode array) will be introduced between the choroid and the sclera. The incision will then be sutured closed before fixating an electronics capsule to the sclera by way of sutures. During the present study, minimally-, or non-invasive IOP measuring techniques will be used to observe this parameter. Owing to the delicacy of the device, manipulation carries a risk of damage to the device that could compromise functionality of active devices intended for future implantation. The physical integrity of the devices will be verified, using X-ray microtomography or similar non-destructive imaging techniques. For comparison purposes, these imaging techniques will be conducted both

4

		prior to and after the procedure to isolate any damage that may be caused as a consequence of surgery. **Apart from additional measurements (IOP) and images (ophthalmoscopy, optical coherence tomography) for the purpose of the study, as well as an expected prolonged surgery/anaesthesia duration, the intervention has no apparent effects on the participants' safety and well-being. The studied intervention is insulated within the orbit and on the globe which is being removed as the primary objective of the surgery. There is therefore a very beneficial ratio between the risks of the intervention and the potential benefits of the study. Even though the participants enrolled to undergo acute implantation of a bionic eye will have no benefits for themselves, this study will contribute significantly towards the clinical application of a novel implant for the blind.** **OTHER POTENTIAL HARMS?** **Psychological: if a participant doesn't fully understand that the operation has no potential to him, (s)he could suffer from psychological harm because of the perspective of recovering sight. To avoid this, the selection of potential participants will exclude anyone with cognitive impairment, an intellectual disability or a mental illness. Consent will be obtained after clearly explaining that no benefit can be expected for the participants themselves and participants will be required to state their understanding of this fact.**
	6b	Explanation for choice of comparators **Safety and efficacy of the surgical intervention will be evaluated on an absolute scale (no comparator within the study). The number of intraoperative adverse events (AEs) and severe adverse events (SAEs) will be recorded and compared to published data of other visual prostheses. The integrity of the device post-implantation is a criterion without a comparator.** **The contralateral eye (no intervention) will be used as a comparator for intraocular pressure.**
Objectives	7	Specific objectives or hypotheses **Research hypotheses:** **The surgical procedure to implant the Phoenix^{99} bionic eye is safe and effective.** • **The intervention does not cause serious adverse events or cause any material damage to critical structures required for electrical stimulation of the retina to be effective (e.g. nerve fibre layer or optic nerve).** • **It allows the positioning of the electrode array in the adequate location in the suprachoroidal space without causing material damage to the device.** • **It allows the visual stimulator capsule to be secured to the sclera via dedicated eyelets to prevent capsule and electrode array displacement or damage.** **Primary objectives:** • **To determine whether the surgical procedure is safe and effective when applied *in-vivo* and, ideally, whether it preserves the tissue structures required for the elicitation of visual percepts using suprachoroidal electrical stimulation. Due to the pre-existing condition(s) that caused - or resulted from - the blindness, it may**

		not always be possible to identify the specific effects of the intervention on intraocular structures. • **To confirm that positioning procedures result in the appropriate positioning of the electrode array when using the procedure in-vivo.** • **To evaluate the effects of the implantation procedure on the physical integrity of the device (macroscopic or microscopic damage)** • **To evaluate the mechanical stability of the device provided by the in-vivo application of the surgical procedure.** **Secondary objectives** • **To evaluate efficacy and efficiency of custom and standard surgical tools and equipment and to propose refinements if required.** • **Confirmation that any intraocular pressure changes caused by the implantation procedure are safe, and to determine whether a specific intervention to compensate for that change is warranted.**
Trial design	8	Description of trial design including type of trial (eg, parallel group, crossover, factorial, single group), allocation ratio, and framework (eg, superiority, equivalence, noninferiority, exploratory) **Exploratory pilot trial, single group, open label study without randomization in allocation.**
Methods: Participants, interventions, and outcomes		
Study setting	9	Description of study settings (eg, community clinic, academic hospital) and list of countries where data will be collected. Reference to where list of study sites can be obtained **All data will be collected at Westmead hospital, Westmead, Sydney, NSW, Australia** **Public hospital**
Eligibility criteria	10	Inclusion and exclusion criteria for participants. If applicable, eligibility criteria for study centres and individuals who will perform the interventions (eg, surgeons, psychotherapists) • **Undergoing planned enucleation procedure for non-cancerous reasons** • **Either gender** • **Aged 18 years or older** • **Inclusion criteria:** ○ **Requires an enucleation procedure for a blind, painful or aesthetically displeasing** • **Exclusion criteria:** ○ **Elevated intraocular pressure (above XX mmHg)** ○ **Low intraocular pressure (below XX mmHg)** ○ **Diagnosed cancer, particularly in the ocular region (globe, optic nerve, orbit)** ○ **Ocular injury or malformation that would prevent identification and manipulation of the tissue involved in the intervention.** ○ **Sensitivity to prolonged anaesthesia (procedure described in this study will make the enucleation procedure longer)** ○ **Cognitive deficiencies, including dementia or progressive neurological disease** ○ **Psychiatric disorders, including depression, as diagnosed by a qualified psychologist**

- **Active infection that can't properly be isolated from the surgical site**
- **Diseases of the inner retina including, retinal detachment, traumatic retinal damage, infectious retinal disease, inflammatory retinal disease.**
- **Inability to visualise the retina due to corneal or other ocular media opacities (corneal degenerations, dense cataracts, trauma, lid malpositions)**
- **Inability to speak or understand English**
- **Pregnancy**
- **Presence of a cochlear implant**
- **Subject enrolled in another investigational drug or device trial for the treatment of their ocular condition**
- **Poor general health, which would exclude them from obtaining a general anaesthetic**
- **Unrealistic expectations of the bionic eye device**
- **Device is left/right specific. Participants can be excluded if no device with the correct orientation is available at the time of the surgery.**

Interventions	11a	Interventions for each group with sufficient detail to allow replication, including how and when they will be administered

All implants used in this intervention were manufactured according to the same detailed manufacturing instructions within the quality management in place at the Graduate School of Biomedical Engineering, level 0 of Samuels Building, University of New South Wales (UNSW), Sydney, Australia. The manufacturing of the implant, as well as the materials composing it have been published [34]

Preliminary data collection

1. **Detailed fundus imaging (for offline data analysis)**
2. **Optical Coherence Tomography (OCT) (for offline data analysis)**
3. **Ocular ultrasound**

Surgical protocol:

Preparation and device implantation

4. **Preparation for surgery**
5. **Anaesthesia induction**
6. **Measure intraocular pressure in both eyes**
7. **Start timer**
8. **Surgical site preparations and disinfection using diluted betadine solution**
9. **Lateral canthotomy and cantholysis**
10. **Dilate pupil with 1% tropicamide, 1% cyclopentolate and 2.5% phenylephrine**
11. **The surgeon sits superiorly**
12. **360 degree conjunctival peritomy with Westcott scissors and conjunctival forceps**
13. **Corneal temporal sutures (6-0 vicryl, spatula needle, toothed forceps, needle holder)**
14. **Isolate the superior and inferior rectus with a muscle hook.**
15. **Isolate the lateral rectus with a muscle hook. Suture the lateral rectus with double armed 6-0 vicryl. Clamp the two ends with an alligator clip, keeping the superior end shorter.**
16. **Cut the lateral rectus**
17. **Identify any large scleral/vortex veins and try to avoid these**

18. Measure an L shaped wound with calipers (11.2mm wide, 3.2mm at one end), 10mm posterior to the limbus. Pay attention to ensuring that the position allows sufficient room for the capsule when the electrode is in place. The electrode should go temporally, posterior to the insertion of the lateral rectus muscle. The position should be such that the lead wire on the capsule exits towards the lateral canthus directly
19. Mark the wound with a marking pen.
20. Incise the 10mm straight wound with a 15 degree blade. NB: The wound needs to be long enough to allow the array to fit but not too long otherwise it will move. It needs to be deep enough not to leave any scleral fibres, but beware of incising too deeply as the uvea will bleed.
21. External diathermy
22. Insert the electrode with silicone covered Kelman Mcpherson forceps while the silicone introducer is still in the wound. Be careful not to bend the electrode. Insert it up the bridge.
23. Cut the 3.2mm "L" with the 15 degree blade.
24. Push the electrode fully in.
25. Suture the wound with 7-0 prolene (interrupted).

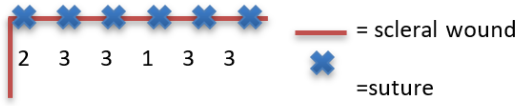

26. Suture the eyelets of the capsule with 7-0 prolene, the two anterior of the capsule, and the more posterior eyelets of the two on the sides if exposure allows.
27. Record intermediate time on timer
28. Measure intraocular pressure in both eyes
29. Detailed fundus imaging (for offline data analysis)
30. Optical Coherence Tomography (for offline data analysis)
31. Ocular ultrasound

Enucleation procedure and device explantation

32. Using a muscle hook, isolate medial rectus using, inferior rectus, superior rectus muscles, suture the muscles with double armed 6-0 vicryl and transect them.
33. Isolate the superior oblique and inferior oblique muscles and transect them.
34. Make a temporal conjunctival relax incision to ease manipulation.
35. Apply gentle forwards traction on the globe and resect the optic nerve, thus liberating the globe from the orbit. Carefully remove the globe together with the implant and store it in 10% formalin.
36. After haemostasis is obtained, position an adequate implant in the orbit and close wounds according to the surgical procedure chosen for the patient.
37. Record total surgery duration from timer

Device imaging and evaluation

38. Transportation of the enucleated eye in-situ implant to the imaging facility.
    - Samples may be required to be shipped/transported overseas to access imaging technologies not available in Australia (e.g. grating interferometry using synchrotron light at Paul Scherrer Institute (PSI), Villigen, Switzerland).

8

39. **Perform micro-CT imaging (or other suitable imaging technologies) of the eye with the device in position**
40. **Explant the device**
41. **Destruction of the eyes according to the local best practice or other based on the informed consent**

11b Criteria for discontinuing or modifying allocated interventions for a given trial participant (eg, drug dose change in response to harms, participant request, or improving/worsening disease)

Procedure should be discontinued if one or more of the following is observed:

- **TBD**

Procedure should be changed to a routine enucleation (without implantation of the subject device) if one or more of the following is observed:

- **TBD**

11c Strategies to improve adherence to intervention protocols, and any procedures for monitoring adherence (eg, drug tablet return, laboratory tests)

Study includes a single intervention per participant and no strategies are required to ensure adherence.

11d Relevant concomitant care and interventions that are permitted or prohibited during the trial

Any concomitant care and interventions are permitted at the exception of interventions that would substantially alter the surgical protocol described above and/or risk to cause damage to the subject device that is unrelated to the proposed implantation protocol.

Outcomes 12 Primary, secondary, and other outcomes, including the specific measurement variable (eg, systolic blood pressure), analysis metric (eg, change from baseline, final value, time to event), method of aggregation (eg, median, proportion), and time point for each outcome. Explanation of the clinical relevance of chosen efficacy and harm outcomes is strongly recommended

Primary outcomes

The primary outcomes of the study are related to the intrinsic properties of the surgical procedure and its effects on the patient and the device. Failure on these critical points would question the safety and effectiveness of the intervention.

- **The safety of the intervention is defined as the number and severity of the adverse events recorded (adverse events are documented and rated by the operating surgeon on a scale of reference e.g CTCAE p.18, an independent expert will review the adverse events and provide scoring) that are related directly or indirectly to the implant or the implantation procedure. Adverse events will be considered to be related to the implant or implantation procedure if they occur before or during closure of the scleral incision or if they involve any of the tissue that was dissected, transected or resected as part of the implantation procedure. Any adverse event involving the retina, as observed using intraoperative or post-operative fundus imaging (e.g. retinal detachment, or retinal, subretinal or suprachoroidal haemorrhage) will be considered to be implant related.**
- **The functionality of passive implants can't be evaluated directly since the devices do not contain electronics. Therefore, the evaluation of the device integrity will be done using high definition**

imaging on the explanted devices. The surgical procedure will be considered a success if it doesn't damage the implant in a way that may compromise its functional longevity. Device inspection will consider macroscopic damage (bare eye inspection) or microscopic (optical microscope, micro-CT or other) to the silicone encapsulation, the conductive platinum tracks, the electrodes or any other part of the implant such as the eyelets used to secure the capsule to the globe.

Secondary outcomes

The secondary outcomes of this study are centred around recommendations and refinements for future surgeries and small technique updates that would increase the likeliness of long term success of the intervention.

- **Surgery duration provides information about the complexity of the procedure as well as it determines the minimal duration of the anaesthesia. Primary surgery duration will be measured from the first cut incision until the last suture of the scleral incision is placed. Surgery duration will be compared to the published values obtained for other visual prosthesis using electrical retinal stimulation.**
- **Implantation of the device in the suprachoroidal space may cause changes in the intraocular pressure because of the incision made to the sclera and the insertion of a foreign body into the globe. Intraocular pressure measurement will be taken after suturing the scleral incision and before enucleating the eye. The intraoperative measurement will be compared to the baseline value obtained preoperatively to give recommendations about active, intraoperative IOP management during surgeries subsequent to this study.**
- **The surgical procedure should allow for the device to be centred around the macula while avoiding interference with the optic nerve. Using intraoperative fundus images, the macula and the optic disc are clearly visible and used as landmarks for the evaluation of the implant position. Static intraoperative fundus images will be acquired for offline analyses and measurement of the distances of interest. Micro-CT will be use post-operatively to obtain quantitative data about implant position relative to the optic disc.**
-

Participant timeline 13

Time schedule of enrolment, interventions (including any run-ins and washouts), assessments, and visits for participants. A schematic diagram is highly recommended (see Figure)

- **Recruitment of patient 1 (up to 6 months)**
- **Patient 1**
  - **Preparation for surgery**
  - **Implantation procedure (see detailed protocol, 2h)**
  - **Enucleation procedure, closure of the surgical wounds (unrelated to this study, see detailed protocol, 1h)**
  - **Patient convalescence and follow-up (1 month)**
- **Validation of the procedure for patient 2**
- **Recruitment of patient 2 (up to 6 months)**
- **Patient 2**
  - **Preparation for surgery**

- **Implantation procedure (see detailed protocol, 2h)**
- **Enucleation procedure, closure of the surgical wounds (unrelated to this study, see detailed protocol, 1h)**
- **Patient convalescence and follow-up (1 month)**

- **Publication of the results (3 months)**

Sample size	14	Estimated number of participants needed to achieve study objectives and how it was determined, including clinical and statistical assumptions supporting any sample size calculations **Number of participants: 2** **Based on the experience previously collected during pre-clinical studies with the subject device as well as clinical data obtained using a similar device, two device implantations will be a sufficient number of interventions to confirm the hypothesis of this study. Simultaneously, the population of potential participants is low and the number of procedures was defined to allow the study to be completed within a reasonable period of time of one year, to avoid external factors (e.g hospital teams or surgeon availability) influencing the results of the present study. Indeed, in the hospital where the study will be conducted, 6 enucleations are typically done yearly.**
Recruitment	15	Strategies for achieving adequate participant enrolment to reach target sample size **1 hospital where 6 enucleations are done yearly. Small percentage of those cases are for non-cancerous reasons therefore patients may need to be grouped from several hospitals in the area.**

Methods: Assignment of interventions (for controlled trials)

Allocation:		
Sequence generation	16a	Method of generating the allocation sequence (eg, computergenerated random numbers), and list of any factors for stratification. To reduce predictability of a random sequence, details of any planned restriction (eg, blocking) should be provided in a separate document that is unavailable to those who enrol participants or assign interventions **N/A, single arm study**
Allocation concealment mechanism	16b	Mechanism of implementing the allocation sequence (eg, central telephone; sequentially numbered, opaque, sealed envelopes), describing any steps to conceal the sequence until interventions are assigned **N/A, no concealment mechanism**
Implementation	16c	Who will generate the allocation sequence, who will enrol participants, and who will assign participants to interventions **N/A, single arm study**
Blinding (masking)	17a	Who will be blinded after assignment to interventions (eg, trial participants, care providers, outcome assessors, data analysts), and how **N/A, open label**
	17b	If blinded, circumstances under which unblinding is permissible, and procedure for revealing a participant's allocated intervention during the trial **N/A**

Methods: Data collection, management, and analysis

Data collection methods	18a	Plans for assessment and collection of outcome, baseline, and other trial data, including any related processes to promote data quality (eg, duplicate measurements, training of assessors) and a description of study instruments (eg, questionnaires, laboratory tests) along with their reliability and validity, if known. Reference to where data collection forms can be found, if not in the protocol

Audio and video recordings of the surgery will be acquired, including a detailed walkthrough by the operating surgeon. Written proceedings of the procedure will be created based on the audio and video recordings. Any observation and discussion will be recorded in the form of handwritten notes by at least one investigator witnessing the surgery. These notes and images will be integrated in the proceedings.

Fundus imaging (preop, intraop) – In-vivo imaging using a direct or indirect ophtalmoscope

- **Trained operators**
- **Same operator throughout the study**

Optical Coherence Tomography (preop, intraop) – In-vivo imaging using dedicated optical coherence tomography imagine system

- **Trained operators**
- **Same operator throughout the study**

Intraocular pressure (preop, intraop) – In-vivo measurement using a tonometer

- **Trained operators**
- **Same equipment at all times**
- **Same operator at all times**
- **Same measurement anatomical location at any time**
- **Multiple measurements at each time point**

Adverse events – Intraoperative and post-operative documentation and evaluation of all investigator observed and patient reported (solicited and spontaneous reporting) adverse events.

- **Trained investigators**
- **Published grading system (or standard) e.g. CTCAE p.18)**
- **Independent rating from a second investigator**

Device integrity – Pre-operative and post-operative imaging and analysis of the device integrity including integrity of the silicone over-moulding, eyelets, hermetic encapsulation, conductive tracks, electrodes, etc.

- **Compare device before and after intervention**
  - **Bare eye**
  - **Microscope**
  - **MicroCT**
  - **Grating interferometry**
- **Trained operators**
- **Multiple independent rating of the integrity**

Surgery duration – Measurement of the surgery duration using a timer, as defined in the study protocol

- **Two trained operators timing operating independently**

Distance to optic disc (Fundus, microCT) – Off-line measurement of the distance between the implant apex and the centre of the optic disc using digital images and a dedicated software (e.g. ImageJ, imagej.net)

- **Landmark positions (implant apex and centre of optic disc) marked by two trained operators independently on the images**

	18b	Plans to promote participant retention and complete follow-up, including list of any outcome data to be collected for participants who discontinue or deviate from intervention protocols **Participant retention is not critical in this study since a single intervention is used to collect all outcome data, including the explanted eye with the device attached. Should a recruited participant withdraw from the study prior to the surgery, no outcome data will be collected. Deviation from protocols are not expected in this study, should nevertheless deviations happen during the intervention they will be recorded and their impact on the results analysed.**
Data management	19	Plans for data entry, coding, security, and storage, including any related processes to promote data quality (eg, double data entry; range checks for data values). Reference to where details of data management procedures can be found, if not in the protocol **TBD**
Statistical methods	20a	Statistical methods for analysing primary and secondary outcomes. Reference to where other details of the statistical analysis plan can be found, if not in the protocol **N/A, outcomes are measured by way of adverse events during surgery and thus statistics are not applicable to such a small scale study**
	20b	Methods for any additional analyses (eg, subgroup and adjusted analyses) **N/A,**
	20c	Definition of analysis population relating to protocol non-adherence (eg, as randomised analysis), and any statistical methods to handle missing data (eg, multiple imputation) **If critical data is missing, conclusions of the study could be compromised due to the low number of interventions planned. Particular care needs to be taken to guarantee quality and timely data collection. On the other hand, since all data will be collected during a single surgery, the data is unlikely to suffer from non-adherence or other factors that could compromise data collection.**
Methods: Monitoring		
Data monitoring	21a	Composition of data monitoring committee (DMC); summary of its role and reporting structure; statement of whether it is independent from the sponsor and competing interests; and reference to where further details about its charter can be found, if not in the protocol. Alternatively, an explanation of why a DMC is not needed **No data monitoring committee is needed for this study. The absence of blinding, as well as the "one-off" nature of the intervention will allow the investigators to critically analyse any adverse events between cases. Device and surgery related adverse events will be weighed according to their severity and whether they pose risks to the.**

	21b	Description of any interim analyses and stopping guidelines, including who will have access to these interim results and make the final decision to terminate the trial **Because the present study uses passive devices and has no potential benefits to the participants, adverse events that have the potential to affect a participant beyond what is expected from an enucleation procedure shall be analysed in detail to avoid reoccurrence. If needed, the study shall be stopped. Because of the nature of the intervention, adverse events could occur that are no threat to the participant because the eye will subsequently be removed. If a detailed analysis of the adverse event(s) reveals that reoccurrence is possible but that it will does not harm the participant, we recommend the study to be continued to increase the amount of data gathered. The final decision to terminate the trial will be taken by the chief investigator, possibly in collaboration with the HREC to whom all serious adverse events will be reported.**
Harms	22	Plans for collecting, assessing, reporting, and managing solicited and spontaneously reported adverse events and other unintended effects of trial interventions or trial conduct **An adverse event (AE) is defined as an untoward medical occurrence in a subject with or without suspicion of causal relationship with the intervention. AEs observed before the beginning of the experimental protocol described in this document will NOT be reported. AEs observed between the beginning of the intervention and until the end of the normal follow-up period for an enucleation procedure (solicited and spontaneously reported) will be documented and analysed to identify a possible causal relationship with the intervention, as opposed to a relationship to the enucleation procedure (not part of the investigation). AEs related only to the enucleation procedure will NOT be reported. If a causal relationship with the studied intervention cannot be excluded, the AEs will be reported. All serious adverse events (SAE) will be reported to the HREC using the appropriate form, including cases where causal relationship with the intervention cannot be demonstrated.**
Auditing	23	Frequency and procedures for auditing trial conduct, if any, and whether the process will be independent from investigators and the sponsor **No auditing planned during trial conduct. Due to the limited size of the trial, reporting of serious adverse events to the HREC is sufficient to ensure trial is conducted adequately.**
Ethics and dissemination		
Research ethics approval	24	Plans for seeking research ethics committee/institutional review board (REC/IRB) approval **The present study protocol and informed consent form (English, Braille and Audio versions) will be reviewed and approved by an accredited HREC at the Westmead Hospital (Westmead, Sydney, NSW, Australia) with respect to the NHMRC National Statement on Ethical Conduct in Research Involving Humans. Research Governance Site Authorization will be obtained from the Chief Executive (or Designee) prior to commencing research, according to the "NSW Health Policy Directive PD2010_056 Research - Authorisation to Commence Human Research in NSW Public Health Organisations". The Research Office at Western Sydney Local Health District (WSLHD) will manage and administer the ethical and governance review process.**

		Participant education and recruitment material, as well as any other requested material will also be reviewed by the HREC. **Following the initial approval of the research protocol and other submitted material, any modification will be reviewed by the HREC. Annual progress reports will be provided to the HREC for review, as well as a final report which will be submitted at the latest 3 months after the conclusion of the study. All reports will contain at least the number of enrolled participants to date, number of enrolled participants that have undergone the experimental surgery, summary of the performed interventions with focus on surgical safety, effectiveness and patients recovery.**
Protocol amendments	25	Plans for communicating important protocol modifications (eg, changes to eligibility criteria, outcomes, analyses) to relevant parties (eg, investigators, REC/IRBs, trial participants, trial registries, journals, regulators) **Substantial alterations or amendments to the protocol (changes that could potentially affect the safety of the participants, the validity of the data and conclusions of the study) will go through a formal approval process by the HREC. An impact analysis of the proposed changes will be documented and provided to the HREC. The impact analysis will include detailed measures that need to be taken to ensure data validity and coherence between the datasets obtained using different protocol revisions. Should the impact analysis reveal no potential harms to the scientific validity of the data, the changes will NOT be reported (journals). Changes that affect patient safety (positively or negatively) will be communicated to all enrolled participants and to the relevant Research Office at WSLHD.** **All documents will be identified on each page by the document name, revision number, date of the latest modification, and the name/number of the study to which it relates. Each document will feature a revision history table describing in detail the changes between each revision and their impact, or a reference to the specific impact analysis.**
Consent or assent	26a	Who will obtain informed consent or assent from potential trial participants or authorised surrogates, and how (see Item 32) • **People that have become blind sometimes experience pain in their eyes which require the non-functioning eye(s) to be removed (enucleation procedure) to avoid further suffering.** • **The investigators will contact several clinicians that are commonly involved with blind people that require an enucleation procedure. The clinicians will be informed of the aims and requirements of the study and given a procedure to follow whenever they identify a potential participant.** • **Participants who require an enucleation surgery for a painful blind eye or cosmetic reasons will be identified by their treating clinician and the investigators will be informed by the clinician of the existence of a potential participant, including relevant, anonymized information required by the research team to validate that the potential participant fulfils all criteria for the study.** • **The clinician will then ask the potential participant if she or he agrees to meet with the investigators (including the surgeon). If the potential participant accepts, their contact details will be transmitted to the investigation team.** • **Upon identification of potential participants, and if the potential participant agrees to meet the investigators, first contact will be made over the phone and a meeting will be organized at the potential subject's convenience and in an adequately private**

15

		location familiar to the potential participant to maximize his/her wellbeing. • **Consent form will be provided in written English, Braille and audio** • **Consent will be obtained by the investigators including audio recording of the consent and written signature.**
	26b	Additional consent provisions for collection and use of participant data and biological specimens in ancillary studies, if applicable **N/A**
Confidentiality	27	How personal information about potential and enrolled participants will be collected, shared, and maintained in order to protect confidentiality before, during, and after the trial **Results of the study will be entirely anonymised in any publication or thesis. The results will focus on the surgical procedure and its outcomes, not on the recipient of the implant.**
Declaration of interests	28	Financial and other competing interests for principal investigators for the overall trial and each study site **[Declaration of the shell company holding the IP will be required]**
Access to data	29	Statement of who will have access to the final trial dataset, and disclosure of contractual agreements that limit such access for investigators
Ancillary and post-trial care	30	Provisions, if any, for ancillary and post-trial care, and for compensation to those who suffer harm from trial participation
Dissemination policy	31a	Plans for investigators and sponsor to communicate trial results to participants, healthcare professionals, the public, and other relevant groups (eg, via publication, reporting in results databases, or other data sharing arrangements), including any publication restrictions **Results from this study will be disseminated internationally in recognized journals and will aim at establishing a best practice for the implantation of bionic eye systems.**
	31b	Authorship eligibility guidelines and any intended use of professional writers
	31c	Plans, if any, for granting public access to the full protocol, participant level dataset, and statistical code
Appendices		
Informed consent materials	32	Model consent form and other related documentation given to participants and authorised surrogates
Biological specimens	33	Plans for collection, laboratory evaluation, and storage of biological specimens for genetic or molecular analysis in the current trial and for future use in ancillary studies, if applicable **The enucleated eyes of the participants will be collected and stored and analysed according to the present protocol. Evaluations will not include genetic or molecular analysis during the present trial or subsequent studies.**

*It is strongly recommended that this checklist be read in conjunction with the SPIRIT 2013 Explanation & Elaboration for important clarification on the items. Amendments to the protocol should be tracked and dated. The SPIRIT checklist is copyrighted by the SPIRIT

References

1. Jager, R.D., W.F. Mieler, and J.W. Miller, *Age-related macular degeneration.* N Engl J Med, 2008. **358**(24): p. 2606-17.
2. Hartong, D.T., E.L. Berson, and T.P. Dryja, *Retinitis pigmentosa.* The Lancet, 2006. **368**(9549): p. 1795-1809.
3. Mantravadi, A.V. and N. Vadhar, *Glaucoma.* Primary Care, 2015. **42**(3): p. 437-+.
4. Humayun, M.S., et al., *Visual perception elicited by electrical stimulation of retina in blind humans.* Arch Ophthalmol, 1996. **114**(1): p. 40-6.
5. Humayun, M.S., et al., *Visual perception in a blind subject with a chronic microelectronic retinal prosthesis.* Vision Res, 2003. **43**(24): p. 2573-81.
6. Ayton, L.N., et al., *First-in-Human Trial of a Novel Suprachoroidal Retinal Prosthesis.* PLOS ONE, 2014. **9**(12): p. e115239.
7. Daschner, R., et al., *Functionality and Performance of the Subretinal Implant Chip Alpha AMS.* Sensors & Materials, 2018. **30**(2): p. 179-192.
8. Hornig, R., et al., *Pixium Vision: First Clinical Results and Innovative Developments*, in *Artificial Vision: A Clinical Guide*, V.P. Gabel, Editor. 2017, Springer International Publishing: Cham. p. 99-113.
9. da Cruz, L., et al., *Five-Year Safety and Performance Results from the Argus II Retinal Prosthesis System Clinical Trial.* Ophthalmology, 2016. **123**(10): p. 2248-2254.
10. Cheng, D.L., P.B. Greenberg, and D.A. Borton, *Advances in Retinal Prosthetic Research: A Systematic Review of Engineering and Clinical Characteristics of Current Prosthetic Initiatives.* Current Eye Research, 2017. **42**(3): p. 334-347.
11. Chowdhury, V., J.W. Morley, and M.T. Coroneo, *Evaluation of extraocular electrodes for a retinal prosthesis using evoked potentials in cat visual cortex.* J Clin Neurosci, 2005. **12**(5): p. 574-9.
12. Bareket, L., et al., *Progress in artificial vision through suprachoroidal retinal implants.* J Neural Eng, 2017. **14**(4): p. 045002.
13. Zrenner, E., et al., *Subretinal electronic chips allow blind patients to read letters and combine them to words.* Proc Biol Sci, 2011. **278**(1711): p. 1489-97.
14. Fujikado, T., et al., *One-Year Outcome of 49-Channel Suprachoroidal–Transretinal Stimulation Prosthesis in Patients With Advanced Retinitis PigmentosaOne-Year Outcome of 49-Channel STS Prosthesis in Advanced RP.* Investigative Ophthalmology & Visual Science, 2016. **57**(14): p. 6147-6157.
15. Endo, T., et al., *Light localization with low-contrast targets in a patient implanted with a suprachoroidal-transretinal stimulation retinal prosthesis.* Graefes Arch Clin Exp Ophthalmol, 2018. **256**(9): p. 1723-1729.
16. Saunders, A.L., et al., *Development of a surgical procedure for implantation of a prototype suprachoroidal retinal prosthesis.* Clin Exp Ophthalmol, 2014. **42**(7): p. 665-74.
17. Villalobos, J., et al., *Development of a surgical approach for a wide-view suprachoroidal retinal prosthesis: evaluation of implantation trauma.* Graefe's Archive for Clinical and Experimental Ophthalmology, 2012. **250**(3): p. 399-407.
18. Bae, S.H., et al., *In vitro biocompatibility of various polymer-based microelectrode arrays for retinal prosthesis.* Invest Ophthalmol Vis Sci, 2012. **53**(6): p. 2653-7.
19. Wong, Y.T., et al., *Efficacy of supra-choroidal, bipolar, electrical stimulation in a vision prosthesis.* Conf Proc IEEE Eng Med Biol Soc, 2008. **2008**: p. 1789-92.
20. Matteucci, P.B., et al., *Current steering in retinal stimulation via a quasimonopolar stimulation paradigm.* Invest Ophthalmol Vis Sci, 2013. **54**(6): p. 4307-20.

21. Matteucci, P.B., et al., *The effect of electric cross-talk in retinal neurostimulation.* Investigative Ophthalmology and Visual Science, 2016. **57**(3): p. 1031-1037.
22. Barriga-Rivera, A., et al., *Cortical responses following simultaneous and sequential retinal neurostimulation with different return configurations.* Conf Proc IEEE Eng Med Biol Soc, 2016. **2016**: p. 5435-5438.
23. Al Abed, A., et al., *A model of electrical stimulation of a retinal cell population using a multi-electrode array.* Conf Proc IEEE Eng Med Biol Soc, 2015. **2015**: p. 2287-90.
24. Khalili Moghaddam, G., et al., *Performance optimization of current focusing and virtual electrode strategies in retinal implants.* Comput Methods Programs Biomed, 2014. **117**(2): p. 334-42.
25. Abramian, M., et al., *Quasi-monopolar electrical stimulation of the retina: a computational modelling study.* J Neural Eng, 2014. **11**(2): p. 025002.
26. Tsai, D., et al., *Survey of electrically evoked responses in the retina - stimulus preferences and oscillation among neurons.* Sci Rep, 2017. **7**(1): p. 13802.
27. Abramian, M., et al., *Activation of retinal ganglion cells following epiretinal electrical stimulation with hexagonally arranged bipolar electrodes.* J Neural Eng, 2011. **8**(3): p. 035004.
28. Matteucci, P.B., et al., *Threshold analysis of a quasimonopolar stimulation paradigm in visual prosthesis.* Conf Proc IEEE Eng Med Biol Soc, 2012. **2012**: p. 2997-3000.
29. Suaning, G.J., et al., *Discrete cortical responses from multi-site supra-choroidal electrical stimulation in the feline retina.* Conf Proc IEEE Eng Med Biol Soc, 2010. **2010**: p. 5879-82.
30. Schuettler, M., et al., *Fabrication of implantable microelectrode arrays by laser cutting of silicone rubber and platinum foil.* J Neural Eng, 2005. **2**(1): p. S121-8.
31. Dodds, C.W.D., et al. *Performance of laser fabricated stimulating electrode arrays for a retinal prosthesis in saline*. in *2009 4th International IEEE/EMBS Conference on Neural Engineering*. 2009. p. 88-91 DOI: 10.1109/NER.2009.5109241.
32. Guenther, T., et al. *Chip-scale hermetic feedthroughs for implantable bionics*. in *2011 Annual International Conference of the IEEE Engineering in Medicine and Biology Society*. 2011. p. 6717-6720 DOI: 10.1109/IEMBS.2011.6091656.
33. Custer, P.L. and C.E. Reistad, *Enucleation of blind, painful eyes.* Ophthalmic Plast Reconstr Surg, 2000. **16**(5): p. 326-9.
34. Eggenberger, S.C., et al., *Implantation and long-term assessment of the stability and biocompatibility of a novel 98 channel suprachoroidal visual prosthesis in sheep.* Biomaterials, 2021. **279**: p. 121191.